DISSERTATION

ULTRA-SHORT PULSE LASER ABLATION OF BIOLOGICAL HARD TISSUE AND DENTAL RESTORATIVE MATERIALS

ausgeführt zum Zwecke der Erlangung des akademischen Grades einer
Doktorin der Naturwissenschaften

unter der Leitung von

a.o. Univ. Prof. Dr. phil. Ernst Wintner
Institut für Photonik E387

eingereicht an der Technischen Universität Wien, Fakultät für Physik

von

Mag. rer. nat. Verena Wieger

97 25 193

Florianigasse 36
7121 Weiden am See

Wien, Februar 2007

Beobachte das Schwimmen der Fische im Wasser,
und du wirst den Flug der Vögel in der Luft begreifen.

Leonardo da Vinci

For my beloved parents
Erwin and Christine

ABSTRACT

For biological hard tissue treatment in medicine mechanical tools are commonly used. In case of dental cavity preparations mainly drills are applied. For implant surgery and orthopaedics besides the drill also saws and diamond discs are in use. In the past decades many efforts have been made to find substitutes for them among laser systems. The reasons for that are manifold: 1) Friction causes high temperatures that damage the adjacent tissue. 2) A smear layer and very rough surfaces are produced by all mechanical tools. 3) The size and shape of traditional tools are often unsuitable for geometrically complicated incisions and for minimal invasive treatment.

Different laser systems in the µs- (10^{-6} seconds) and sub-µs-pulse regime, among them Erbium lasers, have already been tested in the hope to overcome the mentioned drawbacks. After some years of research Erbium lasers are nowadays established as routine tools in dentistry reducing some of the unwanted side effects. For bone surgery some dissensions are still obvious. Although some authors consider Erbium lasers as useful tools in surgery, the results are often not very satisfying and sometimes even controversial. The drawbacks considered are e.g. melting, carbonisation and unfavourable cavity shapes and morphology. They are mainly due to the long pulse durations of these laser systems.

In the present work the applicability of scanned ultra-short pulse lasers (USPL) for biological hard tissue removal was tested. It was shown that cavities with features superior to mechanically treated or Erbium laser ablated cavities can be generated with this innovative method if appropriate scan algorithms and optimal laser parameters are matched. Smooth cavity rims, no micro-cracks, melting or carbonisation and precise geometry are the advantages of scanned USLP ablation. Besides potential painless tooth treatment, good compound between the composite restoration and the tooth may be achieved due to the remaining micro-retentive surface pattern. For bone treatment better healing conditions are expected as the native structure remains unaffected by the preparation procedure.

The uniqueness and novelty of this work is given by the comprehensive compilation of various experimental results to assess the performance of USPL. By focusing different aspects of USPL ablation and linking them together an overall picture could be provided. Therefore pulse durations in the picosecond and femtosecond (1 ps = 10^{-12} s, 1 fs = 10^{-15} s) regime were applied to dental structures and bone tissue. As the removal of dental restorative material is also relevant in this context, several composite materials were involved in these studies. Parameters like ablation rates, which describe the efficiency of the ablation process, and ablation thresholds were determined for the first time and compared to the corresponding Erbium values. The morphology of the tissue surface remaining after laser preparation was investigated and the surface roughness was judged. Selective ablation was stressed and the temperature impact induced by lasers was emphasized. In case of bone tissue, plasma spectra using LIBS (laser induced breakdown spectroscopy) were obtained to distinguish between different substances.

The results of these investigations can be used to develop an USPL laser system for application in surgery. Similar to Erbium lasers commercially available for dental treatments, via mirrors or fibre the laser beam can be guided to a hand-piece with integrated miniature scanner. An incorporated feedback system based on the data of plasma emission spectroscopy can guarantee selective and therefore minimal invasive treatment. With such an USPL system the flexibility of the surgeon and the precision and morphological quality of the treatment can be enhanced.

ACKNOWLEDGEMENTS

I want to express my gratitude to my supervisor a.o. Univ.-Prof. Dr. phil. Ernst Wintner, Photonics Institute, Vienna University of Technology, for giving me the chance to carry out this PhD thesis, for his motivating advices and his support.

Likewise I am very grateful to a.o. Univ.-Prof. Dr. techn. Johann Wernisch, Institute of Solid-State Physics, Vienna University of Technology, for his personal commitment and encouragement, not to forget about his invaluable contributions by doing ESEM analysis.

I like to thank my colleague Dipl.-Ing. Martin Strassl, Photonics Institute, Vienna University of Technology, who helped me to get started and who provided me some graphics for this thesis.

Furthermore I am indebted to HighQ Laser Production GmbH, Hohenems, as well as to the Research Centre for Microtechnology, University of Applied Sciences, Dornbirn, and the Institute of Applied Physics, Johannes Kepler Universität, Linz, for access to their laser systems. Without their cooperation my research work would have not been possible.

I appreciate Alicona company, Grambach, Austria, for providing me their IFM microscope and the Institute of Sensor- and Actuatorsystems, Vienna University of Technology, for use of their diamond saw and their light microscope.

I like to thank Kerr Corporation and Ivoclar Vivadent AG for providing me composite materials.

I am grateful to the Department of Conservative Dentistry, Bernhard Gottlieb University Dental Clinic Vienna, for generous material and sample supply and for access to their Erbium lasers.

I want to thank the Austrian Academy of Sciences for their financial support during the last year of my research by awarding me the DOC-FFORTE fellowship, which provides special funding to women in science.

I appreciate very much that I could do my research work at Photonics Institute. Besides the professional surrounding, I experienced a very familiar atmosphere there. People who contributed to this pleasant feeling particularly were Dipl.-Ing. Heinrich Kofler, Dipl.-Ing. Johannes Tauer, Dr. techn. Martin Weinrotter and a.o. Univ.-Prof. Dr. rer. nat. Georg Reider.

I am especially obliged to my parents for their belief in my potential and abilities, and for passing on their attitude that nothing is impossible.

I sincerely want to thank my friends, most of all Mag. Vera Schneider, Dipl.-Ing. Heinrich Kofler, Andreas Fuhrmann, Günther Leopold, Dipl.-Ing. Johannes Tauer and Christian Sattler, for words of encouragement, their emotional support and for just being there for me.

Although possibly uncommon, I am also grateful to my lovely cats Minki and Sophie for relaxing with them.

CONTENTS

1 INTRODUCTION

Dental tissue treatment which commonly is accomplished by conventional mechanical drills is always associated with pain and heat-induced defects. The reason therefore can be attributed to the sensitivity of the pulp, which reacts to the vibrations of the drill, the pressure applied onto the tooth and the temperature increase due to friction that arises during the drilling procedure. A temperature increase of about 5 C° (Zack, 1965) above body temperature already induces damages. Another problem related to the dental drill is the production of a smear layer that seals the dental tubuli. Prior to restoration of the cavity some etchant has to be applied to remove this smear layer and to make the tubuli permeable for the filling material. Otherwise convenient retention of the restoration cannot be guaranteed. Nevertheless, if this etchant is not removed properly leaving some remnant under the restoration layer longterm damage in form of hypersensitivity can be caused.

First experiments using lasers for dental tissue treatment were already performed in 1964 using pulsed ruby lasers (Goldman, 1964), (Stern and Sognnaes, 1964) which introduced enourmous thermal side effects. Some years later, CO_2 lasers were tested for clinical relevance (Stern, 1972). Since then several studies were conducted on CO_2 laser ablation, making aware of the problematic thermal impact of this laser. (Moritz, 2006, p. 122) Also different other laser types were tested for their applicability in dentistry, among them ArF eximer laser (Frentzen, 1989) and Ho:YAG laser (Niemz, 1993). None of them gained real importance in dentistry because of unwanted side effects or ineffectiveness of ablation. At the end of the 1980s, Erbium systems were considered as surgical tools (Niemz, 1996). As they seemed very promising several improvements were made over the recent years. Nowadays Erbium lasers such as the Er:YAG and Er,Cr:YSGG are already established as useful tools in dental surgery. (Moritz, 2006), (Romanos, 1999) Erbium wavelengths are located close to the absorption maximum of water incorporated in biological hard tissue. Thus, the energy is coupled into the tissue very effectively. Thereby, via immediate heating and vaporization of the water within the irradiated tissue, micro-explosions take place expelling the created small particles.

Combining vibration-free and pain-reduced working procedures the Erbium laser provides more comfort to patients than conventional high-speed drills. Although many efforts were made to find appropriate laser parameters unwanted side effects like collateral damage of adjacent tissue caused by overheating during laser ablation could not be completely diminished. Neither could the goal of pain-free treatment be reached.

In orthopaedics and implant surgery the situation is comparable to dental surgery. Mainly mechanical devices such as drills, burrs, diamond discs and saws are used for bone tissue removal. Again, heat generated by friction becomes problematic. Thereby the arising temperatures can be so high, that the adjacent bone tissue may be damaged. Temperatures of 44°C to 47°C applied to bone tissue over a longer period of time destroy the vital bone cells so that the regeneration cycle is extended (Wang, 2005). Additional drawbacks of common preparation tools can be found in their size and handling, which make them unsuitable for minimal invasive operation. Even signs of wear cannot be disregarded, e.g. dump saws tear out larger fractions of bone material during preparation. The same effect can be observed when saw-blades with an insufficient number of teeth are used. In general, a smear layer and very rough surfaces can be observed for all mechanical tools (Olivier, 2003), (Sasaki, 2002).

Hoping to avoid all these unwanted side effects, also for bone tissue different laser systems in the µs and sub-µs pulse regime, mainly Erbium (El Montaser, 1997), (Kimura, 2001), (Pourzaradian, 2004) and CO_2 (Ivanenko, 1998), (Ivanenko, 2002), (Frentzen, 2003) but also Nd:YAG (Friesen, 1999), (Rohanizadeh, 1999) and FEL (Peavy, 1999), (Spencer, 1999), (Payne, 2001) as well as excimer (Jovanovic, 1997) and Ho:YAG (Buchelt, 1994) lasers have been tested and compared to common mechanical tools. For Erbium lasers the obtained

results are sometimes controversial. Some authors report on the superior tissue quality and on healing processes of laser-treated bone tissue to be comparable or even faster in time than mechanically treated tissue (Keller, 1991), (Pourzaradian, 2004). Others observed a microscopic zone of damage (Li, 1992), (El Monatser, 1997), (Sasaki, 2002), (Anranbat-Dominguez, 2003) which causes a delay in healing. (Nelson, 1989), (Kimura, 2001) Although some drawbacks have to be mentioned, many authors consider Erbium lasers to be very well suited for bone tissue ablation.

In any case, a major advantage of lasers compared to conventional mechanical tools is the contact-free preparation technique. 1. The method is very hygienic and sterile. 2. The laser beam, which is guided by mirrors or fibres inside the system from the laser source to the target, is focused on the tissue surface as it leaves the hand-piece. If the necessary powers are applied, the ablation mechanism starts automatically in the focused area. The application of an external force by the hand of the doctor as needed in the case of drills and saws is superfluous and inconvenient when using lasers. 3. The employment of a hand-piece instead of a saw makes the work of the surgeon easier, so that incisions can be cut in much more flexible way.

Anyhow, further improvements regarding the quality of the ablated cavities in tooth and bone structures as well as the temperature development can only be achieved by applying shorter pulse lengths, especially ultra-short laser pulses (USLP) addressing pulse duration ≤ 30 ps. The reason for that can be found in the fundamentally different interaction mechanism of USLP with matter, the plasma-mediated ablation. The associated shock waves and the thermal influence are significantly smaller than that of the laser preparation techniques in use described above. But still, if the wrong set of parameters is chosen thermal damages can also occur. In any case, in order to initiate plasma formation high power densities are necessary. This can only by accomplished by strong focusing of the USP laser beam yielding focal spot diameters in the µm regime. To treat larger areas scanning of the laser beam, i.e. deflection over a locally limited region is inevitable. Thereby two accumulation effects can be avoided (e.g. Kim, 2001): With an increasing number of laser pulses impacting subsequently on the same tissue spot, the temperature would rise rapidly and the ablation efficiency would be decreased. The reduction in efficiency can be explained by the following: a deep hole acts as hollow waveguide where the cavity walls absorb and reflect part of the laser energy. The deeper the hole, the smaller is the portion of pulse energy available for the actual ablation at the bottom of the cavity so that the ablation efficiency gets reduced.

In general, the morphological characteristics of the remaining tissue are of superior quality. The advantages of scanned USPL ablation exerted on dental and bone tissue are:

- Precise cavity preparation resulting in smooth cavity rims
- No molten or re-solidified zones
- No carbonisation
- No micro-cracks as there is no collateral damage due to thermal load and shock waves
- Almost no temperature increase and therefore no heat transport to the adjacent tissue
- Gentle tissue removal
- Potential for pain-free treatment
- Selective ablation
- Additional feedback by plasma emission

Some of these outstanding properties have already been confirmed by other authors like (Armstrong, 2002), (Kamata, 2004), (Ozono, 2003) and (Schwab, 2004).

1.1 GOALS AND WAYS OF APPROACH

The aim of the study was to test the applicability of UPSL systems for biological hard tissue removal, i.e. tooth and bone structures. Thereby special emphasise is put on selective ablation of different materials. In case of bone structure involving compacta, spongiosa and cartilage, potential selectivity among these tissue types was focused. For investigations of selective ablation of dental tissue just considering dentine and enamel is not enough. In dental praxis, composite filling material often has to be removed to treat secondary caries appearing at the rims of restorations or underneath them. Ablation of composites was therefore a major point of investigation too, particularly because of the fact that hardly any research has been conducted on this topic.

Throughout this thesis a comparison between Erbium and USPL ablation is provided, thereby different Erbium and UPSL systems were involved. In each chapter reporting on the results of my scientific studies material and methods are described separately, comparisons to findings of other authors are provided and a discussion is attached.

This thesis is organised in six main chapters. After this introduction, chapter two gives an overview of the fundamentals. Thereby the principles of laser light generation and especially USLP generation are explained. The anatomy of dental tissue and bone is presented and the nature of composite restorations is described. For completeness also laser-tissue interactions are discussed. Chapter three addresses the technical equipment and the tissue samples used for the studies. Every laser system is introduced and the preparation procedures of the samples are outlined. Chapter four and five make up the core of this work as the scientific results are reported. While chapter four concentrates on dental tissue and composite material, chapter five is devoted to bone substances. For dental tissue and composites ablation rates and ablation thresholds were determined. The morphology of the remaining surfaces after laser ablation was evaluated, selectivity was investigated and roughness of the cavities, important for adhesion of the restoration, was analysed. Chapter five contains ablation rates and ablation thresholds for bone tissues. Furthermore, it provides illustrations of the bone morphology after laser processing mainly carried out on the ESEM. Some results on plasma spectroscopy are presented and temperature measurements are discussed. Finally, a conclusion and an outlook are provided.

2 FUNDAMENTALS

2.1 FUNDAMENTALS OF LASERS

The following chapters were established on basis of references (Reider, 1997), (Koechner, 2003), (Bäcker, 2004) and (Wintner, 2006).

2.1.1 LASER LIGHT GENERATION

The optical concept of laser light generation is based on absorption and stimulated emission of light by a laser medium. The laser medium as an atomic system consisting of atoms, ions and molecules can be described in terms of energy levels E_i, which are discrete energy states that can be occupied by electrons. A change from one to another level can mathematically be stated as

$$E_2 - E_1 = h \cdot \upsilon_{12} \tag{1}$$

where h is Planck's constant and υ_{12} the frequency for radiative 1-2 transitions. Electro-magnetic waves with frequencies corresponding to this energy gap can interact with the system. The transition is then related to either absorption or emission of light with specific wavelengths λ given by

$$\lambda \cdot \upsilon_{12} = c \tag{2}$$

where c is the vacuum speed of light. For the generation of laser light a stronger population of the higher energy level is required called inversion. Therefore external pump sources, e.g. flash lamp or diode laser, have to be applied to cause such a population inversion by exciting the electrons of the lower level and shifting them to an upper one. Electrons of the higher energy level tend to reach their thermal equilibrium again. Spontaneous emission, which is comparable to the common radiative decay, is one possible process to return to the lower energy level. The light emission accompanying this transition is characterized by random direction and phase and is therefore unsuitable for laser light generation. To use the stored energy of the medium for light amplification a further electro-magnetic wave with appropriate frequency corresponding to the energy level difference has to interact with the atomic system. The photons of this wave cause the electrons of the upper state to drop into a lower energy level. The released energy is thereby emitted in form of additional photons amplifying the incident radiation field. This effect is called stimulated emission. The acronym "laser", i.e. light amplification by stimulated emission of radiation, is derived from this process. Stimulated and incident radiations possess the same directional properties, the same polarization, the same phase and the same spectral characteristics. Hence, the excellent properties of laser light like directedness, monochromacy, polarisation and coherence can be explained.

The transitions for most effective laser light generation are schematically outlined in Fig. 1. A four-level system, which is necessary for continuous wave operation, is shown. Using specific pump sources the atoms are raised from the ground level E_0 to E_3. By a rapid decay, which might be radiative or non-radiative, level E_2 is reached. As E_2 has a longer lifetime population inversion can be achieved. Via stimulated emission the transition from E_2 to E_1, the lower laser level, takes place, which is the actual light amplification process. Finally, a fast transition to level E_0 brings the system back to its thermal equilibrium. The fast transition from E_1 to the ground level implicates that E_1 is almost empty and that even the smallest population of E_2 leads to a population inversion.

An alternative system is the three-level system where the laser transition is directly connected to the ground level. Compared to the four-level system, where inversion can easily be achieved, in a three-level system the upper laser level has to be heavily excited via the pump band to become more populated than the ground level. Evidently, the main difference between both schemes is that the threshold for laser operation is much smaller for the four-level system.

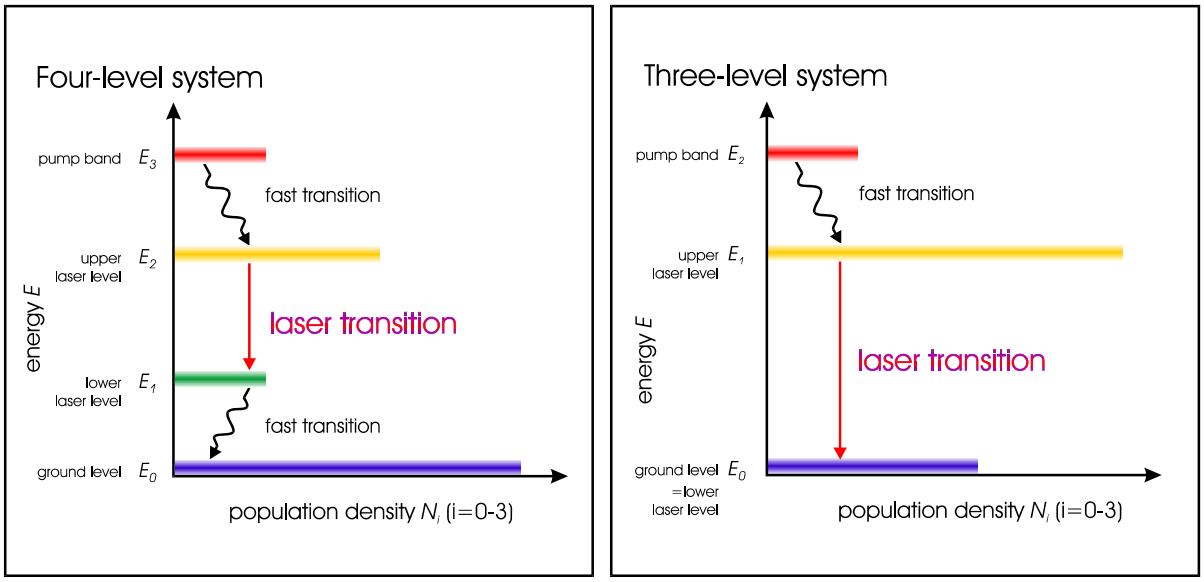

Fig. 1: Four-level system and three-level system. E_i, with i = 0, 1, 2, 3 are discrete energy levels, N_i describes the number of atoms or molecules per unit volume being in one of those states.

Within this thesis just solid-state lasers were used. For such systems crystals or glass hosts doped with ions from rare earth, actinide or iron group of the periodic table of elements are employed as active laser media. In Fig. 2 the transition scheme of Er^{3+} ions embedded in YAG and YSGG crystals is depicted. The whole system can be reduced to four levels. The colour code was chosen, to match the one used in Fig. 1.

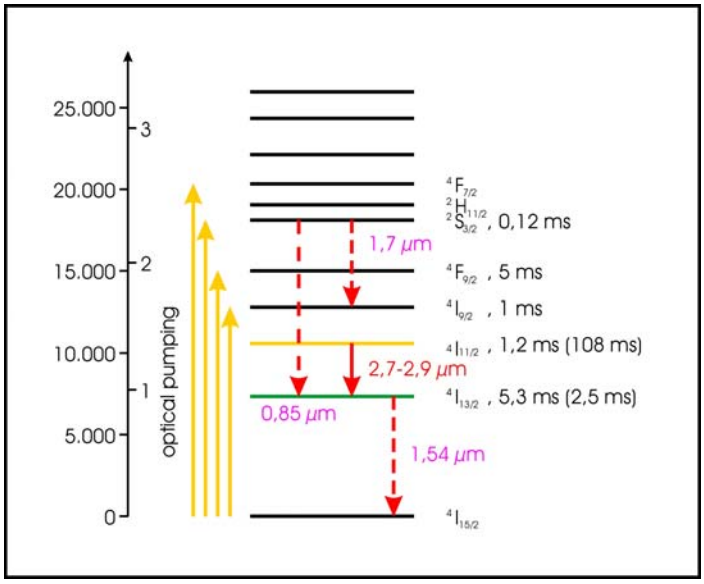

Fig. 2: Laser light generation by Er^{3+} in YAG, YSGG. The lifetimes indicated refer to YAG. The wavelengths 2.7-2.9 µm are presently the most used ones in cavity preparation. The bar on the left addresses the wave number $\bar{\nu}$ ($\bar{\nu} \equiv 1/\lambda$, [$cm^{-1}$]) and the energy in eV, respectively.

The main components of a laser are the laser medium, a pumping source exciting the medium and the optical resonator. A simplified setup is captured in Fig. 3. The resonator consists of mirrors with different reflectivity. The light generated inside the resonator is multiply reflected by these mirrors always passing the active medium. Thereby the light amplification process by stimulated emission of radiation is exploited. As at least one mirror is partially transmitting the laser light which is outcoupled in this way.

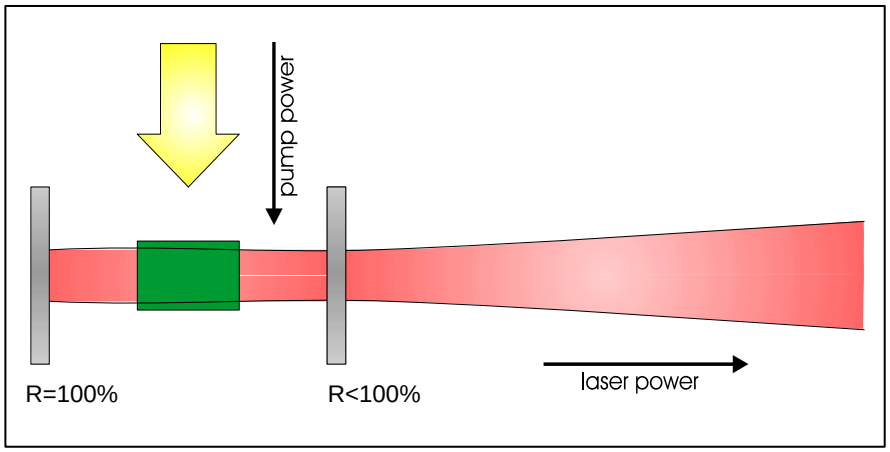

Fig. 3: Free running laser: Basic scheme of a laser consisting of a resonator and an amplifying medium.

The propagating light can be described as a Gaussian beam. Its amplitude and its intensity are distributed according to the Gaussian bell shape. In the paraxial approximation, which means in the vicinity of the propagation axis, given by $r<<|q|$, the beam can mathematically be expressed by

$$E(r,z,t) \approx \frac{B}{q}\exp\left(-\frac{r^2}{w^2(z)}\right)\exp\left(-i\frac{kr^2}{2R(z)}\right)\exp i(\omega t - kz) \tag{3}$$

$$B = E_0 \cdot \exp(k \cdot z_R) \tag{4}$$

$$q = z + iz_R. \tag{5}$$

B is the generalized amplitude and 1/q is the complex generalized wave parameter defined in equation (5), $r = \sqrt{x^2 + y^2}$ is the radius, $R(z)$ the radius of curvature, z the propagation axis and z_R the Rayleigh length. The beam radius $w(z)$ is related to the beam waist w_0 by

$$w(z) = w_0\sqrt{1 + z^2 / z_R^2} \tag{6}$$

where $w_0 = \sqrt{z_R\lambda / \pi}$. Also the divergence given by

$$\theta = \lim_{z<<z_R}\frac{w(z)}{z} = \frac{w_0}{z_R} = \frac{\lambda}{\pi w_0} \tag{7}$$

should be mentioned. In Fig. 4 the main parameters are graphically presented. The intensity distribution in radial direction is especially outlined in Fig. 4 a), where $I/I_{max} = \exp(-2r^2/w^2(z))$ is derived from the expression $\exp(-r^2/w^2)$ of equation (3) as $I \propto |E|^2$.

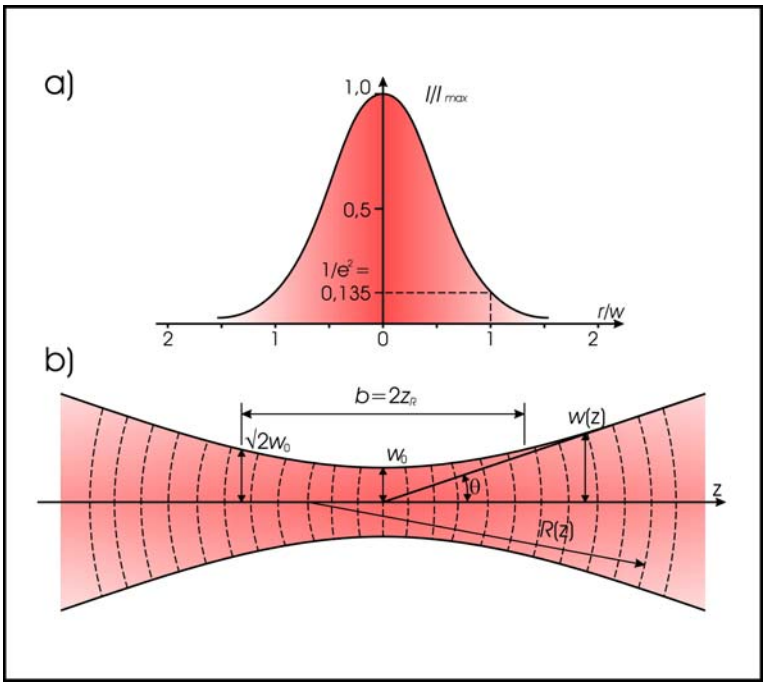

Fig. 4: Gaussian beam. a) Bell-shaped intensity distribution at any cross section at distance z from the waist; I intensity at radial position r, I_{max} maximum intensity at the z-axis. b) Longitudinal cut through the rotationally symmetric Gaussian beam. $b = 2z_R$ is the confocal parameter.

Admittedly, this is a brief survey about laser basics. For detailed information innumerable literature is available. To avoid redundancy just the main aspects are touched. The following chapters are also conceived in this manner.

2.1.2 Generation of Laser Pulses

There are several ways to yield pulsed laser operation. The simplest way is to apply a pulsed pump source. By that quasi-cw radiation with pulse durations in the microsecond regime as evident for free-running Erbium lasers are generated. If high pulse powers are required Q-switching has to be employed. The quality factor Q of the resonant cavity is defined as the ratio of energy stored in the cavity to the energy loss per cycle. Obviously, the higher the quality factor, the lower the losses. Applying this Q-switching technique implicates, that on the one hand energy is stored in the laser medium by means of inversion, on the other hand the losses are kept that high, that laser oscillation is prohibited. Thereby the population inversion reaches a level far above the threshold for laser action. If the high Q value is re-established, a strong laser pulse of typically nanosecond duration is released. Fig. 5 demonstrates the sequence of this process.

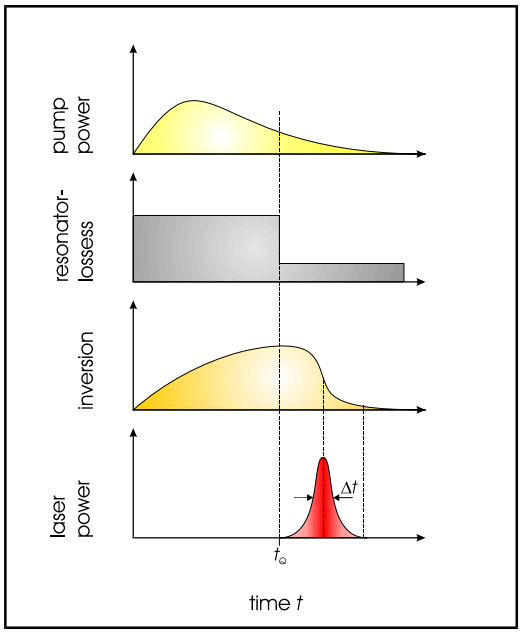

Fig. 5: Q-switching of a laser resonator. During the pumping period the resonator losses are kept high disabling laser action. Towards the end of the flash lamp pulse the inversion reaches its maximum. When the Q-factor of the resonator is switched to a high value, which is related to a rapid reduction of losses, a strong pulse is emitted. t_Q is the time of Q-switching.

Anyhow, Q-switching does not qualify to produce pulses in the pico- and femtosecond pulse regime, mainly focused by this thesis. Therefore a very sophisticated method called mode-locking has to be applied.

2.1.3 MODE-LOCKING

The basis for mode-locking is the temporal interference of laser modes which are the characteristic field distributions in the resonator. The longitudinal modes present in the laser resonator during continuous wave oscillations at free-running operation are widely independent and their phases fluctuate. In the frequency regime, the modes are equidistantly arranged with the mode spacing $\Delta\omega_r = \pi \cdot c / d$, where d is the resonator length. Thereby, the number of modes supported by the oscillator depends on the spectral bandwidth of the laser medium. Assuming that $2N+1$ modes of similar amplitude E_0 and frequencies $\omega_n = \omega_0 + n \cdot \omega_r$ ($n = -N...N$ and ω_0 is the frequency of the central mode) are oscillating in the resonator with random phase Φ_n the complex total field can be stated as

$$E(t) = E_0 \sum_{n=-N}^{N} \exp\left(i[(\omega_0 + n \cdot \Delta\omega_r) \cdot t + \Phi_n]\right). \tag{8}$$

In free-running mode the laser yields a randomly fluctuating output power P_{cw}. Mode-locking, on the other hand, involves a fixed phase relation $\Phi_n = constant$ for all modes at a specific time $t = t_1$. Switching to the time domain, this implicates that at $t = t_1$ all modes constructively interfere forming an intense and very short light pulse. For all other $t \neq t_1$ the modes are cancelling each other out by destructive interference. The pulse repeats itself periodically corresponding to the resonator roundtrip time $t_{rep} = 2 \cdot \pi / \Delta\omega_r = 2 \cdot d / c$. Thereby, the resulting total field strength is given by $(2 \cdot N+1) \cdot E_0$. The superposition of modes leads to a periodically evolving sequence of pulses with a pulse τ_p duration of

$$\tau_p = \frac{t_{rep}}{2 \cdot N + 1}. \tag{9}$$

The peak intensity of these pulses reaches the multiple $I_p = (2 \cdot N+1)^2 \cdot I_0$ of the single intensities I_0. Compared to cw operation, the output peak power is then $P_p \propto N \cdot P_{cw}$. The number of modes contributing to the mode-locking effect is limited by the amplification bandwidth $\Delta\omega_g$ of the laser medium. As

$$\tau_p \geq \frac{2 \cdot \pi}{\Delta\omega_g} \tag{10}$$

the generation of shorter pulses requires media of wide bandwidth. For fs-pulse generation more than 10^5 modes can interfere for pulse formation. Active and passive mode-locking can force the modes to stay in phase. The first technique refers to an external modulation of resonator gains or losses, while the second one addresses an interaction of internal processes. They are described in the following.

2.1.3.1 ACTIVE MODE-LOCKING

For active mode-locking an electro-optic phase modulator or an acousto-optic amplitude modulator have to be placed inside the laser cavity. The modulator is then driven at the frequency spacing of the axial modes. Only radiation passing the absorber at the time of its maximum transmission can propagate in the cavity. The evolving pulse passing the active medium gets amplified. By that mode-locked pulse trains with a repetition rate $1/t_{rep} = c/2 \cdot d$ are generated.

2.1.3.2 PASSIVE MODE-LOCKING

The basis for passive mode-locking is the insertion of a passive nonlinear element, a saturable absorber, into the laser cavity. The pulses arise from intensity fluctuations of the multi-mode laser, as low intensities get suppressed and high intensities get amplified by intensity dependent processes. Thereby a periodic modulation leading to fixed phase relationship of the axial modes is achieved.
The most successful modulation technique is Kerr lens mode-locking (KLM), which produces intensity-dependent changes of the refractive index according to $n = n_0 + n_1.I$. When a Gaussian beam passes a Kerr lens an intensity distribution related graded index lens (GRIN) is formed forcing self-focusing. The higher the intensities the stronger they get focused, hence very low intensities are not focused at all. The graphic in Fig. 6 shows this nonlinear effect, demonstrating that low intensities do not experience self-focusing induced by the Kerr medium termed X. As a consequence, losses at the aperture are caused. High intensities on the other hand undergo self-focusing, so that their transmission through the aperture is not reduced. Pulse shortening is therefore achieved by the nonlinear medium cutting off the low-intensity edges of the pulse.

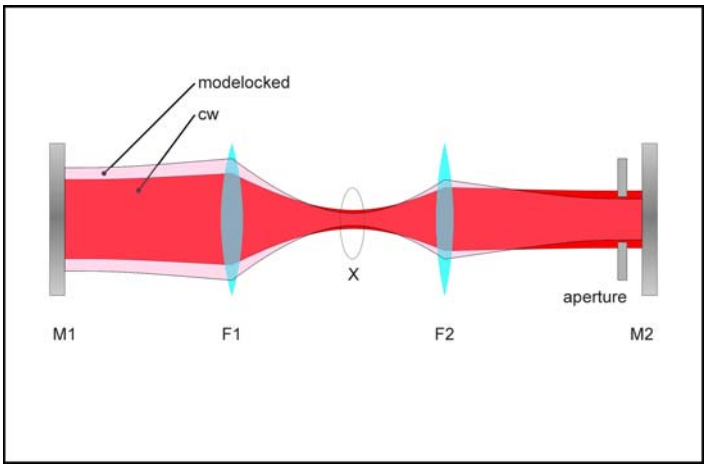

Fig. 6: Kerr lens mode-locking for the generation of ultra-short pulses in a solid-state laser. M_1, M_2...mirrors, F_1, F_2...lenses, X...Kerr lens, AP...aperture, cw...continuous wave operation, ML...mode-locked operation.

In this context also dispersion of the laser medium (dispersion relation: $k = n \cdot \omega / c$,) has to be considered. USL pulses comprise a wide range of frequency components each having its own propagation velocity, i.e. phase velocity $v_{ph} = \omega/k = c_0/n$, whereas the envelope of the pulse is propagating with the so called group velocity $v_g = \frac{c}{n + \omega(dn/d\omega)}$. When passing a dispersive medium depending on its dispersion coefficient high frequency components are either running ahead or lacking behind low frequency parts because of different phase velocities. In case of normal (positive) group velocity dispersion (GVD, $D_\omega = \frac{1}{d\omega}\left(\frac{1}{v_g}\right) > 0$), which is usually present in the laser medium, higher frequency components are delayed compared to lower frequencies. In other words, when a pulse passes the Kerr medium, the leading edge experiences a medium which is getting optically thicker due to the dependence of the refractive index on *I*. Hence, the increase of the refractive index causes a frequency delay of the electric field, i.e. a red-shift of the leading pulse edge. The trailing pulse edge is affected the other way around, leading to a blue-shift. This effect leads to a broadening of the pulse and to a variable instantaneous frequency, called chirp.

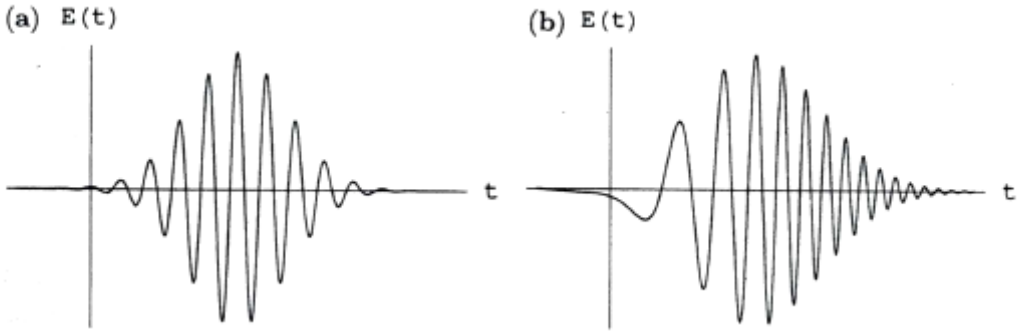

Fig. 7: Amplitude of the electric field of an USL pulse (a) before and (b) after passing a dispersive medium. The introduced change of the instantaneous frequency in the course fo the pulse is called chirp. (Graphic taken from(Bäcker, 2004)).

To compensate this pulse broadening phenomenon, the USL pulse has to be launched through an optical path with negative dispersion. This can be achieved by prism pairs or gratings arranged in a manner that the blue components of the pulse can pass faster than the red ones. Dielectric multilayer cavity mirrors with integrated negative dispersion yield the same result as high frequency components of the pulse are reflected on layers closer to the surface while lower frequencies are reflected at deeper layers.
Self phase modulation, i.e. the creation of a linear chirp by the optical Kerr effect, and negative dispersion are the basis for passiv ultra-short pulse formation.

2.1.4 AMPLIFICATION

Employing either active or passive mode-locking, the desired ultra-short laser pulses can be generated. By active mode-locking approximately N~10^3 modes are linked together activating pulses with ps-durations. Passive mode-locking has to be involved when fs pulses are required as about 10^5 modes are constructively superimposed.
The generation of high energy ultra-short pulses is based on the combination of a mode-locked oscillator, i.e. seed laser, and an amplifier. The oscillator produces initial laser pulses of moderate power and energy. When these pulses pass the amplifier, the energy stored in the active medium due to inversion is extracted and the pulses are intensified. The amplification system mostly uses the same laser gain medium as the seed laser itself. To create the required inversion the gain medium is often pumped transversely by a pump laser. If the necessity for higher amplification arises, multiple-stage amplifier systems, where the oscillator pulses pass the laser medium several times, have to be considered. Another very sophisticated method is regenerative amplification. Thereby an electro-optic shutter (Pockels cell) has to be implemented in the beam path. By activing this shutter single pulses are launched into the cavity. After several roundtrips, when the pulse is sufficiently amplified, the shutter is operated again and the pulse is coupled out.
Before the ultra-short laser pulses pass the active medium they are commonly stretched to reduce their peak intensity. Stretching is done via induction of a chirp therefore referring to chirped pulse amplification (CPA). After the amplification the intensified pulses are compressed again by means of prisms or parallel gratings. Fig. 8 depicts this process.

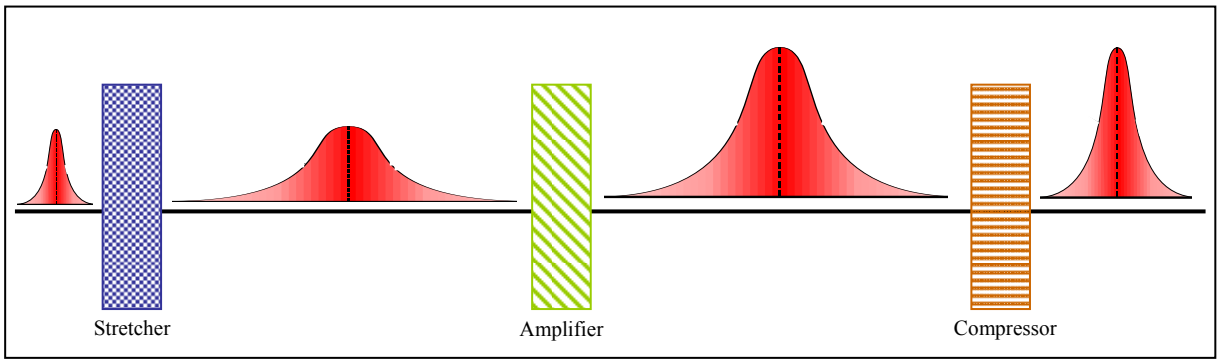

Fig. 8: Processes involved in chirped pulse amplification.

Seed lasers for fs pulse generation typically have PRRs of about 100 MHz and mean output powers of several mW up to hundreds of mW with pulse energies between tens of pJ to nJ. By amplification of these pulses energy gain factors of 10 to 10^{10} can be achieved. The PRRs of amplifiers range from 0.1 Hz up to several MHz. The average output power of amplification systems is again in the hundred mW range as evident for oscillators.

2.2 FUNDAMENTALS OF TISSUE SAMPLES

2.2.1 DENTAL ANATOMY

The main constituents of the tooth are enamel, dentine and the pulp. The dental pulp, building the core of the tooth, is surrounded by dentine. Coronary, i.e. located in the region of the crown, dentine is coated by enamel, while cementum covers dentine along the root. The tooth is embedded in the jaw bone, the mandible. Fig. 9 provides a cross-section through an incisor.

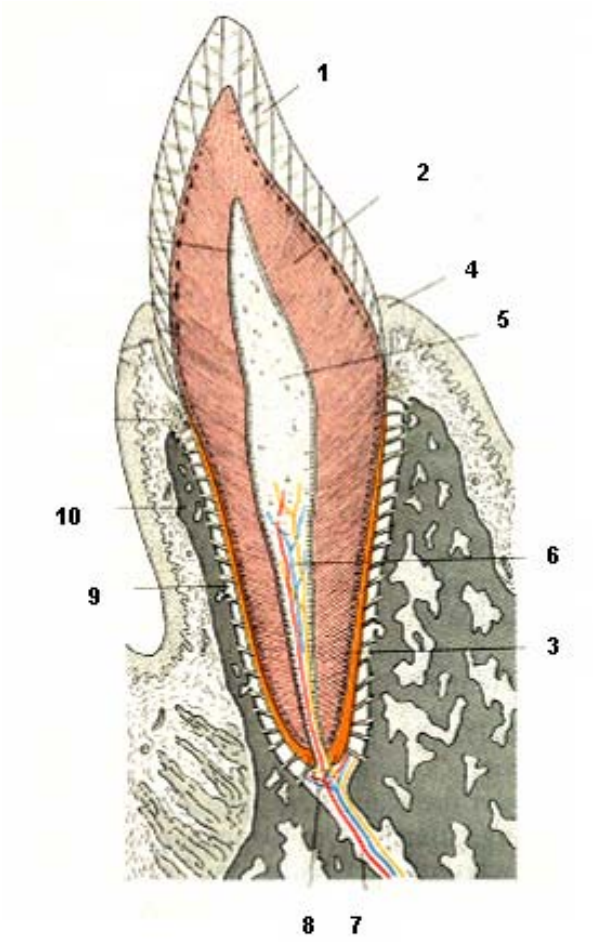

Fig. 9: Anatomy of the human tooth: (1) enamel, (2) dentine, (3) cementum, (4) gingiva, (5-7) pulp, (8) root channel, (9) periodontium, (10) mandible. (Frick, 1992)

Enamel is composed of about 95 % (by weight) of hydroxyapatite, 4 % free water and 1 % organic matter like proteins. Hydroxyapatite, with the chemical formula $Ca_{10}(PO_4)_6(OH)_2$, is a mineralized compound. Its substructure, which consists of tiny crystallites, forms hydroxyapatite prisms that assemble throughout the enamel. Considering that 20000-30000 prisms per mm² are arranged, these prisms are quite narrowly spaced. The diameter of enamel prisms ranges from 4 µm to 6 µm, their maximum length is about 2500 µm. Due to the high anorganic fraction and the low water content enamel is the hardest substance of the body exceeding even the mechanical hardness of dentine and bone. Indeed, it has to stand extreme loads caused during the chewing process and withstand chemical decomposition induced by nutrition constituents.

Dentine has a lower mineralization degree than enamel. It is made up of 70 % (per weight) hydroxyapatite present as amorphous structure, 20 % organic matrix and about 10 % water. The organic matrix mainly consists of collagen fibres providing certain elasticity. The micro-structure of dentine is characterised by small tubuli, which are essential for the growth. Their diameters range from 100 nm down to 3 µm and their maximum length is about 5000 µm. Per mm² 12700-68000 tubuli can be found. Dental tubuli located at the periphery of the pulp contain odontoblasts, i.e. dentine generating cells. They are nourished by the pulp and are able

to produce peritubular dentine throughout the whole life of the tooth. Thereby, the important function of defending dentine and the pulp against pathological processes like caries formation is fulfilled.
The pulp is a soft tissue that mainly consists of blood vessels, nerves and different types of cells, among them odontoblasts and fibroblasts. The latter are connective tissue cells producing collagen proteins thereby contributing to the stability of the tooth, but like odontoblasts they also contribute to regulation mechanisms. The pulp is very sensitive to temperature. Increases of up to 5 °C above body temperature are tolerated, i.e. that no damages are introduced or pain is caused. Temperatures between 43 °C and 46 °C applied for a maximum of 10 minutes already lead to reversible damages. Reaching 46 °C and more the pulp gets irreversibly damaged as the native protein structure cannot be repaired anymore. The pulp is connected to peripheral blood vessels via the root canal. The tooth itself is embedded in gingiva sealing the transition towards the jaw bone and preventing the tooth from bacteria attack. Additionally, it is sheathed by the periodontium and anchored in the mandible. (Niemz, 1996), (Glock, 2000), (Bäcker, 2004)
Caries formation is the most frequent pathological process affecting the tooth. Insufficient oral hygiene and wrong nutrition are the main initiators. Decay of dental hard tissue is caused by metabolic products of bacteria forming a plaque layer on the tooth surface. The micro-organisms generate lactic and acetic acid, which results in a reduction of the pH value. The crystal lattice of hydroxyapatite is decomposed and calcium is washed out by saliva. Hence, the demineralization process turns the hard enamel into a porous and permeable structure, appearing as dark coloured spots and areas. In an advanced stage, dentine can be demineralised and furthermore the pulp can be infected by the micro-organisms causing inflammation and sometimes enormous pain.

2.2.2 BONE ANATOMY[1]

Vital bone plays an important role inside the body as it provides a support as well as protection of inner organs. It acts as storage facility for calcium and phosphorus and as repository for haemopoietic tissue, i.e. the blood forming marrow. Bone is a living tissue that is constantly busy with renewing and remodelling processes adapting to the physical demands of the human being or the mammal in general. Different bone tissue types can be distinguished: Compacta or cortical bone, spongiosa, also called cancellous or trabecular bone, and cartilage. Compacta and spongiosa are mineralized connective tissues; cartilage is less mineralized supporting tissue. About 80 % of skeletal weight is represented by compacta, the hardest among the mentioned bone matters. Compacta is a macroscopically dense bulk material without visible gaps. Spongiosa reveals a spongy or honeycomb-type structure. A meshwork of fine ramified trabeculae with its marrow filled intra-trabecular space is characteristic for this tissue. The transition from compacta to the inner lying spongiosa is fluent. The outer bone shell is commonly covered by periost, which is tight connective tissue, endost is attached inside. Most bones are built up like that, enclosing spongiosa in a compacta surrounding. Just in very long bones like femur or humerus spongiosa is replaced by marrow. Fig. 10 provides a visual impression of the bone architecture. Furthermore, a sketch outlines the main elements of bone.
Compact bone typically consists of 3-7 µm thick lamellae, which are layers made of collagen fibrils. Depending on their location, different types of lamellae can be identified. Lamellae are, for example, part of so-called osteons. This is a complex of a central Havesian canal surrounded by 4-20 concentrically arranged lamellae. The central canal embraces blood vessels and nerves among other tissues. Besides that, lamellae fill also the spaces between

[1] Chapter 2.2.2 is mainly based on references (Rumpf, 2001), (Kuhne, 1998) and (Afilal, 2004).

osteons. But even there, where osteons are missing like in spongiosa parts of lamellae are present. Finally, the outer and inner surfaces of bone are coated by several lamellae. The outer ones, located below the periost, are connected, while the ones close to spongiosa are often disrupted. As mentioned before periost builds the outermost layer of bone. It is extended over the whole surface and leads into cartilage at the joints and into tendons and ligaments.
Considering their micro-anatomical structure, three different bone cells are responsible for formation and remodelling mechanisms of bone tissue: Osteoblasts, osteocytes and osteoclasts. Osteoblasts are involved in bone formation by producing collagen and extracellular matrix, so called osteoids, which build the basic organic substance. By the release of enzymes these cells mineralise and remain embedded in their extracellular matrix. Thereby they become osteocytes. Osteocytes are placed in lacunae, which are small holes that are located throughout the mineral phase of the bone substance. Via cell-appendices they are connected among each other and coupled to osteoblasts. That way, bone metabolism and mineral balance are regulated. Osteoclasts are large, mobile and strongly polar cells, with up to 50 cell nuclei. They are engaged in bone resorption processes, where special enzymes dissolve hydroxyapatite leading to decomposition of bone cells.

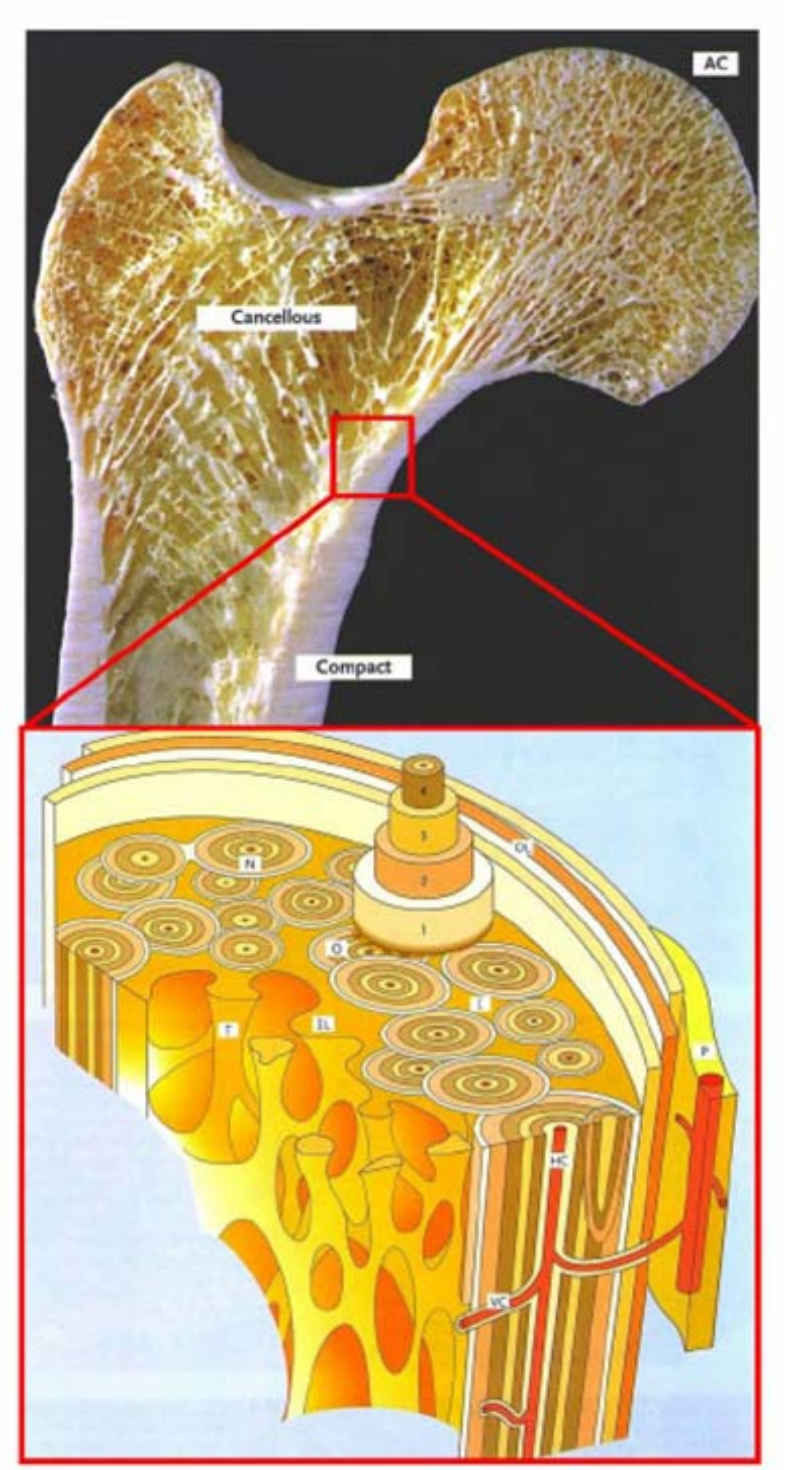

Fig. 10: Section through dried femur showing its internal architecture. Spongiosa with its trabecuar meshwork can be distinguished from compact bone tissue. The schematic magnification depicts the main structures of bone tissue: (O) osteons, (N) newer osteons, (I) interstitial lamellae, (P) periosteum, (HC) Harvesian canals, (VC) Volkmann's canals, (T) trabeculae, (1, 2, 3, 4) concentric lamellae in each osteon. (Rumpf, 2001)

2.2.2.1 PHYSICAL PROPERTIES OF BONE TISSUE[2]

Obviously, the chemical composition of bone tissue is strongly related to its physical properties. It is composed of 50-60 % hydroxyapatite, 15-20 % water, 20 % organic matter, 5 % carbonates, 1 % phosphates and 1-2 % proteins. (Niemz, 1996) Cartilage possesses a much higher water content of 55-58 %. While the amount of hydroxyapatite influences mechanical properties of the tissue, the water fraction determines its thermal characteristics. Anyway, bone is an anisotropic substance, so that mechanical properties vary with location and direction. That means that not just the mineral content is solely responsible for mechanical properties but also the collagen fibrils and the histological structure of the tissue, i.e. percentage of osteons. For example, the mineral content suspends pressure and the collagens absorb tension. Elasticity emerges also from the interaction between the mentioned tissue components. It varies between 12 and 23.1 GPa. For comparison, elasticity of steel is 207 GPa and that of india rubber is 0.001 GPa. Bone can stand stretching of up to 2 %, above that larger fractures are caused.

Concerning thermal properties of bone tissue, heat conductivity and specific heat are of special importance when laser treatment is performed. Heat conductivity is a measure to describe a material's ability to release heat in its surrounding, whereas the specific heat reflects the potential to store and accumulate heat. During laser irradiation a certain fraction of light is always transformed into heat. Especially for longer pulse durations this effect appears on a larger scale. Anyhow, heat diffusion out of the volume absorbing laser radiation is an unwanted process, as thermal damages to the adjacent tissue might be induced. Heat conductivity $\bar{\lambda}$ of bone can be calculated according to the following equation

$$\bar{\lambda} = 0.006 + 0.57\frac{w_{H_2O}}{\rho} \qquad [\mathrm{W/m \cdot K}] \tag{11}$$

where ρ is the density of the tissue given in kg/m³ and w_{H2O} is the water content also expressed in kg/m³. For the specific heat $\bar{c}$ a similar equation, employing the same variables, can be stated

$$\bar{c} = 1.55 + 2.8\frac{w_{H_2O}}{\rho} \qquad [\mathrm{J/gK}] \tag{12}$$

The connection between those parameters is given by the temperature conductivity

$$\kappa = \frac{\bar{\lambda}}{\rho \cdot \bar{c}} \qquad [\mathrm{m^2/s}] \tag{13}$$

which is about $1.2 \cdot 10^{-7}$ m²/s for most tissues. The dynamic of heat distribution inside the irradiated tissue is characterised by the thermal relaxation time

$$\tau = \frac{d^2}{4 \cdot \kappa} \qquad [\mathrm{s}] \tag{14}$$

where d represents the optical penetration depth, which is the reciprocal of the absorption coefficient α. The last equation comprises all these parameters

[2] Chapter 2.2.2.1 is mainly based on references (Rumpf, 2001), (Kuhne, 1998) and (Afilal, 2004)

$$\tau = \frac{1}{4 \cdot \alpha \cdot \kappa} = \frac{\overline{\lambda}}{4 \cdot \alpha \cdot \kappa \cdot \overline{c}} \tag{15}$$

These equations are taken from (Afilal, 2004) pages 17-19. In Table 1 heat conductivity and specific heat of bone and cartilage among other materials are listed. Table 2 contains absorption coefficients of the main tissue components of bone as well as of enamel and muscle. As they were obtained for the Er:YAG laser wavelength of 2.94 µm they are of relevance within this thesis.

Table 1: Heat conductivity and specific heat of different materials. (Rumpf, 2001), (Afilal, 2004)

Material	Heat Conductivity [W/m·K]	Specific Heat [J/gK]
Bone	0.2 – 0.4	1.2 – 2.4
Cartilage	0.6	3.5 – 3.8
Tooth	0.65	1.17
Fatty tissue	~0.3	1.93
Water	~0.58	4.183
Blood	0.62	3.22
Steel	46.02	0.477

Table 2: Absorption coefficients of single tissue components, enamel and muscle for the Er:YAG laser wavelength of 2.94 µm. (Afilal, 2004)

Material	Absorption Coefficient [cm^{-1}]
Compacta	3800
Spongiosa	5900
Hydroxyapatite	648
Water	12000
Collagen	1330
Dentine [3]	4640
Enamel [3]	2170
Muscle	1

2.3 DENTAL RESTORATIVE MATERIALS[4]

Aesthetic dental restorative materials are made of composites. Initially, the material is pasty to allow cavity preparations including plastic shaping. After the restoration, chemical or physical hardening techniques, depending on the specific composite, have to be applied. Thereby a stable polymer network is built. As their name "composites" suggests, they are composed of several chemical substances that determine their characteristics. In the following a brief overview is provided.

[3] From (Mitra, 2002) p. 78.

[4] References (Ivoclar Vivadent, 1990), (Ivoclar Vivadent 1992), (Ernst), (Lonnroth, 1997), (Schärer, 1998) (Kultermann, 2001) and (Ivoclar Vivadent, 2004) were used to write chapter 2.3.

2.3.1 COMPOSITION OF COMPOSITES

The main constituents of composites can be arranged in three groups:

1. organic composite matrix
2. dispersive phase
3. compound phase

The first group contains monomers, co-monomers, initiators, stabiliser and other additives. The dispersive phase comprises the anorganic filler particles. The compound phase is made of silanes that act as intermediators between the fist mentioned phases.

2.3.1.1 ORGANIC COMPOSITE MATRIX

Monomers commonly used are multifunctional methacrylates like Bis-GMA[5], Bis-EDMA[6], UDMA[7] and TEDMA[8] as they fulfil the required demands. The have to

- be toxicologically harmless and biocompatible
- have good physical properties
- be chemically stable
- resist discolorations
- be very reactive
- be stable during storage
- show remote polymerisation-shrinkage.

After radical activation the polymerisation process starts building the bulk material. Monomers are responsible for chemical properties of the composite like polymerisation rate, polymerisation shrinkage, water absorption and viscosity.
Because of the fact that the used monomers are rather large in molecular size, their viscosity is accordingly high and the filler cannot be merged in the needed extent. The processing is also negatively affected. Therefore matrix diluters, the so called co-monomers, which are partly integrated in polymers, are added. Co-monomers decrease the rest-monomer concentration and increase cross-linking considerably. Indeed, due to their minor molecule size stronger polymerisation shrinkage as well as increased water absorption have to be mentioned.
Initiators are matrix components, which decay into radicals and therefore start and maintain the polymerisation reaction. A series of requirements have to be met. They have to

- decay rapidly at low room temperature
- create highly reactive radicals
- be unaffected by storage
- cause no colourations
- be non-toxic
- be colourless
- be scentless.

[5] Bisphenol-A-diglycidyl-methacrylate
[6] Ethoxylated bisphenol-A-dimethacrylate
[7] Urethan-dimethacrylate
[8] Triethyleneglycol-dimethacrylate

Two different activation mechanisms can be distinguished, chemically and physically activated systems. Chemically activated systems are so called Redox systems. The initiator is organic peroxide and a tertiary amine acts as co-initiator. In the case of two-component composites by mixing of two pastes containing the initiator (catalyst) and the co-initiator (base), radicals are generated and the polymerisation gets induced. This reaction mechanism is the basis for cold curing systems. Physically activated systems employ a photo-initiator for light-curing purposes. Benzoinmethylether is the photo-initiator in UV-light activated systems, which nowadays are scarcely used. They got redeemed by cold/blue-light systems, which employ campherchinon. The reaction mechanism involves an H-abstraction. Co-initiators are tertiary amines, which act as H-donators. For light-activated systems also exposure time and light intensity as well as colour and transparency of the composite play an important role. Hot curing is another physical activation process. The basic principle for hot curing is the decay of the initiators into radicals at high temperatures. Such initiators are mostly peroxides. Hot curing is solely applied for composite inlays.
The break-up reaction occurs due to erasure of radicals by combination of two radical endings, by disproportion of elements or by getting together an initiator radical and a macro-radical. Macro-radicals are generated during the growth process and allow molecules to link to each other.
Other components of the organic matrix are inhibitors. Their task is to slow down the hardening process after mixing the components together. They intercept the generated radicals and decelerate so the polymerisation process. This effect guarantees also enough processing time to establish the restoration. Additionally, inhibitors increase the durability of single components. Therefore, adequate inhibitors are added to light activated systems to avoid the reduction of durability caused by daylight and artificial light.
Other ingredients are photo-stabilisers and pigments. As the UV part of the sunlight reduces rest-monomers in the cured composite, leading to discoloration, photo-stabilisers are added to inhibit this process. Pigments, mostly iron oxides, are added to yield a certain colour of the composite material. Optical brighteners and plasticizers are also elements of the organic matrix.

2.3.1.2 DISPERSIVE PHASE

The dispersive phase consists of fillers that make up 50 vol. % of the composite and determine the physical and mechanical properties of the composite, such as stability, shrinkage, thermal expansion and handling. To yield certain x-ray opacities, fillers get provided with elements or compounds of higher atomic number such as Barium, Strontium, Yttrium or Ytterbium. Fillers have to fulfil certain criteria. The have to

- be colourless
- be water- and chemicals-resistant
- have a refractive index between 1.45 and 1.55
- be non-toxic
- be very hard
- strengthen the surrounding polymer.

Only glasses or glass-ceramics, some silicates and silicon-dioxide show these characteristics. Fillers mainly made of ceramic, glass or quartz can be divided into four groups: macro-filler, micro-filler, micro-filler complexes and hybrids. Each of them is characterised briefly in the following.

MACRO-FILLERS

The average particle sizes range from 0.5 to 5 µm (total particle size 0.1-100 µm). The high filling degree causes only remote shrinkage and a low expansion coefficient. To achieve better polishing conditions and a higher abrasion resistance smaller and rounded macro-fillers are used. Nevertheless, macro-filled composites have a rather rough surface compared to micro-filled composites. This enhances abrasion and plaque retention. Today macro-filler composites are scarcely used.

MICRO-FILLERS

The micro-dispersive pearls have a particle size distribution of 0.005-0.8 µm with an average particle size of 0.04-0.15 µm. They show outstanding aesthetic features, good polishing conditions, and low abrasion. Unfortunately, their low fraction of fillers (50 % per weight) leads to reduced mechanical stability and large polymerisation shrinkage.

MICRO-FILLER COMPLEXES

To compensate the drawbacks mentioned within micro-fillers and to control the consistency of composites pre-polymers are added to micro-filled composites. Two types of pre-polymers are commonly used: splinter-shaped, pre-polymerized micro-fillers, with a particle size between 1 and 200 µm and ball-shaped, pre-polymerised, micro-filled complexes. Their particle size ranges from 10 to 30 µm.

HYBRID COMPOSITES

Hybrid composites contain a combination of macro- and micro-fillers. Due to the different grain sizes, from 0.01 up to 30 µm, the highest filling degree (80 vol.%) can be achieved, because the interspaces between the coarse grained particles can be filled by the fine grained ones.

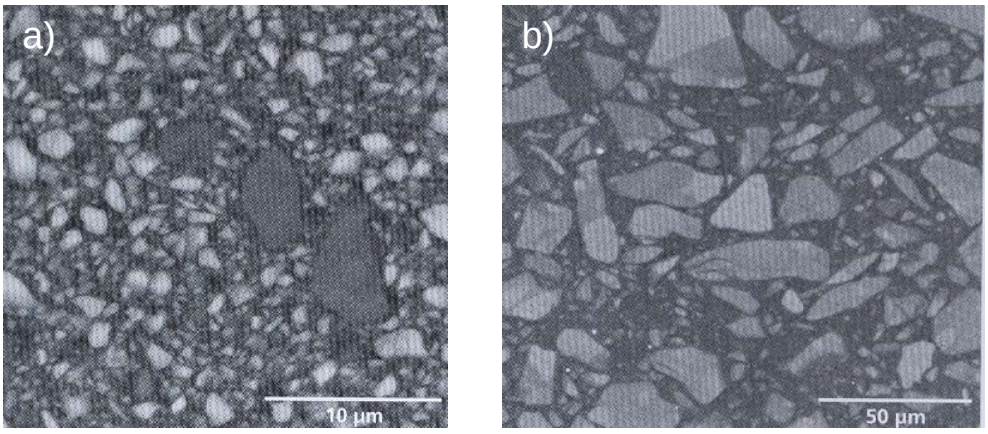

Fig. 11: SEM of the polished surfaces of a hybrid composite a) and a micro-filler complex b). (From (Ivoclar Vivadent, 2004) p. 27.)

2.3.1.3 COMPOUND PHASE

To couple the anorganic fillers to the organic matrix an inter-mediator has to be applied. Such inter-mediators are silanes. Their silicon contingent reacts with fillers via H-bridge formation and its methacrylacid rest merges with the matrix.

2.3.1.4 Effects of Different Composite Components

The combination of fillers and monomers controls physical properties like bending strength, compression strength and hardness. A higher filling degree enhances hardness and compression strength and reduces water absorption by the material. Hardness and water absorption are also influenced by the polymerisation rate, which depends on type and amount of monomer and initiator. A higher polymerisation rate improves many composite properties; among them are also colour stability and shrinkage. Reduction of polymerisation shrinkage is a very crucial aspect. The tensions that appear during the polymerisation process may cause gaps between the filling material and the cavity wall and lead to problems like secondary caries. The reason for polymerisation-shrinkage can be found in the distance of the C=C double bond between the monomer molecules, which is larger after polymerisation. Low-molecular monomers like methylmethacrylate show higher shrinkage due to the high double bond amount per defined volume than highly molecular compounds like the frequently used Bis-GMA. Polymerisation shrinkage can be reduced by higher filler- and lower monomer content, respectively. Additionally, correct handling and processing of the complete adhesive system eliminates the above mentioned problem.
The ways the different constituents work together are very manifold. The following figure demonstrates which components influence important composite characteristics.

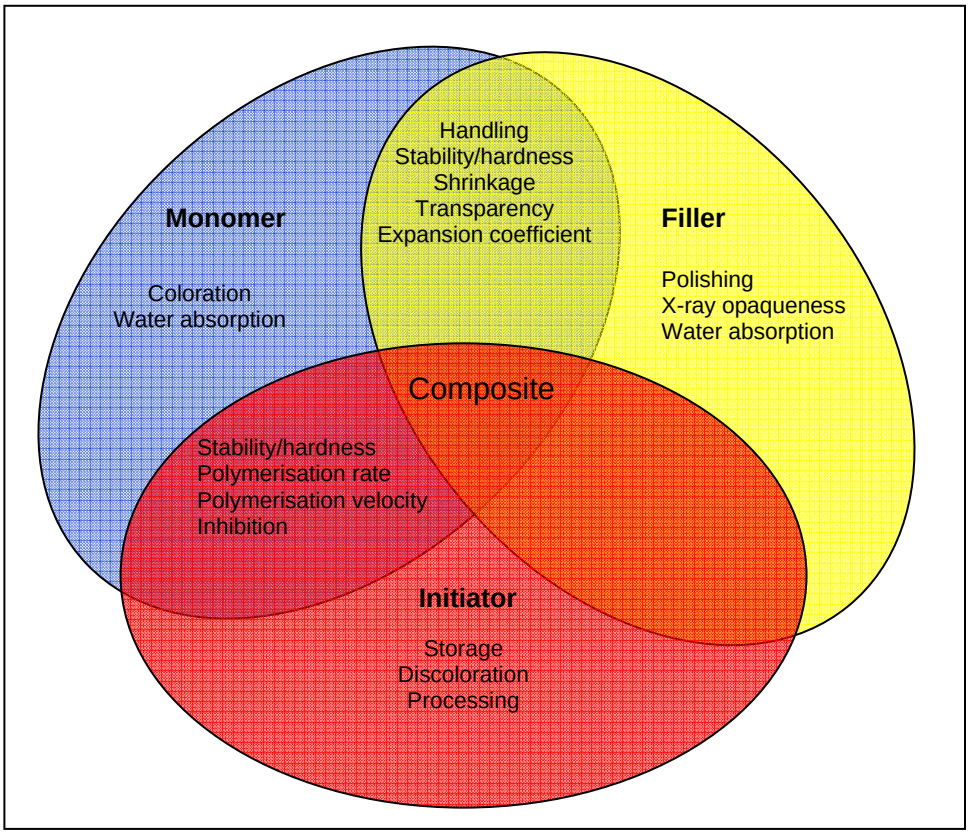

Fig. 12: Interactions of the single components of a composite[9].

2.3.2 Adhesive Agents

Composites cannot be applied directly onto the tooth surface. Several steps involving conditioning, priming and bonding are necessary to yield good interconnection. The following paragraphs describe the single components of the filling procedure.

[9] Graphic established on basis of (Ivoclar Vivadent, 1990), p. 15, Fig. 22.

2.3.2.1 CONDITIONER/ETCHANT

The smear layer is considered as a minor compact and stable layer that does not yield enough adhesion to the underlying tooth structure as well as to the adhesive above. For good adhesion the dissection of collagen fibrils by demineralisation is necessary, so that they can be linked to the synthetic. The removal of the smear layer gets accomplished by conditioners such as citric acid, phosphoric acid, poly-acrylic acid and others. Two distinct etching techniques are common: selective etching technique, where enamel etching and subsequent dentine etching with another acid is performed, and total etching technique where enamel and dentine get etched in a single operation with the same acid. The treatment of dentine is more elaborate. The smear layer caused by mechanical cavity preparation consists of polished dental hard tissue, collagen remnants, hydroxyapatite crystals, tubular liquid and water. This layer is too compact to be removed by water irrigation and therefore acid-etching has to be performed. Acid-etching removes the smear layer including the smear plugs, which seal the entrances of the dental tubules. By that the diffusivity of the prepared surface is warranted. But also the exposure of collagen fibrils is achieved. This is necessary as they have to establish a compact binding on molecular level (molecular entanglement) with the monomers of the adhesive.

2.3.2.2 PRIMER

The principle duty of a primer is to improve the compatibility of the hydrophilic dentine surface and the hydrophobic composite. The primer mostly is a solution of different substances using a hydrophilic solvent. This solvent allows the hydrophilic monomer, the basic module of the primer, to penetrate as deep as possible into the demineralised inter- and peritubular dentine and into the exposed collagen meshwork. Simultaneously, the water contained in the tubules gets expelled. The hydrophilic monomer is an agent between the hydrophilic humid dentine surface and the monomers of the adhesive. Good compatibility of primer and humidity is essential for two reasons: to work under dry conditions in the humid oral cavity is problematic and humidity saves the exposed collagen fibrils from collapsing. Collapsing collagen fibrils would lead to decreased adhesion.
Self-conditioning and self-etching primer respectively take an exceptional position. They are a combination of conditioning substances like acids and acid monomers for example and classical primer substances. They have been developed to simplify the processing procedure and to avoid mistakes.

2.3.2.3 BONDING

After dentine conditioning and application of the primer, an unfilled or in some cases micro-filled synthetic, the so-called bonding, that also contains initiator systems for self- or light-curing purposes is applied and polymerised. This is the agent between the pre-treated dentine and the infiltrated monomers, respectively, and the composite monomers. Combinations of primer and bonding have also been developed.

2.3.3 PROCESSING

The single steps of processing shall be outlined:

1. etching
2. rinsing and drying
3. application of the primer, short dwelling and subsequent drying
4. application of the bonding including light curing
5. application of the composite as restoration
6. light curing

2.3.4 ADHESIVE INTERCONNECTION

After the smear layer removal primer and bonding are applied and the composite is inserted. Thereby a hybrid layer can be observed, which consists of polymerised methacrylate from composite and dentine. This hybrid layer is generated because monomers penetrate into the uppermost dentine layer. Subsequent polymerisation creates the interpenetrating network. Additionally, monomers of the bonding penetrate into the open dental tubules and into their anabranches and form retentive bonding tags after polymerisation. Both hybrid layer and tags are responsible for the micro-mechanical adhesion.

2.4 LASER-TISSUE-INTERACTION[10]

2.4.1 WATER-MEDIATED ABLATION

Erbium laser ablation is associated with thermal laser-tissue interaction. The water molecules incorporated in biological hard tissue possess a pronounced absorption peak around the Infrared wavelength of 3 µm. At room temperature this maximum coincides with the Er:YAG laser wavelength of 2.94 µm, for rising temperatures this peak is shifted to somewhat lower wavelengths and its amplitude is reduced. The water absorption coefficient of $\lambda = 2.94$ µm at room temperature is $\mu_a = 13000\ cm^{-1}$, the one of $\lambda = 2.78$ µm, the Er,Cr:YSGG laser wavelength, is just $\mu_a = 7000\ cm^{-1}$(Stock, 1997). For temperatures where laser ablation is performed, wavelengths of 2.94 µm and 2.78 µm are absorbed with almost similar efficiency.

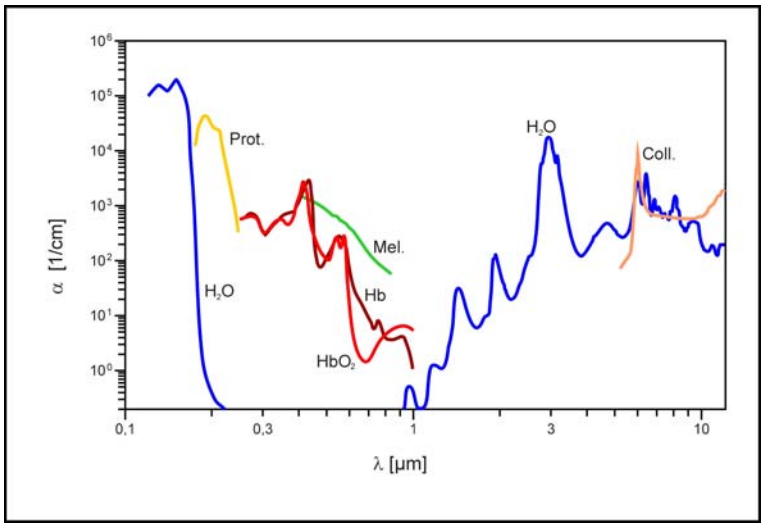

Fig. 13: Absorption coefficient of several types of tissue recorded at room temperature. (Vogel, 2003) (Prot. = protein, Mel. = melanin, Coll. = collagen., Hb = deoxygenated haemoglobin, HbO_2 = oxygenated haemoglobin)[11]

[10] Chapter 2.4 refers to (Wintner, 2000), (Bäcker, 2004) and (Moritz, 2006).
[11] Diagram provided by M. Strassl.

The laser light is absorbed by the H_2O molecule thereby altering its rotational and vibrational states. The energy increase leads to changes in length and eigenfrequencies of the OH-bonds. After a certain lifetime the excited molecule gets back to its ground state and the absorbed energy is set free again. The energy released due to non-radiative decay is converted into heat, which finally initiates ablation. In Fig. 14 a)-e) the different steps of water-mediated ablation are outlined. When the laser beam gets focused on the surface the water embedded in the tissue absorbs the energy contained in the laser pulses (Fig. 14a). The water gets heated up and expands (Fig. 14b). As a consequence micro-cracks are induced (Fig. 14c) and micro-explosions occur which throw the tissue particles out (Fig. 14d). A cavity with a quite rough surface is remaining (Fig. 14e).

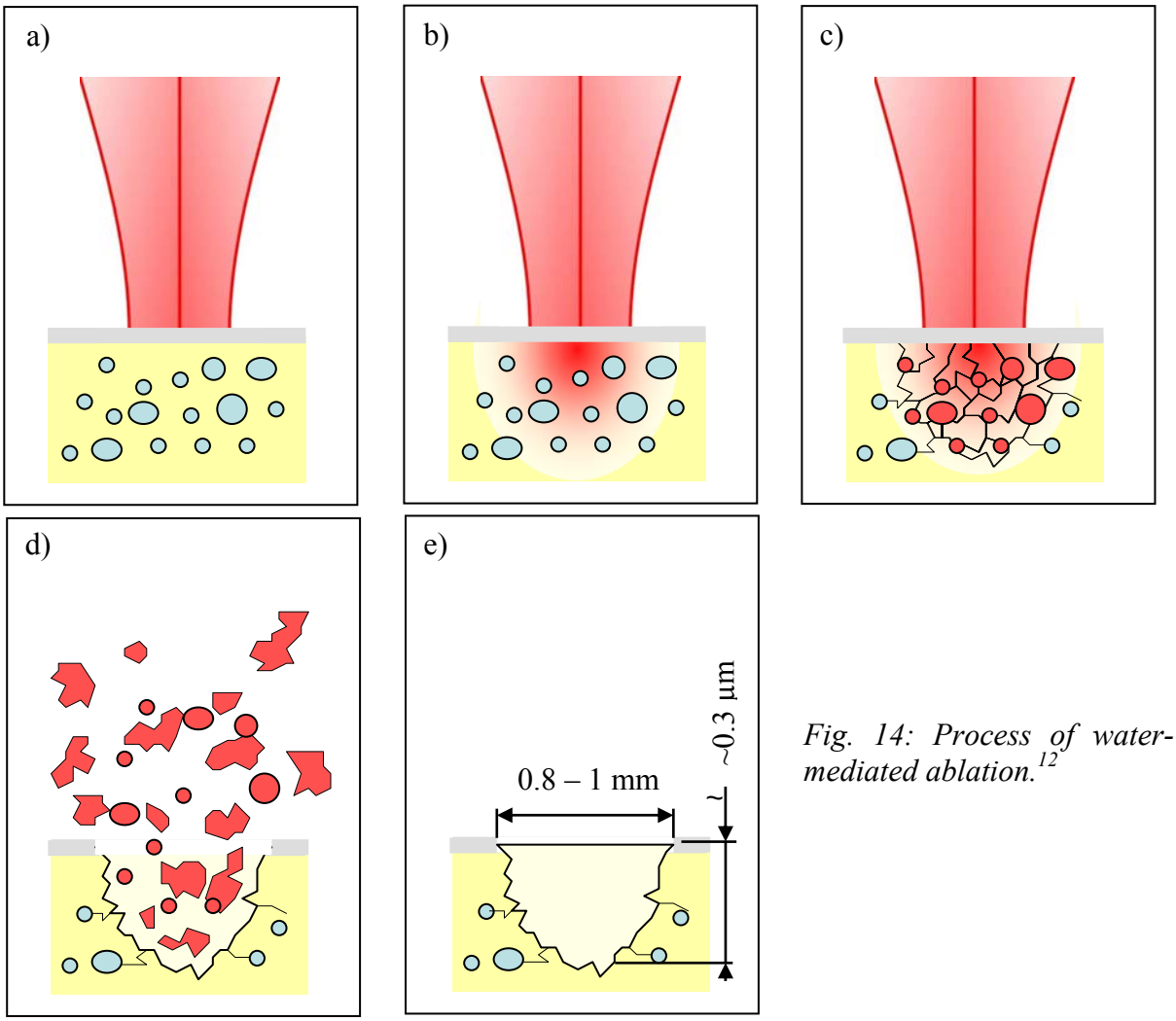

Fig. 14: Process of water-mediated ablation.[12]

Crucial factors for efficient ablation are pulse duration and pulse shape of the incident laser pulses. The leading pulse edge is the trigger for ablation. A steep rising edge of the pulse and a fast rise time are necessary for rapid vaporization of water. Under these conditions, the energy is coupled into the tissue very effectively so that the penetration depth of the incident radiation is also kept low. The contribution of the trailing pulse edge to enhance the ablation depth is modest. The energy stored in the trailing edge penetrates the tissue in form of heat bearing the potential to injure adjacent tissue layers. Therefore, a rapid decay of the pulse after the maximum is reached is beneficial. Not just the temporal pulse profile but also the spatial profile influences ablation. Especially when very sensitive tissue has to be processed

[12] Provided by M. Strassl.

minimal invasively, like dentine around the pulp, laser parameters near the ablation threshold have to be chosen. To reach the ablation threshold at low energies a Gaussian profile corresponding to the TEM_{00}-mode is favourable. (Temporal and spatial profiles of the Erbium systems involved in this study are discussed in more detail in chapters 3.1.1 and 3.1.2.)
A last remark on water-mediated ablation has to be made. The water fraction of the tissue and its distribution affect the ablation efficiency, i.e. a lower percentage of water corresponds to less effective ablation. This is the reason why enamel with a water fraction of about 12 vol. % reveals higher ablation thresholds and lower ablation rates compared to dentine with 24 vol. %. During laser treatment the tissue is additionally dehydrated to some extent. To avoid reduced ablation efficiency a water-spray has to be applied. Besides re-hydration, an increase of the absorption of the laser beam is achieved. Additionally, the water-spray acts as coolant and prevents from irreversible damages if used appropriately.

2.4.2 PLASMA-MEDIATED ABLATION

The shorter the pulse durations for given pulse energies, the higher become the pulse peak powers as well as the related power densities. Combining these high power densities with sufficient focusing, power densities up to several TW/cm² can be achieved at the tissue surface. The strong electric field in the area of the focal spot initiates non-linear processes leading to plasma formation. Plasma creation is started by multi-photon absorption (MPA): The irradiation intensity is that high that valence electrons are enabled to absorb multiple photons. The energy gained by MPA is enough to overcome the band gap energy and the electrons leave the atom generating the plasma. By absorption of energy form the incident radiation the free electrons are further accelerated. In the plasma the high-energetic free electrons collide with other atoms. Thereby a part of their energy is transferred and additional electrons are set free. This avalanche process is called impact ionization (IMI). The increase of the carrier density is driven by MPA being the prevailing process during the leading pulse edge. The trailing pulse edge is dominated by the IMI. Fig. 15 demonstrates this behaviour.

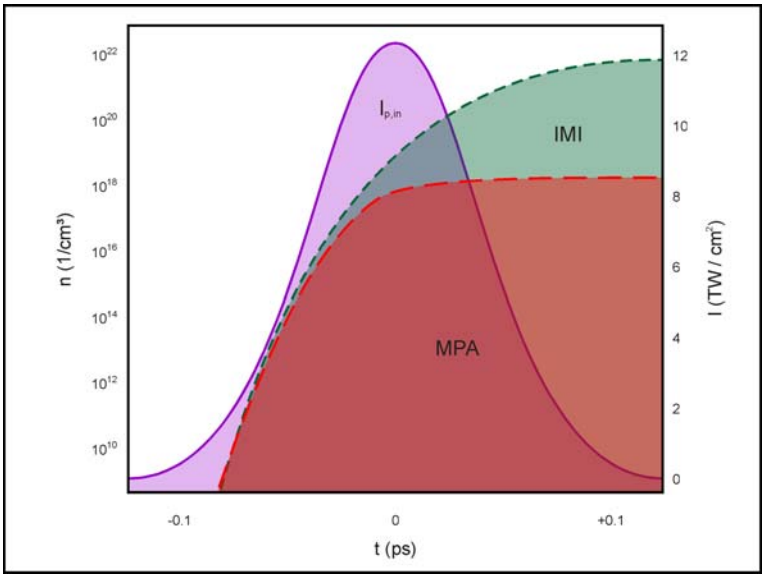

Fig. 15: Plasma generation correlated to the temporal pulse profile: During the leading pulse edge electrons as predominantly created by multi-photon absorption (MPA). After the pulse peak the electron density is mainly increased by impact ionisation (IMI).[13]

[13] Provided by M. Strassl.

Free electrons absorb a considerable percentage of the incident light, so that the plasma is heated rapidly. Additionally, the plasma gets highly reflective as soon as a critical electron density n_c is reached. The reflectivity of the plasma, known as shielding effect, is of great importance for the temperature development inside the tissue. The trailing pulse edge, that contains energy which is not needed for plasma formation, is shielded by the reflectivity of the plasma. The underlying tissue is thereby prevented from excessive heat transfer. The effect of plasma reflection is shown in Fig. 16.
The ablation threshold is defined as the fluence or energy density expressed in J/cm², that is needed to create the critical electron density n_c within the pulse duration. By reaching n_c, which is in the order of 10^{19} to 10^{21} per cm^3 [14], the binding energy of the matter is overcome leading to vaporization (Rubenchik, 1999). For fs pulses MPA suffices to generate n_c, while for longer pulse duration both processes, MPA and IMI, are involved. The shielding effect just works, when the ablation threshold is surpassed and the critical electron density is exceeded, $n > n_c$. If $n < n_c$, the pulse passes the plasma layer and penetrates the underlying tissue layers. The energy transferred to the matter is transformed into heat. The heat distributed over a larger volume is insufficient to evaporate the matter completely. Thus, material expulsion accompanied by collateral damages occurs.

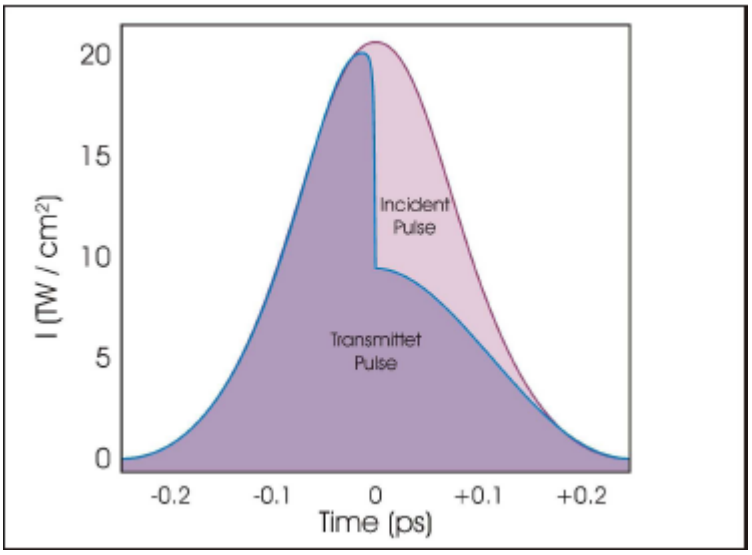

Fig. 16: Due to the shielding effect only part of the incident pulse energy is transmitted to the matter. [15]

Exploiting the shielding effect, nearly the whole energy transferred during the ablation process is deposited in a thin layer of about 1 µm thickness. When the plasma gets expelled due to thermodynamic laws almost all energy confined in this layer gets removed again. The ablation itself takes place after the pulse has terminated (Neev, 1996), (Salle, 1999). The deposited energy determines the thickness of the ablated layer and the expulsion velocity. As the reflectivity of the plasma has to be considered, an increase in pulse energy does not lead to a linear increase of penetration depth. Ablation depths per pulse are typically around 1 µm. The expulsion occurs within a few ns (London, 1999).
The whole process is summarized and schematically outlined in Fig. 17: The USPL beam is strongly focused onto the tissue surface (a). Free electrons are created generating the plasma (b). Due to hydrodynamic laws the plasma expands and gets ejected (c). The remaining cavity

[14] (Bäuerle, 2000), p. 276.
[15] Provided by M. Strassl.

is much smaller compared to an Erbium laser ablated cavity, but its surface features are more favourable because of the gentler ablation mechanism (d).

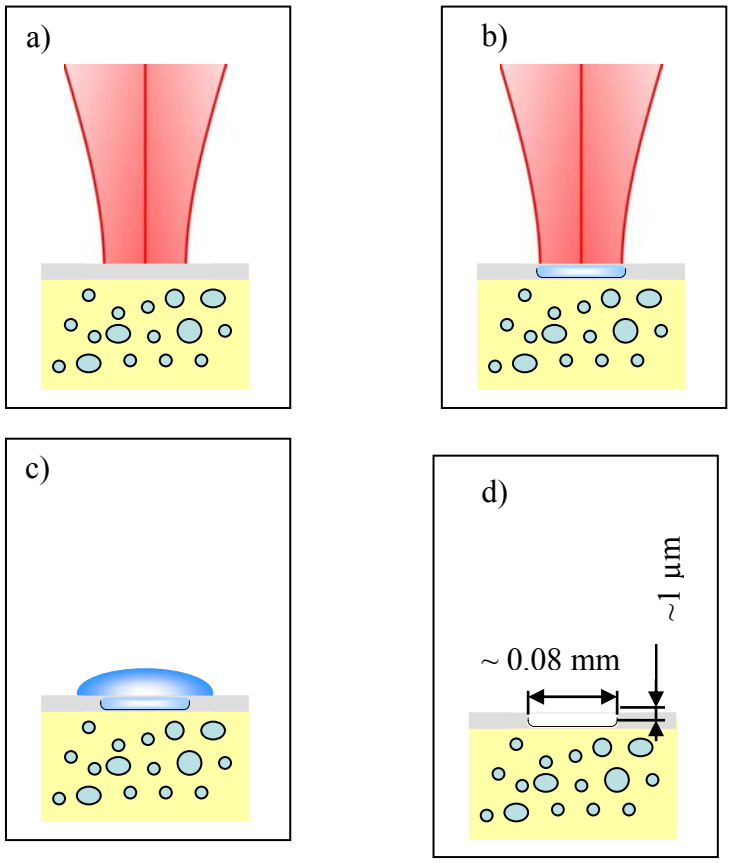

Fig. 17: Process of plasma-induced ablation.[16]

2.4.3 Ablation with Gaussian Laser Pulses

The radial fluence profile of a Gaussian beam is given by the well known equation:

$$\Phi(r) = \Phi_0 e^{-\frac{2r^2}{w_0^2}} \tag{16}$$

where $\Phi(r)$ is the fluence at the radial distance r, Φ_0 is the maximum fluence and w_0 is the radius of the beam waist. Assuming that a defined material dependent ablation threshold exists and that material perforation occurs when this threshold is exceeded equation (16) can be rearranged to

$$r_{th}^{\,2} = \frac{w_0^{\,2}}{2} \ln\left(\frac{\Phi_0}{\Phi_{th}}\right) \tag{17}$$

where r_{th} represents the radius of the ablation site at the ablation threshold Φ_{th}, which implicates that at the rims of the damage zone the threshold fluence is reached[17]. On basis of

[16] Provided by M. Strassl.

[17] Involving the concept of laser-induced optical breakdown the dependence of Φ_{th} on the critical electron density leading to material damage can be derived. The theoretical aspects of this concept are treated in (Bonse, 2001), chapter 2.

the Lambert-Beer law a logarithmic dependence on the ratio of the fluences Φ_0/Φ_{th} can also be stated for the etch depth per pulse

$$d(\Phi) = \frac{1}{\alpha_{eff}} \cdot \ln\left(\frac{\Phi_0}{\Phi_{th}}\right), \tag{18}$$

where α_{eff} is the effective absorption coefficient. The following figure demonstrates all these correlations.

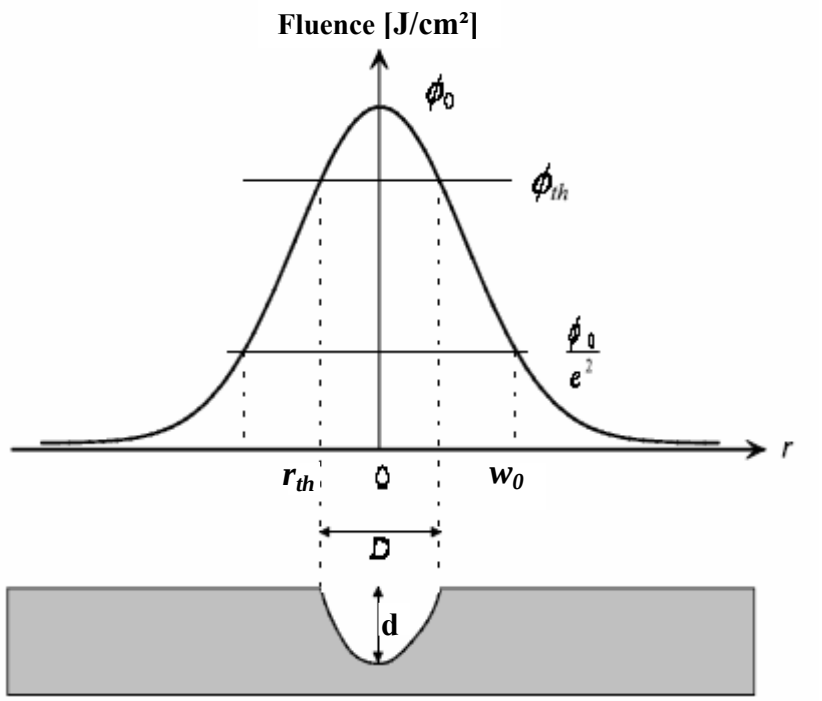

Fig. 18: Ablation with a Gaussian beam profile demonstrating the dependence of the damage radius r_{th} on the threshold fluence Φ_{th}. D is the diameter of the ablated cavity, d is the etch depth. (Figure taken from (Bonse, 2001).)

3 TECHNICAL EQUIPMENT AND SAMPLES

3.1 LASER SYSTEMS

As the main purpose of this work was to judge the suitability of innovative USPL in comparison to commercial Erbium lasers, several laser systems were involved in the conducted studies. In the following all of them are described.

3.1.1 FOTONA FIDELIS PLUS II[18]

This laser, produced by Fotona company, Ljubljana, Slovenia, incorporates two laser sources, an Er:YAG (Erbium-doped Yttrium Aluminium garnet, $Y_3Al_5O_{12}$) and a Nd:YAG (Nd = Neodymium) laser, which can alternatively be chosen depending on the intended medical treatment. The Er:YAG modus is recommended for dental hard tissue procedures while the Nd:YAG modus should be used for soft tissue preparations. According to the purpose of this research just the Er:YAG laser was used. Referring to the manufacturer the system specifications are:

Table 3: Laser characteristics of Fotona Fidelis Plus II stated by the manufacturer.

Wavelength	2940 nm
Maximum Pulse Energy	1.5 J
Maximum Pulse Width	1000 µs
Maximum Frequency	50 Hz
Maximum Power	20 W

During the experiments the pulse repetition rate was adjusted to 20 Hz to be comparable to the Biolase Waterlase, and the pulse energy, displayed on the front panel, was varied between 100 mJ and 300 mJ yielding powers from 2 W to 6 W. Ablation was performed with an air-water spray which was continuously adjustable by turning a wheel.
As all involved Erbium lasers were in use for dental applications, it was expected that the output parameters resemble their front panel setting because of the duty of frequent maintenance. Nevertheless, Strassl et al. (2000) already have shown that average output power and pulse energy values differ from their pre-setting. Erbium laser crystals are pumped by a flash lamp. The reasons for the deviations are discharge fluctuations of the pumping source. Hence, laser parameters were measured using a pyro-electric head (Ophir Laser Star with head Ophir PE50DIF/Er, Jerusalem, Israel) positioned at a distance of 12 mm from the tip that coupled the laser beam out. Table 4 contains the obtained results. All of them are averaged over about 100 data points. Additionally, the corresponding fluences are listed up when for the case considering a focal spot diameter of 900 µm is regarded.

[18] www.fotona.si

Table 4: Comparison of displayed and measured output parameters of the Fotona Fidelis Plus II Er:YAG laser.

Displayed Power [W]	Measured Average Output Power [W]	Displayed Pulse Energy [mJ]	Measured Pulse Energy [mJ]	Fluence [J/cm²]
2	1.39	100	86	13.52
3	2.09	150	103	16.19
4	2.75	200	138	21.69
5	3.43	250	171	27.88
6	4.12	300	207	32.54

The measured average powers and pulse energies are around 30% lower than indicated on the front panel. One important factor that contributes to these deviations is the age of the system as defects and alignment errors occur during time. Until use for the experiments the Fotona system has been installed for approximately three years. Also the type of delivery system and the out-coupling tip affect the emission characteristics. In case of the Fotona laser the laser beam was delivered via a 7-mirror articulated arm. By guiding the beam through this mirror system more losses are induced than by the use of a fibre, especially when the mirrors are misaligned. The contribution of the tip to reduced laser parameters is given by its shape. The laser beam of the Fidelis Plus II was coupled out by a conically shaped sapphire tip (RO7). When the beam passes the tip, similarly to a waveguide it experiences total reflection on the surfaces parallel to the optical axes, so that the laser light remains confined. At the cone of the tip the angle of incidence α_i is smaller than the angle of total reflection α_t, $\alpha_i < \alpha_t$, so that a part of the laser light gets refracted. Thereby transversal electro-magnetic modes (TEM) of higher order are created. The highest intensities are reached with the $TEM_{0,0}$ representing the ideal Gaussian beam profile. All higher modes encourage the reduction of the intensity.
The intensity distribution of the laser can be visualized by irradiating thermal paper (Pelican telefax paper) at low pulse energies. Fig. 19 shows such an intensity distribution. The ring-shaped pattern is the indicator for higher TEM modes. If just the $TEM_{0,0}$ mode had been present a single central peak would have been visible.

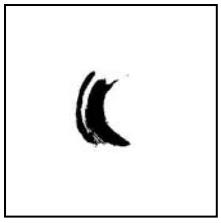

Fig. 19: Visualisation of the TEM mode of the Fotona Fidelis Plus II Er:YAG laser.

The ring-shape of the intensity distribution is more pronounced on the left side of the picture above. Due to alignment tolerances of the tip and the beam axis, on one side more light is coupled out.
The temporal pulse shape of this laser system was also recorded. An infrared-B sensor and an oscilloscope (Velleman PC 500i, Gevere, Belgium) were employed to measure the pulse shape. As example Fig. 20 contains the pulse profile for the 3 W pre-setting.

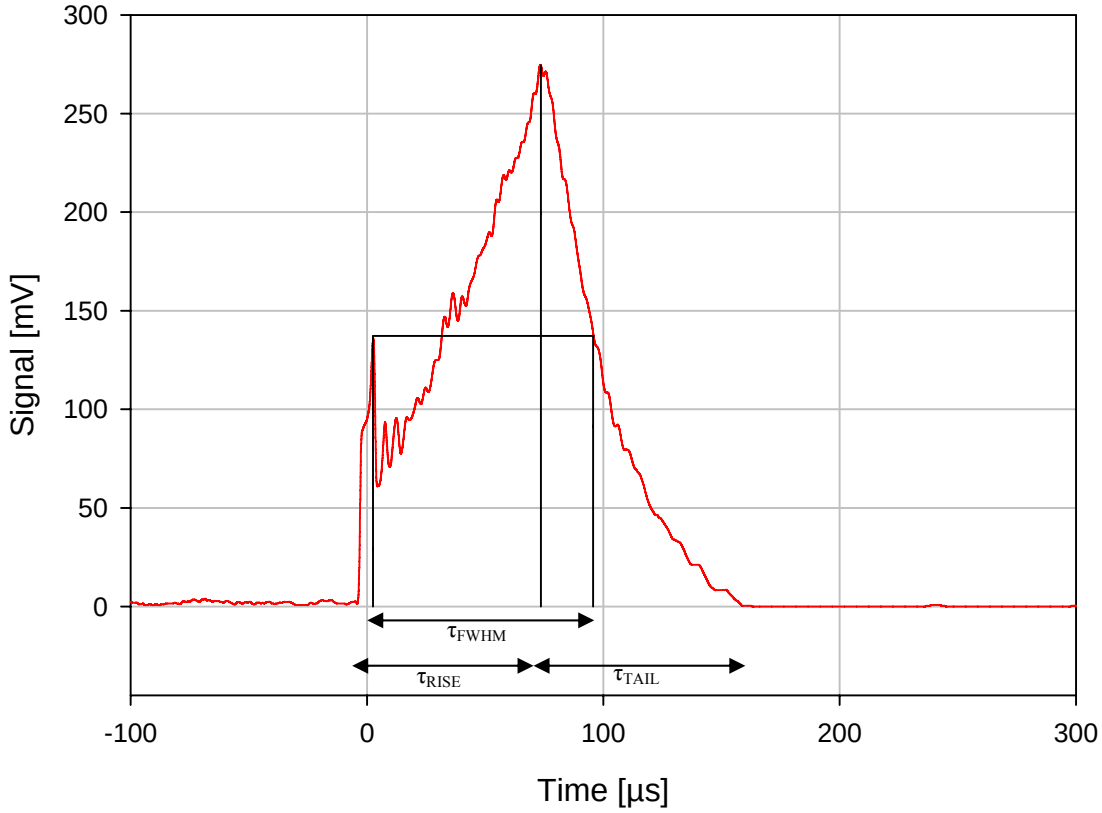

Fig. 20: Smoothed temporal pulse profile of the Fotona Fidelis Plus II Er:YAG laser obtained at 3 W.

As the original data points exhibited large spikes the pulse profile was smoothed, which means that the sliding average over 10 neighbouring data points was built. Pulse duration at full width half maximum (τ_{FWHM}), rise time (τ_{RISE}) and pulse tail (τ_{TAIL}) as well as the pulse peak power were derived. The FWHM was measured from the first peak appearing in the smoothed profile as the original data in this area were located above the 50% intensity line. The rise time was determined from the beginning of the pulse to the pulse peak. The pulse tail, which equals the decay time, was obtained as the duration from the pulse peak to the baseline at the end of the pulse. This procedure was repeated for all laser settings. Table 5 presents the results.

Table 5: Measured laser pulse characteristics of the Fotona Fidelis Plus II Er:YAG.

Measured Pulse Energy [mJ]	Pulse Duration FWHM [µs]	Rise Time [µs]	Pulse Tail [µs]	Pulse Peak Power [kW]
86	77	82	64	1.29
103	93	79	86	1.45
138	99	87	97	2
171	104	93	106	2.61
207	108	97	107	2.84

Obviously, the pulse parameters depend on the applied pulse energies of the system. In general, pulse duration, rise time and decay time increase with rising pulse energy. The only exception is the rise time, which decreases first from 82 µs to 79 µs when the pulse energy is changed from 86 mJ to 103 mJ. In all other cases a continuous but not linear increase can be seen. Actually, the percentage growth gets smaller with rising power. The growth rates for the pulse durations are for example 20.8 %, 6.5 %, 5.1 % and 3.8%. The increase of the pulse peak power with rising pulse energy is plausible. Although applicable for the Fotona laser, the enlargement of the temporal pulse parameters cannot be taken for granted like the following chapter reveals.

3.1.2 BIOLASE WATERLASE[19]

The Biolase Waterlase is an Er,Cr:YSGG laser (Erbium- and Chromium-doped Yttrium Scandium Gallium garnet). Like the Fotona Fidelis Plus II it is also commercially available for dental applications. The systems specifications are listed in Table 6.

Table 6: Laser parameters of the Biolase Waterlase Er,Cr:YSGG system stated by the manufacturer.

Wavelength	2780 nm
Maximum Pulse Energy	300 mJ
Maximum Pulse Width	150 µs
Fixed Frequency	20 Hz
Maximum Power	6 W

In contrast to the Fotona Fidelis Plus II the Biolase system has a fixed pulse repetition rate of 20 Hz. On the front panel just the output power and the air-water-mixture can be chosen.
With the same experimental setup as described before, laser parameters were measured and compared to the stated values. Table 7 shows the deviations between measured and displayed power values and between calculated and measured pulse energy values. Knowing the average power P and the pulse repetition rate PRR the pulse energy E_P was calculated as $E_P = P/PRR$. Additionally, the corresponding fluences resulting from a focal spot diameter of 750 µm were established.

Table 7: Comparison of displayed and measured laser parameters of the Biolase Waterlase Er,Cr:YSGG laser.

Displayed Power [W]	Average Output Power [W]	Calculated Pulse Energy [mJ]	Measured Pulse Energy [mJ]	Fluence [J/cm²]
2	2.2	100	110	24.90
3	3.35	150	168	38.03
4	4.57	200	227	51.38
5	5.71	250	283	64.06
6	6.89	300	344	77.87

[19] www.biolase.com

It is very interesting, that the measured parameters are around 13% higher than the displayed ones. This laser system was in use for approximately 5 years, while providing hardly any maintenance. Adjustments of the interior setup of the system are therefore necessary, because excessive average powers or pulse energies can be harmful for the patient. Besides that, the high output values compared to the Fotona laser can partly be explained by the implemented fibre delivery system, which introduces lower losses than a mirror articulated arm. Additionally, the intensity distribution of the laser beam, out-coupled by a conically shaped sapphire tip, contributes to the obtained results, as the central peak is quite pronounced. Its shape, depicted in Fig. 21, implies a quasi Gaussian intensity profile, which is typical for fibre based delivery systems.

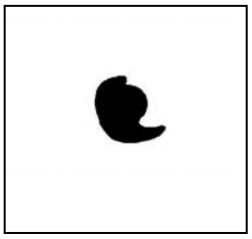

Fig. 21: Visualisation of the TEM mode of the Biolase Waterlase Er,Cr:YSGG laser.

Moreover, the temporal pulse characteristics are also very promising. A look at Fig. 22 reveals that the pulse has a steep rising edge and short pulse duration. One drawback might be seen in the rather long pulse tail. It bears the potential of influencing the tissue adjacent to the ablation site negatively by the generation of heat. Indeed, the decay times of the Er,Cr:YSGG laser are around 4.8 times higher than that of the Fotona Er:YAG laser. All these findings are summarised in Table 8.

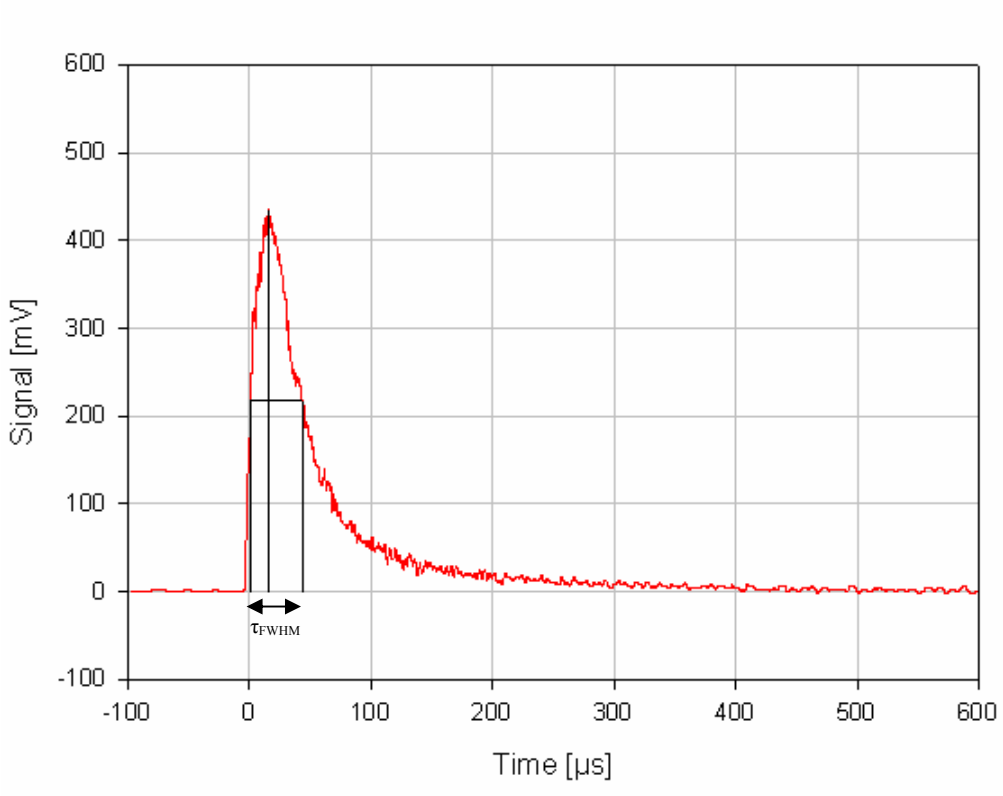

Fig. 22: Smoothed temporal pulse profile of the Biolase Waterlase Er,Cr:YSGG laser.

Table 8: Laser pulse characteristics of the Biolase Waterlase Er,Cr:YSGG laser.

Displayed Power [W]	Pulse Duration FWHM [µs]	Rise Time [µs]	Pulse Tail [µs]	Pulse Peak Power [kW]
2	51	19	386	1.48
3	53	26	384	2.78
4	50	25,5	439,5	3.04
5	43	23	442	4.73
6	46	27	498	5.09

In contrast to the Fotona system, a continuous elongation of the pulse duration could not be observed for this laser. Instead of this a change of the FWHM in a rather narrow range of 43 µs to 53 µs was detected. A similar behaviour was derived for the rise time of the laser pulse. Due to considerable signal fluctuations the length of the pulse tail could just be determined approximately. Together with the calculated pulse peak powers these data are presented in Table 8. For laser ablation with this Er,Cr:YSGG system several settings listed in Table 9 were recommended.

Table 9: Recommended laser settings for tooth treatment.

	Power	Air	Water
Dentine	3.5 W	65 %	55 %
Caries	2.5 W	20 %	20 %
Enamel	5.5 W	90 %	85 %

For the experiments these recommendations were taken into consideration whenever possible, but numerous other settings were tested too.

3.1.3 Nd:Vanadate Lasers

Two Nd:Vanadate ($Nd:YVO_4$) lasers manufactured by High Q Laser Production GmbH[20], Hohenems, Austria, were used. The lasers belong to the so-called "picoREGEN™ series", all-in-one picosecond regenerative amplifier systems. Both lasers have a pulse width at FWHM of 12 ps. The diode pumped solid-state Nd:Vanadate laser crystals emit at a wavelength of 1064 nm. The output beam with high temporal and spatial stability is of $TEM_{0,0}$ mode. Its beam quality can be characterised by $M^2 \leq 1.2$. Differences between the two systems are listed in Table 10.

[20] www.highQlaser.com

Table 10: System parameters of the two Nd:Vanadate 12-picosecond laser systems stated by the manufacturer.

	IC-1500 REG AMP	IC-10000 REG AMP Microprocessing
Average Output Power	1.5 W	>10 W
Pulse Repetition Rate	0-5 kHz	0-100 kHz
Pulse Energy	300 µJ @ 5 kHz	500 µJ @ 10 kHz, 200 µJ @ 50 kHz, 80 µJ @ 100 kHz

The IC-1500 REG AMP with lower frequency of 5 kHz was involved in the first experiments concentrating on selective ablation of composite materials and tooth structures. Thereby it was operated at 620 mW average output power, which implies a pulse energy of 124 µJ. The IC-10000 REG AMP Microprocessing was applied for ablation rate measurements of dental restorative materials and dentine. It was therefore adjusted to frequencies of 35 and 50 kHz, respectively, and a pulse energy of 100 µJ.
In both cases the laser treatment was performed with the r-φ-scanner. While scanning the laser beam over the surface, single laser pulses could be applied. Fig. 23 shows the remaining cavity after laser ablation by a single pulse with the IC-1500 REG AMP. The Gaussian profile is slightly deterred. Instead of a circular rim of the cavity an elliptical one is evident. The diameter of the large semi-axis of the crater equivalent to the focal spot diameter is about 33.7 µm.

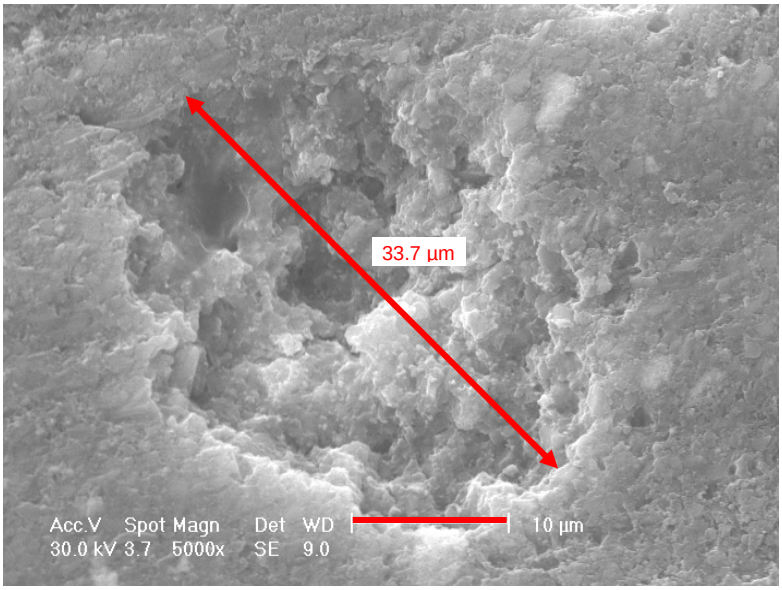

Fig. 23: ESEM of a single laser pulse of 124 µJ pulse energy applied by the 12 ps Nd:Vanadate IC-1500 REG AMP focused on dentine. The resulting focal diameter is ~33.7 µm.

3.1.4 Yb:Glass Lasers

For investigations of selectivity and morphology an Ytterbium:Glass laser was used in addition to the Nd:Vanadate laser. This system, named IC-1040-400 fs REG AMP which is part of the "femtoREGEM^{TM} series" of High Q Lasers, is also a diode-pumped solid-state laser. Its centre wavelength is 1040 nm and its regular pulse width at FWHM is 350 fs. Other laser parameters are listed in Table 11.

Table 11: Laser parameters of the Yb:Glass laser for 350 fs laser pulses.

	IC-1040-400 fs REG AMP
Average Output Power, max.	500 mW
Pulse Repetition Rate	0-10 kHz
Pulse Energy	250 µJ @ 1 kHz

For the experiments conducted a stretcher was inserted. By introducing a chirp the pulse width was extended to 700 fs. That was necessary as the components of the r-φ-scanner would have been damaged due to the high power densities associated with lower pulse widths. It was operated at 1 kHz pulse repetition rate and 100 µJ pulse energy.
Again, high stability and $TEM_{0,0}$ beam profile are promised, which can be confirmed by the CCD image in Fig. 24. An M^2 value of ≤ 1.2 is stated by the manufacturer.

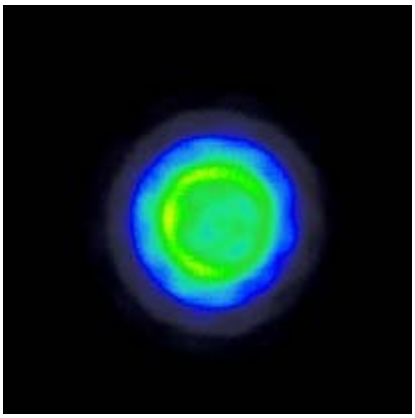

Fig. 24: CCD image of the 700 fs Yb:Glass laser beam.

For the experiments an iris was inserted into the beam path. The resulting spatial intensity distribution can be seen in Fig. 25. The $1/e^2$-diameter determined out of the diagram is 98.5 µm.

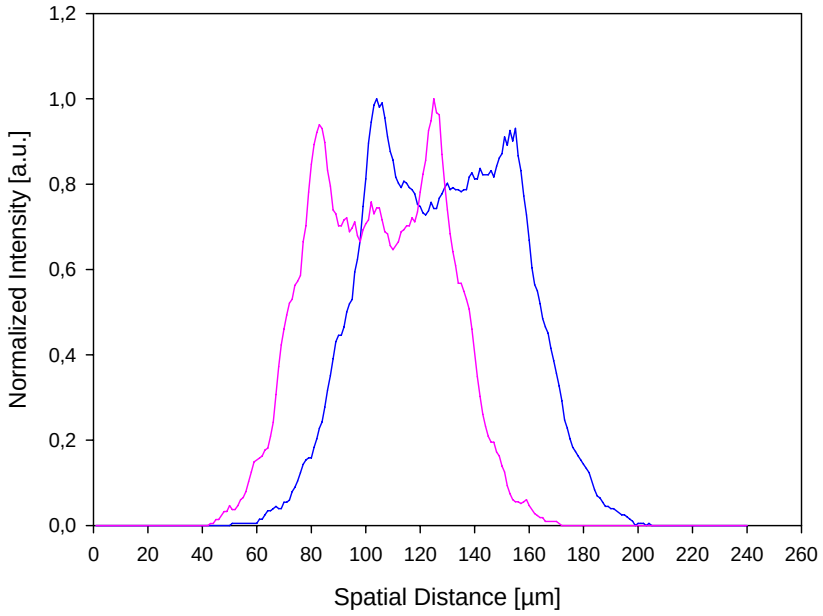

Fig. 25: Spatial intensity profile of the 700 fs Yb:Glass laser beam launched through an iris.

Another Yb:Glass laser fabricated by High Q Lasers, the IC1040-300 fs YB REG AMP, was used to determine the ablation rates of bone materials and of dental restorative materials. For this type of experiments the r-φ-scanner was not employed, so that ultra-short laser pulses of 330 fs could be applied. Beam quality and profile are the same as described before. Again, the PRR was variable between 0 and 10 kHz. Nevertheless, it was operated just at 1 kHz, thereby yielding the maximum average pulse energy of 130 µJ. The laser beam was directed through a lens of 100 mm focal length. Applying the knife-edge-method (Bachmann, 2003), the resulting 1/e²-diameter of the focal spot was determined to be 72.4 µm. That is demonstrated in Fig. 26.

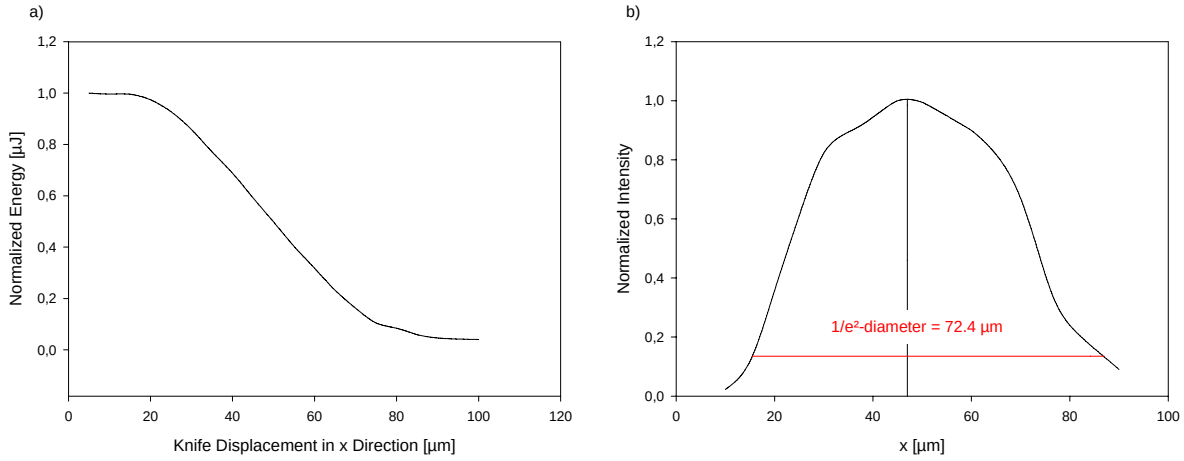

Fig. 26: a) Normalized and b) integrated energy density profile, to determine the 1/e²-diameter of the focal spot, which is 72.4 µm.

3.1.5 TI:SAPPHIRE

The last system to be described is the Hurricane-i laser fabricated by Spectra-Physics. It is a Ti:Sapphire ($Ti:Al_2O_3$) laser with adjustable pulse duration in the span of 130 fs up to 7 ps. For all the experiments involving this laser a PRR of 1 kHz was utilized. Again, its specifications are outlined below.[21]

Table 12: Laser parameters of the Hurricane-i Ti:Sapphire laser.

Wavelength	~800 nm
Pulse Width	130 fs-7 ps
Pulse Energy at 1 kHz	> 1 mJ
Frequency	0-10 kHz

For ablation rate and ablation threshold measurements of dental composites and bone tissue, the focal spot diameter after focussing the laser beam through a lens of 35 mm focal length, had to be determined. On basis of the following equations the experimental setup was arranged:

[21] From: Manual of the Hurricane-i laser, Spectra-Physics, 2003.

The beam width of a propagating laser beam is given by the Gaussian equation

$$w(z) = w_0 \sqrt{1 + \left(\frac{z - z_0}{z_R} \right)^2} \tag{19}$$

where $w(z)$ is the beam radius at a distance z, w_0 the radius of the beam waist, z_0 the beam waist location and z_R the Rayleigh length given by

$$z_R = \frac{\pi w_0^2}{\lambda}. \tag{20}$$

At the distance z_R from the waist the beam radius increases by a factor $\sqrt{2}$. The equation is just valid for an ideal laser beam. The propagation of real beams is affected by the quality factor M^2. Considering this quality factor and using capital letters for the symbols above, equation (20) can be adapted to real conditions:

$$Z_R = \frac{\pi W_0^2}{M^2 \lambda}. \tag{21}$$

Replacing z_R in equation (19) by the capital Z_R, the beam width for real conditions can be expressed.
The experiment was then performed acquiring the beam width at numerous distances along the propagation direction. The setup employing a CCD camera is presented in Fig. 27.

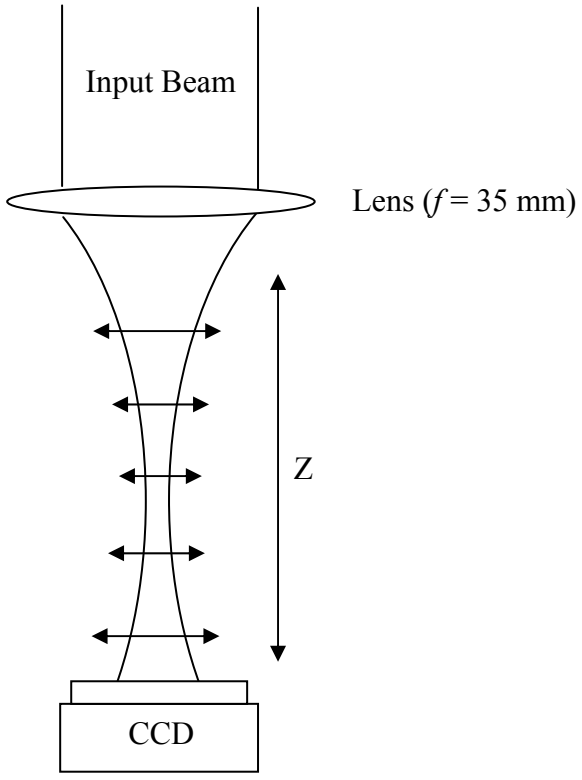

Fig. 27: Experimental setup to determine the focal spot diameter of the Ti:Sapphire laser beam after focusing through a lens of f = 35 mm.

Different pulse durations of the Hurricane- i laser are adjusted by changing the position of the grating inside the pulse compressor. To make sure, that these changes in the optical path did not result in changes of the focal spot diameter, the measurement of the beam waist was performed for 150 fs and 7 ps. The obtained data were entered in a plot and fit by a Gaussian function according to equation (19), where Z_R is considered.

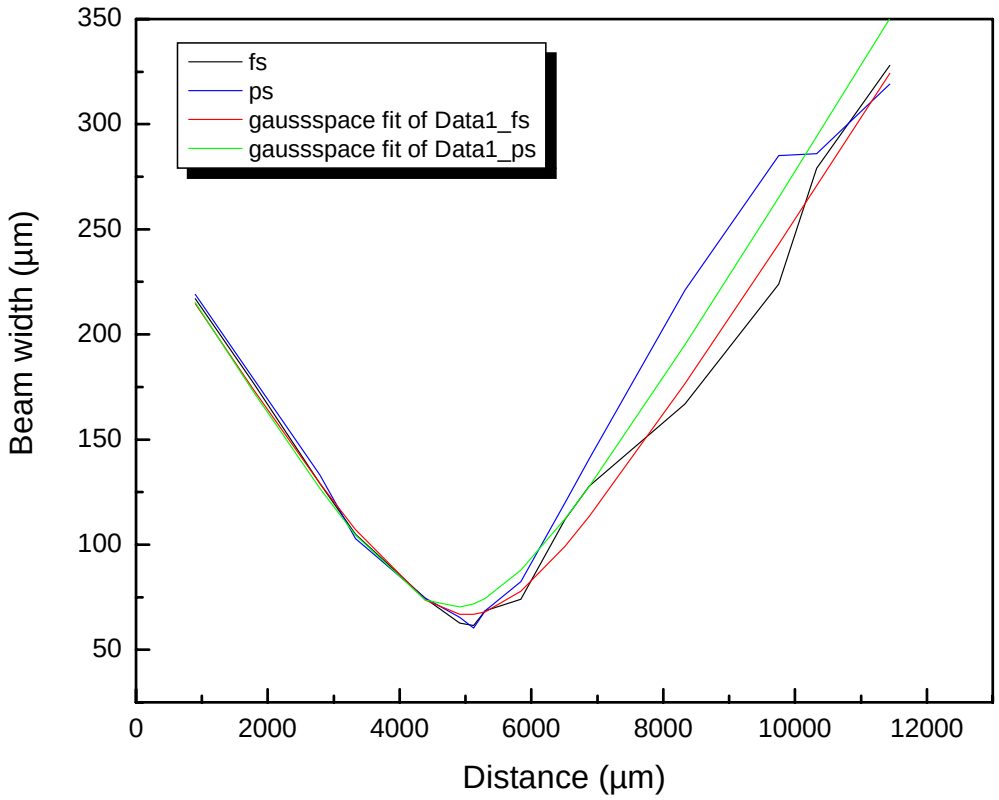

Fig. 28: Beam width drawn versus distance to determine the beam waist.

For the shorter pulse duration an imperceptible smaller focal diameter of 67 µm instead of 70 µm was retrieved, implicating that hardly any changes of the ablation conditions occur when the pulse width is elongated from 150 fs to 7 ps. Other parameters determined by the Gaussian fit were the beam divergence, Rayleigh length and the M² factor. They are summarized in the table below.

Table 13: Measured beam parameters of the Hurricane-i laser.

	Beam Waist [µm]	Beam Divergence [rad]	Rayleigh Length [µm]	M^2
τ = 140 fs	67	0.025	1323	1.8
τ = 7 ps	70	0.026	1299	1.9

Due to the good circular symmetry of the beam, measurements for both vertical and horizontal cross sections were considered unnecessary. Its intensity distribution is depicted in Fig. 29.

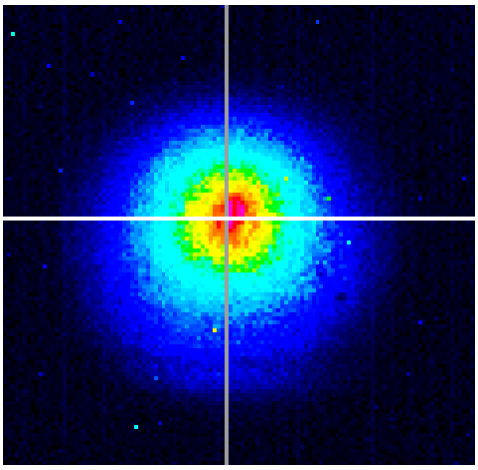

Fig. 29: Intensity distribution of the Hurricane-i Ti:Sapphire laser beam.

3.2 SCANNERS

3.2.1 R-φ-SCANNER

Ultra-short pulse laser ablation is plasma mediated. Sharp focusing is necessary to achieve the high power density needed for plasma formation. The resulting spot diameters are so small (some tens of µm to ~0.1 mm) that they are just suitable for micro-preparations. For the treatment of larger areas the laser beam has to be moved over the surface in a defined pattern. In the present study a lateral scanning device working in r-φ-coordinates was applied generating circular shapes of the scan pattern able to simulate the mechanical drill. By the use of the scanner two accumulation effects can be avoided (Kim, 2001), (Niemz, 1996): With an increasing number of laser pulses impacting subsequently on the same tissue spot, on the one hand the temperature rises rapidly and on the other hand the ablation efficiency is decreased as the energy stored in the laser beam gets reduced due to absorption and reflection on the cavity walls before reaching the cavity bottom for further ablation.

The prototype r-φ-scanner used for some experiments reported in this thesis has been developed by LINOS Photonics GmbH & Co. KG, Munich[22]. The scanner incorporates two main optical components, an oscillating galvo mirror, deflecting the laser beam in radial direction, and a fast rotating prism, altering the φ-component. The galvo mirror can be operated at oscillation frequencies up to a maximum of 600 Hz and at different freely defined mirror functions, such as sin, |sin| or triangle. The prism can be rotated constantly by a motor with velocities between 10 and 5000 rpm. Both, mirror and prism parameters can be adjusted and controlled via PC. By choosing different amplitudes of the mirror offset, mirror functions and rotation velocities, a variety of circular scan patterns can be generated.

The prism consists of two parts, a Schmidt-Pechan prism and half of a Penta prism, which are separated by an air gap. Ideally, the optical image of a beam entering the rotating prism parallel to the optical axis is a circle. Unfortunately, alignment imperfections of the prism faces enclosing the air gap introduce a tumbling error resulting in some artefacts in the generated scan pattern. (For more details see (Bäcker, 2004)).

[22] www.linos.de

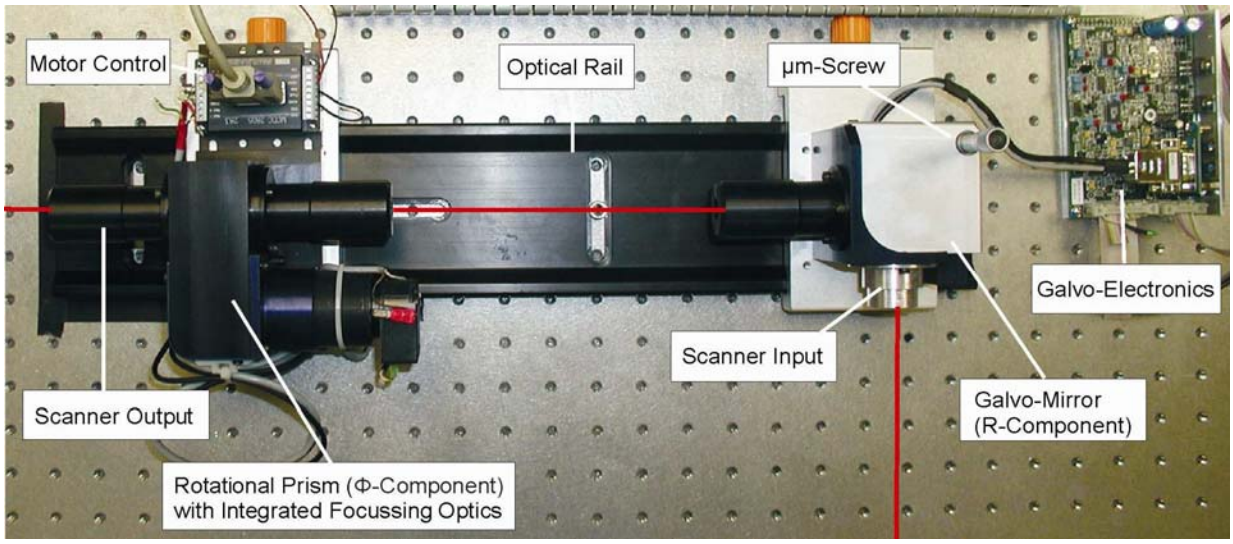

Fig. 30: Top view of the prototype r-φ-scanner. As the laser beam (red line) passes the galvo mirror and the rotating prism the circular coordinates r and φ are adjusted. (The figure is taken from (Bäcker, 2004).)

3.2.1.1 SCAN ALGORITHMS

By systematically varying the scanner parameters numerous scan algorithms were produced. The procedure to find appropriate algorithms involved Matlab simulations followed by experimental verifications. For these experiments a red diode laser mounted on the r-φ-scanner and a CCD camera (WinCamD, DataRay Inc., USA) were used to display the intensity distribution of the scanned area. The algorithms were evaluated according to the following criteria: The energy distribution should be as homogenous as possible and the energy density ratio of the central peak to the surrounding body, determined from the CCD images, should be as low as possible. In the best case a flat top energy profile should be achieved. The so found algorithms were tested in dental tissue afterwards.
Among all the selected algorithms two of them performed best. The scanner parameters of these algorithms for a PRR of 1 kHz are listed in Table 14. If higher PRR are applied, the rotation velocity of the prism as well as the mirror frequency have to be adjusted by multiplying the concrete values with the scaling factor (e.g. PRR = 35 kHZ → scaling factor = 35).

Table 14: Scan parameters for 1 kHz PRR.

Algorithm	Prism Rotation [rpm]	Mirror Function	Mirror Frequency [Hz]	Mirror Amplitudes [Vpp]	Mirror Offset [V]	Mirror Offset [mm]
2	57.14	sin	8.07	3.2	0.06	0.04
13	57.14	|sin|	0.11	2.6	0.2	0.15

3.2.1.2 CORRESPONDENCE OF SIMULATION AND EXPERIMENTS

In the work of Bäcker (2004) many scan algorithms were simulated and experimentally tested. In the scope of this thesis the procedure shall be described briefly: To start with, the Matlab simulations are shown in the following for algorithm 13, using the same number code like Bäcker. Fig. 31 a) contains the simulated scan pattern assuming an infinitesimal small

diameter of the laser beam for better visualisation. As no information about the energy density profile is contained in this picture a Gaussian pulse shape with a focal spot diameter of $2 \cdot w_0 =$ 70 µm ($1/e^2$-level) was superimposed to every data point yielding distributions as seen in Fig. 31 b) or 3-dimensional surface plots displayed in c).

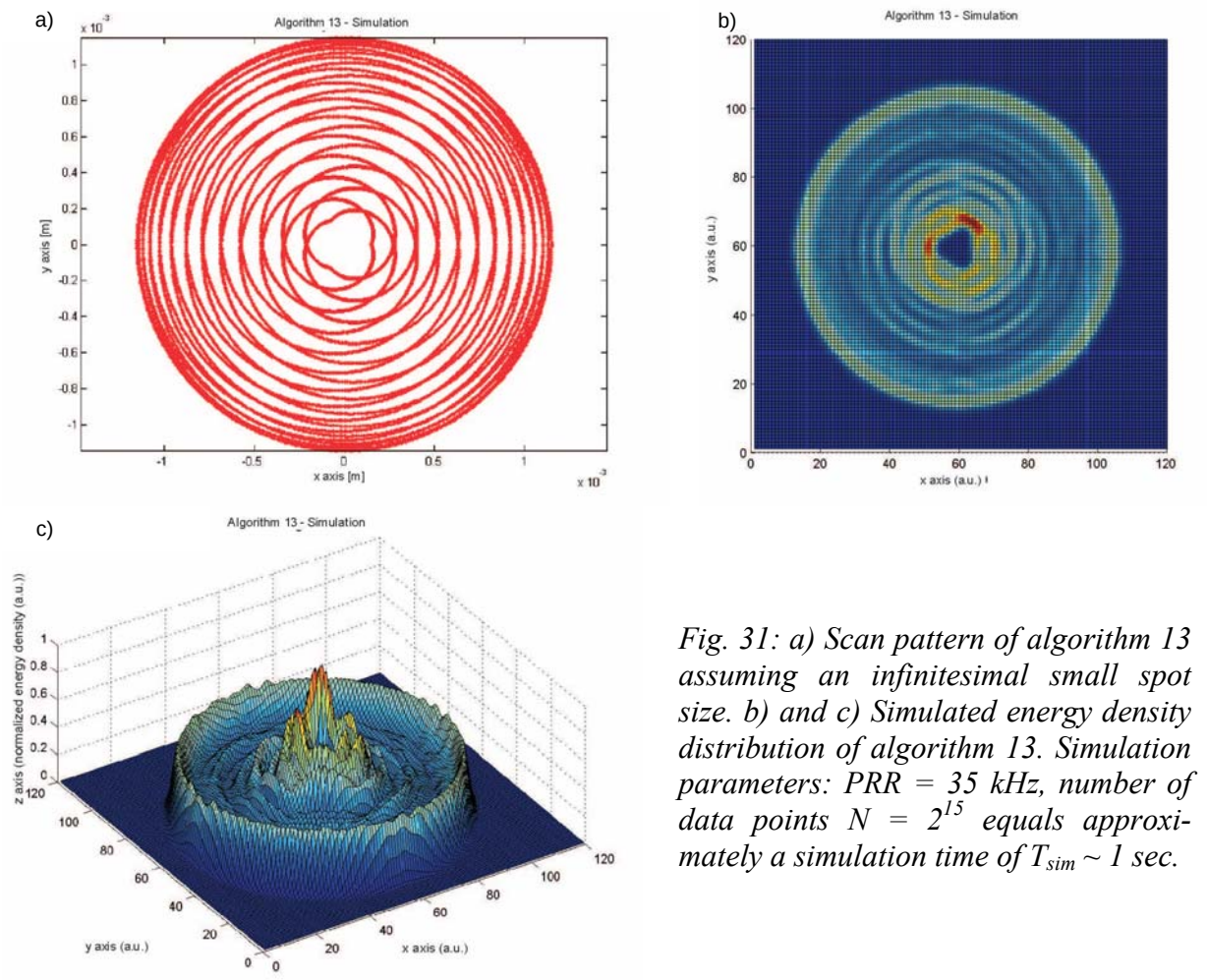

Fig. 31: a) Scan pattern of algorithm 13 assuming an infinitesimal small spot size. b) and c) Simulated energy density distribution of algorithm 13. Simulation parameters: PRR = 35 kHz, number of data points $N = 2^{15}$ equals approximately a simulation time of $T_{sim} \sim 1$ sec.

The first experimental data to be compared to the Matlab simulations above were CCD images of the intensity distribution generated by an r-φ-scanned pilot laser beam. The captured energy density distributions were obtained at different integration times. To visualise the scan pattern evident in Fig. 32 an integration time of just 0.5 seconds was chosen. To analyse the energy density distribution the profiles were averaged over 5 seconds. This case is shown in Fig. 33. Despite the tumbling error introduced by the alignment imperfection of the prism, simulated and actual scan pattern and energy density profile agree very well. The tumbling error is noticeable in the asymmetric cycles, which are in particular pronounced at the rims of the scanned area and in the centre with its slightly distorted energy density peak. In Fig. 33 also the cross section of the CCD image of algorithm 13 is shown. As stated above, the energy density distribution should resemble a homogeneous flat top profile. The cross section of the energy density profile demonstrates the tendency towards that goal.

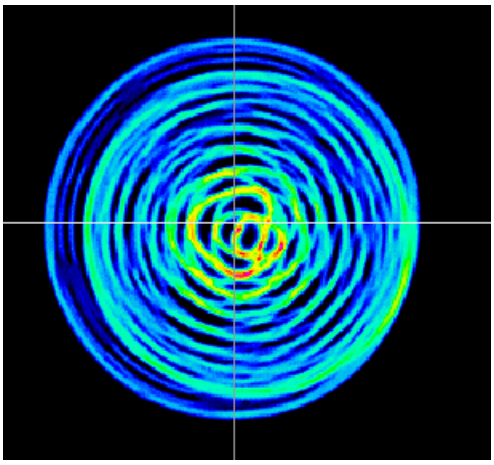

Fig. 32: Energy density distribution of the r-φ-scanned pilot laser applying algorithm 13 captured by the CCD-beam profiler. Integration time: 0.5 sec.

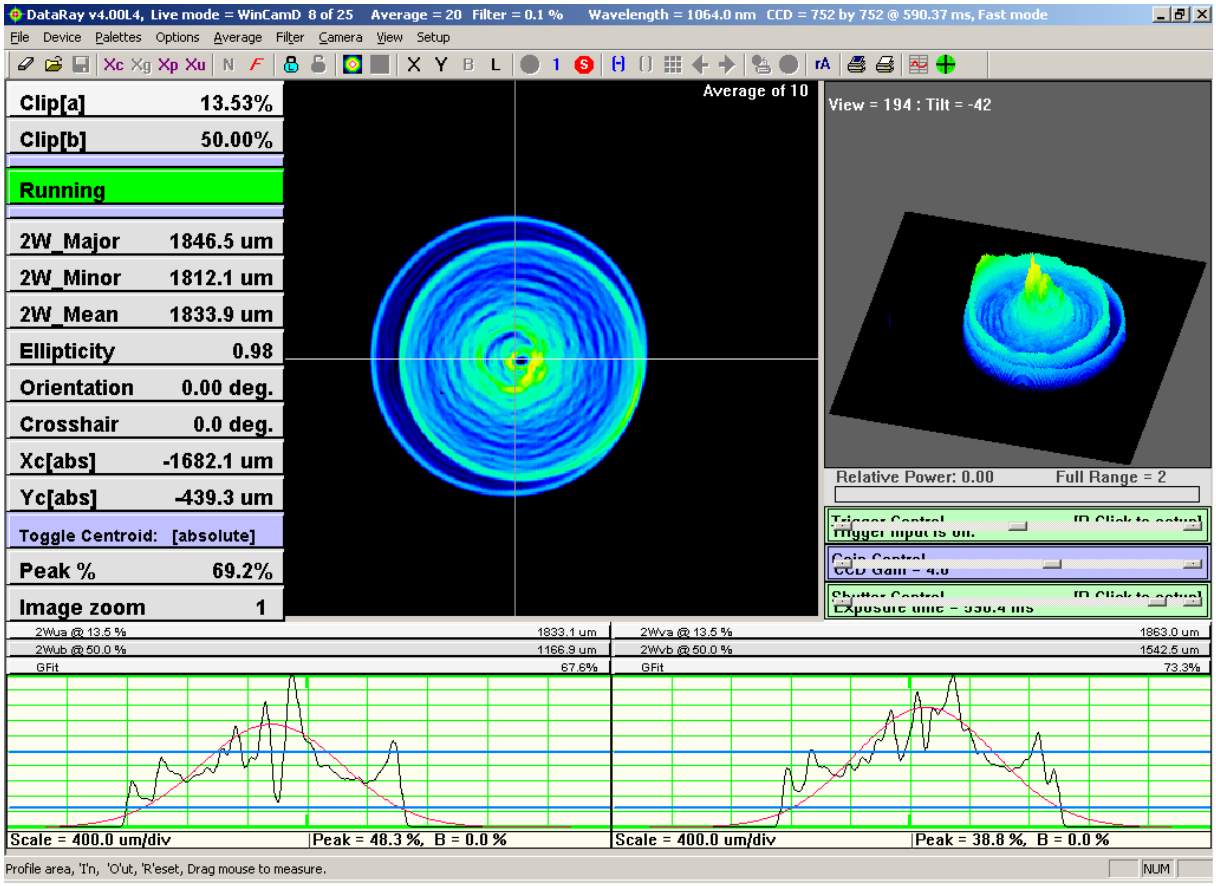

Fig. 33: Top and side view of the energy density distribution of algorithm 13 captured by the CCD camera. τ_{int} = 0.5 sec, τ_{avg} = 5 sec. Additionally, the cross section of the energy density profile is depicted. The red curve represents the Gaussian profile.

The last step in the testing procedure to judge the applicability of the r-φ-scanner was to perform USPL ablation. Bäcker worked with dentine slices and two fs laser systems. Via ESEM analysis the scan patterns of the processed cavities were evaluated and compared to the simulations and CCD images. Also morphological aspects were taken into consideration. Bäcker concluded that Matlab simulations and experimental verifications were in good agreement.

The surface morphology of r-φ-scanned USPL cavities generated in dentine is discussed in every detail in chapter 4.3.3 where some scanning electron micrographs of the processed cavities are presented. To avoid redundancy, at this point just a reference to the mentioned chapter shall be made.
To complete the description of the scan patterns used in the present study, the second algorithm shall be introduced. In Fig. 34 the simulated scan pattern and energy density distribution are captured. The same simulation parameters as for algorithm 13 were chosen to be able to compare the results.

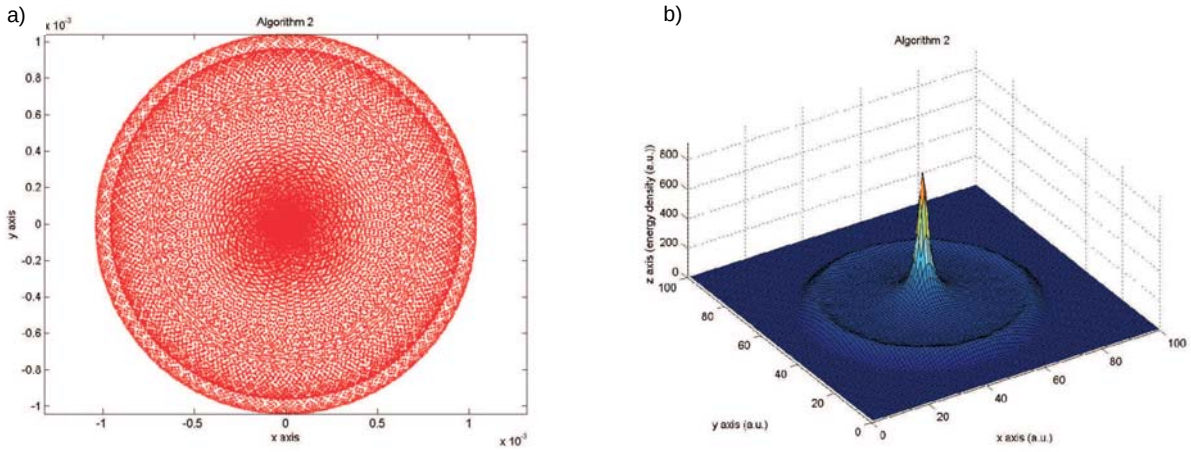

Fig. 34: a) Simulation of the scan pattern of algorithm 2 assuming an infinitesimal focal spot. b) Energy density distribution over the scanned area with a superimposed Gaussian beam profile of 70 µm beam waist. Simulation parameters: PRR = 35 kHz, number of data points N = 2^{15} corresponding to a simulation time of around 1 sec.

In Fig. 35 the image of the scanned pilot laser beam obtained with the CCD camera is shown. Compared to algorithm 13 a more pronounced central peak is visible. The alignment errors of the prism are again obvious, not only in the outer circles but also in the centre which does not exhibit one single peak as predicted by the simulations, but two of them.

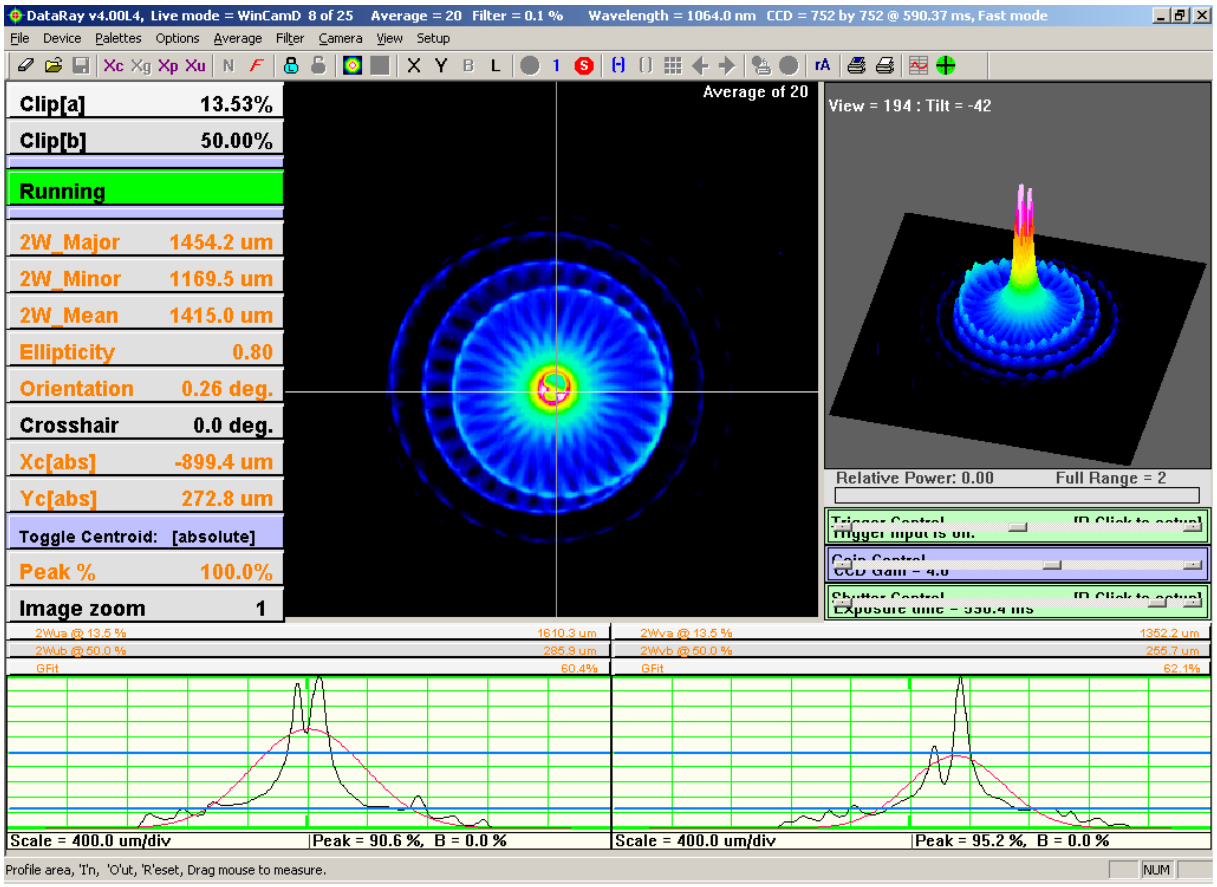

Fig. 35: Top and side view of the energy density distribution of algorithm 2 captured by the CCD camera. τ_{int} = 0.5 sec, τ_{avg} = 10 sec.

3.2.1.3 SCANNER SETUP

For each experiment the laser beam was launched into the scanner via a telescope. The beam diameter entering the r-φ-scanner was adjusted to 2 mm. Smaller diameters would have destroyed the optical components of the scanner as too high energy densities would have been generated. Each run was started with the determination of the galvo mirror offset. Therefore two steps were necessary, the mechanical adjustment of the micrometer screw and the electronic adaptation of the oscillation function offset. During the experiments the electronic offset had to be readjusted from time to time as it is sensitive to temperature.
The laser beam deflected according to the applied algorithm exits the scanner through a focusing lens of 80 mm focal length. The samples fixed on a translation stage were positioned in the focal plane.

3.2.2 X-Y-SCANNER

The second scanner involved in the studies was the SCANcube 7 manufactured by SCANLAB AG, Puchheim, Germany. It incorporates two silver-coated tilted mirrors each connected to a separate linear Galvanometer scanner. The first mirror steers the beam in y-direction, while the second mirror performs the x-deflection. A lens of 100 mm focal length attached at the exit of the scan cube focuses the beam. The scanner components are designed for a wavelength range of 450 nm – 2500 nm. The utilizable aperture is 7 mm. In cw laser operation a maximum power densitiy of 30 W/cm² shall not be exceeded when using the scanner. For 50 ns pulses the limiting power density is 10 MW/cm². Extrapolation down to 20

ps and less yields that ≥ 3 GW/cm² seem to be acceptable. The scanner components can stand a maximum laser power of 6 W.

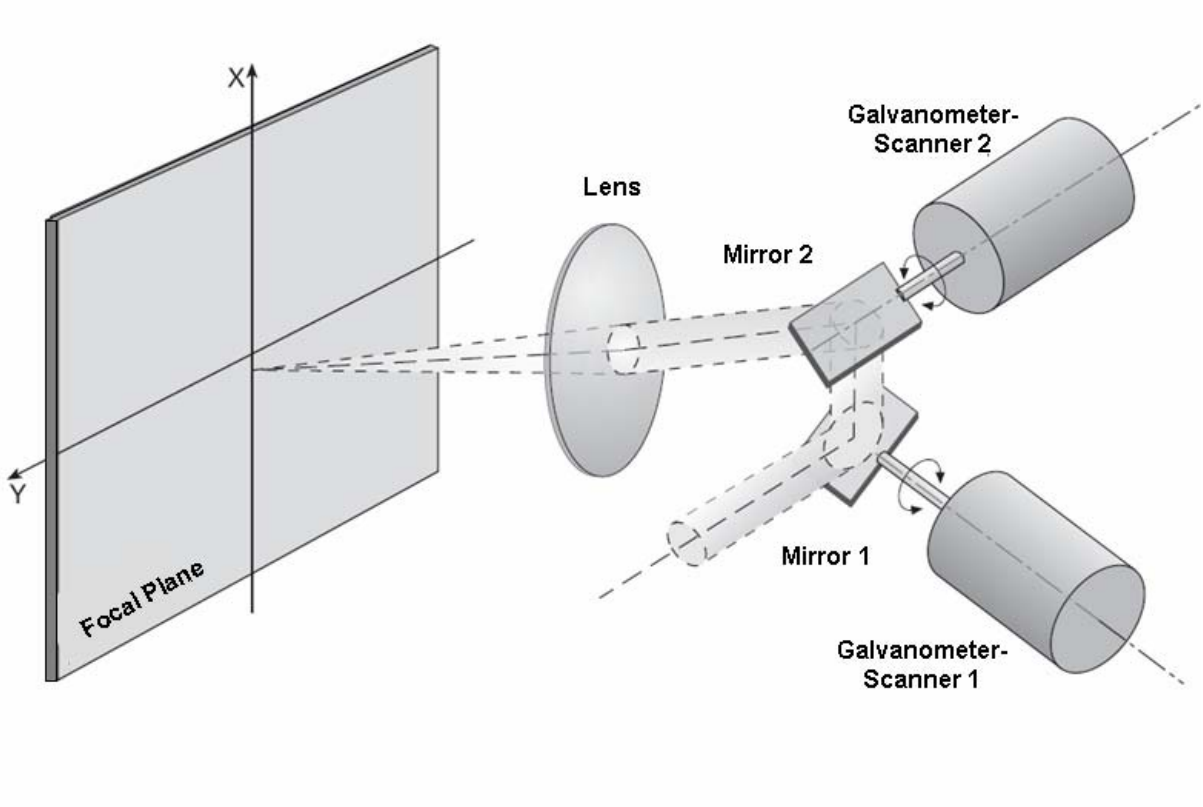

Fig. 36: Principle of the x-y-scanner. [23]

For the conducted experiments an Archimedic helix was scanned. The distance between the arcs is determined by the focal spot diameter. To achieve certain overlaps an appropriate scaling factor has to be used. Similar considerations have to be made concerning the overlap of the focal spots along the spiral traces. In that case the scan speed has to be adjusted.
The energy distribution obtained by an Archimedic spiral was simulated by my colleague M. Strassl (2007). Fig. 37 presents some of his results. The goal to achieve flat top profile can be achieved easily with this scanning method.

[23] (Scanlab Manual, 2005), p.5.

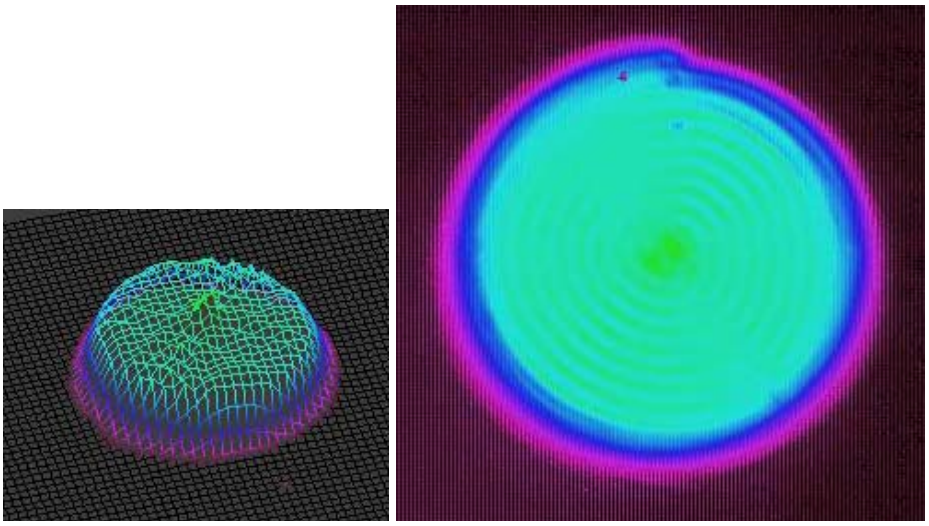

Fig. 37: Energy distribution of an Archimedic spiral.

3.3 TISSUE SAMPLES

3.3.1 TOOTH SAMPLES

For the experiments extracted caries free human third molars were collected. To expose dentine the occlusal enamel was removed using a diamond saw under water cooling (Accutom-2, Struers). Subsequently dentine was polished. When just enamel was used, no additional procedure was applied to treat the surface. Before and after laser ablation the samples were kept in pure water to avoid dehydration.

For selectivity analysis, long grooves were opened across the dentine surface using a conventional dental turbine. The restoring procedure was performed according to the manufacturer's instructions, involving the etchant Scotchbond from 3M ESPE, Excite bonding (Ivoclar Vivadent) and a composite. Common recommendations for the filling procedure in dentine are the following: 1) etching with 37% phosphoric etchant for 10-15 seconds, 2) removing all etchant gel with vigorous water spray for at least 5 seconds, 3) drying the excess water with a burrst of dry air so that a wet shimmering surface is visible, 4) applying the bonding gel and rub the surface for at least 10 seconds, 5) fixing the gel with an air stream, 6) light curing for about 10 seconds, 7) inserting the composite filling material in small layers, 8) light curing of the composite layers for about 40 seconds. The permissible layer thickness and the duration of light polymerisation depend on the filling material. For light curing the Spectrum 800 (DentSply, UK) polymerisation lamp was employed. Laser cavities were then generated at the dentine-composite border affecting both regions. Selective ablation was judged on the amount of tissue removed in both materials.

3.3.2 COMPOSITE BLOCKS

Numerous composites from different manufacturers were acquired. Table 15 contains a list of all restorative materials involved in the studies.

Table 15: List of composites.

Manufacturer	Product
Kerr Hawe	Point 4
	Premise Enamel
	Premise Body
	XRV Herculite Dentine
	XRV Herculite Enamel
Ivoclar Vivadent	Heliomar
	Compolgass F
	Tetric Flow
	Tetric Ceram
3M ESPE	Z100

Composite blocks were built by filling the paste into hollow cylinders with an inner diameter of 6 mm and a height of 1.5 – 2 mm or into cubes of 5 mm side length. As described above the pasty composite has to be hardened by means of light curing. Therefore, a new halogen polymerisation lamp named Swiss Master Light by EMS, Geneva, Switzerland, was employed. As stated by the manufacturer, working with a power density of 3 W/cm² a composite layer of 2 mm thickness can be hardened in 4 seconds. As the composite was irradiated with 1.8 W/cm² it was decided to harden it for 10 seconds. The prepared samples were kept under dry conditions before and after laser ablation.

3.3.3 BONE SAMPLES

Fresh spongiosa, compacta and cartilage were obtained from a nearby butcher. Spongiosa was derived from hip joints, compacta descended partly from ribs but mostly from femur, cartilage was taken from different joints. For a small number of experiments human spongiosa was used. Obviously, it was hard to get, so for most of the experiments bovine bone tissue served as sample. To justify the use of bovine instead of human bone the following comparison can assist.

Table 16: Specific densities and compositions of human and bovine spongiosa and compacta.[24]

Bone Tissue	Origin	Specific Density [g/cm³]	Water Fraction [Vol. %]	Mineral Fraction [Vol. %]	Organic Fraction [Vol.%]	Anorganic Faction [Vol. %]
Spongiosa	Human	1.92	27.0	33.9	34.9	4.2
	Bovine	1.93	28.1	33.5	34.2	4.2
Compacta	Human	1.99	23.9	37.7	33.8	4.6
	Bovine	2.00	25.2	36.6	33.6	4.6

[24] From www.ubicampus.mh-hannover.de/~bmt/bio/kapitel_6/6_2.php

Bone tissue was stored in saline solution (0.2 % NaCl) and refrigerated before and after the preparation procedure. Whenever possible, bone tissue was ablated within one week at the latest. Just human spongiosa was stored a little bit longer. To assure that the composition and morphology of the tissue did not change during storage in NaCl, scanning electron micrographs were obtained from both freshly extracted and stored spongiosa. Fig. 38 gives evidence, that no decomposition of the hard tissue structures was observed. Just the intra-trabecular material, mainly fat and blood tissue, got washed out to some extent. The trabeculae themselves remained unaffected. As no alteration of hard tissue was observed tissue samples kept in saline solution were used throughout the experiments.

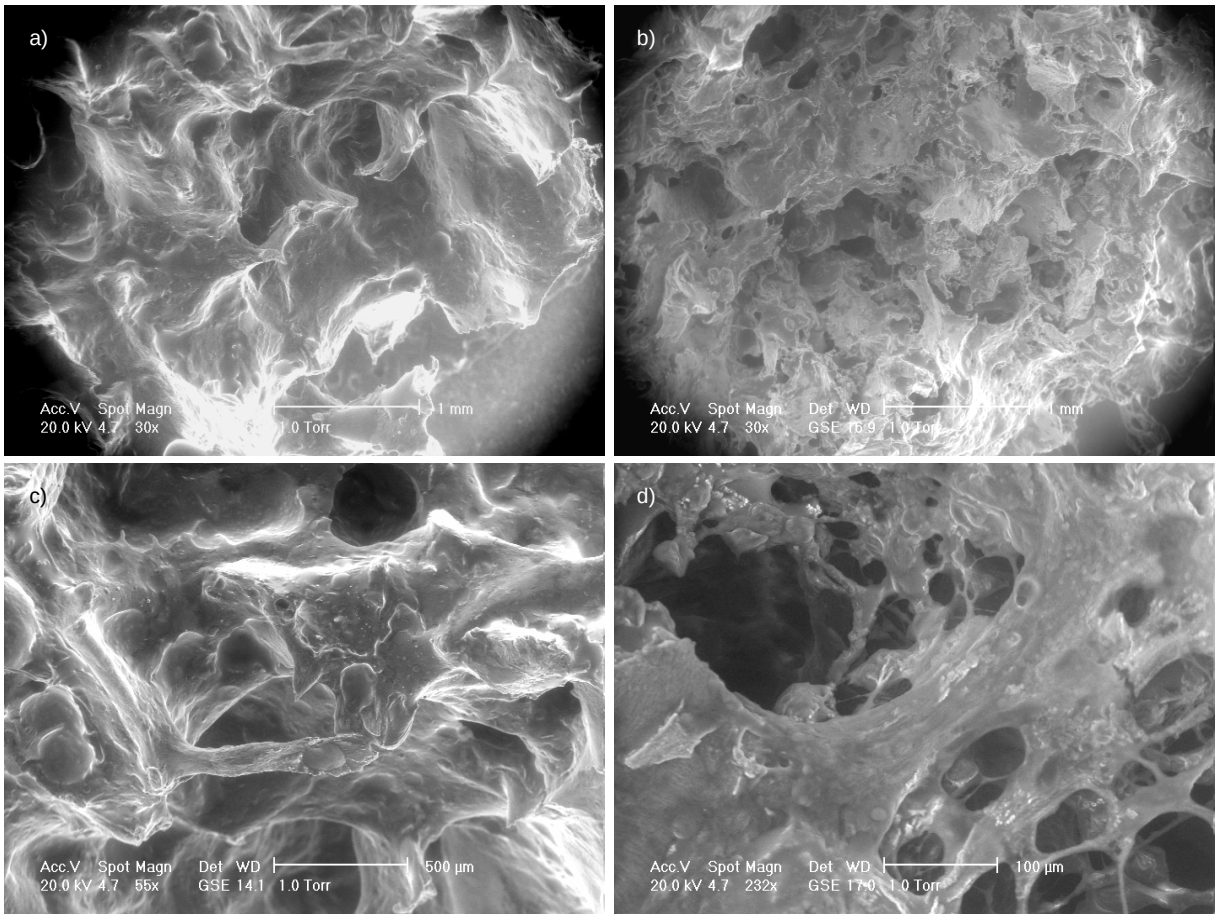

Fig. 38: ESEM micrographs of human spongiosa. a) and c) capture fresh spongiosa, whereas b) and d) depict spongiosa stored in saline solution for 14 days. During storage the hard bone structure did not change. Just fatty tissue and blood vessels dissolved.

For better handling, bone tissue was cut into blocks of about 1 cm^3 using a diamond saw under water cooling. To preserve the trabecular structure of spongiosa and to avoid plugging of the small channels inside the spongy tissue no other preparation than cutting was performed. Similar considerations were made concerning cartilage. Unlike to that, compacta samples were additionally ground to expose even surfaces.

4 EXPERIMENTAL RESULTS AND DISCUSSION - TOOTH

4.1 ABLATION RATES

4.1.1 ERBIUM LASER ABLATION RATES

4.1.1.1 MATERIALS AND METHODS

Erbium laser systems involved in ablation rate measurements were the Fotona Fidelis Er:YAG and the Biolase Waterlase Er,Cr:YSGG laser. Cavities were generated with front-panel power settings ranging from 2 to 6 W. Ablations were always accompanied by an air-water spray. With each laser setting 6 cavities were prepared for a defined period of time.
The experiments were performed in dentine, enamel and different composite materials. Concerning teeth, extracted caries free human permanent third molars were collected, which were stored in pure water until use. For dentine ablation, the occlusal enamel was removed using a diamond saw under water cooling (Accutom-2, Struers). Before and after laser ablation the samples were weighted employing a µg-balance to determine the total mass loss. The average over all 6 total mass values was included to calculate the mean total ablated volume according to $V = m/\rho_{d/e}$, where the densities are given by $\rho_d = 2.14$ g/cm³ for dentine and $\rho_e = 2.97$ g/cm³ for enamel[25]. In a last step the mean ablated volume per pulse was established by dividing the averaged total volumes by the number of applied laser pulses (N), which is the product of pulse repetition rate (PRR) times the duration of ablation (D), N = PRR·D.

Table 17: Computation of the ablation rates of dentine and enamel.

Setting	D [s]	N	Weight [g]	Difference [g]	Mean Mass-Loss [g]	Mean Volume [cm³]	Mean Volume/Pulse [mm³]
3 W 20 Hz 60% Water 65% Air	15	300	1.161		0.008	0.0037	0.0125
			1.155	0.006			
			1.147	0.008			
			1.137	0.01			
			1.129	0.008			
			1.122	0.007			
			1.113	0.009			

As the density of the composite samples was not known, another method was involved to determine the ablation rates in terms of volume per pulse. Therefore, imprint material commonly used in dentistry was considered. As this material is capable of reproducing tooth structures exactly it was assumed that it fits the demands of the experiment, which are to attach closely to the surface of the cavities, to be able to fill even very small holes and to imprint the cavities accurately without any excess material. As all these issues were confirmed, the laser ablated cavities were weighted, filled with imprint material and weighted again. The difference between the mass values gave the weight $m_{i,c}$ of the imprint model of the cavity. By producing blocks of imprint material with defined volumes V_i and measuring their masses m_i, the density of the material was determined $\rho_i = m_i/V_i$, so that at least the total ablated volume of the cavity could be calculated: $V_c = m_{i,c}/\rho_i$. This procedure was applied for

[25] From www.lib.umich.edu/dentlib/Dental tables/Density.html

all cavities per sample. Finally, the mean ablated volumes per pulse were retrieved in a similar way as for dentine and enamel.

4.1.1.2 RESULTS

4.1.1.2.1 DENTINE AND ENAMEL

As a first aim, the results were compared on basis of the front-panel power settings of the lasers. As both Erbium systems were in use for dental applications, it was expected, that due to regular maintenance the pre-settings and output parameters resemble. Thereby, a direct comparison of the Fotona Fidelis Er:YAG and the Biolase Er,Cr:YSGG ablation rates was possible as exactly the same laser settings could be chosen, i.e. powers of 2, 3, 4, 5 and 6 W and a fixed pulse repetition rate of 20 Hz. The following table lists the obtained results.

Table 18: Mean ablated dentine and enamel volumes per pulse of the Fotona Fidelis Er:YAG and the Biolase Er,Cr:YSGG laser for increasing front panel power settings.

	Power [W]	Ablated Volume per Pulse [mm³]	
		Fotona Er:YAG	Biolase Er,Cr:YSGG
Dentine	2	0.0043	0.0062
	3	0.0067	0.0125
	4	0.0101	0.0181
	5	0.0121	0.0234
	6	0.0161	0.0275
Enamel	4	0.0044	0.0063
	5	0.0059	0.0093
	6	0.0079	0.0115

In general, dentine ablation rates obtained with the Fotona system are about 42 % lower than those of the Biolase system. Concerning enamel, the situation is similar as deviations of ~33 % can be observed. As the absorption coefficient of water (μ_a = 7000 cm^{-1}) for the Er,Cr:YSGG laser radiation is only about 55 % compared to the Er:YAG laser (μ_a = 13000 cm^{-1}) (Stock, 1997), the performance of the Er:YAG laser should be superior.
This discrepancy motivated the measurement of the output parameters of the laser systems. As it turned out, relying just on the front panel power settings is insufficient to develop useful data. Actually, the measured average output powers deviate significantly from the front panel power settings for each laser system. The output powers of the Biolase system are around 13 % higher than the displayed values, whereas the Fotona laser emits on average 31 % less power than indicated. A more detailed discussion of measured Erbium laser parameters can be found in chapter 3.1.
Using the measured laser parameters, a second attempt was made to analyse the ablation rates. The basis for the new discussion is the radiant exposure or fluence. Table 19 lists the ablation rates in this new context. More impressing, Fig. 39 depicts dentine ablation rates versus incident laser fluence in a semi-logarithmic plot.

Table 19: Mean ablated dentine and enamel volumes per laser pulse for the Fotona Fidelis Er:YAG and the Biolase Er,Cr:YSGG laser for varying laser fluences.

	Fotona Er:YAG		Biolase Er,Cr:YSGG	
	Fluence [J/cm²]	Ablated Volume per Pulse [mm³/pulse]	Fluence [J/cm²]	Ablated Volume per Pulse [mm³/pulse]
Dentine	13.5	0.0043	24.9	0.0062
	16.2	0.0067	38.0	0.0125
	21.7	0.0101	51.4	0.0181
	26.9	0.0121	64.1	0.0234
	32.5	0.0161	77.9	0.0275
Enamel	21.7	0.0044	51.4	0.0063
	26.9	0.0059	64.1	0.0093
	32.5	0.0079	77.9	0.0115

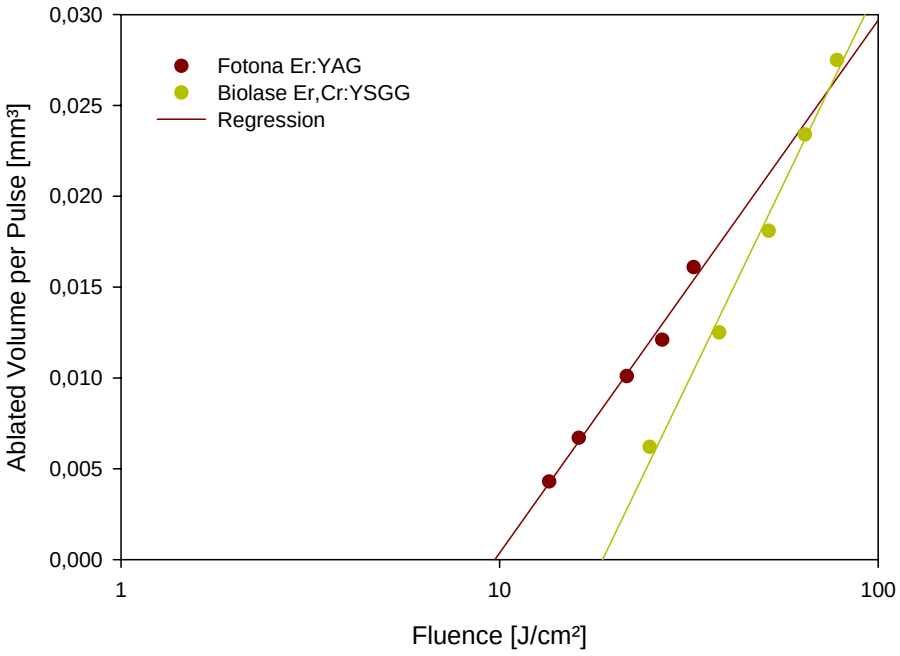

Fig. 39: Erbium laser ablation rates of dentine vs. laser fluence. Brown dots: Er:YAG. Green dots: Er,Cr:YSGG.

Due to different measured pulse energy values and focal spot diameters of the two Erbium laser systems the single fluence values are not directly comparable. Nevertheless, by drawing regression lines, interpretation of the results is permitted. Obviously, in a wide fluence range the ablation rates of the Er:YAG system are higher than that of the Er,Cr:YSGG laser. This finding is in accordance with the above mentioned absorption coefficients of the two laser wavelengths. For higher laser fluences the ablation behaviour turns over, so that the Er,Cr:YSGG laser performs slightly better. This is also in agreement with the results of Vogel and Venugopalan (2003) who report on the changes of the absorption coefficients for both Erbium laser wavelengths with rising fluences. The high absorption coefficient of the Er:YAG laser wavelength declines monotonously with increasing radiant exposure and gets

even less than that of the Er,Cr:YSGG. At fluences where laser ablation takes place the performance of both systems should at least be comparable.
Fig. 40 demonstrates this behaviour referring to the optical penetration depth, which is the reciprocal of the absorption coefficient. For low fluences the optical penetration depth of λ = 2.94 µm lies well below that of λ = 2.79 µm, therefore offering better spatial confinement. Above Φ_0>0.4 J/cm² the opposite is the case. Reaching radiant exposures of ~10 J/cm² the optical penetration depths and therefore the absorption coefficients of both laser sources are comparable.
For the conducted experiments the turning point, indicating higher ablation rates for Er,Cr:YSGG instead of Er:YAG, is located at much higher fluences (>70 J/cm²) than Vogel and Venugopalan suggested. Some reasons to explain this shift can be found: 1) The quoted authors investigated just the optical properties of water and not of dentine. 2) For sure the experimental setup was different. 3) The graphs in Fig. 39 contain not enough data in the region of interest to determine the concrete turning point. The value of >70 J/cm² stated here is a rough approximation and is dependent on various influencing parameters, e.g. temperature.

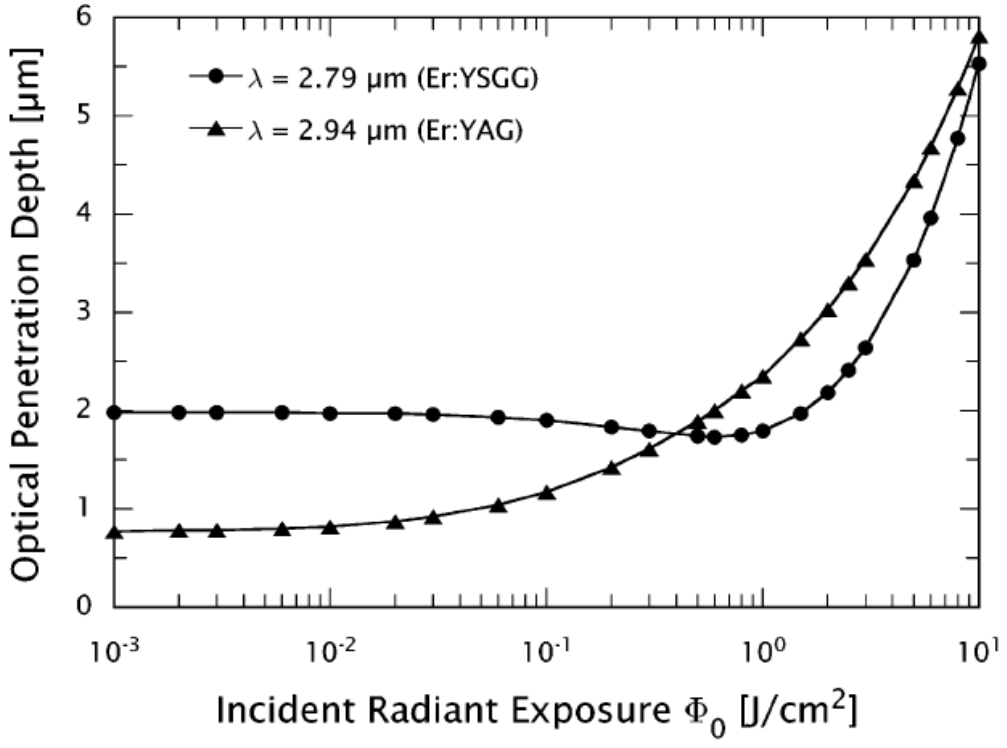

Fig. 40: Variation of the optical penetration depth of water with incident radiant exposure (Vogel and Venugopalan, 2003).

4.1.1.2.2 COMPOSITES

Composite ablation rates were determined with the Biolase Er,Cr:YSGG laser as it has shown the best laser characteristics among Erbium systems. In the following table different types of dental restorative materials and their ablation rates for 1.7 W and 4.5 W laser ablation, corresponding to fluences of 19 J/cm² and 51 J/cm², respectively, are listed. The ablated volumes per pulse were determined with the imprint method.

Table 20: Ablation rates of various dental composite materials obtained with the Biolase Er,Cr:YSGG laser applying fluences of 19 J/cm² and 51 J/cm², respectively.

Composites	Ablation Rates [mm³/pulse]	
	19 J/cm²	51 J/cm²
Tetric Ceram	0.0026	0.0161
Tetric Flow	0.0036	0.0187
Heliomar	0.0041	0.0213
Point 4	0.0047	0.0233
Premise	0.0031	0.0176
Z100	0.0021	0.0156
XRV Herculite	0.0031	0.0176

Although the ablation rates of all composites are on the same scale, deviations among different filling materials are apparent. Ranking the composite samples according to their material removal per laser pulse at 19 J/cm² from the highest to the lowest amount, Point 4 occupies the first position with $47 \cdot 10^{-4}$ mm³/pulse whereas Z100 can be found on the last place yielding $21 \cdot 10^{-4}$ mm³/pulse. The ranking remains consistent for higher applied laser powers. On average, the ablated volume per pulse is about 5.8 times higher for the 51 J/cm² ablation compared to the lower setting.

The effective removal of composite material is guaranteed by its chemical composition and the related absorption of Erbium laser wavelengths. On the one hand, there is enough water present in all composites for strong absorption around 3 µm but also other components like quartz and PMMA resin substantially absorb in the mid-IR region. (Dumore, 2000) Kalachandra et al. (1997) investigated the transmittance of BIS-GMA depending on the wavenumber and report on a reduction of transmittance at a stretching frequency of 3458.32 cm^{-1} corresponding to a wavelength of ~2.89 µm. This broad absorption band belongs to OH-group of BIS-GMA. As the mentioned components are apparent in some of the above listed composites, although in different concentrations, the observed deviations of the ablation rates can be described. For example, the concentration of BIS-GMA in Tetric Ceram is 8.3 wgt.-% whereas Tetric Flow contains 13.6 wgt.-% (Ivoclar Vivadent, 2000). On that basis the higher ablation rates of Tetric Flow may be explained.

Comparing composite ablation rates to that of dentine implicates that selectivity of Erbium laser ablation is not very pronounced. A dentine volume of 0.0181 mm³/pulse ablated with the Er,Cr:YSGG laser at 51 J/cm² fits quite well into the range achieved in composites for the same fluence. While for Z100, Tetric Ceram, Premise and XRV Herculite the tissue removal procedure is slower compared to dentine, Tetric Flow, Heliomar and Point 4 can be removed faster. A clear tendency concerning selectivity valid for all tested materials could therefore not be found.

4.1.2 USPL ABLATION RATES

4.1.2.1 MATERIALS AND METHODS

Ablation rates generated by ultra-short laser pulses were determined using either the 12 ps Nd:Vanadate laser, the 330 fs Yb:Glass laser or the Hurrican-i Ti:Sapphire laser with variable pulse duration. The first experiments were performed with the Nd:Vanadate laser in combination with the r-φ-scanner. The aim was to determine the ablated volume per laser pulse to judge the effectiveness of USPL compared to Erbium systems. Therefore dentine and different composite materials were ablated. Again, the imprint method was used to reconstruct the volume of the cavities so that the ablation rates could be calculated.
Additional ablation rate measurements in composites were done with the Yb:Glass and the Ti:Sapphire laser. Thereby, line scans were conducted. The depths of the remaining grooves were measured out by means of digital light microscopy with implemented software. The motivations for these experiments were manifold: 1. I was interested in the dependence of the ablation rates on varying radiant exposure. 2. The influence of different laser wavelengths on the ablation rates raised some curiosity. 3. And the dependence of composites ablation rates on changing pulse duration afforded some attention.

4.1.2.2 RESULTS - R-Φ-SCANNED ND:VANADATE LASER

The 12 ps Nd:Vanadate laser was operated for a duration of 15 seconds at a pulse energy of 100 µJ and a PRR of 50 kHz yielding 5 W. As the focal spot diameter was 33.7 µm this setting corresponds to a fluence of 11.2 J/cm². Algorithm 2 was applied to the r-φ-scanner. The trace left behind on the tissue surface after one round trip of the scanner can be seen in Fig. 41.

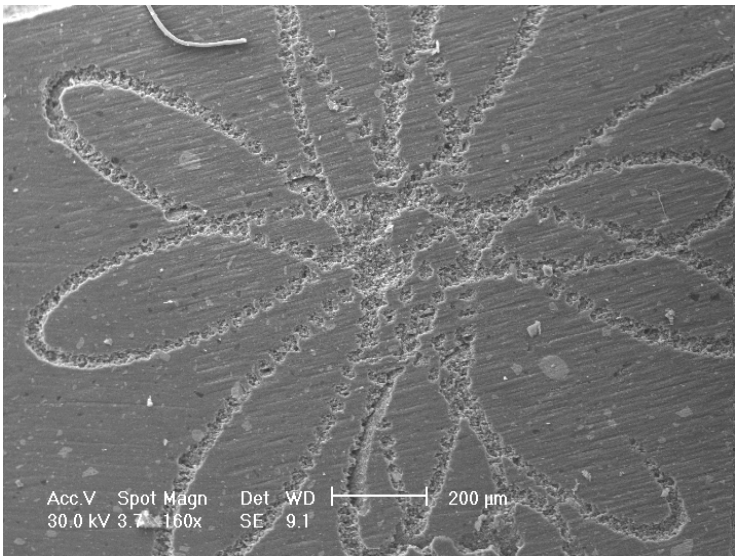

Fig. 41: Pattern resulting from r-φ-scanned 12 ps Nd:Vanadate laser treatment. E_P = 100 µJ, PRR = 50 kHz, D_{foc} = 33.7 µm, Φ = 11.2 J/cm². The trace visible in the ESEM picture is the result of one round trip.

This scanning electron micrograph can serve as evidence, that the overlap of subsequent laser pulses can be assumed to be about zero. This is true for all segments of the curve with exception of the bends. Nevertheless, considering each laser pulse impacting onto a new tissue spot is a quite satisfying approximation. On that basis the ablated volume per pulse was

determined by dividing the total ablated volume by the number of applied laser pulses. The results for composites and dentine are listed in the following table.

Table 21: Ablation rates of dental composite materials obtained with r-φ-scanned Nd:Vanadate laser pulses. Laser parameters: τ = 12 ps, PRR = 50 kHz, E_P = 100 µJ, Φ = 11.2 J/cm².

Composites	Ablation Rates [10^{-6} mm³/pulse]
Tetric Ceram	5.18
Tetric Flow	4.15
Heliomar	5.53
Point 4	5.81
Premise	6.08
Z100	8.71
XRV Herculite	7.88
Dentine	0.32

Among composites Tetric Flow yields the lowest ablation rates with $4.15 \cdot 10^{-6}$ mm³/pulse, Z100 the highest with $8.71 \cdot 10^{-6}$ mm³/pulse. In relation to that dentine ablation rates are one order of magnitude smaller. This is a striking peculiarity that has to be emphasized: In contrast to Erbium lasers the USPL ablation rate for dentine is much lower than that of all investigated composite materials. As secondary caries appears preferably at the rims or underneath of dental restorations, in dental praxis the filling material has to be removed prior the treatment of biological tissue. Therefore, the idea to preferably remove composite resin of old restorations and preserving the dental tissue applies very well for USPL.
Within this context a last aspect should be taken up, which is the speed of the tissue removal process. Therefore USPL ablation at 5 W and Er,Cr:YSGG laser ablation at 4.5 W shall be considered as the average output power can roughly be compared. The amount of tissue removed by a single USLP is a multiple of 10^{-6} mm³ (at least for composites), which is a factor 10^4 less than the corresponding Erbium values. Evidently, this is due to the different pulse energies used, i.e. 100 µJ for USPL and 225 mJ for the Erbium laser. Hence, the comparison of the ablation rates of single laser pulses is not very convenient. A better approach is to look at the total volume ablated during 1 second irradiation. Here the PRR is taken into account as it is one of the main factors influencing the speed of ablation. In case of the Nd:Vanadate laser the PRR was 50 kHz, the Erbium laser has just been operated at 20 Hz. Referring to Table 22 the wide gap between the ablation rates observed for single pulse laser ablation has vanished. For Z100 and XRV Herculite, USPL ablation works even faster than Erbium laser ablation. Just dentine removal lasts >22 times longer when applying the USPL.

Table 22: Total ablated volume after one second laser irradiation with the Er,Cr:YSGG laser at 4.5 W (E_P = 225 mJ, PRR = 20 Hz) and the Nd:Vanadate laser at 5 W (E_P = 100 µJ, PRR = 50 kHz).

	Er,Cr:YSGG 4.5W	Nd:Vanadate 5W
	[mm³/sec]	[mm³/sec]
Tetric Ceram	0.322	0.259
Tetric Flow	0.374	0.208
Heliomar	0.426	0.277
Point 4	0.466	0.291
Premise	0.352	0.304
Z100	0.312	0.436
XRV Herculite	0.352	0.394
Dentine	0.362	0.016

4.1.2.3 RESULTS - LINE SCANS

For further investigations ablation rates were defined as etch depths per pulse. Therefore, the experimental setup had to be modified. For the results presented in the following chapters line scans were performed. The samples mounted on a motorized linear translation stage were moved perpendicular to the incident laser beam with a certain pre-defined velocity. Thereby grooves were generated which afterwards were measured out by means of digital light microscopy with implemented software.

4.1.2.3.1 THEORETICAL BACKGROUND

When line scans are conducted to determine the ablation depth per laser pulse, one has to consider that subsequent laser pulses overlap spatially to some extent because of the dimension of the focal spot area. By this overlap the ablation depth is influenced. To get the etch depth achieved by a single pulse the geometrical overlap factor has to be implemented in the calculation. This was done by introducing the equivalent pulse number according to the following equations (Ivanenko, 2005):

$$n = PRR \cdot w / v \tag{22}$$

$$N_{eq} = N_{pass} \cdot n \tag{23}$$

$$\delta D = D / N_{eq} \tag{24}$$

n is the geometrical pulse overlap factor on the tissue, PRR marks the pulse repetition rate, w is the beam waist at 1/e² level, v is the velocity of the line scan, N_{eq} is the equivalent pulse number, N_{pass} is the number of passes of the scans, D represents the depth of the ablated grooves, and δD is the desired ablation depth per laser pulse.

4.1.2.3.2 YB:GLASS LASER

Line scans were first done with the IC1040-300 fs YB REG AMP Yb:Glass laser described in chapter 3.1.4. Its specifications are a centre wavelength of 1040 nm and pulse duration of 330 fs. It was operated at 1 kHz pulse repetition rate, thereby yielding the maximum average pulse energy of 130 µJ. As it is designed for technical applications the USPL was used in open beam propagation. The beam diameter at the exit of the system was 1.7 mm. After passing a λ/2-plate to attenuate and regulate the pulse energy, the laser beam was directed through a convex lens of 100 mm focal length resulting in a focal spot diameter of ~72.4 µm given at $1/e^2$-level. The samples were fixed on a motorized x-y-z translation stage and positioned in the focal plane of the laser. Grooves of 4 mm length were generated for decreasing pulse energy values from 130 µJ to 10 µJ in steps of 10 or 5 µJ, respectively.
Ablation rates expressed in etch depths per laser pulse were just obtained for composite materials. The results retrieved with the 330 fs Yb:Glass laser are depicted in Fig. 42.

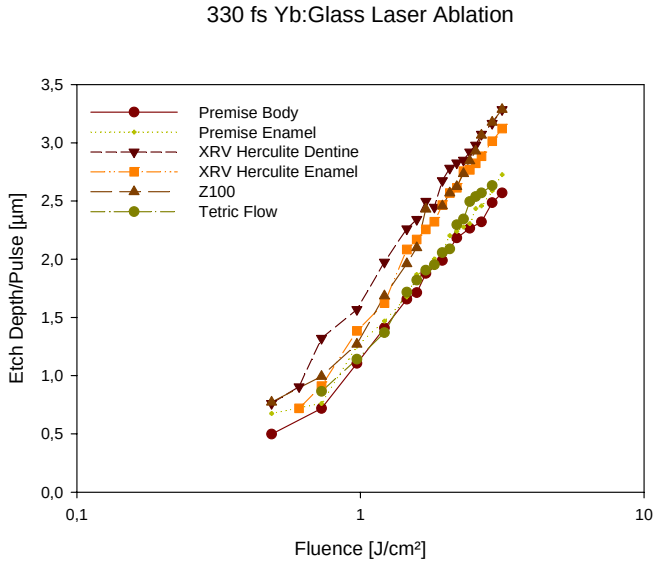

Fig. 42: Correlation between etch depth per pulse and laser fluence of the 330 fs Yb:Glass laser. Data are plotted in a semi-logarithmic plot to show the linear dependence.

For the chosen fluence range the data obey the theoretical law of equation (18) stating the logarithmic dependence of the etch depth on the applied fluence. Besides this, differences in the ablation rates of all composite materials are evident. The highest ablation rates for all applied fluences can be found for XRV Herculite Dentine, the lowest for Premise Body. Very interesting is the comparison of the ablation rates for dentine and enamel restorations, respectively. Intuitively I would expect, that composites for dentine fillings get removed faster that those for enamel restorations as the same situation is given for dentine and enamel themselves. This statement is just valid for XRV Herculite Dentine and XRV Herculite Enamel but not for Premise Body (composite filling for dentine) and Premise Enamel where the differences are not that distinctive.

4.1.2.3.3 TI:SAPPHIRE LASER

The experimental setup for the line scans performed with the Ti:Sapphire laser was similar to the one described before with the exceptions that a lens of 35 mm focal length and another filter to adjust the pulse energy were used. The laser beam diameter was 6 mm. Energy values used for these experiments cover the range between 240 µJ and 40 µJ. The laser was operated at 1 kHz PRR. Pulse durations were adjusted to 150 fs, 500 fs, 2 ps and 7 ps by changing the

position of the gratings inside the system and by controlling it via Michelson-Morley interferometer. The results are presented in Fig. 43.

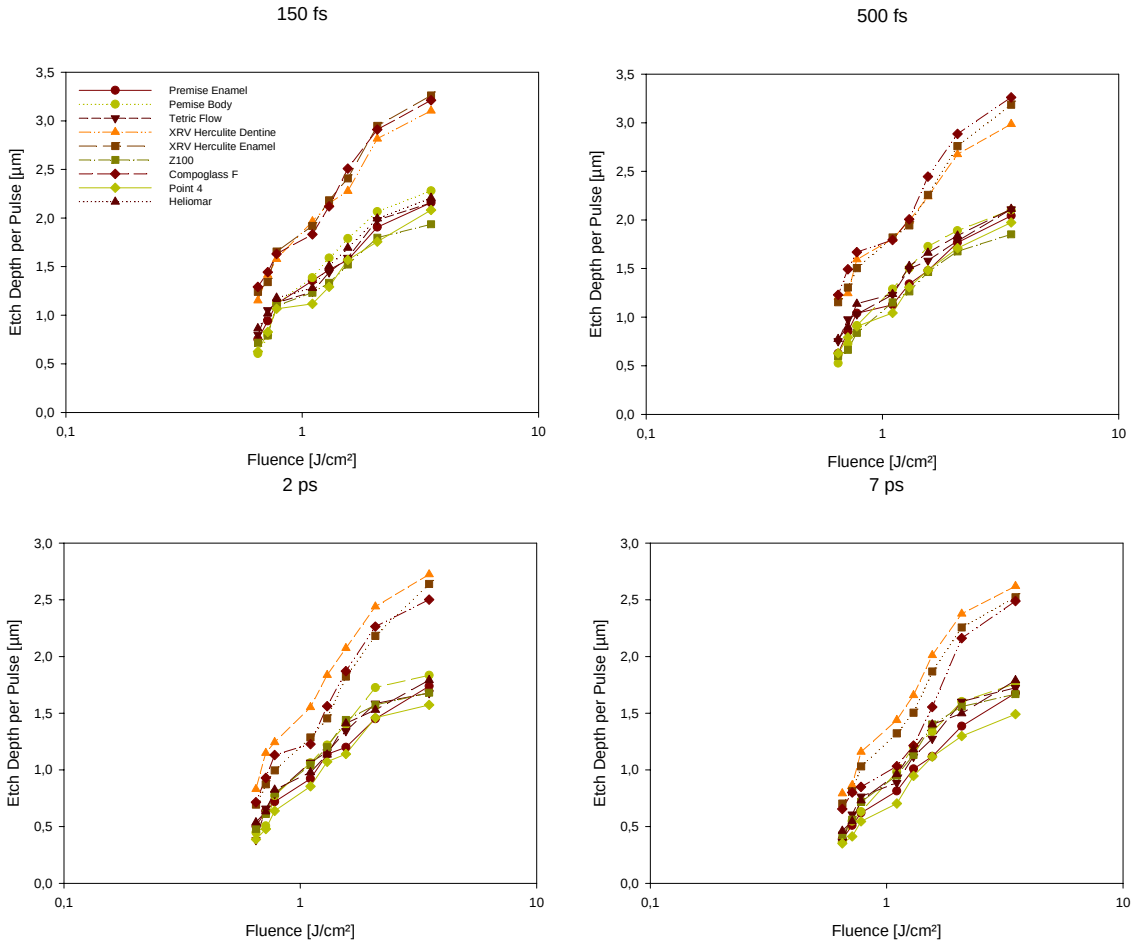

Fig. 43: Semi-logarithmic plots of the ablation rates of various dental composite materials drawn versus laser fluence. Data were generated applying the Ti:Sapphire laser for pulse durations of 150 fs, 500 fs, 2 ps and 7 ps.

It was chosen to depict the data without regression of the single curves. Nevertheless, the arrangement of the data in these semi-logarithmic plots suggests the linear dependence of ablation rates and fluences given by equation (18) anyway. Among all composites XRV Herculite and Dentine as well as Compoglass F expel the largest amount of tissue per laser pulse, while etch depths of all other composites lie clearly below.
Fig. 44 illustrates the correlation between ablation rates and rising pulse durations. Obviously, etch depths per pulse get reduced when elongating the pulse width. This decrease can be observed when turning from 150 fs to 500 fs as well as for changes from 2 ps to 7 ps. This decline is even more pronounced, when stepping from fs to ps.

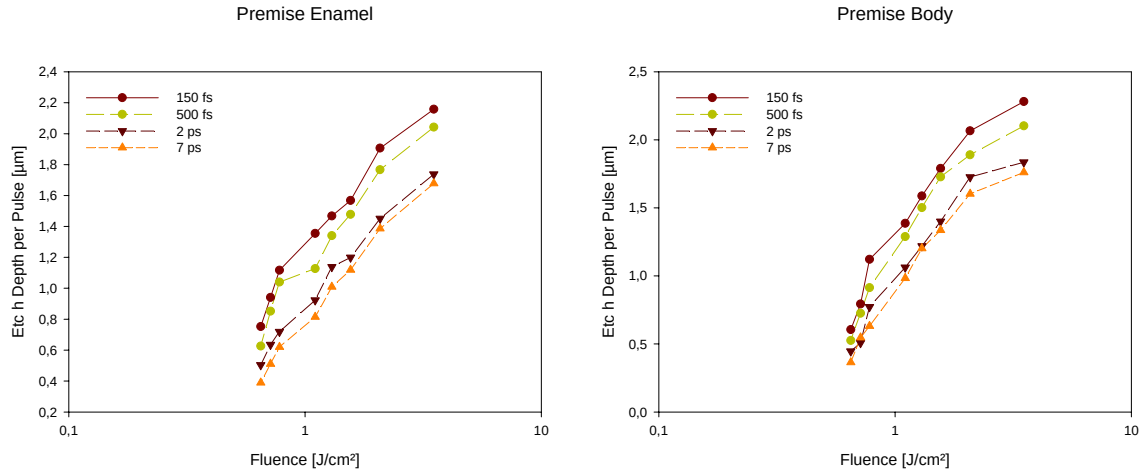

Fig. 44: Etch depth per pulse in Premise Enamel and Premise Body for rising pulse durations.

A last question focusing on ablation rate measurements of composites arises: Which system performs better, the Yb:Glass laser or the Ti:Sapphire laser? As laser ablation with both systems was conducted with different pulse durations, an answer to this question can be provided with some wariness. Insertion of the obtained data for fs laser ablation of Yb:Glass and Ti:Sapphire into one plot reveals that especially for lower fluences, ablation rate values resemble. Fluences above ~1.3 J/cm² lead to higher ablation rates for 330 fs Yb:Glass compared to 150 fs or 500 fs Ti:Sapphire laser ablation. Fig. 45 depicts the situation for Premise Enamel and Tetric Flow. To some extent this behaviour can be explained by enhanced impact ionisation caused by higher pulse energies, as this effect is more impressive for longer wavelengths.

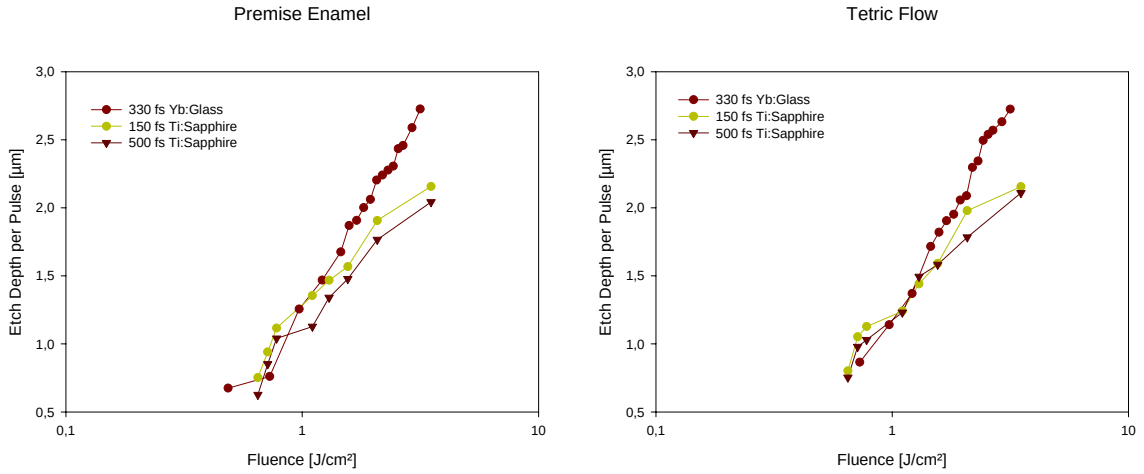

Fig. 45: Comparison of the ablation rates achieved with the Yb:Glass and the Ti:Sapphire laser, respectively.

4.1.3 CONCLUSION

It was shown that material removal by USPL can be very effective when certain laser parameters are applied and that ablation speeds comparable to Erbium systems can be achieved. Moreover, the small ablation rates per pulse compared to Erbium systems ensure precise preparations without any collateral damages. For minimal invasive dental treatments these properties are not enough. Decisive is the potential of selective tissue processing, which was demonstrated for the Nd:Vanadate USPL. A more exhaustive discussion of selectivity is provided in chapter 4.4.

4.2 ABLATION THRESHOLDS

The ablation threshold of a material for a certain set of laser parameters addresses the minimum fluence at which ablation occurs. It is therefore one of the main determinant of laser ablation. In the following, ablation thresholds of dental tissue as well as of composite restorative materials are discussed.

4.2.1 ERBIUM LASER ABLATION THRESHOLD

Erbium laser thresholds were experimentally determined in dentine. For enamel a rough estimation was derived. Nevertheless, other authors have already reported on Erbium ablation threshold of dental structures. A selection of results can be provided.

4.2.1.1 MATERIAL AND METHODS

Again, ablation was performed with the Fotona Er:YAG and the Biolase Er,Cr:YSGG laser for varying fluences. On the basis of ablation rate measurements ablation thresholds were determined. The experimental setup was therefore the same.

4.2.1.2 RESULTS

In Fig. 46 the ablation rates are drawn versus laser fluence. The diagram contains the same information as Fig. 39 in chapter 4.1.1 Just another scaling of the x-axis has been chosen, i.e. a linear scaling. Additionally the equations of the regression lines are captured. The ablation thresholds were established by fitting a regression line to the data and extrapolating it to the abscissa. Dentine threshold values of 5 J/cm² and 8 J/cm² for Er:YAG and Er,Cr:YSGG, respectively, were obtained.

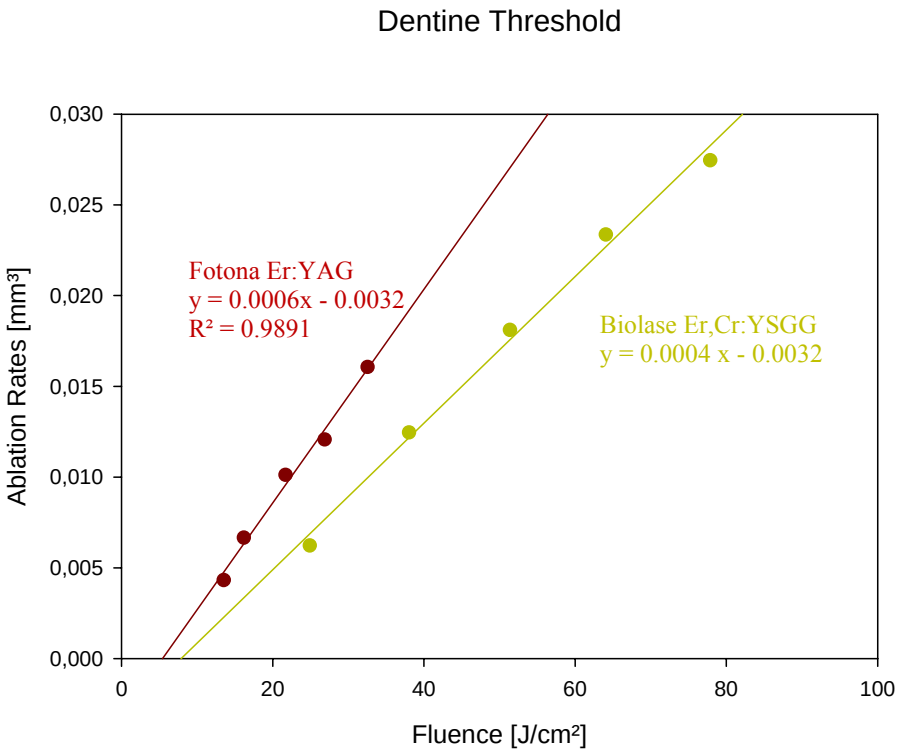

Fig. 46: Determination of dentine ablation thresholds with the Fotona Er:YAG and the Biolase Er,Cr:YSGG laser.

Wannop et al. (1993) investigated 250 µs Er:YAG laser performance and defined a threshold value for dentine ablation of 10 ± 2 J/cm². This value is a little bit higher than the one calculated here. Nevertheless, Wannop et al. worked with 250 µs laser pulses in comparison to ~100 µs involved in the conducted experiments.
Several workgroups have already concentrated on Erbium ablation threshold in enamel. Wannop et al. quoted above report on a threshold of 25 ± 8 J/cm² for their Er:YAG systems. Apel and his colleagues (Apel, 2002 b) experimented with an Er:YAG laser with a pulse duration of 150 µs and got a threshold range of 9-11 J/cm². The same experiments were done with an Er,Cr:YSGG laser yielding 10-14 J/cm². In another report of the group around Apel (Apel, 2002 a) ablation thresholds in enamel for varying pulse durations of the Fotona Fidelis Er:YAG system were discussed. Their results are the following: For 700 µs the threshold is in the range of 9-10 J/cm², for 350 µs pulses a value of 8 J/cm² is recommended and for 150 µs and 100 µs radiant exposures of 7 J/cm² suffice to start the ablation. They themselves compare their obtained values to 7–9 J/cm² determined by Fried et al. (1997), to ~10 J/cm² stated by Hibst et al. (1989) and at least to 8 J/cm² obtained by Belinkov et al. (1993).

4.2.2 USPL Ablation Threshold of Composites

4.2.2.1 Background Information

On basis of equation (17) the threshold fluence can be determined by entering the squared radii of the ablation sites and the applied pulse energies in a semi-logarithmic plot. Regression tools applying the least squares fit and extrapolation $r^2 \rightarrow 0$ allow calculating the ablation threshold. For low fluences the data within this non-linear plot arrange in a line with a slope directly related to the Gaussian beam waist. This method has already been described by J. M. Liu (1982) and its accuracy has been proven to be quite satisfying.

4.2.2.2 MATERIALS AND METHODS

Different methods can be applied to determine the ablation threshold according to the theoretical law mentioned above. The first possibility is to measure out the cavity diameters generated by single pulse laser ablation for varying pulse energies. This method can be modified by using multiple laser pulses hitting a single spot and taking accumulation effects into account. None of them is applicable to the requirements of this study. The aim was to use the same method for all USPL experiments. Although multi-pulse and maybe even single-pulse laser ablation could have been performed for composite materials, bone samples would have caused some problems because of their natural structure. Therefore it was decided to scan the laser beam linearly across the surface of the samples and measure the remaining groove diameters via light microscope.

Laser systems employed were the Yb:Glass laser with 330 fs pulse duration and the Ti:Sapphire laser with 150 fs, 500 fs, 2 ps and 7 ps. The Yb:Glass laser beam passed a λ/2-plate to attenuate the pulse energy. An energy range of 130 µJ to 10 µJ in steps of 10 or 5 µJ was covered. To regulate the pulse energy of the Ti:Sapphire system filters were employed. In contrast to the λ/2-plate, where a continuous reduction of the energy was possible, the filters allowed the adjustment of certain discrete values between 240 µJ and 5 µJ with different increments. Nevertheless, lower energies did not produce any perforation. Therefore a reasonable analysis of the data was limited to the range of 240 µJ to 40µJ yielding less data-points compared to the investigations with the Yb:Glass laser. The thresholds of several composite materials were derived. Fig. 47 captures the regression procedure.

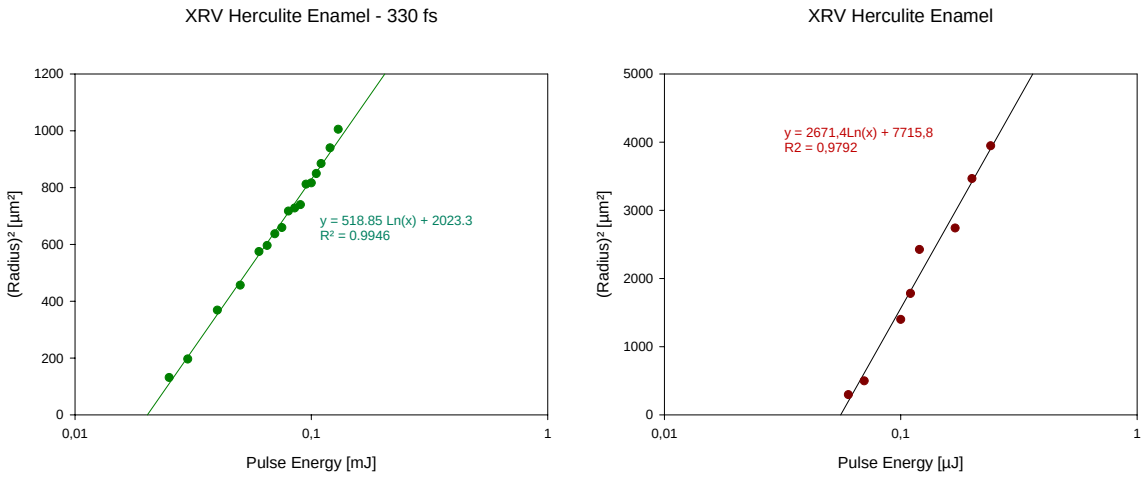

Fig. 47: Determination of the ablation threshold for 330 fs Yb:Glass laser ablation (left) and 500 fs Ti:Sapphire laser ablation (right) of XRV Herculite Enamel.

4.2.2.3 RESULTS

Ablation thresholds for both laser systems and all investigated materials are listed in the following tables.

Table 23: Thresholds of 330 fs Yb:Glass USPL ablation of different composite materials.

Composite Material	Ablation Threshold [J/cm²]
Tetric Flow	0.75
Premise Enamel	0.61
Premise Body	0.48
XRV Herculite Enamel	0.62
XRV Herculite Dentine	0.43
Z100	0.61

Table 24: Ti:Sapphire laser ablation thresholds of different composite materials for 150 fs to 7 ps.

	Ablation Thresholds [J/cm²]			
Pulse Duration	Compoglass F	Premise Enamel	Premise Body A2	Heliomar A3
150 fs	0.27	0.30	0.35	0.24
500 fs	0.44	0.38	0.43	0.35
2 ps	0.56	0.58	0.51	0.48
7 ps	0.60	0.63	0.58	0.59

	Ablation Thresholds [J/cm²]				
Pulse Duration	Tetric Flow	XRV Herculite Dentine	XRV Herculite Enamel	Point 4	Z100
150 fs	0.25	0.25	0.30	0.36	0.27
500 fs	0.39	0.34	0.33	0.48	0.44
2 ps	0.57	0.44	0.53	0.51	0.46
7 ps	0.64	0.54	0.56	0.56	0.59

For each considered laser system and specific pulse duration the ablation thresholds of all composite types are within the same fluence range, e.g. for 150 fs Ti:Sapphire ablation Heliomar A3 possesses the lowest threshold with 0.24 J/cm² and Point 4 the highest with 0.36 J/cm². A similar interval just shifted for about 0.10 J/cm² to the right along the fluence axis can be found for other pulse durations: 500 fs – [0.33 J/cm², 0.48 J/cm²], 2 ps – [0.44 J/cm², 0.58 J/cm²], 7 ps – [0.54 J/cm², 0.64 J/cm²]. 330 fs Yb:Glass laser ablation gives threshold values between 0.43 J/cm² and 0.75 J/cm². Although 330 fs pulse duration is located between 150 fs and 500 fs, the ablation thresholds of both laser systems in this regime differ. With the exception of XRV Herculite Dentine and Premise Body, thresholds of the Yb:Glass laser exceed even 500 fs thresholds of Ti:Sapphire. The reason therefore is surely the difference in the wavelength of the laser systems.

4.2.3 ABLATION THRESHOLD OF DENTINE AND ENAMEL

For sound dentine and enamel and also for carious dentine ablation thresholds obtained with a Ti:Sapphire laser can be derived from literature. Serbin et al. (2002) focused on laser ablation of tooth substances with pulse durations from 120 fs to >2 ps. Ablation thresholds were determined after directing 100 pulses onto the tissue surface and analysing it in a scanning electron microscope. Their results are depicted in Fig. 48.

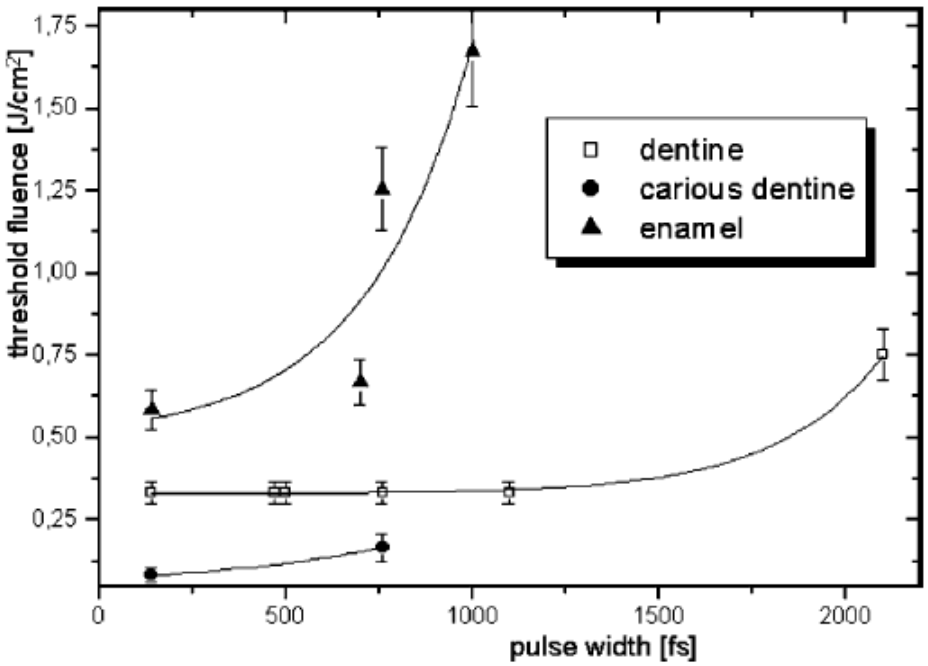

Fig. 48: Dependence of the ablation threshold on the pulse width of the applied laser pulses. (From (Serbin, 2002))

For 120 fs Ti:Sapphire laser ablation the highest threshold was found for sound enamel with > 0.5 J/cm² followed by sound dentine with >0.3 J/cm². Carious dentine revealed a threshold of just <0.12 J/cm². Similar values can be stated from Lubatschowski et al. (2002). For all applied pulse durations composite thresholds of this study are lower than enamel thresholds reported by Serbin et al. Pulse durations of 150 fs and 500 fs yield comparable values for composite and dentine, while for longer pulse widths dentine thresholds are situated well above composite thresholds (~2 ps correspond to a threshold of 0.75 J/cm² in dentine). That implies that selectivity is very pronounced for enamel and composite ablation. Distinct ablation thresholds of composite and dentine appear just at higher pulse durations.
B. M. Kim et al. (2001) determined ablation thresholds for dentine for a broader range of pulse durations, i.e. 130 fs to 20 ps. The laser system employed was the Spectra-Physics Tsunami with λ = 800 nm. It was found that the threshold for dentine increases with the square root of the pulse duration for pulses longer than 5 ps. The threshold scaling differs from $\tau^{1/2}$ when the pulse duration is shorter than 5 ps. To give some examples, for 130 fs a threshold fluence of 0.75 J/cm² was derived, which is already higher than the values listed in Table 24 for 150 fs ablation of composites, for 20 ps 3.8 J/cm² are already necessary to start the tissue removal procedure. Rode et al. (2003) again worked with Ti:Sapphire and 95 fs and 150 fs, respectively. For both pulse durations the obtained threshold in enamel was 2.2 ± 0.1 J/cm². Neev et al. (1996 a) concentrated on 350 fs Ti:Sapphire laser ablation. Thresholds of 0.5 J/cm² for dentine and 0.7 J/cm² for enamel are reported and compared to 20 J/cm² for 1 ns laser ablation in dentine. Seka et al. (1996) applied also 350 fs laser pulses to get the ablation

threshold of dentine. In contrast to Neev et al. (1996 a) a wavelength of 1053 nm was used. The corresponding threshold fluence was ~1 J/cm² and therefore slightly higher than that of 350 fs Ti:Sapphire ablation. For composite ablation with the Yb:Glass laser at λ =1040 nm and τ = 330 fs thresholds between 0.4 J/cm² and 0.7 J/cm² were determined (see Table 23). A vague comparison between 350 fs ablation at 1053 nm of tooth and 330 fs ablation at 1040 nm of composites suggests selectivity in this case.

4.2.4 CONCLUSION

Summing up and neglecting thereby the slight deviations between single threshold values, USPL thresholds of tooth substances and restorative materials are in any case lower than Erbium thresholds, with 5-8 J/cm² in dentine and even more in enamel. Moreover, USPL tend to need lower fluences to start composite ablation than tooth ablation. In general higher ablation thresholds for tooth structures compared to composites are favourable to be able to perform selective and therefore minimal invasive treatment. Although distinct ablation thresholds for different tissue types support this effect, they are not sufficient to guarantee selective treatment. In this context, also ablation rates have to be considered which are discussed in chapter 4.1. Only a combination of lower ablation thresholds and higher ablation rates for composite fillings in contrast to dentine and enamel, respectively, leads to secure and differentiated ablation.

4.3 MORPHOLOGY

4.3.1 TREATMENT WITH A MECHANICAL DRILL

As commonly dental drills are used for cavity preparations some micrographs of the remaining morphology are provided in Fig. 49 and Fig. 50. The crack in Fig. 49 arose from dehydration during ESEM investigation. Although the morphology of drilled cavities is often referred to as very smooth and even the pictures below give another impression. Obviously, several steps were caused on the cavity inclinations by the shape of the drill. The surface is branded by the rotation of the drill visible as stripe like traces. As expected the whole cavity is covered by a smear layer. Therefore an etchant has to be applied to open the tubuli and make them permeable for the primer to form tags for retention. Fig. 51 depicts the magnification of a cavity rim after etching.

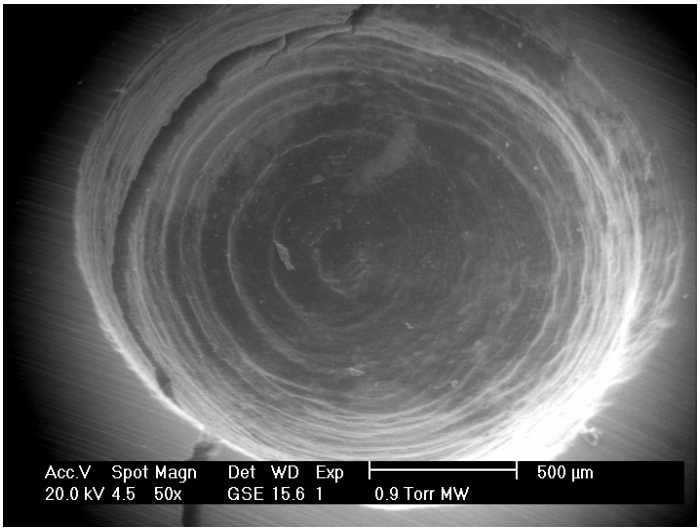

Fig. 49: Overall view onto the drilled cavity.

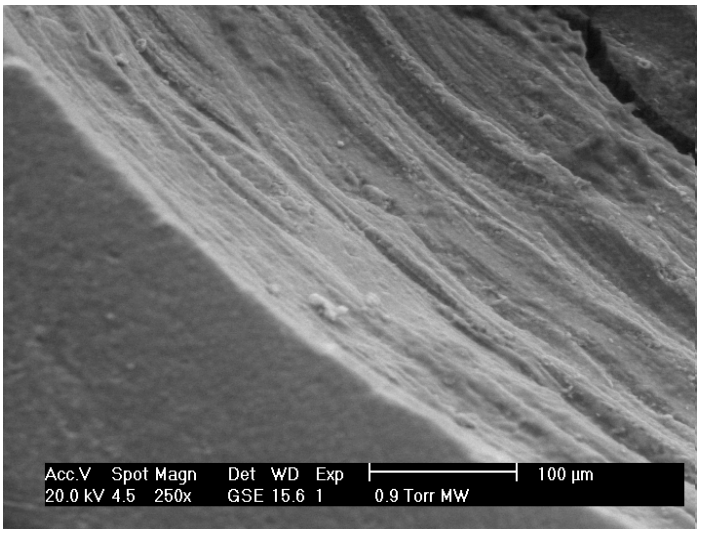

Fig. 50: Magnification of the cavity rim. The produced smear layer covers the dental tubuli.

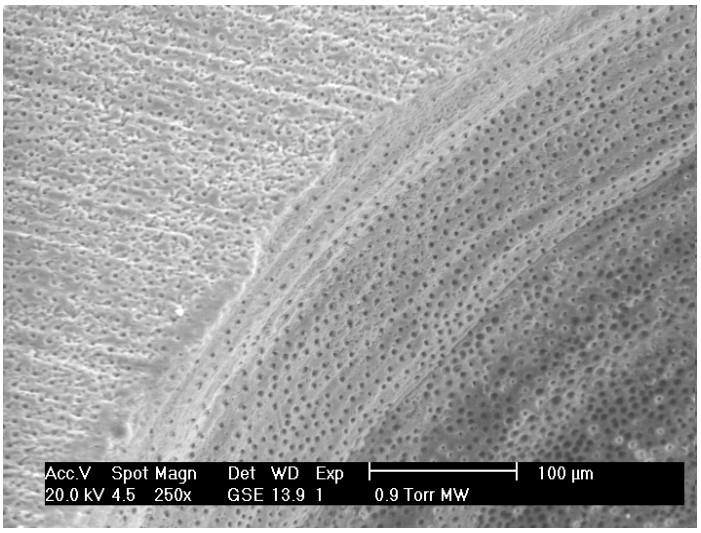

Fig. 51: Magnification of the cavity rim. After etching the dental tubuli are opened.

4.3.2 ERBIUM LASER TREATMENT

4.3.2.1 MATERIAL AND METHODS

Dentine of human permanent teeth was exposed by removing the uppermost enamel layer by means of a diamond saw under water cooling. The Biolase Er,Cr:YSGG laser was applied with a power of 3.5 W and 5 W, respectively with the cooling air-water spray. Cavities were generated free hand. Scanning electron micrographs were obtained.

4.3.2.2 RESULTS

The cavity shapes generated by Erbium laser ablation strongly depend on the skills of the surgeon. Therefore, not too much attention shall be paid on the appearance of the entire cavity. Nevertheless, typical for Erbium treated tissue is, that the cavity rims are not as exactly defined and as sharp as for the drill shown above.

Following some suggestions of a practitioner, Er,Cr:YSGG laser processing of dentine was performed with an average output power of 3.5 W. Thereby an air-water spray with 65 % air and 55 % water was used. The surface shown in Fig. 53 was made with this setting. It captures the characteristic scaly surface with its unevenness and irregularities. Some micro-cracks indicated by the red bars are visible. With the setting of 3.5 W the dental tubuli are open. As discussed later on, this surface does not satisfy the demands for good adhesion between restoration and tooth structure. Additional etching might therefore be necessary.
The higher average power of 5 W leaves a different surface. As obvious in Fig. 54, the chosen combination of laser power and air-water spray was inadequate. The surface is all over covered with melting, which can be identified as round artefacts. Even the dental tubuli are sealed as a result of melting.

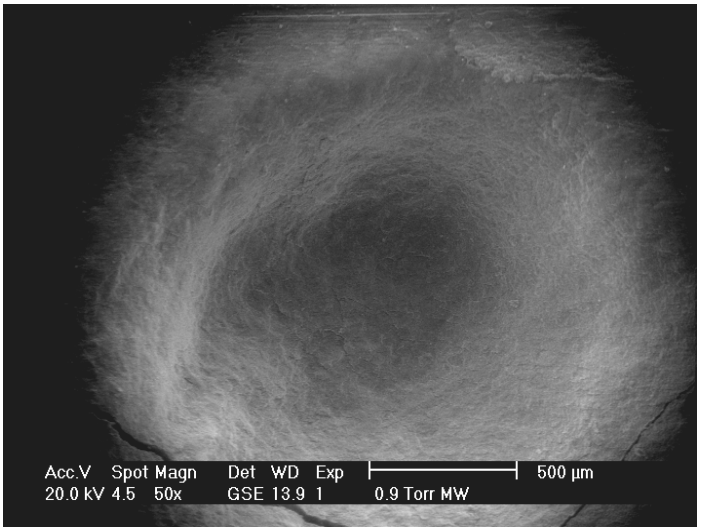

Fig. 52: Cavity in dentine excavated by the Er,Cr:YSGG lasert.

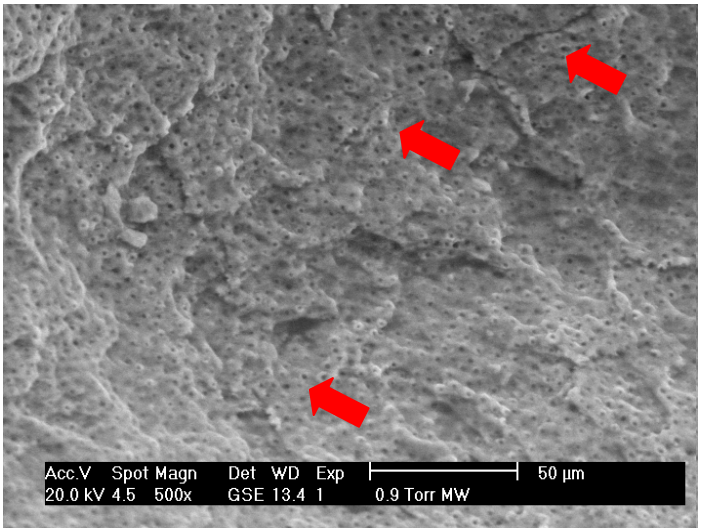

Fig. 53: Morphology of Er,Cr:YSGG laser treated dentine with 3.5 W output power.

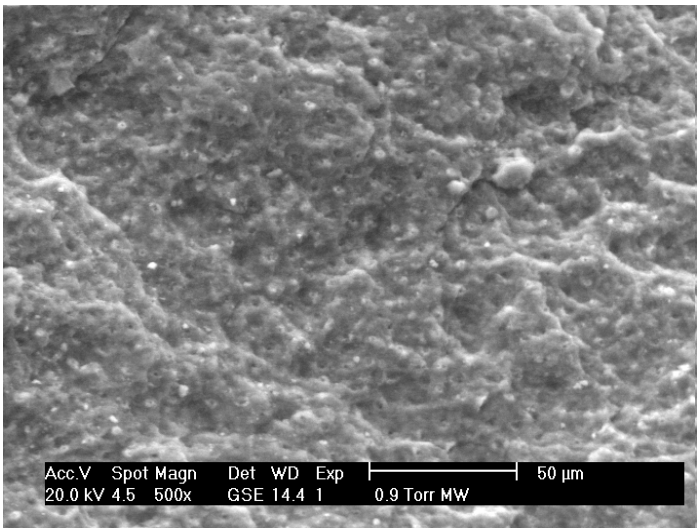

Fig. 54: Morphology of Er,Cr:YSGG laser treated dentine with 5 W output power.

4.3.3 USPL TREATMENT

USPL processing requires high power densities (up to TW/cm²) to generate free electrons via multi-photon absorption for plasma formation. To reach these high power densities strong focusing of the laser beam onto the tissue surface is necessary. The resulting spot diameters, usually some ten µm to ~0.1 mm, are that small that they are just suitable for micro-preparations. Treatment of larger areas makes scanning inevitable. Besides that, scanning of the laser beam hinders consecutive pulses from impacting onto the same spot on the tissue surface thereby avoiding certain accumulation effects: With an increasing number of pulses applied onto the same spot the ablation efficiency per pulse drops. (Kim, 2001) A crater produced by a single pulse with Gaussian beam profile has a slightly conical shape. This conical shape gets even more pronounced when a series of Gaussian pulses hits the same tissue spot. (Rubenchik, 1999) The deeper small cavities and therefore the steeper the cavity inclinations, the more they act as hollow waveguides, i.e. incoming light is scattered and multiply reflected as well as partly absorbed by the cavity walls. Thus a significant part of the pulse energy gets lost on its way to the hole's ground where the next ablation should occur. (Strassl, 2002) In this context, the heat transfer to the surrounding tissue layers is another aspect to be considered when a longer pulse train is delivered to the same tissue spot. The pulse energy absorbed by the cavity walls is insufficient to ablate material, but causes some temperature rise in the adjacent tissue instead. (Niemz, 1996) Summing up, the deeper the cavities, the more energy is absorbed by the walls and converted into heat. Thereby, the ablation efficiency is reduced, as just a small fraction of pulse energy is left for the actual ablation process on the bottom of the cavity.

In the conducted experiments USPL ablation of dentine has been performed employing the prototype r-φ-scanner. According to the selected scan algorithms, each laser pulse hitting the tissue surface can be considered to be the first one as the overlap of subsequent pulses is almost zero. Thus, the mentioned unwanted accumulation effects can be avoided. The function of the r-φ-scanner and the correspondence between simulation and experiments has already been discussed in chapter 3.2.1. In the following, morphological aspects of circularly scanned USLP are emphasized.

4.3.3.1 MATERIALS AND METHODS

Morphological analysis of scanned USPL ablation involved the Yb:Glass IC-1040-400 fs REG AMP laser with a centre wavelength of 1040 nm. Its regular pulse width of 350 fs was extended to 700 fs to protect the scanner components from excessive and therefore harmful power densities. A PRR of 1 kHz and a pulse energy of 100 µJ were adjusted. The second laser applied was the Nd:Vanadate IC-1500 REG AMP laser, with a wavelength of 1064 nm and a pulse length of 12 ps. It was operated at 5 kHz with a pulse energy of 120 µJ. Both laser systems are described in chapter 3.1. Experiments were performed in dentine applying algorithm 2 as well as algorithm 13.

4.3.3.2 RESULTS

Scanning electron micrographs of dentine ablated with 700 fs Yb:Glass laser pulses following traces according to algorithm 2 are depicted in Fig. 55 to Fig. 57. 12 ps Nd:Vanadate laser ablation applying algorithm 13 are captured in Fig. 58 and Fig. 59. Comparing the shape of the ESEM cavities to the discussed Matlab simulations and the energy density distribution captured by the CCD beam profiler, the similarity is obvious. Slight deviations just occurred in the middle of the ablated craters, where the central peak is not as developed as predicted by the simulations. This is a result of accumulation effects. Nevertheless, the geometry of the entire cavities is impressing anyway. Remarkable are the very sharp rims and the geometrically well-defined surfaces reflecting the scan pattern. The riffled structures on the bottom and inclinations are caused by interference phenomena in the scan pattern. These phenomena occur due to interferences between the rotation frequency of the rotating prism and the oscillation frequency of the galvo mirror. In Fig. 56 a magnification of this riffled pattern on the cavity inclination typically for algorithm 2 is presented. For algorithm 13 interference phenomena lead to wave-like structures on the cavity bottom which can be seen in Fig. 59. These fine micro-structures enlarge the surface of the cavity and may yield favourable conditions for good compound with restorative material. Moreover, complete absence of a smear layer and exposed dental tubuli might allow a direct application of restorative materials in dentine without previous etching. In Fig. 57 showing a further magnification of the cavity rim and its inclination the opened tubuli are obvious. In none of the micrographs signs of molten or re-solidified zones, micro-cracks as well as split off debris can be identified. The non-existing collateral damages give evidence of the absence of thermal load and shock waves. (The large cracks appearing in the general views of the USPL cavities happened during ESEM analysis due to desiccation.) The overall impression of USPL cavities is therefore much superior the drilled or Erbium laser processed dentine.

Concerning the scan pattern itself, some improvements have to be made. The stair-like structures in the side walls corresponding to the circles visible in the top views of the cavities are the results of the alignment imperfections of the rotating prism. As explained earlier, the prism consists of two parts separated by an air gap. The prism faces of the used prototype r-φ-scanner are not fully parallel, therefore introducing a tumbling error. Nevertheless, with the available experimental setup this error could not be eliminated. In further improvements of the scanner this imperfection has to be corrected to achieve uniform scan patterns. In general, this prototype scanner is very sensitive to adjustments and exterior influence like temperature changes. To demonstrate this, the micrograph in Fig. 58 was chosen. In that case, the off-set was not arranged correctly leaving the middle part of the cavity untouched. On the other hand, when the adjustments were made accurately a central peak of laser energy generated a hole as the laser beam crossed this area more often according to the scan algorithm. To achieve well-balanced cavity geometry approaching flat top profile a shutter has to be implemented to spare this central region from excessive ablation.

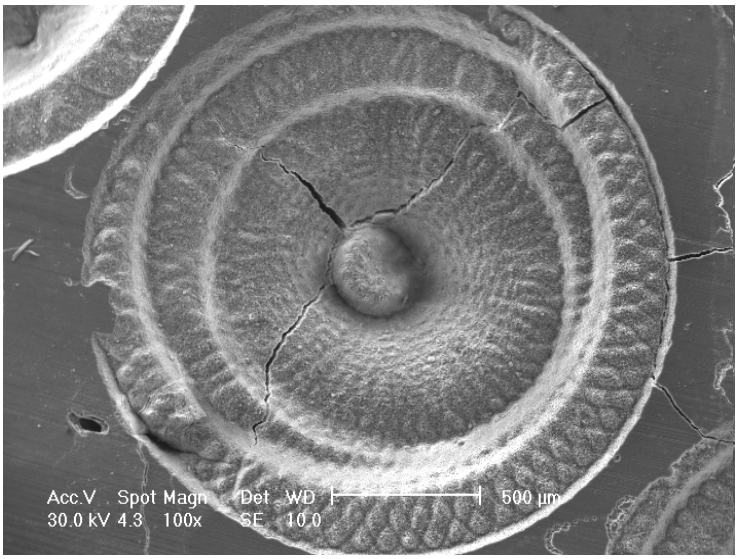

Fig. 55: SE micrograph of an r-φ-scanned cavity in dentine. Yb:Glass laser, τ = 700 fs, E_P = 100 µJ, PRR = 1 kHz, algorithm 2. The cracks originate from dehydration during ESEM investigation.

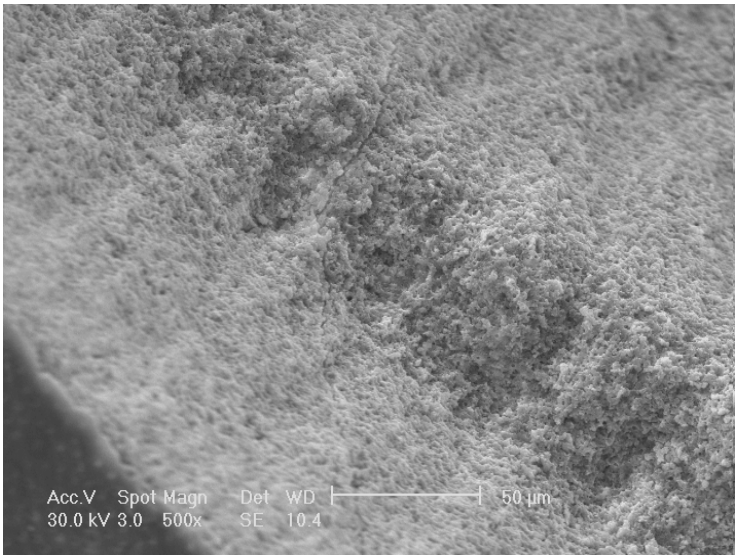

Fig. 56: View onto the inclinations of the cavity shown in Fig. 55. The fine micro-retentive pattern is visible as well as a regular surface morphology left after r-φ-scanned USPL ablation.

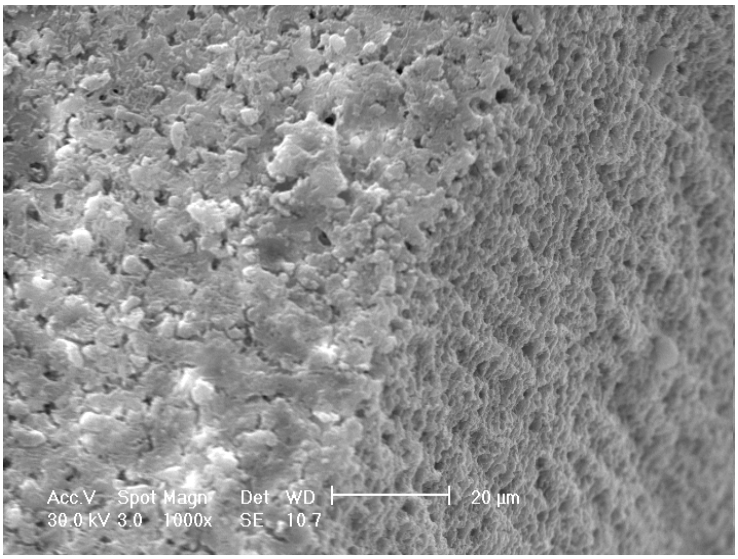

Fig. 57: Magnification of the defined rims of the cavity depicted in Fig. 55. The inclinations demonstrate the absence of a smear layer. There is no evidence of carbonisations or melting.

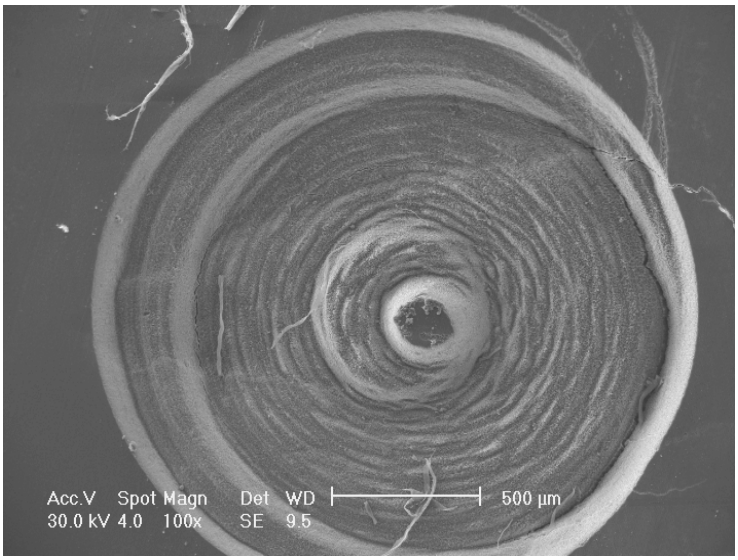

Fig. 58: SE micrograph of a circularly scanned USPL cavity in dentine applying algorithm 13. Nd:Vanadate laser, τ = 12 ps, E_P = 120 µJ, PRR = 5 kHz. The crack along the inner circle appeared during ESEM analysis.

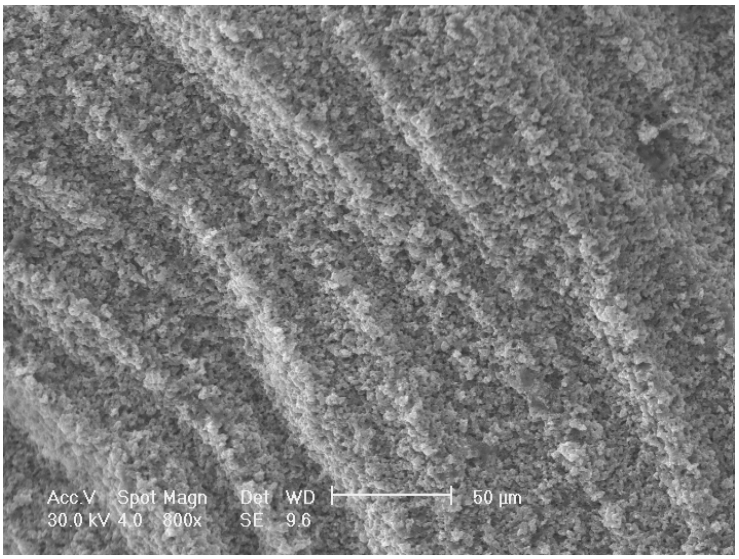

Fig. 59: Magnification of Fig. 58 capturing the cavity bottom. The wave-like structure associated with algorithm 13 is visible. Open tubuli, no melting, carbonisation or micro-cracks are some of the benefits to be seen in the micrograph.

For practical realisation the misalignment of the scanner prism has to be removed, the sensitivity of the scanner components have to be improved and a shutter has to be implemented to achieve the desired geometrical features. Besides these geometrical issues which can be handled, the surface resulting from scanned USPL ablation has proven to be of high quality. As USPL ablation of dentine was performed with 700 fs and 12 ps the question arises, which pulse duration yields the better results and is therefore more suitable for dental hard tissue removal? Analysing the surface morphology of the cavities generated within this study nearly no difference can seen between the shorter fs and the longer ps laser ablation, neither macroscopically nor microscopically. Including the results of other workgroups suggest that shorter pulse duration yields the better surface morphology.
Niemz M. H. (1994) reports on 30 ps Nd:YLF laser ablation of enamel with 1 kHz PRR, 1 mJ pulse energy and a focal spot diameter of 30 µm giving a fluence of 141 J/cm². He created 1x1 mm² cavities by scanning the laser beam as well as holes by fixing the beam position and applying 1000 pulses onto the same spot. Distributing the laser pulses spatially over the target left no signs of thermal damage. The hole generated by the pulse train was surrounded by a zone of molten substance within a distance of 100 µm. Niemz concluded, that these results prove that ps laser pulses can induce thermal damage, if more heat is generated than diffused per unit time during a multiple overlap of consecutive pulses. Similar results were published by Niemz M. H. (1995) when he also concentrated on the ablation of human dentine. The same laser system was used to generate cavities with square or circular geometries. The cavity features with precise, clean and sharp edges and conditioned bottom for good adhesion of filling materials are quite satisfying. Neev et al. (1996 a) worked with 350 fs Ti:Sapphire laser on enamel and dentine. They applied 100 laser pulses with a fluence of 1 J/cm² for dentine and 3 J/cm² for enamel at 10 Hz onto the same tissue spot and observed little evidence of molten hydroxyapatite. Exposed tubuli are present in dentine. In general, a clean and damage-free surface was detected. Kim et al. (2001) performed laser ablation of dentine with the Spectra-Physics Tsunami laser at 1 kHz for pulse durations of 130 fs, 1 ps, 5 ps and 10 ps with fluences two times the ablation threshold, which were 0.75 J/cm² for 130 fs, >1 J/cm² for 1 ps, <2 J/cm² for 5 ps and about 2.7 J/cm² for 10 ps. They observed differences in ablation crater morphology for cavities generated with 130 fs-1 ps and 5 ps-10 ps. Walls and edges of the craters created by pulse durations of 1 ps and shorter show comparatively smooth

surfaces. Dentine tubules were mostly intact and open. 5 ps and 10 ps show rough surfaces and molten edges. They concluded, that a larger fraction of absorbed energy of 5 ps and longer is used for heating the material rather than for material removal, which also results in a reduction of the ablation efficiency. Several authors who investigated USPL ablation of tooth structures can be cited. Surely, all of them used different laser systems, laser parameters and experimental set-ups, so that their experiments and their results are individual. As this short excerpt of publications shows, no clear and generally valid answer can be given, if fs or ps laser pulses perform better. It is not just a matter of pulse duration but also of many other parameters influencing the ablation quality, i.e. PRR, scan algorithm and scan speed which are mainly feeding accumulation effects as well as the pulse energy. On the one hand the pulse energy is manifested in the fluence, which is necessary to start the ablation, on the other hand the pulse energy together with the pulse duration are responsible for heat conduction. So if the set of laser and scanner parameters used for tissue ablation is well balanced even with ps laser pulses excellent results can be achieved.

4.4 SELECTIVITY

After fitting the composite into the processed cavity, the pasty filling material has to be light cured to finish the restoration procedure. The composite material polymerizes and hardens. Due to polymerisation the bulk material shrinks to a certain extent depending on the composition of the dental restorative mass as well as on the diligence of the dentist. As a consequence of shrinkage gaps between restoration and tooth surface are caused leading to unsealed regions. The restored site is therefore susceptible for bacteria infiltration. The result is that secondary caries appears, commonly at the rims of existing restorations or underneath them. A further dental treatment is then necessary to remove that newly built caries. By that, first the composite material has to be removed to expose the caries affected regions which are treated in a second step. Selective removal of different types of tissues is the basis for minimal invasive treatment. In general, laser systems possess the potential of selective material ablation which is already expressed by distinct ablation thresholds and ablation rates.

4.4.1 ERBIUM LASER TREATMENT

For a fixed set of parameters the amount of material removed by Erbium laser depends on the water content of the tissue. For dentine and enamel the situation is clear: Dentine incorporates more water then enamel, ergo the ablation rates of dentine are higher than that of enamel. This was proven in chapter 4.1.1 where also composite ablation rates were stressed. Now, some more interest is paid on selective removal of tooth substance and composite material.

4.4.1.1 MATERIALS AND METHODS

Enamel and dentine of extracted human molars were used for the experiments. To expose dentine, the occlusal enamel of some tooth samples was removed by means of a diamond saw. Afterwards, grooves were made in enamel as well as dentine using a common mechanical drill. According to the manufacturer's instructions, the filling procedure was performed, applying etchant, bonding and composite material (Tetric Flow). The laser system employed for these investigations was the Biolase Waterlase Er,Cr:YSGG. As just qualitative aspects were considered, the hand-piece was simply held by hand without fixation. The sapphire tip was moved slowly across the dentine-composite border. The ablation sites were examined via ESEM.

4.4.1.2 RESULTS

For dentine ablation a power of 2.25 W and an air-water mixture of 65 % air and 55 % water were adjusted on the front panel of the laser system, in case of enamel ablation a power of 3.75 W, 95 % air and 80 % water were chosen. The obtained micrographs are shown in the following.

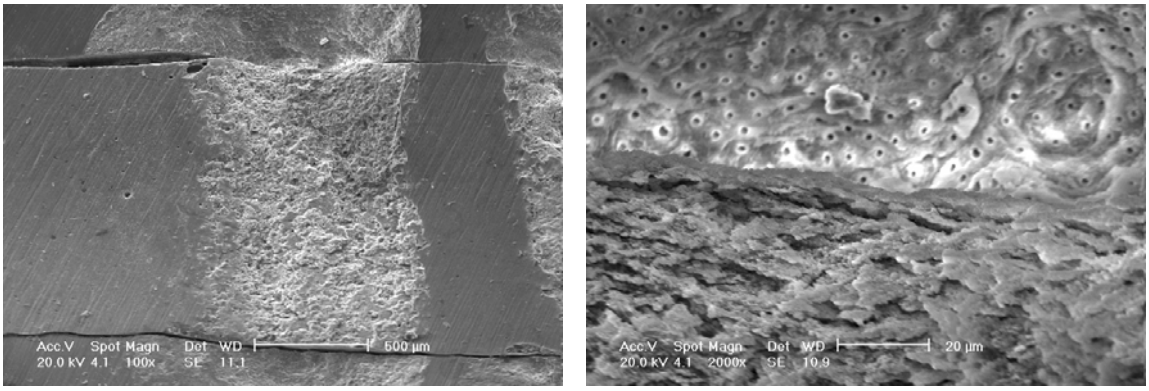

Fig. 60: Scanning electron micrograph of the selective Erbium laser ablation of composite and dentine. Left: The composite bulk is surrounded by dentine. The laser beam crossed the composite-dentine border perpendicularly. Right: Magnification of the border at the ablation site. Dentine can be identified by its opened tubuli.

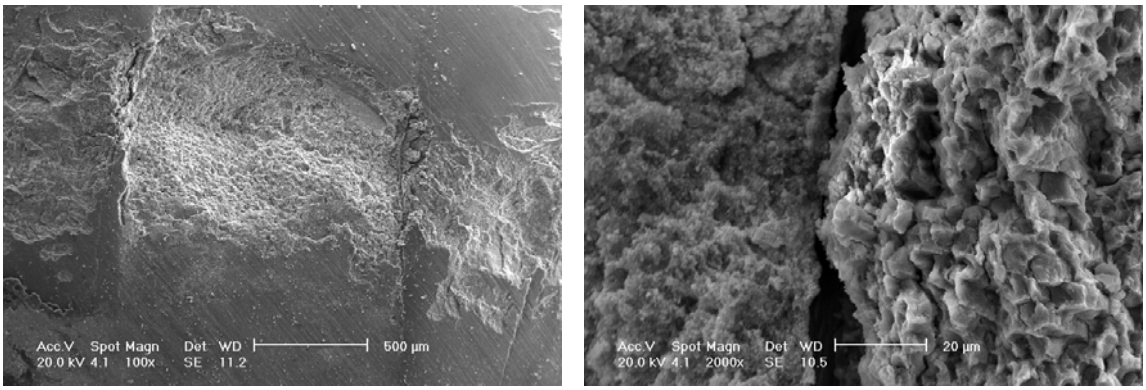

Fig. 61: Erbium laser ablation of enamel and composite. Left: Composite can be seen in the middle part of the ESEM. Enamel is adjacent on both sides. The laser beam was directed across the border. Right: Magnification of the border. Enamel prisms on the right side of the image are obvious.

In Fig. 60 the composite filled groove visible as horizontal bar can easily be distinguished from the adjacent dentine. Obviously, the Er,Cr:YSGG laser ablation with the chosen setting is quite selective. Comparing Tetric Flow and dentine ablation sites, the amount of material removed by the laser is higher for dentine. Also other laser settings were tested in this context yielding mainly the same results. In some cases, selectivity is not as pronounced, i.e. that a preference for stronger ablation of dentine or composite, respectively, cannot be discerned. Indeed, this behaviour is not favourable for minimal invasive treatment of biological tissue. Nevertheless, one has to note that this finding cannot be generalized. For other types of composite material and different laser parameters the outcome may be different. Anyway, these investigations can just give a visual impression of the accurate results obtained for ablation rate measurement presented in chapter 4.1. The same is valid, if enamel and

composites are concerned. Due to the higher ablation threshold and the lower ablation rates of enamel compared to composites selective ablation is more advantageous. A look at Fig. 61, where enamel appearing at the left and right side of the micrograph gets less ablated than composite, confirms this.
At this point, the morphology of the ablation sites shall also be mentioned. In the magnification of the dentine-composite border in Fig. 60 dentine can easily be identified by the small black spots representing the opened tubuli. The dentine surface appears relatively smooth with some wave-like ripples. Especially in the left upper part of this SE image irregular micro-cracks are visible. Moreover, also some signs of molten and re-solidified deposits are evident. These artefacts are the results of dehydration due to overheating by the laser. Inappropriate laser parameters or the handling and guiding of the beam across the surface may explain these issues. The magnification of the composite-enamel border in Fig. 61 shows a fissured and irregular enamel surface on the right side of the micrograph. The typical enamel structure with its enamel prisms is remaining after laser ablation. Unfortunately, micro-cracks wind their way through this prisms. Erbium laser ablation of composite left either a flaky or a gravelled surface depending on the applied average power. As composite has to be removed anyway to treat the underlying caries affected dental tissue the morphology of composite is irrelevant as a matter of fact.
Experiments equal to the one reported here have not been performed yet by any other workgroup although selectivity of laser ablation has already been concerned. For example Lizarelli et al. (2003) determined the ablation rates of three types of composites and dental tissue applying the Fotona Twin Light Er:YAG laser at different fluences. As the overall ablation rates were 5 to 10 times higher for composite compared to enamel, secure removal of those materials with little effect on enamel should be possible. For permanent dentine ablation rates were not very different to that of resins with a removed volume equal or even higher to composites. This finding is in good agreement with the discussion above. A controversial result was obtained by Alexander and his workgroup (2002), who stated that free-running 100-300 µs Erbium lasers were not well suited for selective ablation, since enamel and composite got ablated to similar rates. Their study demonstrated, that third harmonic (355 nm) laser ablation of a Q-switched Nd:YAG laser with 10 ns pulses is capable of removing residual composite left after de-bonding orthodontic brackets without damaging the underlying enamel. Dumore and Fried (2000) analysed TEA CO_2 laser ablation operating at 9.6 and 10.6 µm with 200 ns pulse duration at FWHM and Q-switched Er:YAG laser ablation with 150 ns pulse duration. An excerpt of their article says, that although there is enough water present in composites for strong absorption at 2.94 µm, the principal components of dental composites, namely quartz and PMMA resin indicate substantial absorption in the mid-IR range with the strongest absorption occurring near 9.6 µm due to the quartz filler where the absorption exceeds 1000 cm^{-1}. Their experimental results are in accord with this statement. While TEA CO_2 laser pulses were suited for selective removal of orthodontic bracket adhesives, the Er:YAG laser failed to fulfil this goal. Between fluences of 10-20 J/cm² enamel was ablated more rapidly than composite, at fluences larger than 20 J/cm² the ratio of the ablation rates for composite and enamel is near unity.
It is impossible to find a consensus in this context, because of the variety of composite available either for dental restorations or for orthodontic bracket adhesion, not to forget about the wide range of Erbium lasers parameters.

4.4.2 USPL TREATMENT

In contrast to Erbium laser ablation, where water is the trigger for laser ablation, USPL ablation is independent of an initiator for plasma generation. Responsible for starting the ablation process is just a sufficiently high pulse peak power to generate the necessary free electrons. It is therefore solely a matter of dielectric properties of the considered material. As the following discourse reveals USPL ablation performed in sound and carious dentine as well as in composite is highly selective, thereby accomplishing the desired needs.

4.4.2.1 MATERIALS AND METHODS

The 12 ps IC-1500 REG AMP Nd:Vanadate laser with a frequency of 5 kHz and a pulse energy of 124 µJ was applied for selectivity analysis. The laser beam launched through the r-φ-scanner was deflected according to the scan parameters of algorithm 2 and 13, respectively. Human third molars were used for ablation. The occlusal enamel was removed by a diamond saw to expose dentine. Again, grooves were generated using a common mechanical drill and restored afterwards in the usual way employing etch gel, bonding and the composite, which was either Tetric Flow or Tetric Ceram. The prepared samples were positioned in the focal plane of the laser beam. Regions at the dentine-composite border were irradiated. The processed cavities were evaluated by means of scanning electron microscopy and IFM analysis tools, respectively. IFM stands for Infinite Focus microscope, which is a light microscope with implemented three-dimensional analysis software developed by Alicona Imaging Company, Grambach, Austria. It automatically obtains series of two-dimensional pictures in different planes of the cavity which are fit together to three-dimensional images. These images can also be used for volume, area and profile analysis.

4.4.2.2 RESULTS

Fig. 62 presents a circular cavity on the dentine-Tetric Ceram border. To generate this cavity, algorithm 2 was applied and laser treatment was performed for 2 minutes. The large cracks spreading over the whole cavity in Fig. 62 a) are again due to dehydration during ESEM analysis. The magnification of the crater in Fig. 62 b) contains a crevice exactly at the boundary of dentine and composite. This gap can be ascribed to polymerisation shrinkage of composites. By dehydration this gap formation is additionally enhanced. Concerning selectivity, the performance of the USPL is very impressing as a clear distinction between dentine and composite ablation sites can be made. In unison with the results of ablation rate measurements composite was removed on a much larger scale than dental tissue. The magnification given in Fig. 62 b) shows an abrupt step downwards the cavity inclination when traversing the borderline between dentine and Tetric Flow. Composite was removed without destroying the adjacent biological hard tissue.

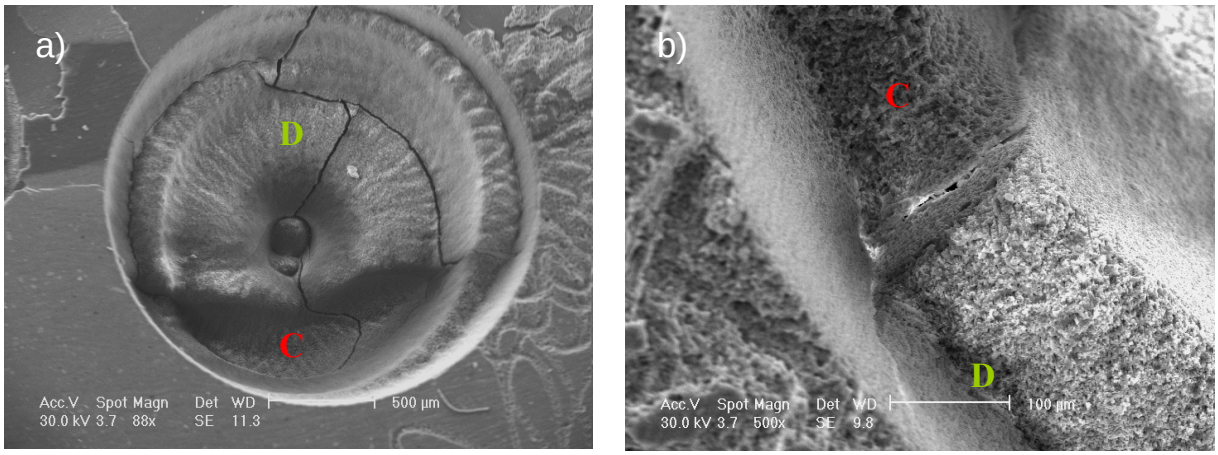

Fig. 62: a) USPL cavity on the dentine-composite border applying algorithm 2. Dentine is marked by D, composite by C. b) Magnification of the ablated dentine-composite border. A large step can be observed when passing from dentine to composite.

Examples of selective USPL ablation applying algorithm 13 are presented in Fig. 63 and Fig. 64. The first one captures a cavity partly obtained in carious and sound dentine. The carious structure indicated by C appears as dehydrated, rough and brittle substrate which can be ablated easier than healthy tissue with its denser and vivid matter. So selectivity of ps Nd:Vanadate laser ablation of can also be reported here. Nevertheless, selectivity in this sense was already investigated by other workgroups[26].

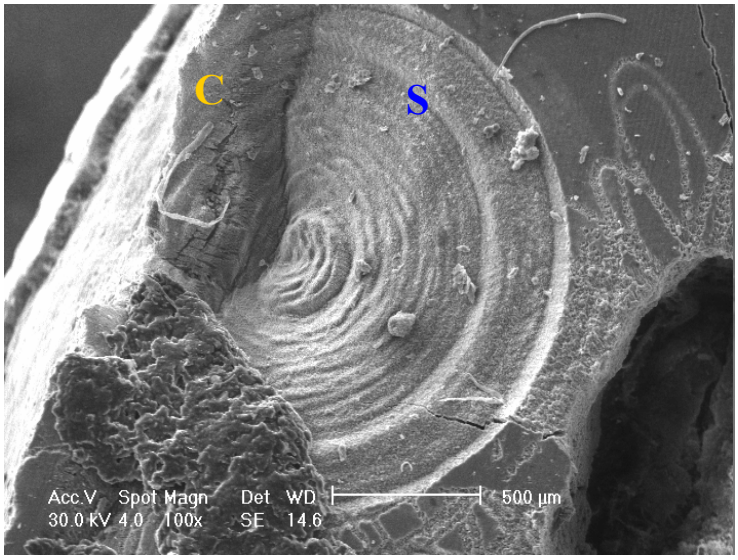

Fig. 63: USPL treated carious (C) and sound (S) dentine.

Until now, selectivity was judged on basis of SE micrographs. To continue in this way an adequate picture of an r-φ-scanned USPL cavity in dentine and composite ablated according to algorithm 13 is depicted in Fig. 64 a). Supplementary, the Infinite Focus light microscope and its analysis software were involved to provide a last incessant aspect of selective USPL ablation of composite and dentine. A three dimensional reconstruction of the generated cavity was obtained to give insight into the precipice created by composite ablation. This 3D cavity model is depicted in Fig. 64 b).

[26] An example of selective removal of caries and dentine by USPL is shown in (Bäcker, 2004) p. 30.

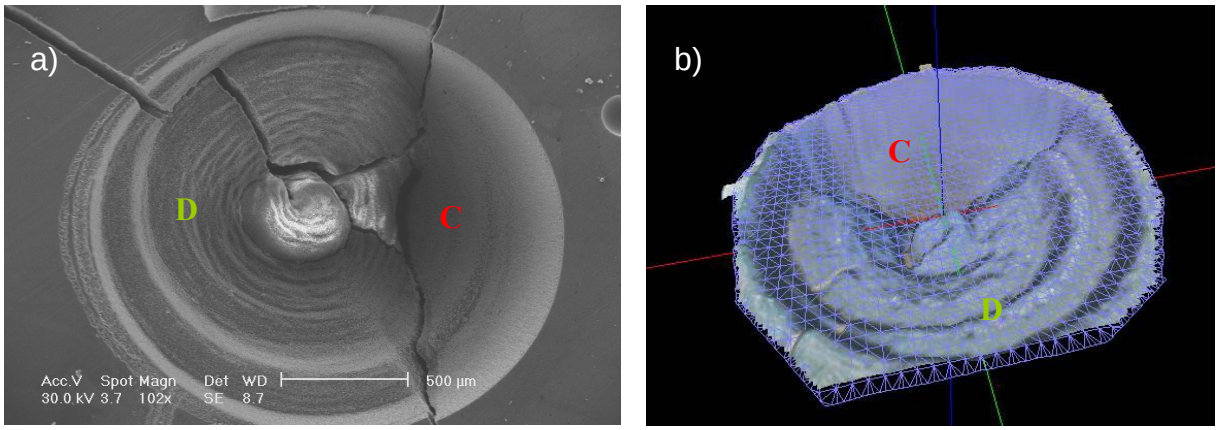

Fig. 64: a) ESEM of ablation crater obtained at the border between dentine (D) and composite (C). Algorithm 13 was applied. b) 3D reconstruction of the same cavity by means of digital light microscopy using IFM.

A very interesting appearance of the cavity geometry is pointed out in Fig. 65 where the profile of a cross-section through the crater is shown. To obtain the depth profile a colour image of the light micrograph already used to reconstruct the cavity model depicted in Fig. 64 b) was generated. After drawing the line indicating the section through the cavity, the depth profile was calculated and visualized. The line was thoroughly chosen to stretch over the two prevailing tissue types. The crossing of the red auxiliary lines in the depth profile corresponds to the point near the cavity centre in the colour picture. This is exactly the region where dentine merges into composite. In the colour image this area is characterized by a green tinge instead of an orange one. This transition is clearly noticeable as step in the depth profile which is marked by the auxiliary lines. To the right of these lines, the deepest region of the entire cavity can be located and assigned to composite.

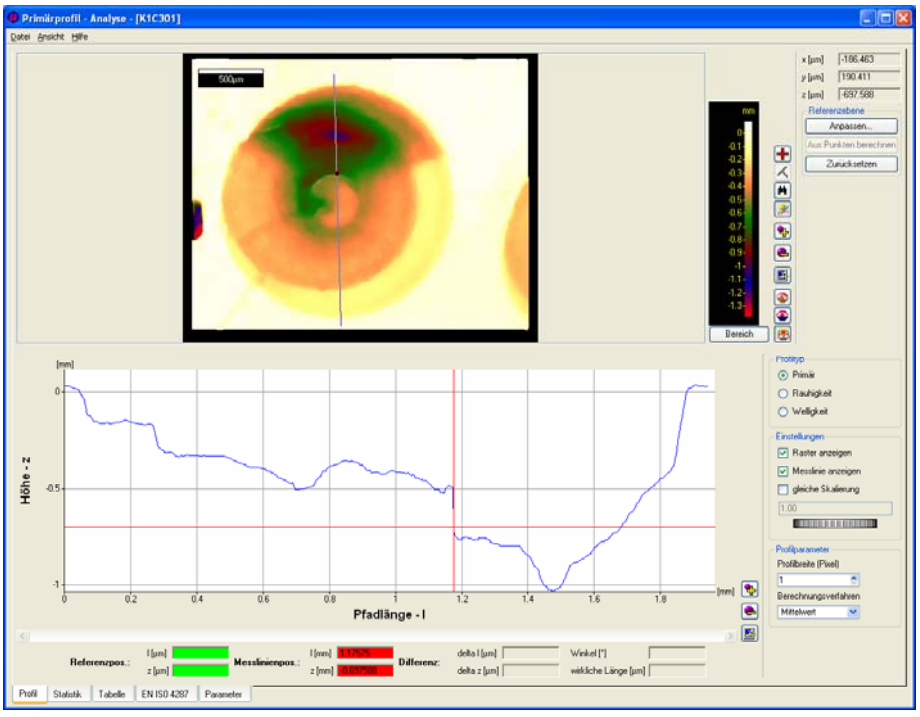

Fig. 65: IFM colour image and depth profile of a USPL treated cavity generated on the composite-dentine border.

Literature inquiry revealed that selectivity analysis of composites and dental hard tissue ablated by scanned USPL has not been focused, although it is a very important topic when old restorations have to be removed in order to treat the underlying or surrounding tooth substance. As mentioned above, just selective ablation of caries and dentine or enamel has already been investigated. But anyway, this was not the main emphasis of the conducted study.
It was demonstrated that Erbium as well as USPL systems are capable of selective tissue treatment. However, in the first case the results do not entirely correlate with the desired effects especially when dentine is concerned. In contrast to that, dentine and composite can be processed very distinctively if USPL are applied. The performance of USPL in comparison to Erbium systems is therefore much more favourable.

4.5 SURFACE ROUGHNESS

Several conditions have to be fulfilled to guarantee good adhesion between the processed dental surfaces and the inserted filling material. One essential issue is that the bottom and the inclinations of the cavity have to possess a roughened surface. Compared to a smooth surface roughening enlarges the area for attachment and forces better compound with the filling material. Concerning dentine, another special requirement arises: As the restoring procedure affords the application of a primer or a combination of primer and bonding in one-bottle-adhesives opened dental tubuli are inevitable. The primer responsible for the interconnection with the collagen net infiltrates these tubuli and forms tags. These tags acting like barbs provide the micro-mechanic anchoring. These criteria can be handled by technical means, when appropriate tools for cavity preparation are applied. The remaining responsibility for thorough cavity restoration lies in the hand of the dentist. The activities embrace for example the right degree of drying of the tissue surface. Dehydration of dentine causes collagen fibers constituting this matter to collapse, thereby reducing the retention of the restoration. Another fact is that the cavities have to be stuffed properly with composite to plug the hole and seal the tooth surface. Light curing has to be done sufficiently long to fix the filling accurately. Also the time span needed for cavity restoration influences the result. Unfortunately, numerous other factors can be found which are related to the experience and ability of the dentist. As these dangers are of human nature they cannot be eliminated totally but reduced by training.
In the following, the technical aspect of cavity preparation is enlightened. Different cavity preparation techniques are analyzed with respect to their surface features.

4.5.1 MATERIAL AND METHODS

Smooth dental surfaces of human permanent teeth were exposed by detaching the occlusal enamel using a diamond saw, which were subsequently ground with carbide paper. Cavities were generated by each of the given items: a common dental drill with additional etching applying phosphoric acid (Scotchbond) for 20 seconds, the Er,Cr:YSGG laser operated at 2 W with supporting air-water spray and the r-φ-scanned 12 ps Nd:Vanadate laser with 124 µJ and 5 kHz applying algorithm 13 without additional water irrigation. Scanning electron micrographs of the cavity bottoms were obtained.

4.5.2 RESULTS

Fig. 66 to Fig. 68 demonstrate the surface features achieved by the mentioned conditioning techniques. Each method yields a characteristic and individual surface. The one remaining after etching is strewn with pikes surrounding the opened dental tubuli. Obviously, the smear layer generated by the drill was removed successfully. The primer can therefore penetrate into the tubuli without obstacles to form the tags.

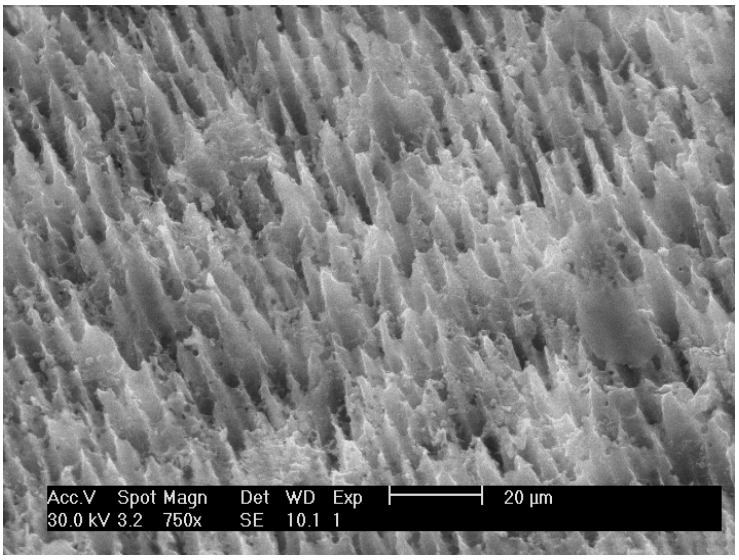

Fig. 66: ESEM of drilled and subsequently etched dentine.

For convenient retention a surface predominantly based on peaks is essential.[27] Looking at Fig. 67 depicting the Er,Cr:YSGG laser treated surface lacks these peaks. Instead of that a scaly surface appears. It has to be emphasized that just the upper part of the micrograph shows dentine, which is evident by the small black spots representing the opened tubuli. Although, the unplugged tubuli are very favourable, the surface is quite smooth compared to the etched one. The retentive strength is therefore reduced.

Several authors have already concentrated on laser conditioning by Erbium lasers. Most of them came to the conclusion that laser irradiation alone is not a valid alternative to acid-etching pre-treatment for composite materials adhesion. (Ceballos, 2001), (Gürsoy, 2003), (Giachetti, 2004), (Sassi, 2004) Others, like Hossain et al. (2001) and (2003), are intercessors of this technique. Their first mentioned study was conducted with the Biolase Millennium Er,Cr:YSGG laser at 3 W with 70% air and 20 % water. Irradiation was performed for 6 seconds. Evaluation was done by judging roughness values. Their second publication reports on micro-leakage tests involving the Kavo Key laser. Enamel was irradiated with 400 mJ at 2 Hz, dentine with 200 mJ. According to them, micro-leakage tests revealed no significant differences between the laser and burr cavities.

The surface in the figure below was generated with a power of 2 W as suggested by an expert. Nevertheless, several other settings were also tested, but in general the results showed the same characteristics. Problematic in this context may be that during laser conditioning the hand-piece was not fixed, so that a uniformly distributed pattern like in case of acid etching cannot be achieved. Nevertheless, when the dentist processes the cavity the hand-piece is not fixed anyway.

[27] http://www.taylor-hobson.com/faqsurfacedetail.asp?faqid=69

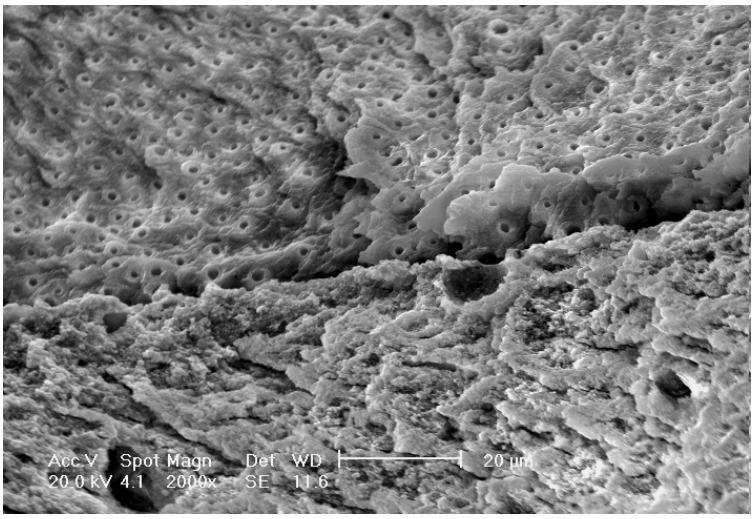

Fig. 67: ESEM of Erbium laser treated dentine (top) and composite (bottom).

The surface features resulting from laser conditioning by the USPL reveals as micro-retentive structure incomparable to the morphology of etched and Erbium laser processed surfaces. This appearance is typical and unmistakable for all USPLs tested during this research. On a somewhat larger scale the surface features can be influenced by the scan pattern, but on the micro-level this filigree structure is evident. Like for the other techniques, the dental tubuli are uncovered facilitating tag formation and therefore sufficient retention. Supplementary, the micro-retentive pattern enlarges the surface and allows good adhesion. The combination of both issues leads to the conclusion that successful cavity restoration might be possible without additional surface roughening methods.

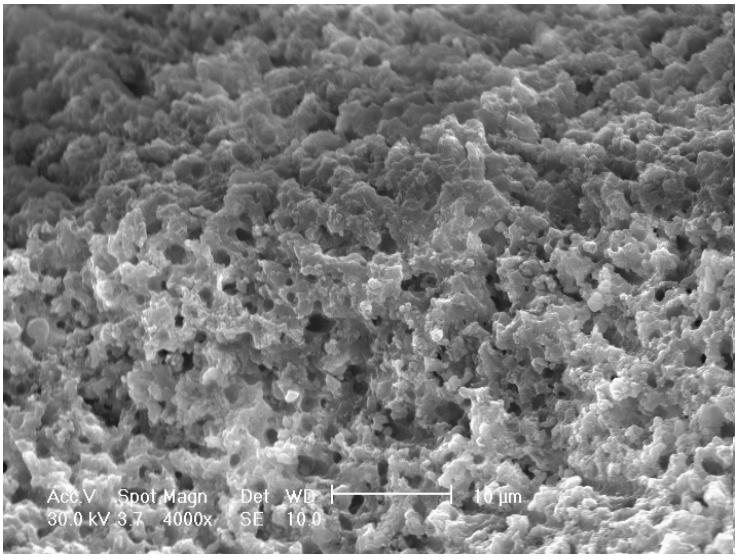

Fig. 68: ESEM of USPL processed dentine.

Surface roughening without additional etching would be very beneficial. As soon as the etchant is spread over the exposed dentine surface it also penetrates into the tubuli. Although the tooth is rinsed afterwards, some etch gel might be left in the tubuli thereby irritating the tubular liquid. The consequence is that the pulp gets hyper-sensitive to pain. Another aspect is, that in case of USPL the separate step for surface conditioning gets superfluous, as the surface remaining after ablation already possess the mentioned advantageous characteristics.

Some attempts were made to perform dye penetration tests with USPL treated cavities to visualize micro-leakage arising from polymerisation shrinkage. As the number of available samples was not sufficient, instead of the results of an extensive study just an impression of the potential of USPL treated dentine can be provided. In Fig. 69 a composite filled USPL cavity is depicted. The cavity was generated with pulses of 100 µJ pulse energy employing the 12 Nd:Vanadate laser used before. Excite from Ivoclar Vivadent, which combines primer and bonding, was directly applied to the laser treated surface renouncing the etchant. After restoring the cavity with composite, the whole tooth with exception of the restored area was covered with nail polish. Then the tooth was immersed in 1 % EOSIN solution. 24 hours later the sample was rinsed in pure water, cut longitudinally through the midline of the cavity and analysed via light microscope.

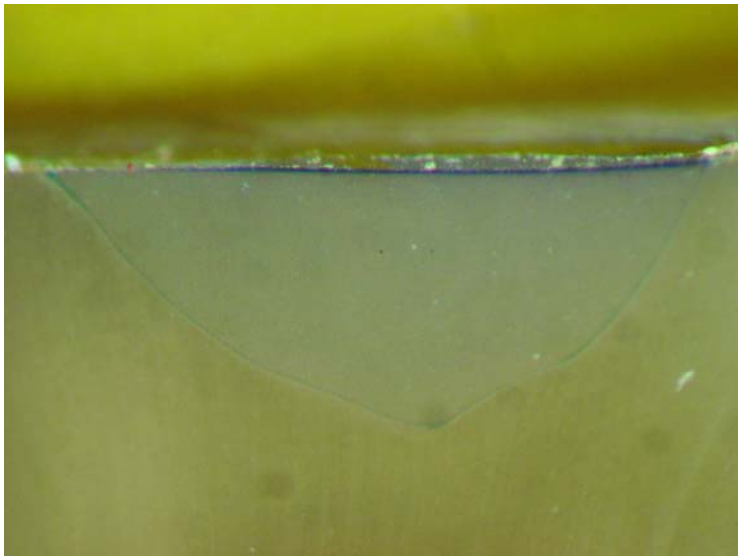

Fig. 69: Restored USPL cavity in dentine.

Along the border line between the filling and dentine there is minor evidence of dye. Anyhow, the cavity was excavated without water-supply. That implicates, that the dentine surfaces dehydrated to some extend. As mentioned before, the whole restoration procedure is very sensitive to dehydration. If the drying procedure for dentine or the bonding is too long the collagen fibres of the tissue collapse that at least the retention is reduced. Further studies have therefore to be done with and air-water spray. Anyhow, the restoration in Fig. 69 is just an example demonstrating the retentive and adhesive potential of USPL treated cavities.

5 EXPERIMENTAL TOOLS AND DISCUSSION - BONE

5.1 ABLATION RATES

5.1.1 ERBIUM LASER ABLATION RATES

As mentioned, the comparison to Erbium systems is the basis to judge the applicability and usefulness of USPL. Therefore not just USPL ablation rates but also Erbium laser ablation rates of bone tissue were determined.

5.1.1.1 MATERIALS AND METHODS

Erbium laser systems involved for the ablation rate measurements were the Fotona Fidelis Er:YAG and the Biolase Waterlase Er,Cr:YSGG. The experiments were performed with bovine compacta and cartilage. Total ablated volumes mainly were obtained with dental imprint mass and µg-balance. Additionally, the IFM method was applied to some of the cavities for ablation rate measurements. The procedure for volume analysis is demonstrated in Fig. 70. After drawing a poly-line around the cavity rims enclosing the region of interest, the IFM software establishes the three-dimensional image of the cavity and calculates the volume between the cavity walls and the attached iso-layer. Deviations of measured volumes with either imprint or IFM method are negligible.

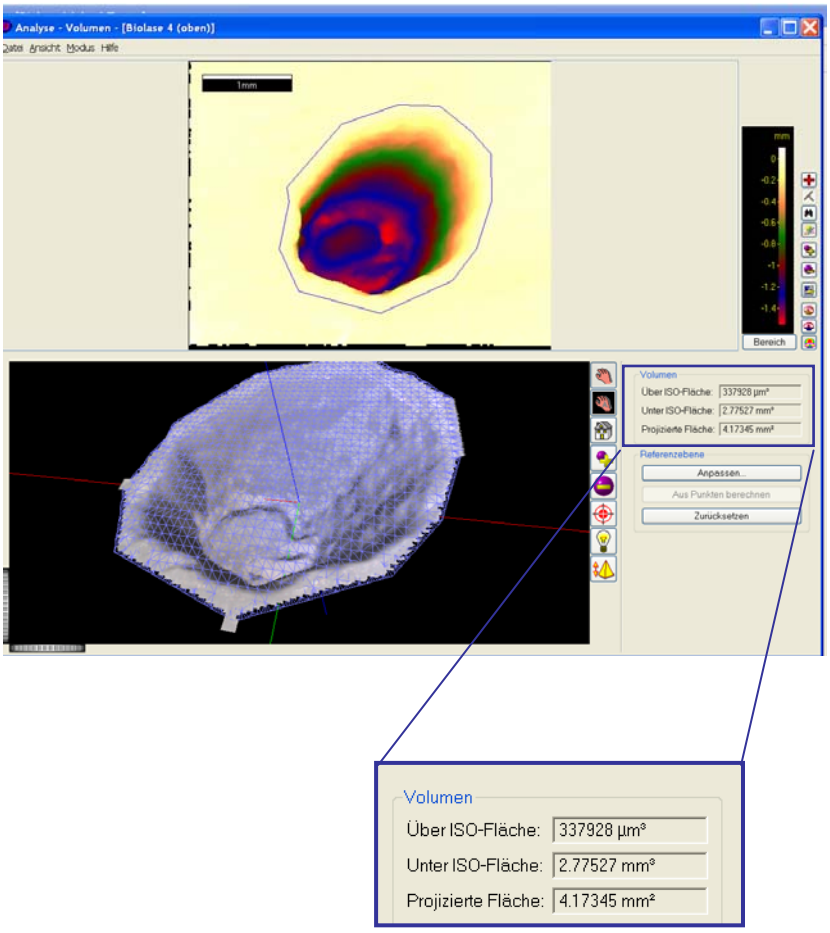

Fig. 70: Determination of the total ablated volume using Infinite Focus Analysis Software.

5.1.1.2 RESULTS

Like for dentine, ablation rates achieved with Erbium lasers were determined as ablated volume per pulse. For each laser setting 6 cavities were generated with a defined number of laser pulses. After averaging the total ablated volumes, the ablation rates were calculated. Ablation rates were established for bovine compacta and cartilage. Even some efforts were made to define the ablation rates of spongiosa. Nevertheless, with the available analysis tools this attempt failed. This can be attributed to the trabecular structure of the tissue, because imprint mass that penetrated into the intra-trabecular space deterred the results. In case of IFM analysis the deep holes between trabeculae also caused problems so that digital cavity reconstruction contained some sources of error and calculation of the cavity volume was too inaccurate. The ablation rates of cartilage and compacta excavated by either Er:YAG or Er,Cr:YSGG laser are captured in Fig. 71 and Fig. 72.

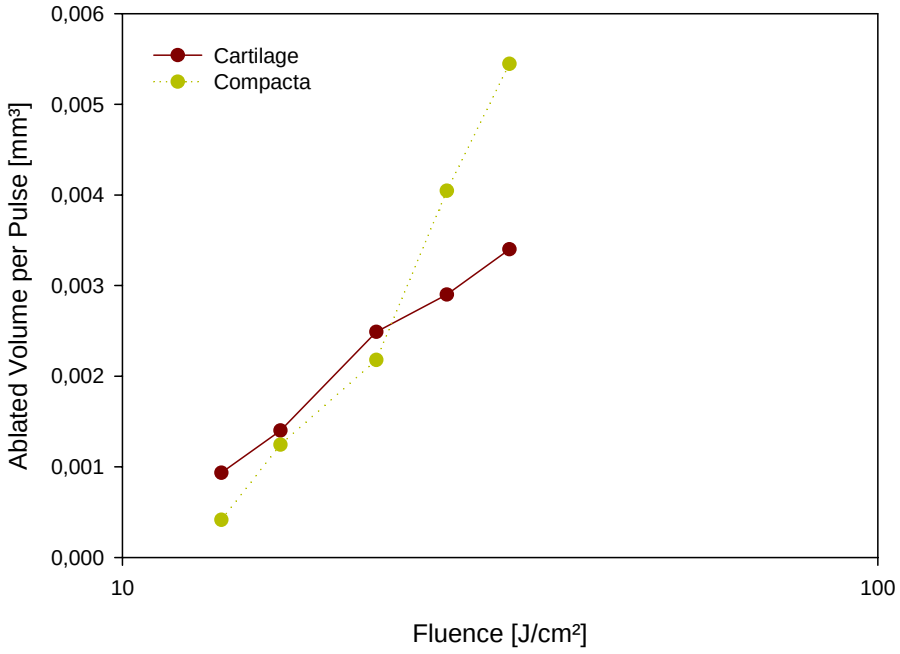

Fig. 71: Cartilage and compacta ablation rates obtained with the Fotona Er:YAG laser for rising fluences.

For fluences up to ~20 J/cm² the ablation rates of cartilage generated with the Fotona Er:YAG laser are slightly higher than that of compacta. With rising fluences the situation turns around: The ablation rates of compacta exceed than that of cartilage and the differences get more distinctive. In chapter 3.1.1 the temporal pulse profile of the Fotona laser is discussed. The pulse duration at FWHM is ~100 µs and the rise time of the laser pulse measured from the beginning of the pulse to the pulse peak for fluences >20 J/cm² is about >90 µs which implicates that the inclination of the leading pulse edge is not very steep. Therefore, the energy contained in this leading pulse edge is released into the tissue in form of heat vaporising the incorporated water. As cartilage contains more water than compacta this effect influences the ablation markedly. A reduction of the water content of the tissue reduces also the ablation rates, because water is the main absorber of Erbium laser wavelengths.
The temporal pulse profile of the Er,Cr:YSGG laser showed better conditions. With pulse durations at FWHM of ~50 µs and rise times of ~25 µs energy deposition into the tissue is more effective. The heat impact by the leading pulse edge is kept low so that the vaporisation effect of water leading to reduced abation rates is insignificant. Therefore, the achieved

ablation rates correspond to the expected behaviour: Softer tissue gets more ablated than harder one, or in other words, cartilage yields higher ablation rates than compacta for all applied fluences.

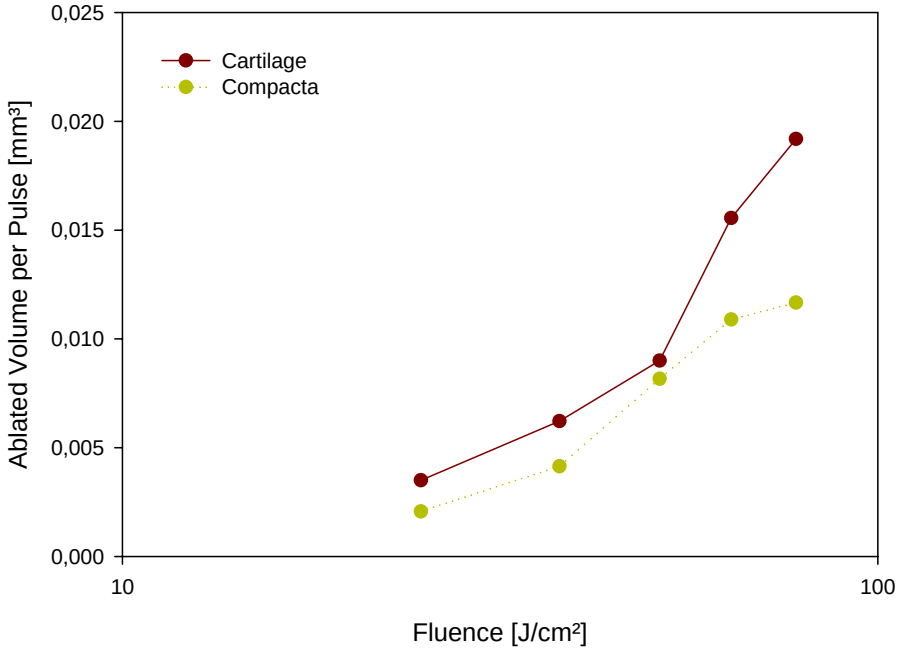

Fig. 72: Cartilage and compacta ablation rates obtained with the Biolase Er,Cr:YSGG laser for rising fluences.

A strict comparison of Er:YAG and Er,Cr:YSGG ablation rates is not possible as different fluence regions were covered during the experiments. This is mainly due to the limited number of laser pre-settings and the deviations of the measured output parameters from their front panel values. Just an impression can be given by comparing Er:YAG and Er,Cr:YSGG laser performance in compacta. As previously discussed, the absorption coefficient of water depends on the laser fluence. For lower fluences water absorption of $\lambda = 2.94$ µm is stronger than for $\lambda = 2.79$ µm. After reaching a certain fluence value the tables are turned. Fig. 73 demonstrates this situation.

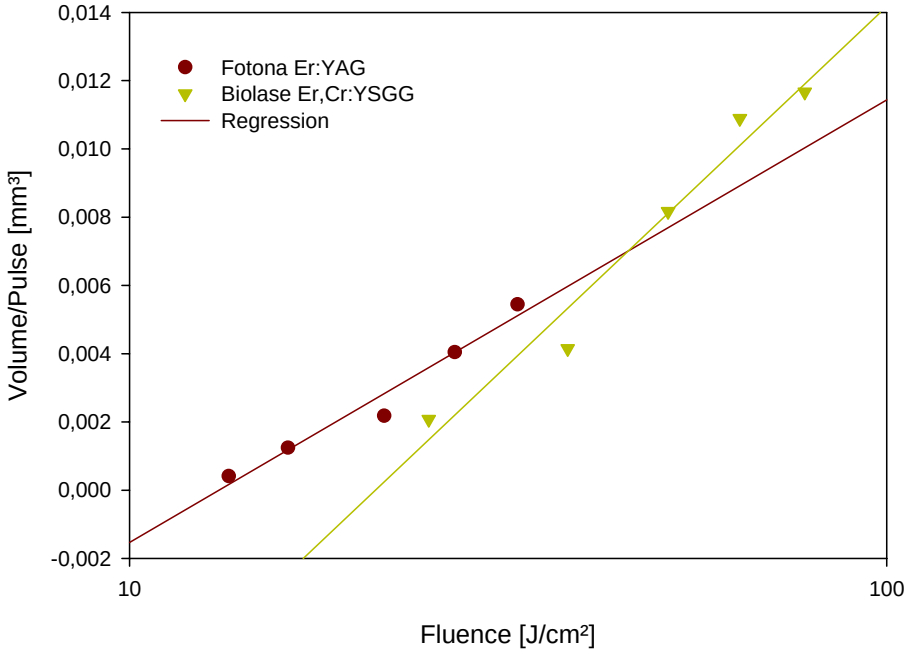

Fig. 73: Compacta ablation rates vs. fluence for Er:YAG and Er,Cr:YSGG laser ablation.

5.1.2 USPL Ablation Rates

5.1.2.1 Materials and Methods

To determine the ablation rates of bone tissue the 330 fs Yb:Glass laser and the Hurricane-i Ti:Sapphire laser with adjustable pulse duration were employed. Line scans were performed and the depths of the remaining grooves were measured out by means of light microscopy. For details of the experimental setup and of the theoretical background see chapter 4.1.2.3. Compacta and cartilage ablation rates were retrieved without any difficulties. Whenever possible, ablation rates for spongiosa were also procured.

5.1.2.2 Results – Yb:Glass Laser

Again, linear scans were performed with the 330 fs Yb:Glass laser at 1 kHz PRR and pulse energies ranging from 40 µJ to 130 µJ corresponding to radiant exposures of 0.97 J/cm² to 3.16 J/cm². The scan speed was 1 mm/s. In Fig. 74 the obtained etch depths per pulse for all three different types of bone tissue are drawn versus rising pulse energies in a semi-logarithmic plot. The equivalent pulse number was considered in the calculations.

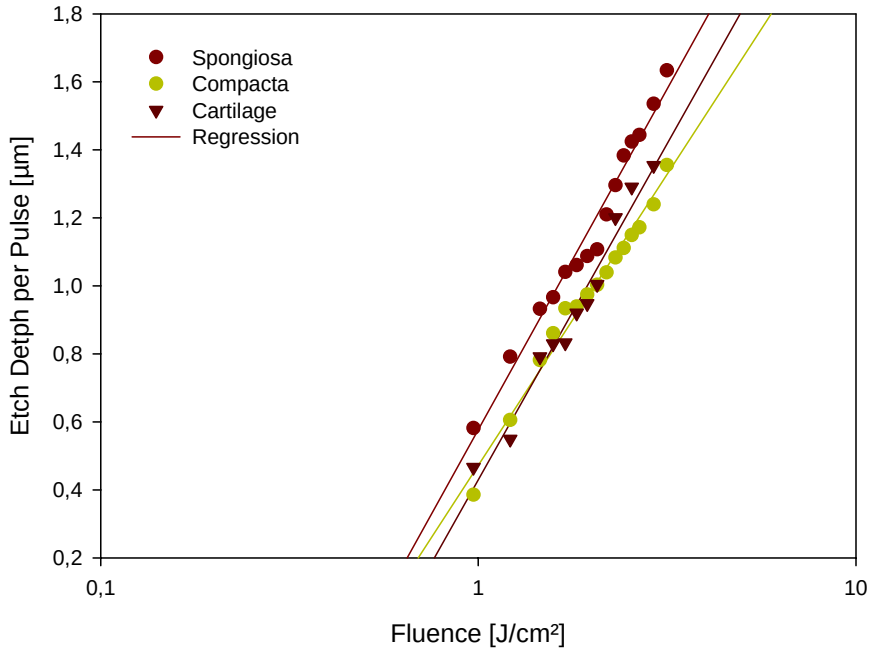

Fig. 74: Etch depth per pulse vs. rising pulse energy obtained in spongiosa, compacta and cartilage with the Yb:Glass USPL.

Strikingly, the ablation rates of all bone samples in the investigated fluence regime are quite close to each other, especially those of compacta and cartilage. The etch depths within spongiosa are slightly higher. The slopes of the graphs above, corresponding to the optical penetration depths differ just a little bit. That implicates that the effective absorption coefficients for the 330 fs ablation at $\lambda = 1040$ nm resemble. For spongiosa the slope of 0.870 µm gives $\alpha_{eff} = 1150$ cm^{-1}, compacta with a slope of 0.744 µm yields $\alpha_{eff} = 1345$ cm^{-1} and for cartilage $\alpha_{eff} = 1060$ cm^{-1} could be calculated from a slope of 0.944 µm.
For the Er:YAG and the Er,Cr:YSGG laser, ablation rates were established as ablated volumes per pulse. In case of the Yb:Glass USPL, etch depths per pulse were considered. As for threshold calculations also the groove diameters were measured out, the ablated volume per pulse can also be determined for the Yb:Glass system. Assuming a Gaussian beam profile resulting in cavities shaped like rotational paraboloides and by knowing the etch depth per pulse and the groove diameters the ablated volumes per pulse were calculated. With values in the range of 10^{-7} mm³/pulse the volumes per pulse ablated by the USPL are very small compared to rates of 10^{-3}-10^{-2} mm³/pulse achieved by Erbium systems.

Table 25: Calculated compacta volumes ablated by a single Yb:Glass laser pulse.

Fluence [J/cm²]	Volume/Pulse [10^{-7} mm³]
1.0	0.57
1.2	3.3
1.6	6.9
1.7	8.2
1.9	9.3
2.1	9.9
2.2	11
2.7	15
3.2	20

The question now is: How can the speed of ablation be accelerated for USPL? The answer is obvious: by enhanced PRR. When larger areas are treated with USPL scanning is necessary. Therefore, for higher PRR also the scan parameters have to be adjusted to avoid extensive overlapping of subsequent laser pulses so that each spot on the tissue surface hit by a pulse can be seen as an untouched one. By that, accumulation effects can by eliminated. Anyway, to get an idea about the necessary PRR the ablation rates in compacta shall be considered. The measurements revealed that a volume of 0.08 mm^3 per second can be processed by the Er:YAG laser when a fluence of 26.9 J/cm^2 is applied, whereas the Er,Cr:YSGG systems needs 37.9 J/cm^2 to remove the same amount. Both systems were operated at 20 Hz. For comparison, Yb:Glass laser ablation at a fluence of 1.9 J/cm^2 shall be focused. This fluence is chosen, as it is about twice the threshold fluence of compacta for this system. To excavate a volume of 0.08 mm^3 per second a PRR of about 9 kHz has to be applied to the USPL. Bearing in mind, that USPL can be operated at much higher PRR, a frequency of 9 kHz is nothing unusual.

5.1.2.3 RESULTS – TI:SAPPHIRE LASER

Ablation rate measurements involving the Hurricae-i Ti:Sapphire laser were done with pulse durations of 150 fs, 500 fs, 2 ps and 7 ps. A pulse energy range of 240 µJ to 40 µJ was covered and line scans were conducted. Again, the ablation rates, defined as etch depth per pulse, were calculated after determining the cavity depths and considering the equivalent pulse number. Fig. 75 shows the results.

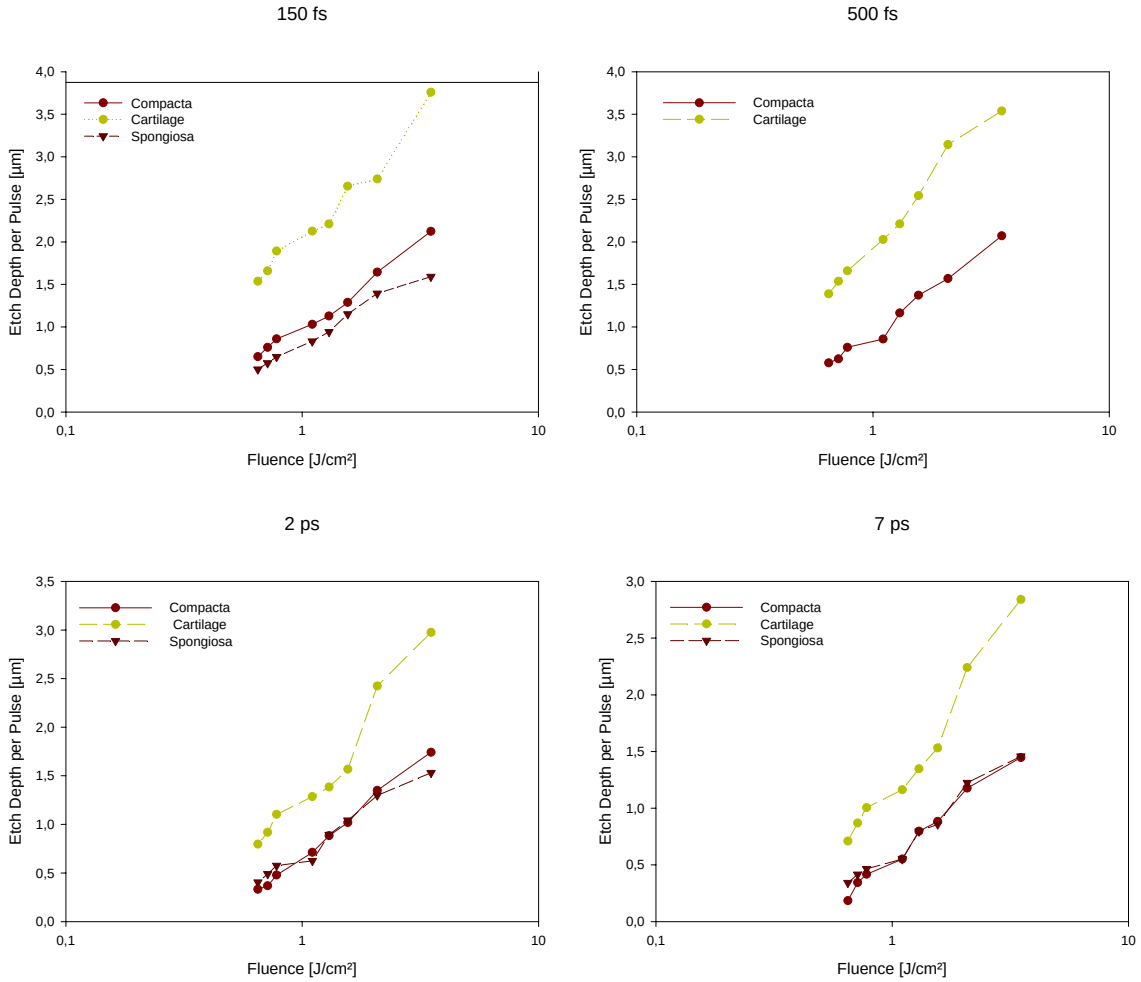

Fig. 75: Semi-log plot of ablation rates [µm] vs. pulse energy [mJ] obtained with the Ti:Sapphire laser applying pulse duration of 150 fs – 7 ps.

For every applied laser setting the etch depths per pulse for cartilage are the highest. 150 fs ablation revealed lower ablation rates for spongiosa compared to compacta, whereas spongiosa and compacta ablation rates are nearly the same for ps laser ablation. This finding is contrary to the one of Yb:Glass laser. Certainly, the reason therefore can be found in the native structure of spongiosa itself. As bone structure fits each individual's needs, differences can appear in the used samples. For some samples the bridge-like trabecula structure can be denser than for others, which means that the intra-trabecular space is smaller. A laser beam hitting the surface of denser spongy tissue removes material more efficient than the same laser beam impacting onto a coarser region. In the second case, there is no guarantee that each laser pulse strikes a trabecula. Instead of that, the pulse may come down into the intra-trabecular space leaving the surrounding hard bone tissue untouched resulting in lower ablated depths. The obtained etch depths of spongiosa can therefore just serve as guidelines.
Alterations of the etch depths per pulse for varied pulse duration fulfill the expectations: ablation rates decrease when the pulse durations get extended. For spongiosa a decrease in ablation rates of 12 % and 13 %, respectively, was noticed when enlarging the pulse width from 150 fs to 2 ps and form 2 ps to 7 ps. Ablation rates of cartilage for 150 fs and 500 fs differ just for about 4 %, that of 2 ps are 6 % lower than that of 7 ps. A more severe reduction is obvious, when the pulse duration is changed from 500 fs to 2 ps. Thereby, the amount of tissue removed by a laser pulse is reduced by 33 %. Differences in ablation rates of compacta for both fs settings are within 7 %. Further elongation of the pulse width induces a down scaling of 27 % and 17 %, respectively. Fig. 76 illustrates these facts.

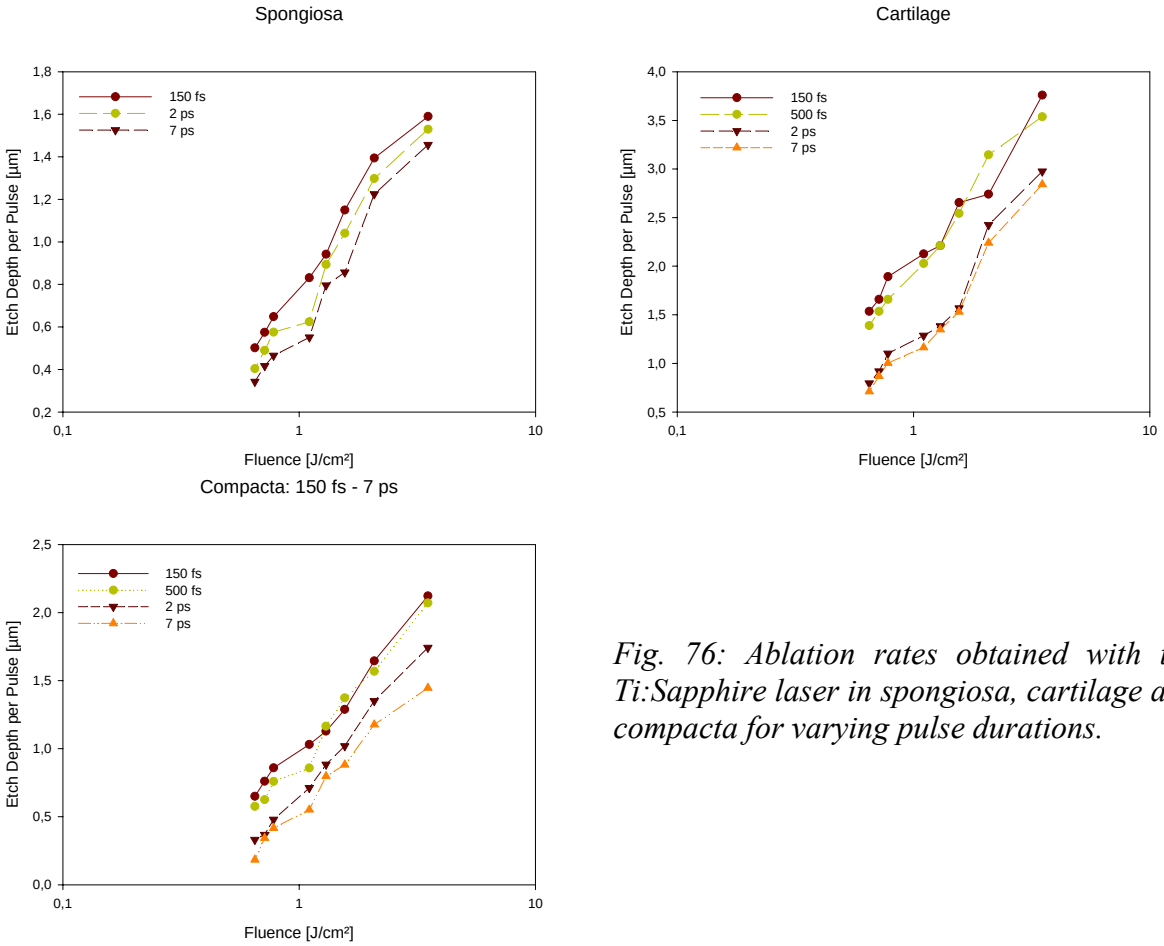

Fig. 76: Ablation rates obtained with the Ti:Sapphire laser in spongiosa, cartilage and compacta for varying pulse durations.

The comparison of Yb:Glass and Ti:Sapphire laser ablation rates is still outstanding. Therefore, etch depths per pulse for all pulse durations of the Ti:Sapphire system as well as for 330 fs Yb:Glass laser ablation are inserted into one plot for each bone material. Fig. 77 demonstrates that spongiosa ablation rates of both systems cover almost the same range. Etch depths in compacta achieved by the 330 fs Yb:Glass laser integrate into the ps ablation rates of Ti:Sapphire. Just cartilage does not fit into the data range obtained by any Ti:Sapphire setting, but lacks behind.

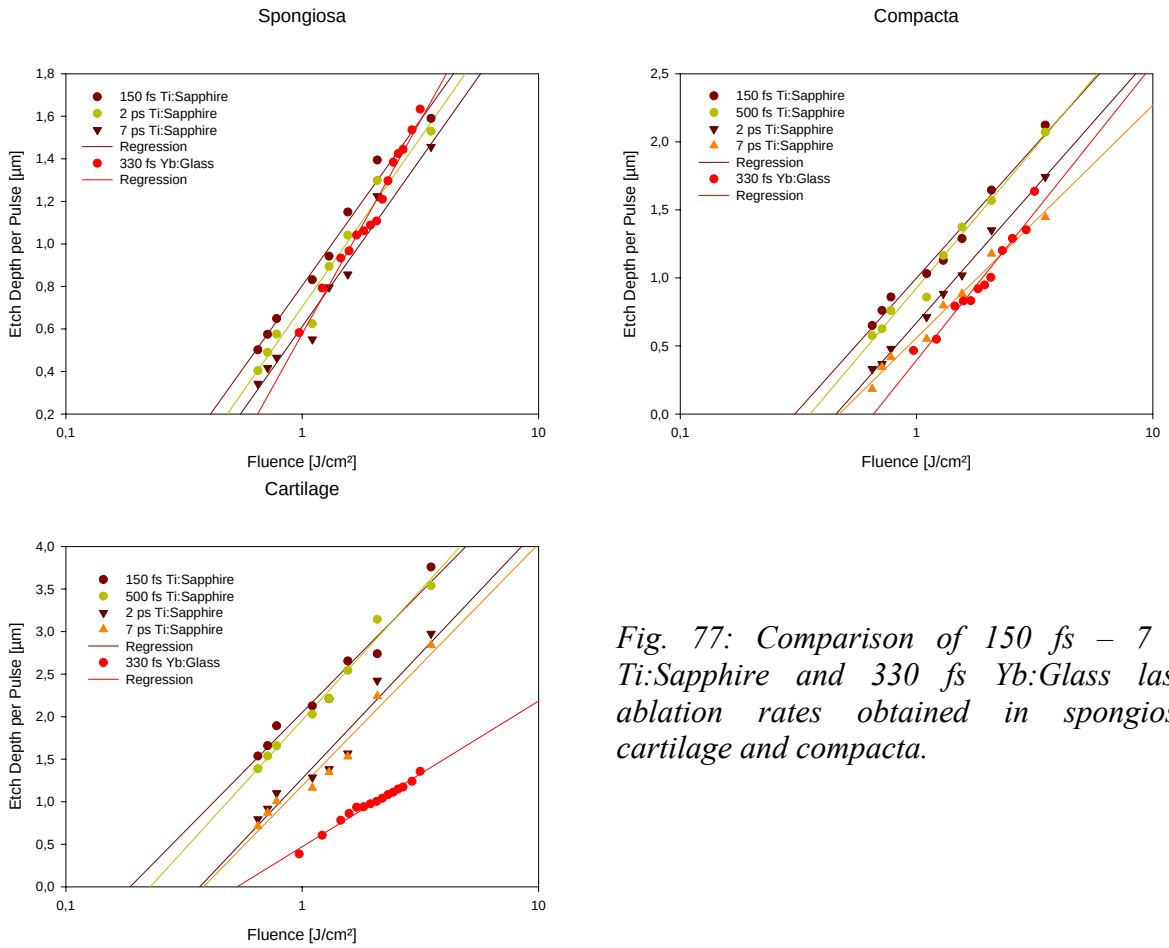

Fig. 77: Comparison of 150 fs – 7 ps Ti:Sapphire and 330 fs Yb:Glass laser ablation rates obtained in spongiosa, cartilage and compacta.

5.1.3 Conclusion

The Ti:Sapphire laser was designed to allow continuous adjustment of the pulse duration. On the other hand, the Yb:Glass laser had a fixed pulse duration. A direct comparison between the two systems would just be possible, when exactly the same parameters could be chosen for both of them. By that, their performance could be evaluated and judged on basis of their ablation rates and thresholds. Nevertheless, the presented study revealed, that ablation rates of USPL are in any case lower than the corresponding Erbium values. This fact is quite advantageous for gentle and damage-free tissue treatment. Choosing appropriate PRR matching with suitable scan parameters the speed of the tissue removal procedure can be accelerated to velocities comparable or even higher than that achieved by Erbium lasers.

5.2 Ablation Threshold

5.2.1 Erbium Laser Ablation Threshold

Out of the data from ablation rate measurements at least the Er:YAG ablation thresholds for cartilage and compacta could vaguely be appraised. For compacta and cartilage threshold values of >11 J/cm² and >7 J/cm² were estimated. Nevertheless, the deviations to values retrieved from literature are remarkable. This is mainly due to the lack of data in the lower fluence range. A brief overview of Erbium ablation thresholds of bone tissue shall provide more reliable data: The workgroup around Jovanvovic (1997) reports on an ablation threshold of less than 5 J/cm² for bovine compact bone. They used an Er:YSGG laser with a temporal pulse duration of 500 µs at FWHM and a focal spot diameter of 480 µm. Walsh and Deutsch

(1989) found a threshold energy density of 2.1-3.4 J/cm² for pig parietal bone. An Er:YAG laser (λ = 2.94 µm) operated in normal spiking-mode with a macro-pulse duration of 200 µs and a 1.1 mm round spot at tissue surface was involved in their study.
N.M. Fried and D. Fried (2001) determined the threshold of an Er:YAG laser in adult bovine skulls. The laser was operated in free-running mode with a pulse duration of 300 µs and in Q-switched mode with 0.5 µs yielding threshold fluences of ~10 J/cm² and <2 J/cm², respectively.

5.2.2 USPL ABLATION THRESHOLD

5.2.2.1 MATERIALS AND METHODS

The method and the laser systems used to determine the ablation threshold in spongiosa, compacta and cartilage are described in detail in 4.2.2. In the following just the results are presented.

5.2.2.2 RESULTS – YB:GLASS

In Fig. 78 the correlation between squared radii and pulse energy according to equation (17) are drawn. For the three types of bone tissue regression of the data yields parallel lines shifted along the x-axis. The lowest ablation threshold belongs to cartilage, followed by compacta. Spongiosa shows the highest threshold value. The thresholds for compacta and spongiosa with 0.77 J/cm² and 0.82 J/cm², respectively, are very close to each other. Nevertheless, the fact that the ablation threshold for spongiosa exceeds that of compacta is somewhat surprising because the harder material is expected to possess the higher threshold. In that context, the native structure of spongiosa has to be considered again. During ablation it cannot be guaranteed that each laser pulse hits a trabecula but penetrates into the intra-trabecular space without removing hard bone tissue. Therefore for spongiosa material removal is not as effective as for compacta. By that the higher ablation threshold for spongiosa compared to compacta may be explained. On the other hand, the lowest threshold for cartilage seems intuitively clear as it is the softest tissue among the three investigated bone materials.
A last remark to the regression according to equation (17) shall be made: The slopes of the regression lines are related to the Gaussian beam waist w of the laser beam. Regression lines for all three bone materials are almost parallel implicating that the slopes are nearly equal. Out of the slopes w = 35.8 µm was calculated for compacta and cartilage, whereas for spongiosa w = 34.3 µm was derived. Comparing it to the value obtained by the knife-edge method which is w = 36.2 µm, especially w = 35.8 µm is in good agreement.

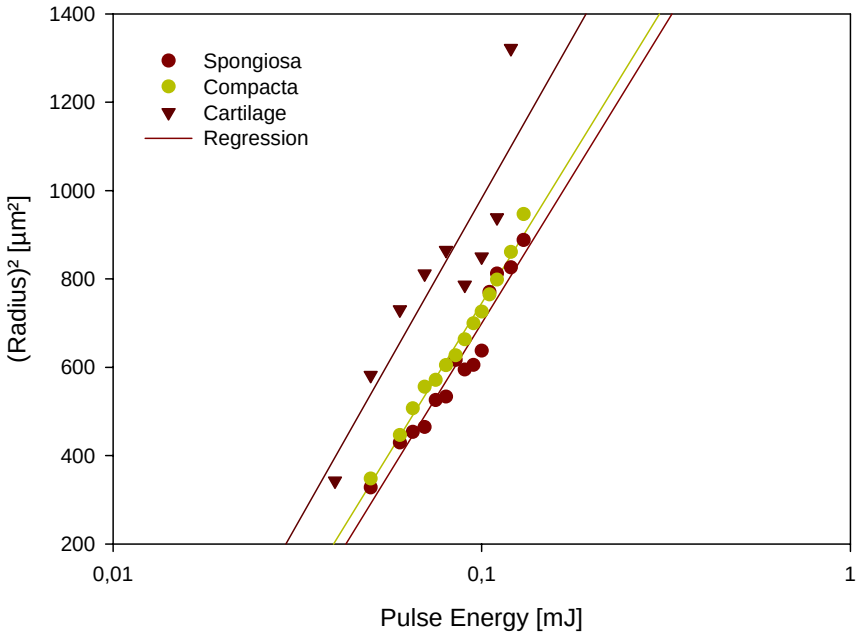

Fig. 78: Determination of the ablation threshold for the 330 fs Yb:Glass laser ablation of spongiosa, compacta and cartilage.

Table 26: Ablation thresholds of the Yb:Glass USPL for bovine spongiosa, compacta and cartilage.

Material	Ablation Threshold [J/cm²]
Spongiosa	0.82
Compacta	0.77
Cartilage	0.54

5.2.2.3 RESULTS – TI:SAPPHIRE

In the same way as for the Yb:Glass laser system ablation thresholds of bone tissue were derived for the Ti:Sapphire laser for pulse durations of 150 fs, 500 fs, 2 ps and 7 ps. The following table lists the results.

Table 27: Ablation thresholds of the Ti:Sapphire laser for bovine spongiosa, compacta and cartilage.

	Ablation Threshold [J/cm²]		
Pulse Duration	Compacta	Spongiosa	Cartilage
150 fs	0.58	0.49	0.20
500 fs	0.60	-	0.40
2 ps	0.75	0.58	0.57
7 ps	0.80	0.69	0.66

For any adjusted pulse duration cartilage needs the lowest fluences to get the ablation started, compacta the highest. In contrast to Yb:Glass, spongiosa thresholds are located between those of compacta and cartilage, which seems reasonable. Anyhow, referring to the arguments above, the trabecular structure just allows determining guide values.
Schwab et al. (2004a, 2004 b) studied Ti:Sapphire USPL ablation of porcine compacta for pulse durations between 130 fs and 1 ps. The threshold for 130 fs lies below 0.7 J/cm² that for 180 fs is about 0.8 J/cm². Out of the diagrams in their article threshold fluences of ~0.9 J/cm² for 500 fs and ~1.2 J/cm² for 1 ps laser ablation are obvious. Threshold values of the conducted study are lower than those of the quoted reference. Nevertheless, thresholds were determined for bovine bone instead of porcine bone used by Schwab. This contributes to the deviations in ablation thresholds.
For extending pulse widths the thresholds increase. This is in agreement with theory: For rising pulse durations the pulse peak powers decrease. Therefore, higher fluences are necessary to initiate plasma formation.

5.2.3 CONCLUSION

Irrespective of the USPL system - Yb:Glass or Ti:Sapphire – the achieved thresholds to start the ablation clearly lie below that of Erbium systems, even when thresholds rise with increasing pulse duration. This can be ascribed to the different pulse regimes and the corresponding ablation mechanisms, which are the water-mediated ablation in case of µs pulses and plasma-induced ablation for USLP. As the pulse energies introduced by USPL are distinctively lower compared to common Erbium laser systems, the temperature released into the surrounding tissue is negligible. Tissue perforation with USPL can therefore happen without collateral damage, which just occurs when high temperatures accompany the ablation process. Micro-cracks, melting and carbonisation can so be avoided. On the other hand this "cold ablation" bears a potential drawback. Due to the lack of temperature increase inside the tissue coagulation effects are omitted. To ensure good operating conditions for the surgeon conventional means of haemostasis have to be applied to stop bleeding. Another possibility is to operate the laser with other parameters to achieve styptic effects. For example, turning off the mode-locking of the USPL system and operating it in the free-running mode may generate laser pulses with durations in the µs regime. These pulses may possess the potential for coagulation.

5.3 MORPHOLOGY

In the following chapters the surface features after bone treatment by mechanical drill as well as by laser systems are analysed. Of course, each preparation technique leads to specific surface characteristics. The differences are not only obvious when mechanical and laser treatment is compared, but even when Erbium and USPL ablation are confronted. In any case, the utmost goal is to achieve a morphological structure similar to native bone tissue. Scanned USPL ablation with a convenient set of parameters approaches this objective.

5.3.1 BONE TREATMENT WITH A MECHANICAL DRILL

5.3.1.1 MATERIAL AND METHODS

A standard mechanical drill was applied with 750 and 2000 roundtrips per minute when holes were drilled in human spongiosa. This setting was suggested by a surgeon who has lots of

practical experience in implant surgery. He also performed the experiments. The generated cavities were investigated under ESEM.

5.3.1.2 RESULTS

Fig. 79 and shows the results for the treatment with 750 roundtrips per minute. Comparable to dental preparations with a drill, a smear layer was produced covering the cavity bottom. Obviously, this layer is not that smooth and homogeneous like the one generated in dentine. Nevertheless, the trabecular structure disappeared. On the cavity walls the native spongy structure can be recognised. Nevertheless, the cut borders of single trabeculae are very edged and pointed as bone material was torn out during the rotation of the drill.

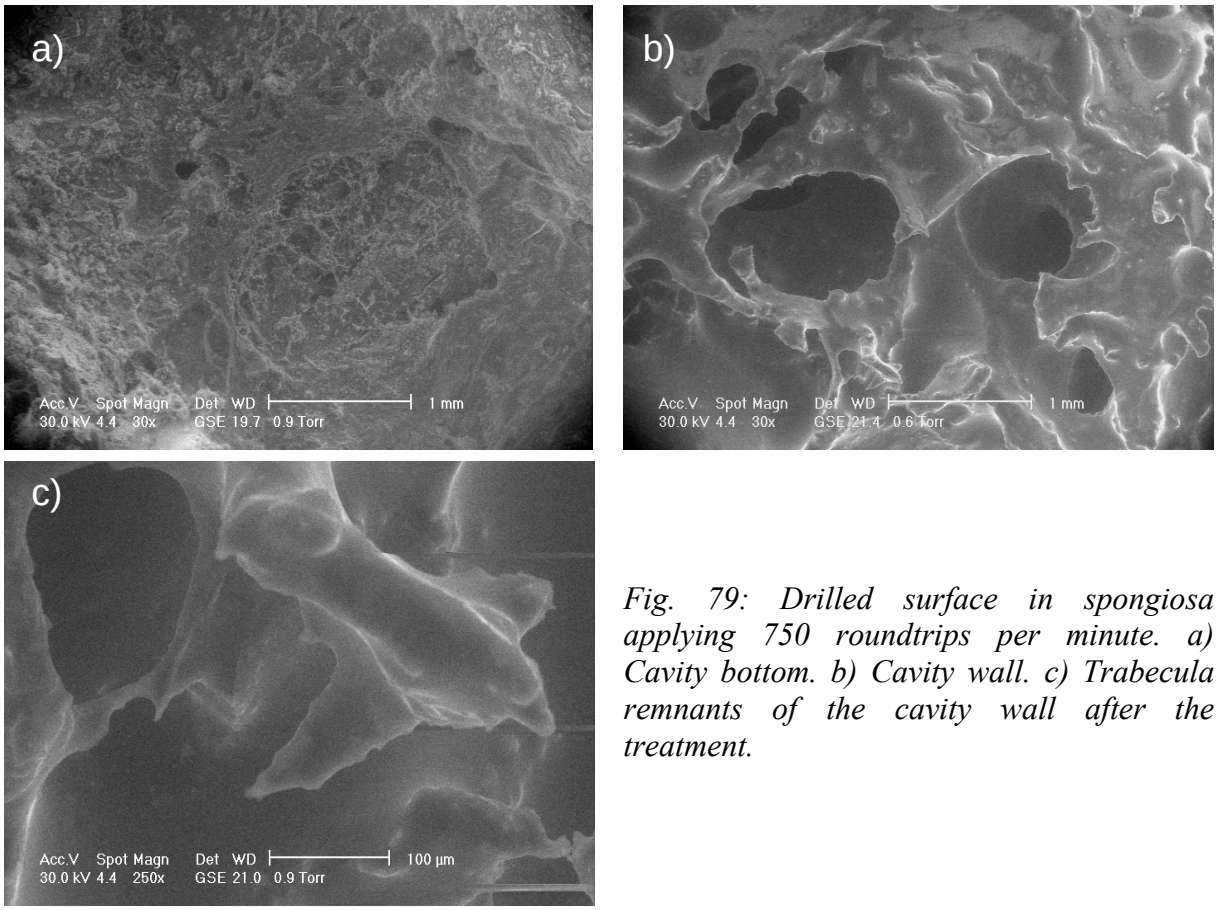

Fig. 79: Drilled surface in spongiosa applying 750 roundtrips per minute. a) Cavity bottom. b) Cavity wall. c) Trabecula remnants of the cavity wall after the treatment.

The morphology produced by 2000 roundtrips per minute looks even worse. Again, some kind of smear layer was generated accompanied by lots of debris. The trabecular structure of the cavity bottom has completely vanished behind this layer. Although single trabeculae can be discovered the general impression of the cavity wall is also very disappointing. Moreover, the bubble-like artefacts present in the magnification of a trabecula give evidence of melting due to friction.

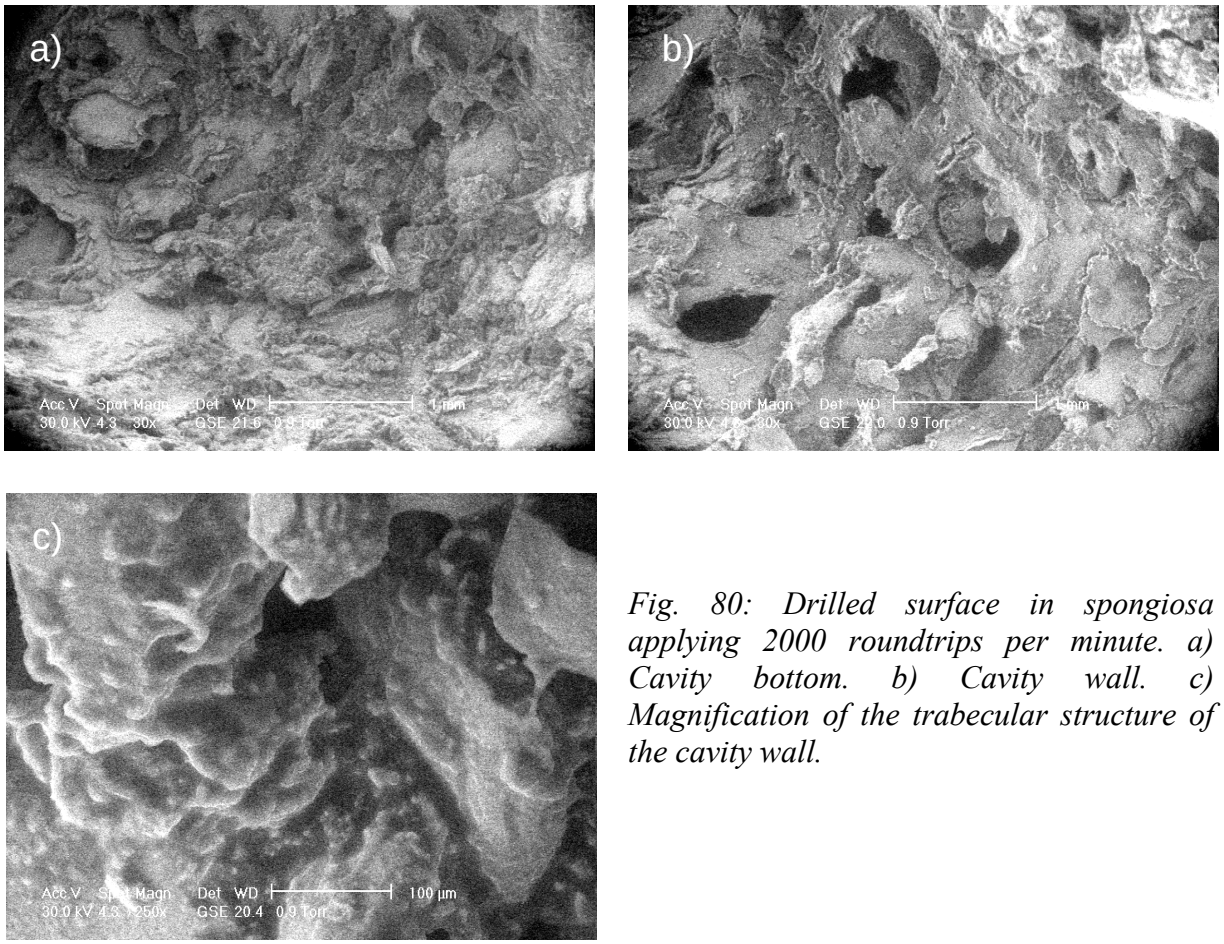

Fig. 80: Drilled surface in spongiosa applying 2000 roundtrips per minute. a) Cavity bottom. b) Cavity wall. c) Magnification of the trabecular structure of the cavity wall.

A comparison of these results to Fig. 81, where the magnification of an untouched trabecula in native spongiosa is shown, is almost impossible.

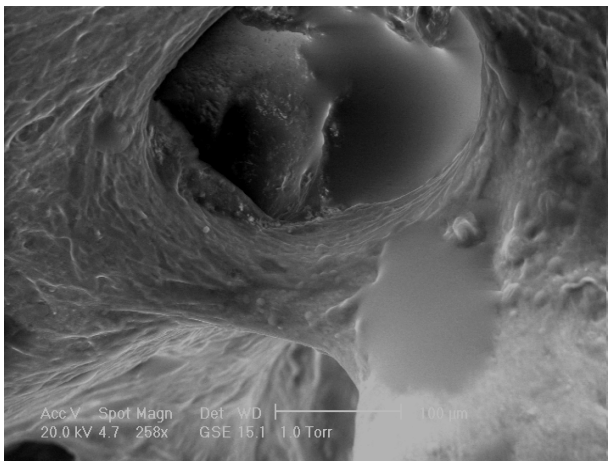

Fig. 81: ESEM of a trabecula in native spongiosa. The bone surface is covered by soft tissue and fat.

The situation is similar for compacta although not that dramatic, because of the relatively smooth natural texture of this tissue. As shown above, especially for higher rotational frequencies of the drill the potential of overheating has to be feared. Also in case of compacta whole tissue particles can be dragged off. All these fact lead to the conclusion, that the goal of damage-free and conservative bone tissue treatment can not be reach by mechanical drills.

5.3.2 ERBIUM LASER TREATMENT

As Erbium lasers are already in use for dental applications, the occasion presents itself to use these systems for bone ablation. In an extensive study several laser parameters were tested. For certain settings the goal of secure tissue treatment gets closer.

5.3.2.1 MATERIAL AND METHODS

Initially, both Erbium systems, the Er:YAG and the Er,Cr:YSGG laser, were applied to judge their performance with respect to the left over morphology. Several power settings were chosen. Ablation was performed with an air-water spray as common for Erbium laser ablation. In further experiments the influence of the air-water mixture on the morphology was investigated. Thereby just the Er,Cr:YSGG laser was involved as it generated better surface quality. The fraction of air and water of the spray could also be adjusted very accurate by defining the percentage share of the mixture.
For the first experiments human spongiosa was used, for the following tests bovine spongiosa, compacta and cartilage were involved. The generated cavities were sectioned across the midline. Afterwards they underwent ESEM analysis. As the cavities were quite deep two micrographs were obtained, one of the top and one of the bottom. Those picture were then fit together to capture the whole cavity. When looking at these pictures just the inner part of the picture has to be regarded. The outermost parts appearing as bulk material originate from the cut of the diamond saw.

5.3.2.2 RESULTS

Favourable as well as disadvantageous cavity features could be obtained with both systems. A comparison between good and bad result for each laser is made. To start with, cavities generated in human spongiosa by the Biolase Er,Cr:YSGG laser are presented in Fig. 82. For the Er,Cr:YSGG system a fluence of 37.9 J/cm² is already too high to prepare spongy tissue without damage. Although the bridge-like structure can be identified, whole trabecular branches got removed. In the general view of the cavity lots of debris is visible. Large cracks are evident and molten regions are indicated. The magnification in Fig. 82 b) confirms this: The trabecula is broken and the surface of the bone tissue is covered by molten and re-solidified zones. The cavity features achieved by applying a fluence of 24.9 J/cm² are quite promising on first sight. Obviously, the tissue got ablated while the trabecular network was preserved. Hardly any debris can be identified. Nevertheless, a closer look reveals that minor cracks appeared and that the cut borders are slightly molten. That implies that a moderate heat transfer to the surrounding tissue took place. Anyhow, this cavity showed the best surface features among all cavities generated in spongiosa by Erbium lasers. For sure, this laser setting bears the potential for further improvements of the morphology.

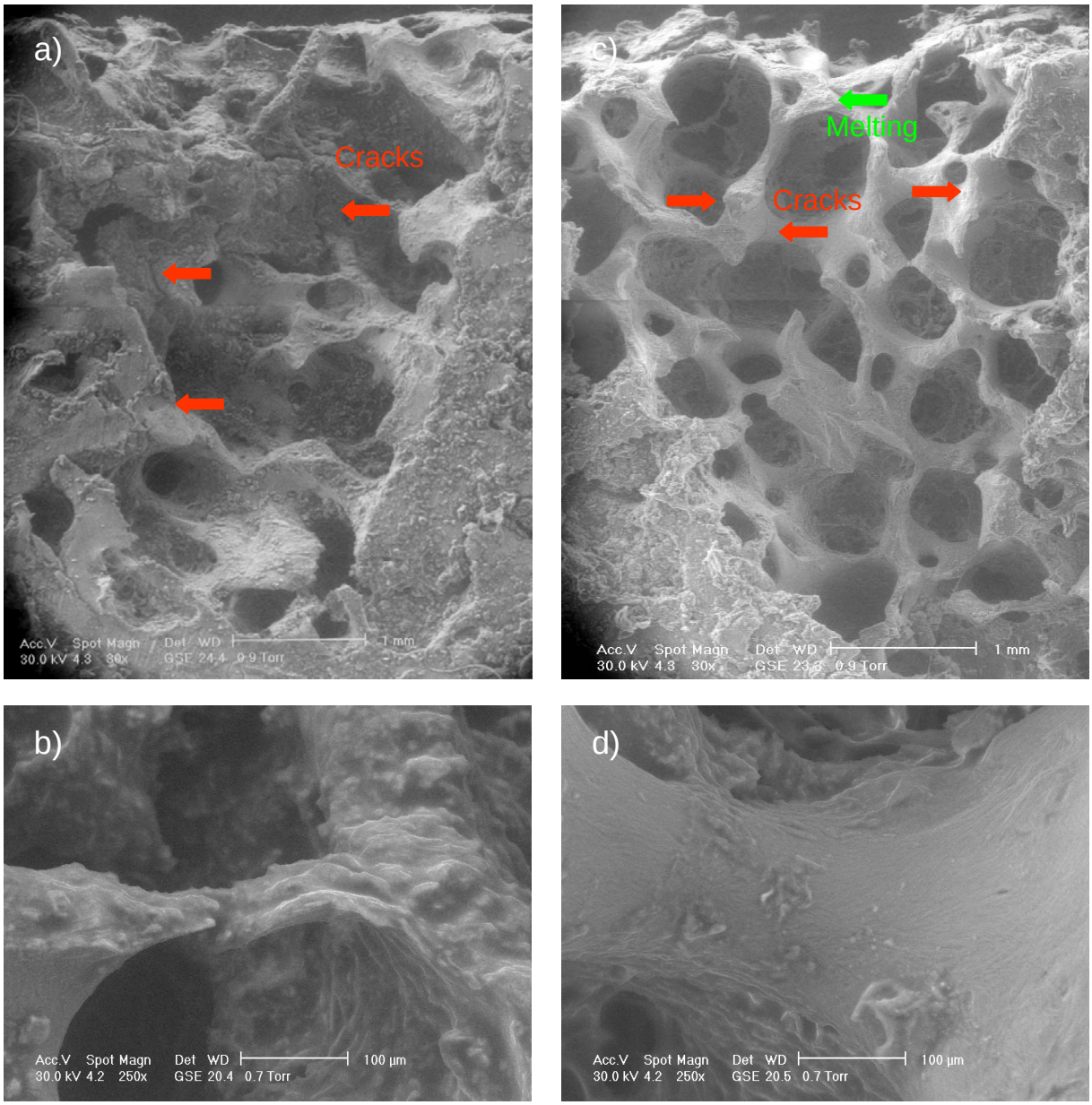

Fig. 82: a) Cavity in human spongiosa generated by the Er,Cr:YSGG laser with 37.9 J/cm² and an air-water mixture of 51 % water and 66 % air. b) Magnification of a trabecula of the cavity depicted in a). c) Cavity in spongiosa generated by the Er,Cr:YSGG laser with 24.9 J/cm² and an air-water mixture of 51 % water and 66 % air. d) Magnification of a trabecula of the cavity depicted in c).

A similar comparison of the results of Er:YAG laser ablation is depicted in Fig. 83. In case of Er,Cr:YSGG laser ablation a negative example was shown for an excessive fluence. Here, unfavourable surface features arose from insufficient fluences. While a fluence of 37.9 J/cm² in case of Er,Cr:YSGG ablation lead to devastation of the trabecular structure, the relatively low fluence of 11 J/cm² of the Er:YAG system exterminate any trabecular branch. Instead of this, extensive melting occurred. Micro-cracks were induced as well. In contrast to the former example, where high pulse energies caused dehydration, too low pulse energies are the reason for crack formation: To generate a cavity the same region has to be passed more often by the laser beam than for higher fluences. As the fluence of 11 J/cm² lies around its threshold value the capability of effective tissue removal is quite low. Thereby more energy is absorbed by the tissue and converted into heat than used for ablation. The consequences are dehydration

causing cracks and melting. Better results with the Er:YAG laser could be achieved with a fluence of 32.4 J/cm². Although the native structure of single trabeculae remained untouched, as Fig. 83 d) demonstrates, whole bridges got eliminated. Again, melting is left on the cut borders and micro-cracks are apparent. Interestingly, these cracks appeared predominately offside the ablation site and not directly on the trabeculae like in case of Er,Cr:YSGG ablation with 24.9 J/cm². An explanation may be, that these areas were in the near vicinity of the ablation site, that again energy was not used for ablation but was converted into heat instead.

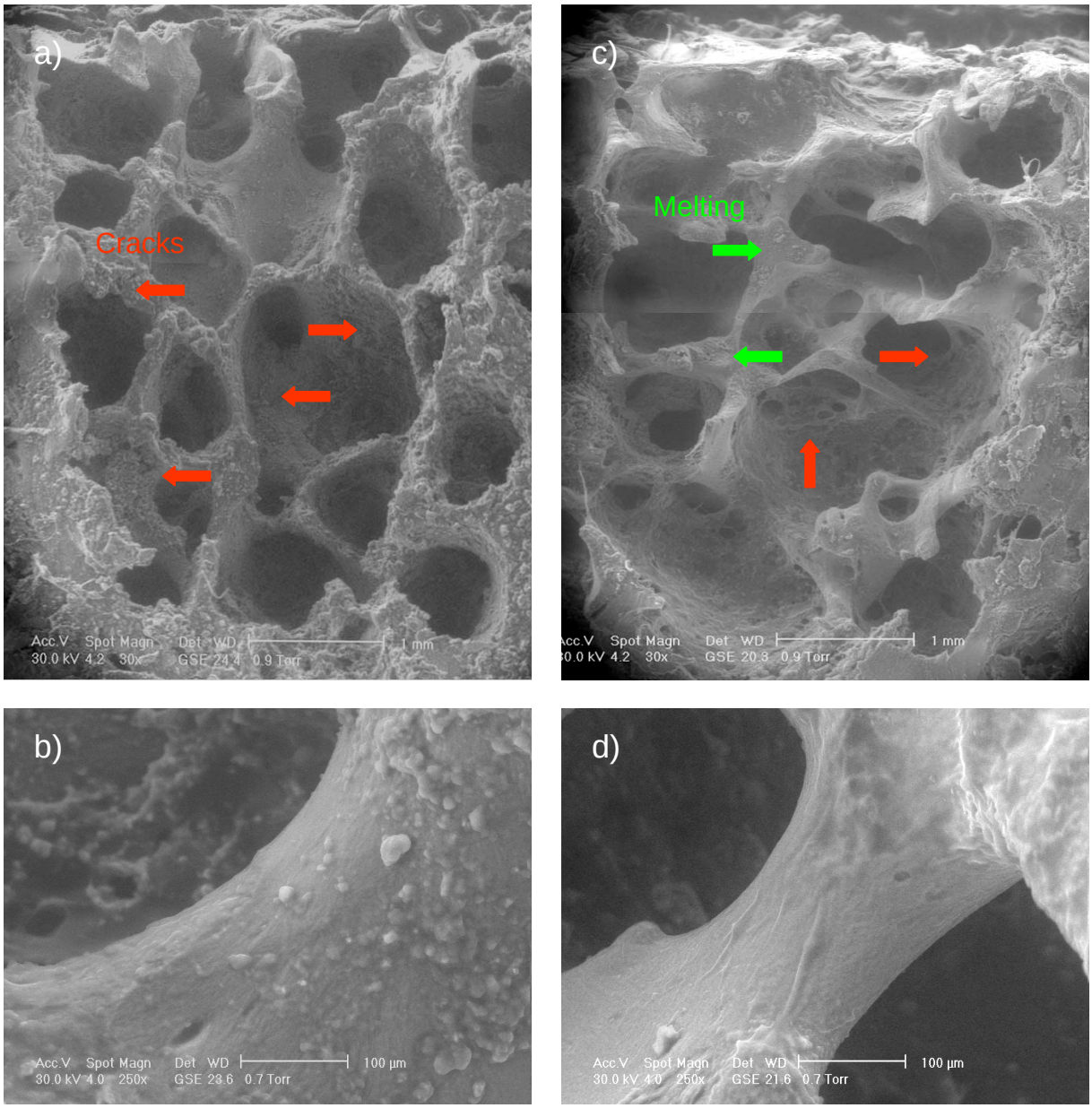

Fig. 83: a) Cavity in human spongiosa generated by the Er:YAG laser with 11 J/cm². b) Magnification of a trabecula of the cavity depicted in a). c) Cavity in spongiosa generated by the Er:YAG laser with 32.4 J/cm². d) Magnification of a trabecula of the cavity depicted in c).

The air-water spray of the Er:YAG laser could be regulated continuously be turning a wheel. Therefore, the exact amount of air and water used during the experiments can not be provided. Anyhow, the air-water mixture can strongly influence the ablation product. Several tests were made trying various fluences combined with different air-water mixtures. It is remarkable that even minor changes of the air or water amount lead to completely distinct results.

Fig. 84 captures two cavities, both ablated with the Er,Cr:YSGG laser with 39.6 J/cm². The cavity which was generated with 60 % water and 65 % air shows an irregular rim and a rough and scaly surface. Decreasing the water amount by 5 % yielded much better quality. The cavity walls are smoother and the rim is more defined. Indeed, the cavity in Fig. 84 b) is among the best results obtained in compacta. Nevertheless, as for all other cavities generated during these investigations some debris is also present in this cavity. Additional rinsing after laser treatment might have removed this debris.

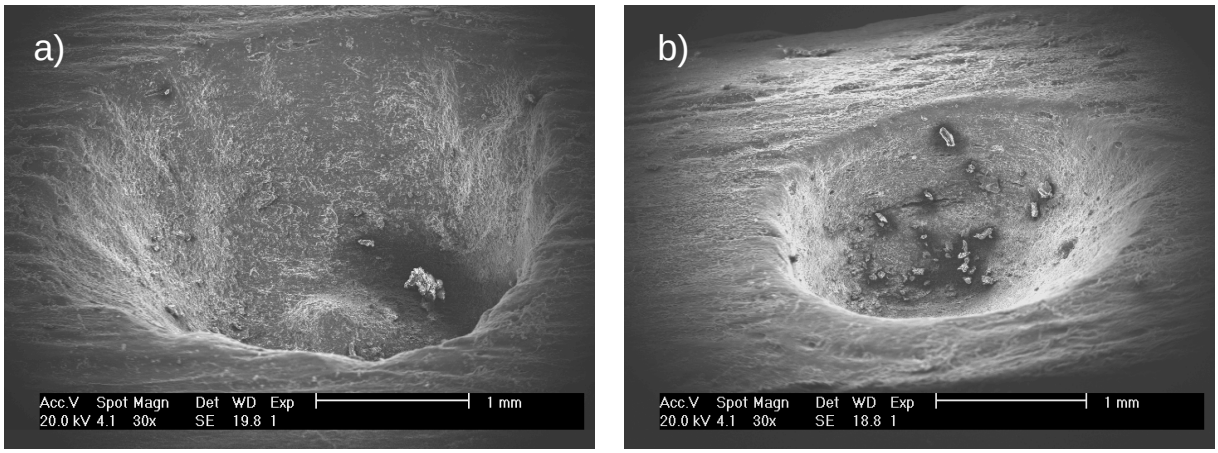

Fig. 84: Er,Cr:YSGG laser ablated bovine compacta with 39.6 J/cm². a) 60 % water and 65 % air. b) 55 % water and 65 % air.

Similar experiments were also performed with cartilage. The results were very sobering as most laser settings destroyed the morphology completely, i.e. the surface was rugged or even changed. Dehydration was the main hazard to be faced accompanied by carbonisation. One of the few cavities with surface features comparable to natural cartilage is depicted in Fig. 85. Indeed, the fluence of 67.9 J/cm² applied for ablation was rather high to excavate tissue of this relatively soft matter. Anyhow, all other results were not even that good. So in general Erbium laser ablation of cartilage with the chosen parameters cannot be recommended.

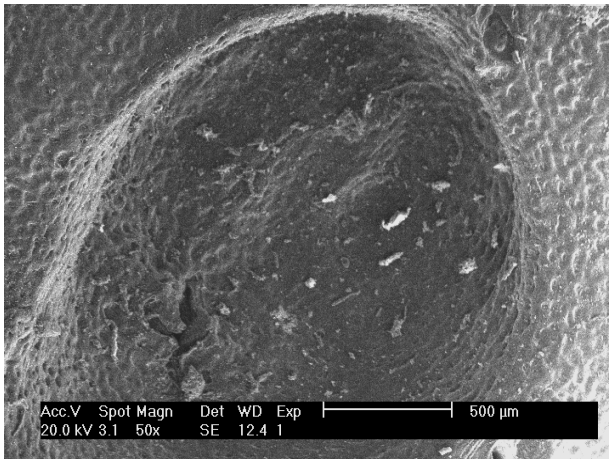

Fig. 85: Bovine cartilage treated with the Er,Cr:YSGG laser with 67.9 J/cm², 55 % water and 65 % air.

5.3.3 USPL TREATMENT

For dental hard substances it has already been shown that scanned USLP are capable of producing cavities with surface feature superior to mechanically treated or Erbium laser ablated tissue. With the same expectations, scanned USPL ablation of bone tissue was performed. As it turned out, the goal of damage-free and minimal invasive treatment is within reach.

5.3.3.1 MATERIALS AND METHODS

The 330 fs Yb:Glass laser and the Ti:Sapphire laser with pulse durations of 700 fs and 7 ps, respectively, were used for these studies. To prepare larger areas the x-y-scanner was employed. Two scan patterns were programmed: A rectangular scan and an Archimedic spiral. The scan patterns were adjusted to the focal spot diameter and the PRR of the laser system, which means that the scan velocity and the distance between two traces of the scan pattern were chosen in order to yield a convenient overlap of subsequent laser pulses. When the overlap is too high accumulation effects influence the surface quality. The ablated cavities were investigated via ESEM.

5.3.3.2 RESULTS

To start with, rectangular scans of 330 fs Yb:Glass laser ablation of bovine spongiosa is presented in Fig. 86. It was ablated with 1.9 J/cm², which is more than twice the threshold value. The overall view shows precise cavity geometry with defined and smooth edges. The natural structure of spongiosa remained untouched without any carbonisation. Although no air-water spray was used no debris is evident. The magnification in Fig. 86 b) captures the cut border of a trabecula taken from the cavity bottom. Compared to the cut borders generated by the mechanical drill or the Erbium system, the one presented is very smooth. No micro-cracks or melting were introduced to the surrounding bone tissue. Looking at the edges of the rectangular cavity, melting caused by accumulation effects is visible. When the laser beam reaches the borders of the scan pattern it has to be shifted along a 90° line. After another 90° shift it moves its way back. Due to this turn an excessive number of laser pulses impacts onto the same tissue area. This effect is even more pronounced at the corners of the cavity. Nevertheless, by the implementation of a shutter this problem can easily be eliminated. Fig. 86 presents trabeculae located near a corner of the cavity. Leaving the melting out of account, it is an example of the non-destructive ablation procedure. The bridge, a little larger than 200 µm, connecting the trabeculae got removed by the laser while the trabeculae themselves did not experience any collateral damages like cracks.

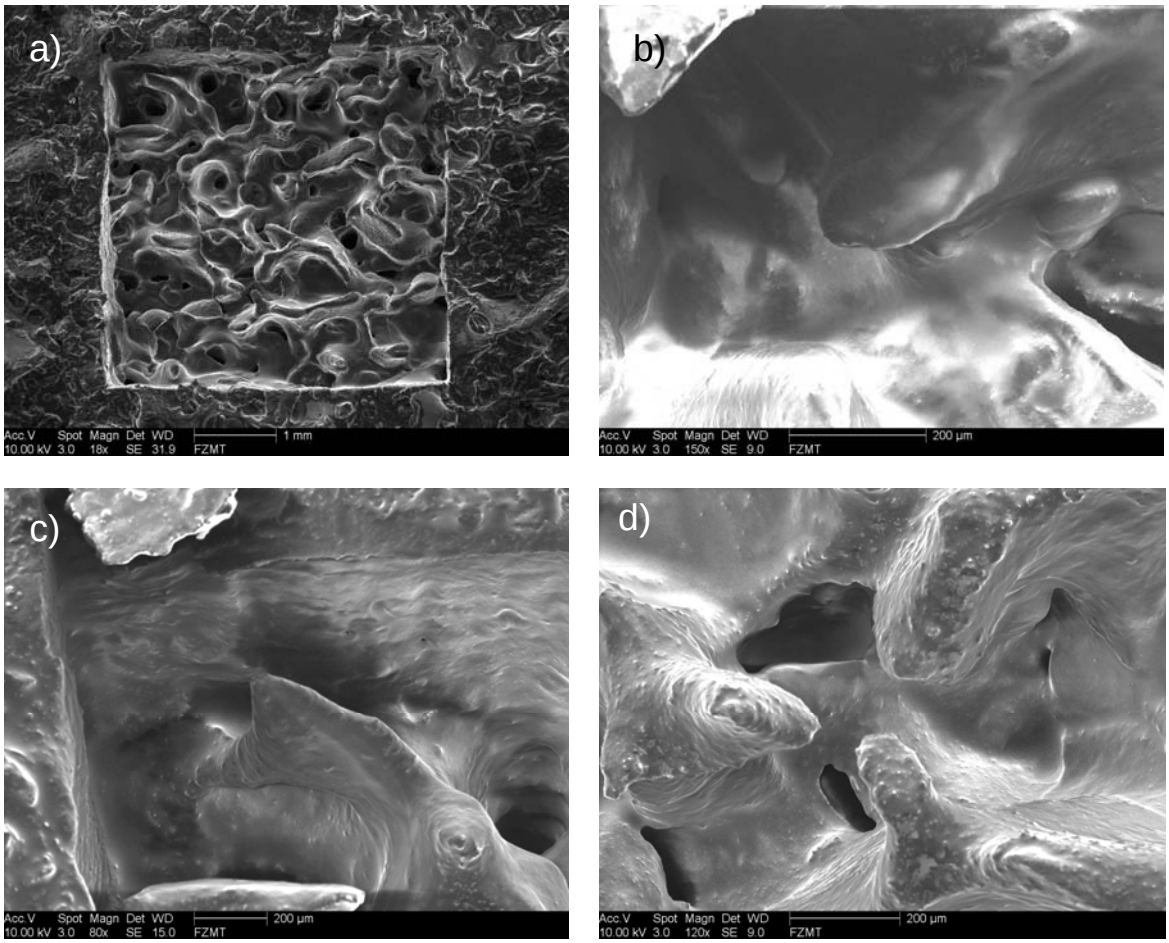

Fig. 86: Rectangular scan in bovine spongiosa ablated by the 330 fs Yb:Glass laser with 1.9 J/cm² and 1 kHz PRR. a) Overall view of the cavity. b) Magnification of the cut border of a trabecula located at the cavity bottom. c) Magnification of the edges of the cavity. d) Trabeculae located near the corner of the cavity.

When scanning the USPL beam according to an Archimedic spiral accumulation effects can be kept under control without the additional use of a shutter. The only issue is, to select proper laser parameters. Fig. 87 captures 700 fs and 7 ps Ti:Sapphire laser ablation of compacta with 0.65 J/cm² and 1 J/cm², respectively. For both settings the cavity features including well defined geometry, smooth cavity rims, the absence of debris and carbonisation are very appreciable. The natural structure of compacta was also not affected by the ablation. Cavity inclinations are clean and free of melting. Just the magnification of the cavity bottom reveals some differences between 700 fs and 7 ps ablation as Fig. 87 c) and f) demonstrate. 700 fs ablation left molten and re-solidified zones on the cavity floor, 7 ps introduced no alterations. A possible explanation may be that the chosen fluence of 0.65 J/cm² is within threshold range for 700 fs ablation and it is therefore ineffectively absorbed for plasma formation.

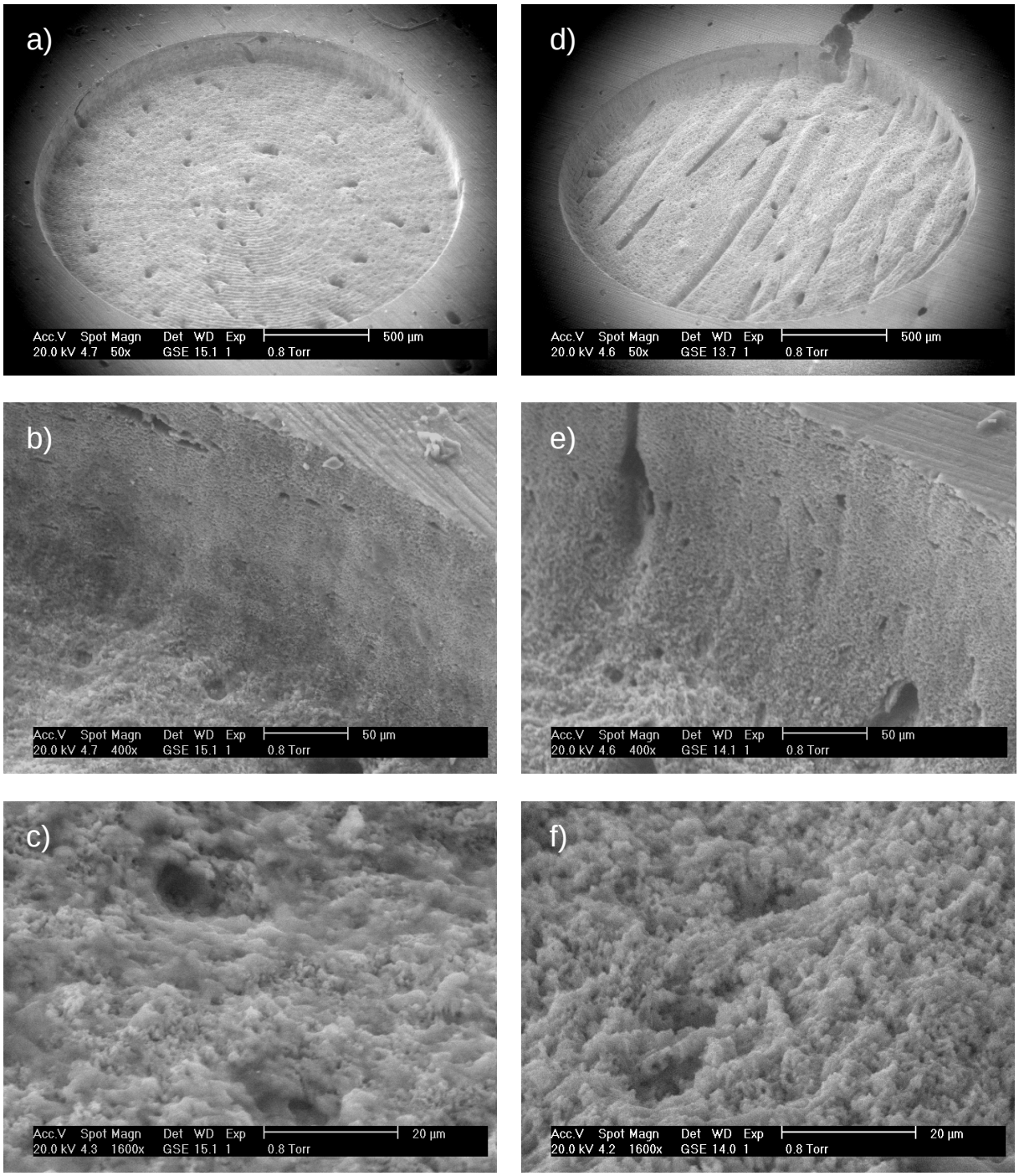

Fig. 87: Bovine compacta ablated by Ti:Sapphire laser pulses scanned according to an Archimedic spiral. Parameters: 1 kHz, 20 roundtrips. a) Overall view, b) magnification of the rim and c) magnification of the bottom of a crater obtained with 700 fs and 0.65 J/cm². d) Overall view, e) magnification of the rim and f) magnification of the bottom of a crater obtained with 7 ps and 1 J/cm².

Results obtained by Ti:Sapphire laser ablation of cartilage are similarly promising. In Fig. 88 700 fs and 7 ps with 0.65 J/cm² and 1 J/cm², respectively, are depicted. The morphology is comparable to the natural structure of cartilage. The surface was not altered. There are no signs of thermal injury. The slight ripples present in both micrographs are artefacts of the tissue itself.

In praxis, cutting of cartilage might be more relevant than drilling circles. Therefore, the scan parameters can be adjusted to yield line scans generating straight cuts. Morphological features of the cut borders are expected to be of same quality as reported here.

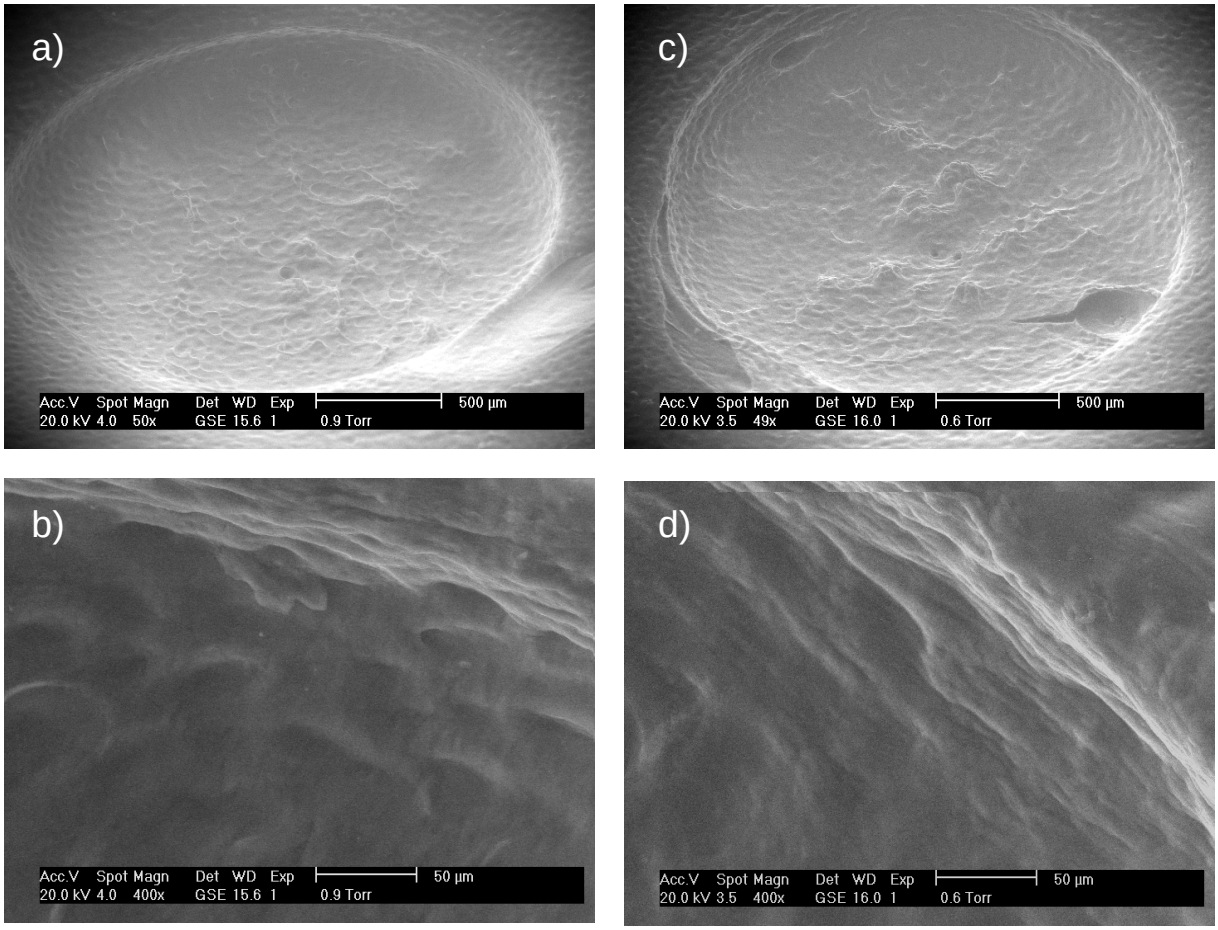

Fig. 88: Bovine cartilage ablated by the Ti:Sapphire laser following the traces of an Archimedic spiral. Parameters: 1 kHz, 20 roundtrips. a) Overall view and b) magnification of the rim of a crater obtained with 700 fs and 0.65 J/cm². c) Overall view and d) magnification of the rim of a crater obtained with 7 ps and 1 J/cm².

Although scanned USPL ablation of spongiosa has already been presented for the Yb:Glass system, some pictures are provided for the Ti:Sapphire ablation of the same tissue. As spongy tissue involved in the latter studies was strongly larded with fat, the appearance of the cavities after ablation is somewhat different. As evident in Fig. 89 bone got ablated properly, but a bubbled fat layer covers the whole cavity. Anyhow, for the following healing process of bone no negative influences of this affected fat layer are expected.

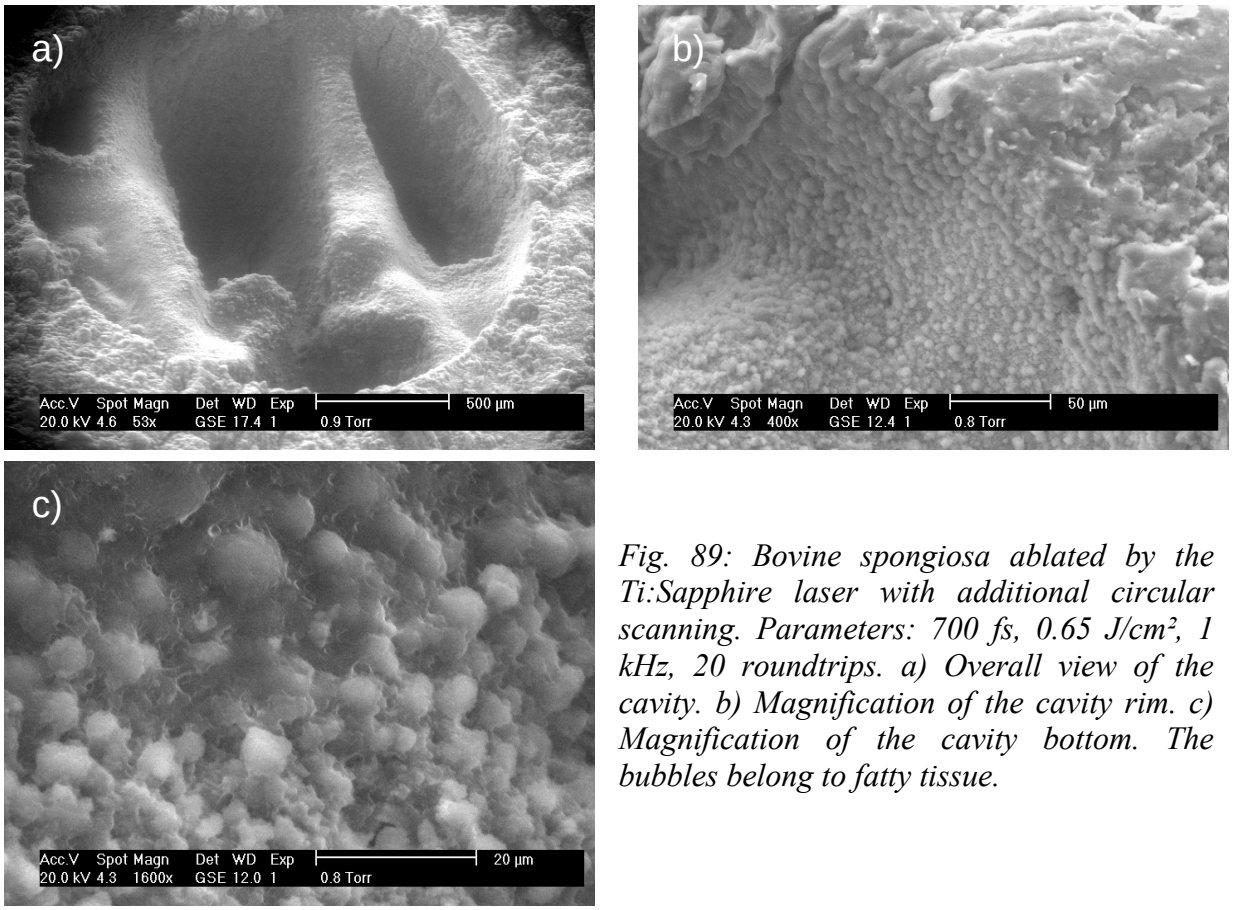

Fig. 89: Bovine spongiosa ablated by the Ti:Sapphire laser with additional circular scanning. Parameters: 700 fs, 0.65 J/cm², 1 kHz, 20 roundtrips. a) Overall view of the cavity. b) Magnification of the cavity rim. c) Magnification of the cavity bottom. The bubbles belong to fatty tissue.

5.3.4 LITERATURE REVIEW

Several authors have already tested the applicability of Erbium laser wavelengths for bone tissue treatment. Their motivations were either to overcome the drawback associated with mechanical instruments like saws and drills or the comparison to other lasers such as CO_2, Nd:YAG and FEL. Unfortunately, the obtained results are sometimes controversial: While some authors report on favourable tissue quality and good healing conditions, others consider Erbium laser prepared surfaces as less beneficial. For example Peavy et al. (1999) ablated bovine femur with 2.9 µm laser pulses with a fluence of 72 J/cm² and describes the remaining surface as uniform with varying degree of melting but no evidence of micro-fissures. On the other hand, the smooth bone texture was broken into slabs by multi-fissures caused by the saw. The laser produced clean cuts, while the saw generated a large amount of debris at the cut site. Kimura et al. (2001), who operated their Biolase Er,Cr:YSGG laser with 625 mJ and 8 Hz yielding 141 J/cm² , were also quite satisfied with their results. They ablated canine mandible and bones from healthy adult mongrel dogs and report on sharp cavity edges, smooth walls, no melting and intact prisms without fusing. The surfaces had a scaly like appearance and debris was just visible at high magnifications. Among the supporter of bone treatment by Erbium lasers are also Keller et al. (1991). This group prepared cortical bone of beagles with 30-50 J/cm² and could not detect any thermal damage just a 10-20 µm fringed seam. The duration of the healing process of the Er:YAG laser osteotomy and that of a normal secondary fracture resemble. This result could not be obtained by Nelson et al. (1989) two years before. When they treated rabbit tibiae with a higher fluence of 141 J/cm² deep cuts with sharp edges and no gross charring or burrning of adjacent bone tissue was produced. Nevertheless, a microscopic zone of damage caused delay in healing. Sasaki et al. (2002) ablated bones of Wistar rats and calvaria compact bone with 35 J/cm² and detected micro-cracks, disorganization and slight re-crystallization of the original apatite and reduction of the

surrounding organic matrix. The list of supporters and opponents of Erbium laser ablation of bone tissue can be continued as it has attracted the interest of various scientists in the past decades. USPL ablation of bones has not been stressed that extensively, as it has just been focused in the recent years. Armstrong and his colleagues (2002) worked on formalin fixed incus and stapes with a 350 fs Ti:Sapphire laser without additional scanning and applied a fluence of 2 J/cm². They detected almost no thermal damage and very little evidence of photomechanical injury. Stapedotomy was round and smooth with no cracks or fractures. Subtle melting of hydroxyapatite occurred just at higher powers. Their conclusion was, that USPL may provide a useful tool for otologic and skull base surgery, where precise hard tissue ablation is required adjacent to critical structures. In the research of Ozono et al. (2003) and Kamata et al. (2004) Ti:Sapphire laser ablation of hydroxyapatite, one of the main components of biological hard tissue, was investigated. One crucial medical issue is to preserve the chemical properties of the machined surface for the following reason: If the chemical characteristics of hydroxyapatite are changed, bone tissue cannot re-grow after laser processing. They confirmed that the P/Ca ratio stayed constant after irradiation with 50 fs and 2 ps at several fluences. The fact that hydroxyapatite was not altered promises good healing conditions for USPL treated biological hard tissue.
Keeping all this information in mind, the conducted study sets the next step towards the applicability of USPL for medical treatment in the near future. The conclusion below summarizes the main findings of this research.

5.3.5 CONCLUSION

Improvement of surface quality of excavated cavities in bone tissue can already be achieved by using Erbium systems instead of common mechanical tools. The drawbacks arising from externally applied forces like friction producing a smear layer or torn out tissue particles leaving fissured bone remnants can so be avoided. Surface features created by Erbium systems can be enhanced by matching several parameters, for instance pulse duration, fluence and pulse repetitions rate, not to forget about the tremendous influence of the air-water mixture. Nevertheless, a surface as homogeneous and smooth as the one generated by scanned USPL cannot be reached, because of the micro-explosions that are part of the ablation process of Erbium lasers. When the plasma initiated by USLP gets expelled, thin layers with thicknesses of a few µm are evaporated. By that, tissue is gently ablated layer by layer leaving a well-balanced morphology. Anyhow, the hazard of melting has to be faced for Erbium as well as for USP lasers. In the first case, elongated pulse width, excessive pulse energies, accumulation effects and insufficient cooling by the air-water spray are responsible for that. In case of scanned USPL, special care has to be taken to choose fluences well above threshold value and to avoid extensive overlapping of subsequent pulses. But even when inappropriate laser parameters are erroneously selected for ablation of bone, the risk of destroying whole areas of tissue can be completely eliminated by using USPL as the conducted study revealed. The application of an air-water spray is not necessary to enhance the crater morphology of USP lased cavities. Anyhow, for longer treatments syringing might be helpful to avoid dehydration of the tissue and to keep the temperature increase, although very low, under control.

5.4 LASER-INDUCED BREAKDOWN SPECTROSCOPY

For minimal invasive and selective treatment of different types of tissue a feedback system has to be established to reliably distinguish between them. Laser induced breakdown spectroscopy (LIBS) or sometimes referred to as laser induced plasma spectroscopy (LIPS) as a non-contact in-situ method for elemental chemical analysis of the composition of substances, no matter if solid, liquid or gaseous, is therefore best suited.

5.4.1 BACKGROUND INFORMATION

When focusing a short high intensity laser pulse onto the surface of the sample of interest free electrons are generated. Subsequently, plasma is formed near the surface of the target by avalanche ionisation. This process is called optical breakdown. When the high density plasma expands into the ambient atmosphere the hot and radiating plasma plume cools down. The optical plasma emission is composed of transitions lines of the material's constituents. By detecting these transition lines of the plasma via a grating spectrometer information about the quantitative and qualitative composition of the target can be gained.
LIBS, which is applicable in a wide range of fields like material processing, space applications and also diagnostics, can be performed with ns-, ps-, and fs-pulses. The latter are especially advantageous for analysis of biological samples with high spatial resolution. For detailed information about LIBS and the various contributing processes to the work of Stehrer (2005) is referred. Besides the analysis of the chemical composition of metals, a solid theoretical background and instructions for a convenient experimental setup are provided.
Optical emission spectroscopy is just based on intrinsic light emission of the laser induced plasma. Therefore no other excitation source is needed. As a consequence, the experimental setup is quite simple and adaptable to automation and remote sensing. By that, even the temporal and spatial evolution of the plasma can be reproduced. (Capitelli, 2004)

5.4.2 MATERIALS AND METHODS

Performing LIBS nearly no sample preparation is necessary as laser ablation yields a fresh surface after each laser pulse. Spongiosa, compacta and cartilage, the targets of interest, were just cut to guarantee an even surface. The Hurricane-i Ti:Sapphire laser operated at a low PRR of 20 Hz was used for this studies. The plasma spark induced on the tissue surface was captured by a high resolution spectrometer, into which the light emitted from the plasma was coupled. This spectrometer, i.e. a fibre, was combined with a time resolved detector. All these units were computer controlled to ensure correct timing. The experimental setup is shown in Fig. 90.

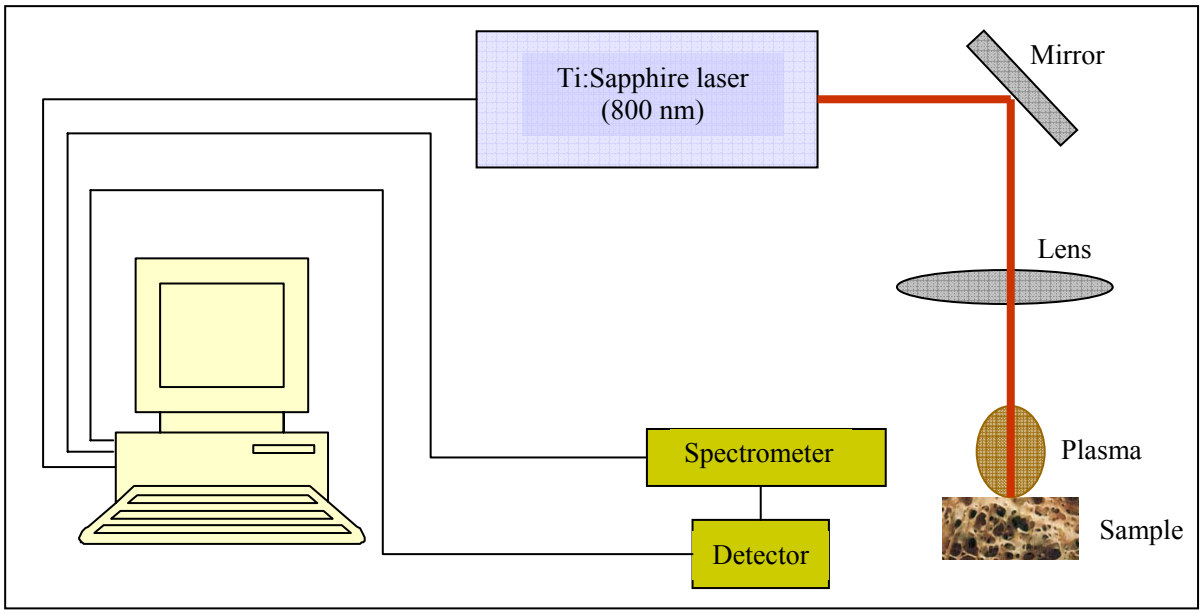

Fig. 90: Experimental setup for LIBS.

Wavelength regions around 422 +/- 18 nm and 526 +/- 18 nm were investigated. Measurements were performed on three different spots on the tissue surface. Five spectra were obtained from each spot. The spectra were then averaged to eliminate inconsistencies. Peaks arising from the spectral continuum, which correspond to a transition from an upper exited level to a lower excited level, were identified to be mainly Ca lines using the atomic spectra database of the National Institute of Standards and Technology[28]. For spectra in the field of 526 +/- 18 nm also P lines were found.

5.4.3 RESULTS

LIBS spectra of both wavelength regions and all bone samples are depicted in Fig. 91 and Fig. 92. All plots are normalized to their highest peak corresponding to Ca. The height of the remaining peaks gives their relative intensity in comparison to these Ca transition lines. The peaks appearing at 422.67 nm can solely be attributed to Ca. Besides Ca also P can be identified in the spectra obtained at 526.56 nm.

[28] http://physics.nist.gov

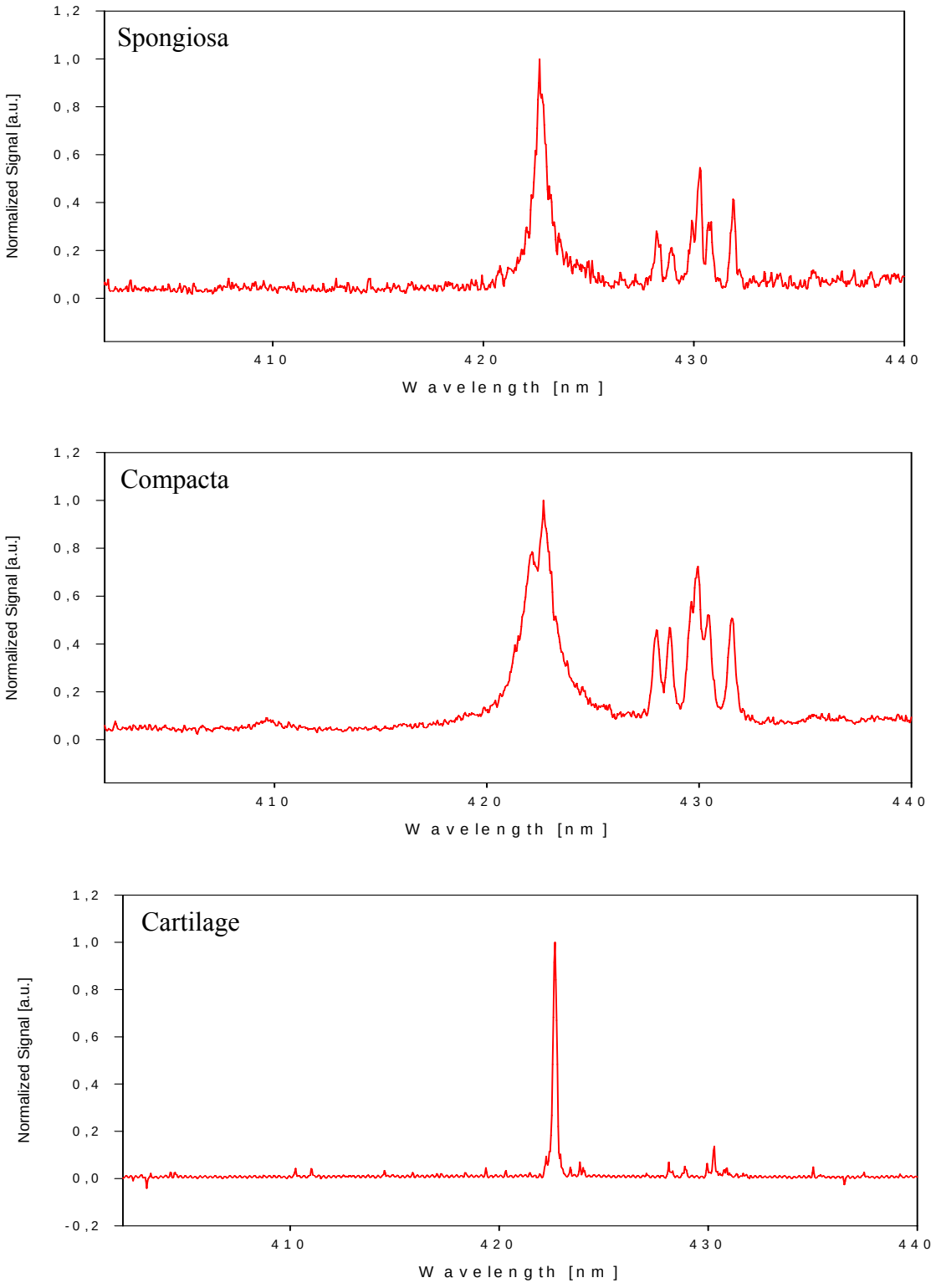

Fig. 91: LIBS spectra of spongiosa, compacta and cartilage depicting Ca peaks in the wavelength region of 422 +/- 18 nm.

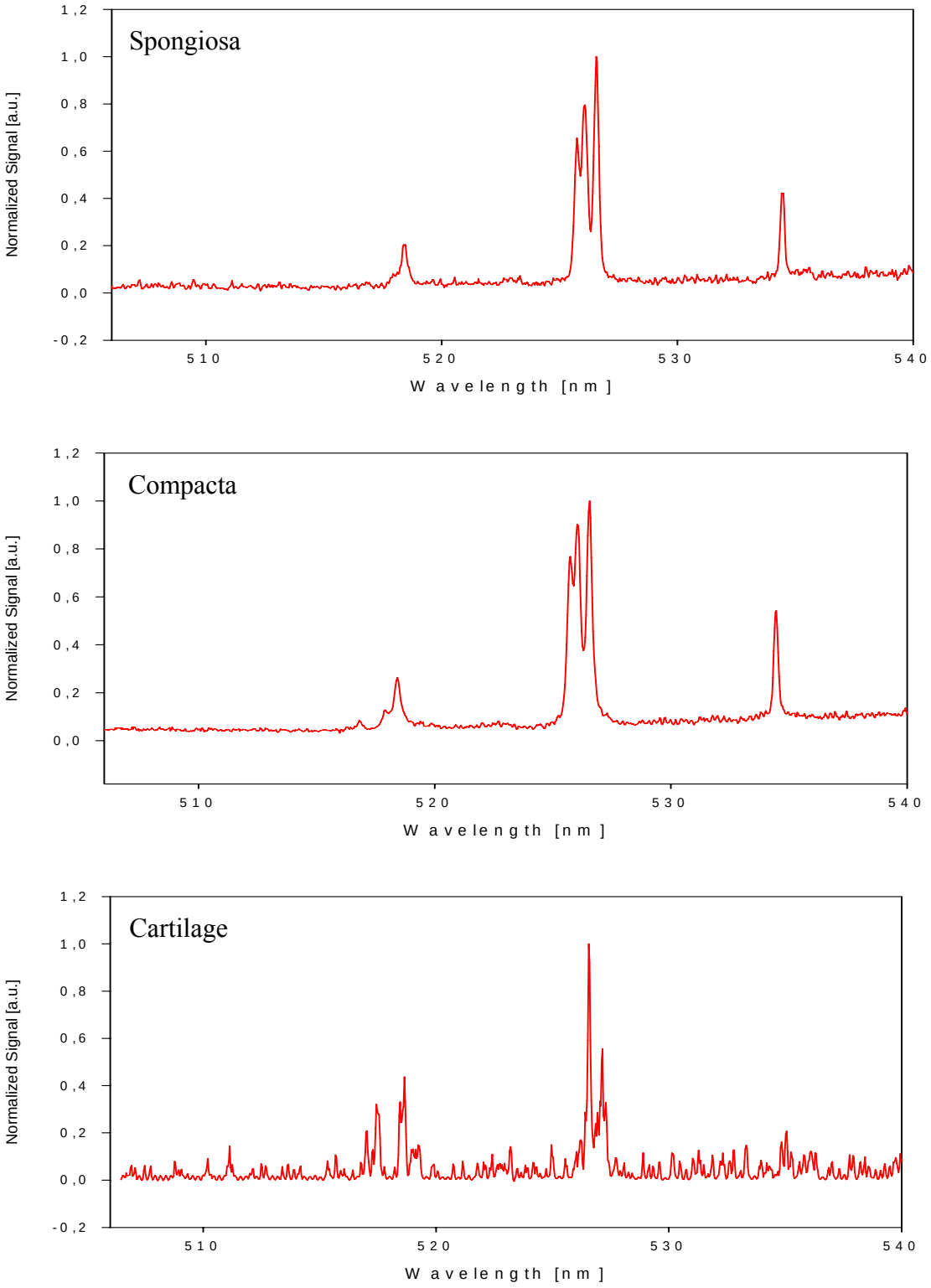

Fig. 92: LIBS spectra of spongiosa, compacta and cartilage depicting Ca and P peaks in the wavelength region of 526 +/- 18 nm.

For each spectral range, the ratios of the peaks present in all materials were established and listed in Table 28 and Table 29. The ratios of the P intensity lines were also compared to the Ca peak with maximum signal. The relative intensities can now be used to distinguish between different types of materials, as they are directly related to their real concentration inside the tissue.

Table 28: Ratios of Ca peaks in the region of 422 +/- 18 nm for spongiosa, compacta and cartilage.

Ca-Peaks	Relative Intensity		
Wavelength [nm]	Spongiosa	Compacta	Cartilage
422.67	1	1	1
430.25	0.605	0.709	0.105
431.87	0.435	0.516	-

Table 29: Ratios of Ca and P peaks in the region of 526 +/- 18 nm for spongiosa, compacta and cartilage.

Wavelength [nm]		Relative Intensity		
Ca-Peaks	P-Peaks	Spongiosa	Compacta	Cartilage
518.88		0.228	0.269	0.437
	525.35	0.625	0.776	0.091
526.17		0.787	0.901	0.171
526.55		1	1	1
	534.47	0.413	0.532	0.207

Besides a somewhat different appearance especially in the lower spectral range, cartilage can easily be distinguished from spongiosa and compacta by its generally lower ratios. One exception is the Ca peak at 518.88 nm, where a relative intensity of 0.437 exceeds those of spongiosa and cartilage. Although, the comparison between spongiosa and compacta affords a closer look, a distinction between those materials is also possible without a doubt. The ratios of the Ca peaks of 430.25 nm and 431.87 nm are ~18 % higher for compacta compared to spongiosa. The spectra around 526 nm reveal also higher ratios for compacta, no matter if Ca or P lines are concerned. Indeed, the 518.88 nm and 526.17 nm Ca peaks of compacta exceed their spongiosa counterparts for 18 % and 14 %, respectively. The P lines at 525.35 nm and 534.47 nm are even 24 % and 29 % higher.
Obviously, plasma spectroscopy is a valuable source to distinguish between different bone materials. A loop control system can be developed to automatically interrupt laser ablation when LIBS signalizes, that biological tissue, that actually should be spared, was touched. A feedback system based on LIBS can therefore enhance selective and finally minimal invasive USPL treatment.

5.5 TEMPERATURE MEASUREMENTS

Bone tissue can just stand moderate temperature increase, otherwise damages are introduced. The worst consequence of excessive heat impact is that the vital bone cells get destroyed and the regeneration process of the bone tissue gets extended or even inhibited. Absolute temperatures of >43 °C applied for seconds to minutes already yield irreversible damages like membrane damages with oedema or denaturations of enzymes. Temperatures of >60 °C

applied for less then a second can even lead to necrosis. A list of hazards to be feared from temperature rise is provided in Table 30. It is taken from (Keller, 1998).

Table 30: Temperature related damages of bone tissue.

Temperature	Duration	Consequences	Effect
37 – 43 °C	Minutes to hours	Heating up, oedema	reversible
43 – 60 °C	Seconds to minutes	Membrane damage with oedema, denaturation of enzymes	irreversible
60 – 100 °C	< 1 second	Coagulation, necrosis	
100 – 300 °C		dehydration, vaporisation of water	
> 300 °C		Carbonisation, vaporisation of tissue	

In agreement with the table above, most authors consider 47 °C, which represents an increase of 10 °C above body temperature, applied for one minute as critical temperature to harm the tissue. As the temperature rise inside the tissue is one of the crucial determinants of successful cavity preparation, it has to be considered when judging the suitability of a laser system for bone tissue ablation.

5.5.1 MATERIALS AND METHODS

Temperature measurements just involved the Biolase Er,Cr:YSGG laser operated at 20 Hz and different fluences. Blocks of bovine compacta, spongiosa and cartilage were used. In distances of 2 and 4 mm holes were drilled into the tissue samples. These holes were filled with thermo paste and thermo couples connected to a thermometer were inserted. The thermo paste fulfilled two aims: 1. it served as fixation for the thermo couple, 2. guarantees better conditions for heat conduction. On the surface of the tissue sample the position of the thermo couple was marked and exactly this position was irradiated for a certain time period. Laser ablation of bone was performed with the air-water spray acting as coolant. Without this spray the tissue surface would have been completely carbonized. Keller (1998) has already mentioned in his scientific report, that sufficient cooling by an air-water spray is necessary to reduce thermal effects when higher pulse repetition rates than 6 Hz are applied.
For each laser setting several measurements were conducted and recorded properly. By averaging these data the results presented immediately were derived.

5.5.2 RESULTS

A selection of graphs representing the heat accumulation during ablation is depicted in Fig. 93. All of them show the temperature increase when applying a fluence of 34 J/cm². Ablation was performed for 40 seconds, with exception of spongiosa where the laser was turned off after 30 seconds irradiation. Data for compacta, spongiosa and cartilage are captured. In general, the temperatures reached in 2 mm depths are much higher than those detected 4 mm below the surface. The slopes of the graphs obtained for a depth of 2 mm are also steeper compared to their 4 mm counterpart, which holds especially for spongiosa and cartilage. In contrast to compacta, for spongiosa and cartilage a relatively narrow peak is evident. Compacta on the other hand possesses a quite elongated maximum, indicating that heat inside the tissue accumulated during ablation diffuses slowly to its surrounding.

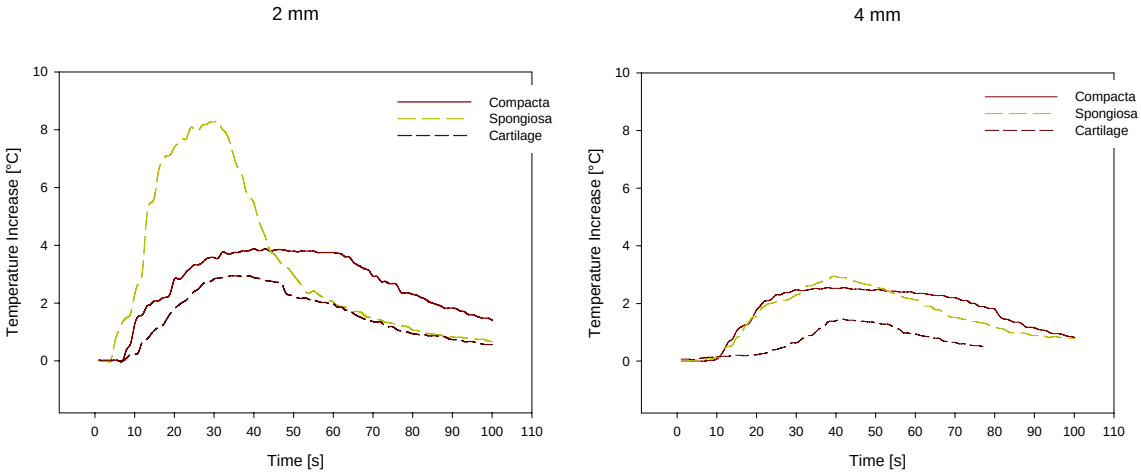

Fig. 93: Temperature increase inside compacta, spongiosa and cartilage in 2 mm and 4 mm depth below the ablation site induced by Er,Cr:YSGG laser ablation.

The specific heat capacity expresses the capability of a material to change its temperature when a certain amount of energy is brought into the tissue. Because of the vast temperature increase in spongiosa compared to the other bone materials its specific heat is expected to be the lowest among those materials. Referring to Rumpf (2001) the situation is somewhat different. The following table containing specific heat capacities and heat conductivities of the materials to be discussed presents an excerpt of his work. Although these values are supposed to represent parameters for human bone they can be used as guidelines for the current interpretation.

Table 31: Comparison of thermal parameters of compacta, spongiosa and cartilage.

Parameter	Equation	Symbol	Compacta	Spongiosa	Cartilage
Specific Heat Capacity	$\bar{c} = \frac{\Delta Q}{\Delta T}$ [29]	$\bar{c}$ [J/gK][30]	1.2-1.3	1.2-2.4	3.5-3.8
Heat Conductivity	$\bar{\lambda} = \frac{1}{3} v l \rho \bar{c}_V$ [31]	$\bar{\lambda}$ [W/mK]	0.2-0.3	0.3-0.4	0.6

The specific heat capacity of cartilage is the highest, followed by spongiosa and compacta. Higher values of the specific heat capacity implicate, that more energy is necessary to induce a temperature increase of 1 °C. The consequence is that the heat accumulated during a defined time period by applying certain energies is lowest for the material with the highest heat capacity value. Therefore the results are in good agreement with theory, especially when cartilage is compared to the other bone materials. For spongiosa and compacta deviations from theory can be noticed, when temperature increases in a depth of 2 mm were measured. Here, the trabecular structure plays a major role. When the trabecular network is not that densely woven, the heat absorption capacity of the tissue is even higher as blood contributes to this effect. Nevertheless, as the intervals for their specific heat capacities overlap results

[29] $\bar{c}$ …specific heat capacity, ΔQ…transferred heat, ΔT…temperature-difference

[30] Temperature differences can either be expressed in K or °C.

[31] $\bar{\lambda}$ …heat conductivity, v…mean velocity of the particles involved in heat exchange, l…mean free path length, ρ…density of the matter, $\bar{c}_V$ …specific heat capacity for a constant volume

like the one above are permitted. This overlap can especially be used for the interpretation of the temperature curves measured for compacta and spongiosa in a depth of 4 mm.
A last consideration involving Fig. 93 refers to the peak of the curves depicted. Obviously, the peaks of spongiosa and cartilage are narrower compared to compacta, implicating that the heat induced in compact bone is released into the adjacent material much slower. This finding is correlated to the lower heat conductivity of compacta compared to spongiosa and cartilage. As the heat conductivity of cartilage is the highest its peak should be the narrowest. The temperature measurement in 2 mm depth cannot serve as example, as irradiation of spongiosa was stopped 10 seconds earlier than cartilage treatment. On the other hand, temperature measurement 4 mm below the surface reflects this situation very well.
Temperature curves were additionally developed for 45 J/cm² and 57 J/cm² treatments. Their shapes resemble mostly with that of the graphs above. The presentation of all graphs would not contribute any surplus value to this work. As these results are also of some interest, they are presented as well, although in a different way. For better quantification the temperature increases of all materials accumulated after 10, 20 and 30 seconds irradiation are now arranged in Table 32. 2 mm below the ablation site spongiosa experiences the highest temperature increases for all applied fluences, followed by compacta and cartilage. The temperature of cartilage does not increase at all during the first 10 seconds of irradiation. In 4 mm depth compacta is on top especially for 20 seconds laser treatment and more.

Table 32: Temperature increase inside compacta, spongiosa and cartilage after a defined period of time.

Fluence [J/cm²]	Depth [mm]	Material	Temperature Increase [°C]		
			10 s	20 s	30 s
34	2	Compacta	1.25	2.83	3.58
		Spongiosa	2.28	7.4	8.28
		Cartilage	-	1.8	2.84
	4	Compacta	0.08	1.78	2.48
		Spongiosa	0.15	1.55	2.3
		Cartilage	-	0.22	0.63
45	2	Compacta	1.78	5.57	7.75
		Spongiosa	2.56	8.08	8.4
		Cartilage	-	2.38	4
	4	Compacta	0.1	1.97	2.72
		Spongiosa	0.2	1.77	2.51
		Cartilage	-	0.93	1.83
57	2	Compacta	3.55	6.54	8.48
		Spongiosa	2.86	8.47	8.73
		Cartilage	-	4.3	6.25
	4	Compacta	0.7	3.64	6.03
		Spongiosa	0.36	1.98	2.73
		Cartilage	-	1.23	2.02

In the worst case, an increase of more than 8 °C above body temperature within 30 seconds laser irradiation is reached in distances of 2 and 4 mm, respectively. That means that the temperature increase at the surface of the treated sample is even higher. Considering that the threshold for bone survival is about 47 °C for 1 minute belonging to an increase of 10 °C

within 1 minute (Eriksson and Albrektsson, 1983), the thermal impact of the temperatures achieved in this study is already harmful. Kimura et al. (2001) measured the temperature rise on the surface of canine mandibular bone during Er,Cr:YSGG laser ablation at 141 J/cm². They operated their laser at this fluence as satisfying surface quality was achieved with that setting. The temperatures increase for 10 second irradiation was less than 4 °C, whereas 30 second irradiation showed a maximum increase of 15 °C (or an average of 12.6 °C) that was beyond the limit. Interestingly, they speculate that there would be no thermal effects on adjacent bone tissue for treatments less than 30 seconds, as a rise of 10 °C was just detected for less than 10 seconds. Nevertheless, such assumptions are quite risky.
In a study of Schwab et al. (2004 a) temperature development in cochlea were simulated by using a drilled PMMA body filled with 0.3 ml of water. The rise in temperature of the target space upon laser bombardment with a free-running Er:YAG and a fs laser was registered with the aid of temperature sensors. Changes of about 1.75 °C, 4 °C and 5.25 °C were detected after 10 minutes Erbium laser irradiation at ~28 J/cm² (3.7 Hz), 49 J/cm² (3.7 Hz) and 68 J/cm² (3 Hz) respectively. The USPL with a wavelength of λ = 780 nm was operated with a pulse duration of 100 fs and a PRR of 3 kHz. The temperature changes in water during USPL ablation are presented in Fig. 94. For each curve (starting from 18 °C) the maximum temperature is stated as well as the applied laser power. With a focal spot diameter of 80 µm the powers of 30 mW, 60 mW and 120 mW correspond to fluences of 0.2 J/cm², 0.4 J/cm² and 0.8 J/cm², respectively. Out of the diagram changes of 1.5 °C, >2 °C and 4.5°C after 10 minutes irradiation are evident for the three settings. By analysing the gradients of their temperature curves Schwab et al. inferred that for a given power output, the fs laser releases only half the amount of heat emitted by the Er:YAG lasers. They even conclude that thermal damage to the adjacent tissue may virtually be ruled out.

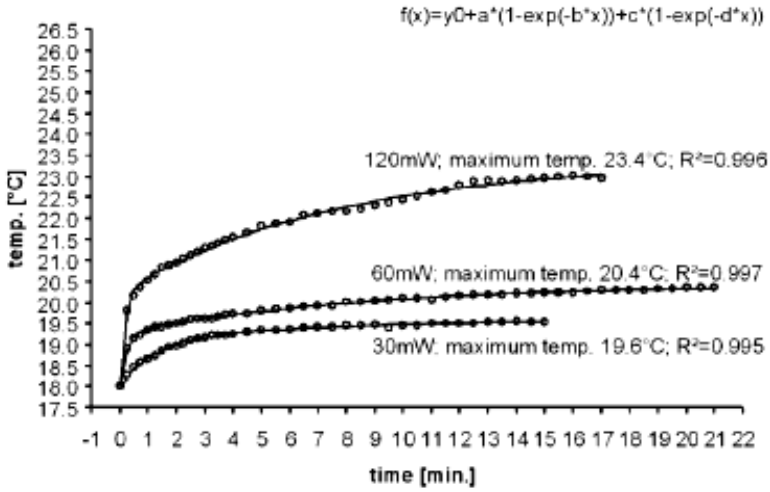

Fig. 94: Temperature change in water with a fs laser. (Taken from (Schwab, 2004 a).)

Comparable to the results obtained by Schwab et al. for the temperature increase in water after laser irradiation, even for bone substances reduced heat impact by USPL compared to Erbium systems can be expected. Nevertheless, temperature rise near the ablation site during USPL treatment could not be determined in own experiments as suitable devices for the measurements like IR cameras were not available. Although scarcely existing, at this stage it has to be referred to literature. Undoubtedly, a comprehensive study to investigate heat accumulation effects induced by USPL has to be performed to judge their suitability in surgery. Anyhow, as USPL ablation is already initiated by very low fluences the heat impact can be kept in a tight rein.

6 CONCLUSION AND OUTLOOK

The main results of this thesis are outlined in the following enumeration:

Tooth and Composites

- Etch depth per pulse achieved by USPL in dental hard tissue and composite restorations are in the µm-region and therefore much lower than Erbium ablation rates. The USPL ablation procedure can be enhanced by applying PRR of some tens of kHz. Ablation rates per second are then comparable to Erbium rates.
- Selective ablation is very pronounced for USPL as dentine revealed lower ablation rates than composites, which is beneficial for minimum invasive secondary caries treatment. This cannot generally be reported for Erbium systems. Depending on the composite sometimes the controversial effect can be observed, i.e. composite gets equally or even less ablated than dentine.
- Ablation thresholds in dentine amount to 5 J/cm² for Er:YAG and 8 J/cm² for Er,Cr:YSGG, while enamel ablation is started at even higher fluences. Fs laser ablation thresholds of the same tissues are below 1 J/cm². USPL thresholds of composites determined in this study are lower than those of tooth structures. Again, this fact contributes to selective ablation. With rising pulse duration thresholds increase and ablation rates decline at constant fluence.
- The remaining dentine surface after Erbium laser treatment is quite fissured and scaly. It strongly depends on the air-water spray as insufficient cooling and hydration, respectively, lead to micro-cracks, melting or carbonisation. The morphology of USPL processed cavities in dentine involving a scanner shows superior tissue quality. An appropriate set of laser and scanner parameters leads to surfaces with no evidence of melting, carbonisation or micro-cracks. In contrast to cavities excavated by Erbium lasers the cavity rims after scanned UPSL treatment are well defined and smooth.
- Scanned USPL ablation leaves a fine micro-retentive pattern. Although its appearance is distinct from an etched surface this regular structure bears the potential for good compound to dental filling material without additional etching. On the other hand, supplementary etching is recommended after Erbium conditioning because of the scaly appearance of the tooth surface.

Bone

- Like for tooth and composites ablation rates per pulse achieved with Erbium lasers in each bone material are higher than USPL ablation rates in the same tissue. Volumes in the order of 10^{-3}-10^{-2} mm³ per pulse can be excavated with Erbium lasers. Therefore fluences of tens of J/cm² have to be applied. USPL are capable of just removing volumes in the order or 10^{-7} mm³ per pulse while applying about 2 J/cm². For preparations within a reasonable duration higher pulse repetition rates have to be used.
- As Erbium laser ablation strongly depends on the water content of the tissue, cartilage possesses higher ablation rates than compacta. For USPL systems the situation is similar. Cartilage, the softest tissue, reveals the highest ablation rates, followed by compacta, the densest bone tissue. Spongiosa occupies the last position. This is a result of its native structure. Not every laser pulse is capable of hitting a trabecula but penetrating into the intra-trabecuar space failing to contribute to ablation.
- Depending on the pulse duration and on the type of bone tissue, threshold values from 2 J/cm² up to 10 J/cm² are reported for Erbium lasers. USPL ablation thresholds determined in this study are well below 1 J/cm². To give examples, a threshold of 0.2

J/cm² was found for 150 fs Ti:Sapphire ablation of cartilage and 0.8 J/cm² for 2 ps Ti:Sapphire laser ablation of compacta. 330 fs Yb:Glass laser ablation affords 0.82 J/cm² to start ablation in spongiosa. Again, rising pulse duration cause decreased etch depths per pulse and increased thresholds for fixed fluences.

- The tissue morphology after preparation with a mechanical drill is characterised by torn out tissue particles and a smeared surface. Erbium laser ablation is capable of yielding appreciable surface features. With a fluence of 24.9 J/cm² good results were obtained in spongiosa with the Er,Cr:YSGG laser. Treatment of cartilage with Erbium lasers was not that successful, neither was the ablation of compacta, as a very rough and scaly surface was remaining. USPL ablation of bone material was conducted with an x-y-scanner. In general, the native tissue structure was preserved. Although the gentle tissue removal procedure was demonstrated in spongiosa with 330 fs Yb:Glass laser at 1.9 J/cm² by performing rectangular scans, overheating and therefore melting can occur at the corners of rectangles. The beam of the Ti:Sapphire laser was scanned according to an spiral. For 7 ps, 1 kHz, and 1 J/cm² presentable results were achieved. For 700 fs 1 kHz, 1 J/cm² slight melting was evident. A convenient match of scan and laser parameters is therefore inevitable. No morphological differences as well as no changes in the native structure could be detected for 700 fs, 0.65 J/cm² and 7 ps, 1 J/cm² ablation of cartilage at 1 kHz.
- During laser ablation laser induced-plasma spectroscopy was performed. The relative intensities of the identified Ca peaks allow differing between spongiosa, compacta and cartilage.
- Temperature measurements involving Erbium lasers indicate that they might damage the tissue. Treatment without damage is just possible for a few seconds. In the worst case a temperature increase of >8 °C was detected at a depth of 2 mm below the ablation site after 30 seconds irradiation with a fluence of 57 J/cm². This can already cause some worries, as the threshold fluence for bone survival is 47 °C applied for 1 minute. Additional water cooling or shorter treatment duration can therefore be suggested.

Considering all these aspects, superior performance can be attributed to USPL systems in comparison to Erbium laser. Anyhow, further research has to be conducted in this field. Temperature measurements in dental tissue are already under way. In vitro studies on temperature development in bone in the near vicinity of the ablation site still have to be performed. Different geometries of the scan pattern have to be tested and scan and laser parameters have to be correlated perfectly. For dental cavities micro-leakage studies are outstanding, to assess if USPL conditioning alone is really sufficient to guarantee good adhesion to the restoration. For bone in vivo studies on the healing process of USPL treated tissue should be conducted.

An USPL system for surgical applications in implant surgery and orthopaedics can then be developed. A feedback system based on the data of plasma spectroscopy to distinguish between different tissue types has to be integrated. This feedback system combined with an online monitoring modus enhances selective and also minimum invasive treatment. Furthermore, the scanner has to be miniaturised and incorporated into a hand-piece to be operated by the surgeon. This USPL system can bring several advantages for the surgeon and the patient such as flexible and secure treatment of tissue, gentle tissue preparations, pain free tooth treatment or in case of bone better healing conditions.

7 REFERENCES

Afilal S.: Ablationsmechanismen von biologischem Hartgewebe bei Bestrahlung mit kurzgepulsten CO_2-Lasern. PhD Thesis, Mathematisch-Naturwissenschaftliche Fakultät, Heinrich-Heine Universität Düsseldorf, Germany, 2004.

Alexander R., Xie J., Fried D.: Selective Removal of Residual Composite from Dental Enamel Surfaces Using the Third Harmonic of a Q-Switched Nd:YAG Laser. Lasers Surg Med 30, 2002, 240-245.

Apel C., Franzen R., Meister J., Sarrafzadegan H., Thelen S., Gutknecht N.: Influence of the Pulse Duration of an Er:YAG Laser System on the Ablation Threshold of Dental Enamel. Lasers Med Sci 17, 2002 a, 253-257.

Apel C., Meister J., Ioana R.S., Franzen R., Hering P., Gutknech N.: The Ablation Threshold of Er:YAG and Er:YSGG Laser Radiation in Dental Enamel. Lasers Med Sci 17, 2002 b, 246-252.

Armstrong W., Neev J., Da Silva L., Rubenchik A., Stuart B.: Ultrashort Pulse Laser Ossicular Ablation and Stapedotomy in Cadaveric Bone. Lasers Surg Med 30, 2002, 216-220.

Arnabat-Dominguez J., Espana-Tost A.J., Berini-Aytes L., Gay-Escoda C.: Erbium:YAG Laser Application in the Second Phase of Implant Surgery: A Pilot Study in 20 Patients. Int J Oral Maxillofac Implants 18, 2003, 104-112.

Bachmann L., Zezell D.M., Maldonado E.P.: Determination of Beam Width and Quality for Pulsed Lasers Using the Knife-Edge Method. Instrumentation Science and Technology 31 (1), 2003, 47-52.

Bäcker A.: Ablation of Dental Hard Tissue by Scanned Ultrashort Laser Pulses, Diploma Thesis, 2004.

D. Bäuerle: Laser Processing and Chemistry. 3rd Edition, Springer-Verlag Berlin, Heidelberg, 2000.

Belinkov A.V., Erofeev A.V., Shumilin V.V., Tkachuk A.M.: Comparative Study of the 3 µm Laser Action on Different Tooth Tissue Samples Using Free-Running Er-Doped YAG, YSGG, YSP and YLF Lasers. Proc SPIE 2080, 1993, 60-67.

Bonse J.O.: Materialbearbeitung von Halbleitern und Nitridkeramiken mit Ultrakurzen Laserpulsen. PhD, Fakultät II – Mathematik und Naturwissenschaften, Technische Universität Berlin, 2001.

Buchelt M., Kutschera H., Katterschafka T., Kiss H., Lang S., Beer R., Losert U.: Er:YAG and Ho:YAG Laser Osteotomy: The Effect of Laser Ablation on Bone Healing. Lasers Surg Med 15, 1994, 373-381.

Capitelli M., Casavola A., Colonna G., De Giacomo A.: Laser-Induced Plasma Expansion: Theoretical and Experimental Aspects. Spectrochimica Acta Part B 59, 2004, 271-289.

Ceballos L., Osorio R., Toledano M., Marshall G.W.: Microleakage of Composite Restorations after Acid or Er:YAG Laser Cavity Treatments. Dent Mat 17, 2001, 340-346.

Dumore T., Fried D.: Selective Ablation of Orthodontic Composite by Using Sub-Microsecond IR Laser Pulses with Optical Feedback. Lasers Surg Med 27, 2000, 103-110.

El Montaser M., Devlin H., Sloan P., Dickinson M.: Pattern of Healing of Calvarial Bone in the Rat Following Application of the Erbium-YAG Laser. Lasers Surg Med 21, 1997, 255-261.

Eriksson A.R., Albrektsson T.: Temperature threshold levels for heat-induced bone tissue injury: A vital-microscopic study in the rabbit. J Prosthet Dent 50, 1983, 101-107.

Ernst C.P., Willsershausen B.: Quo vadis Komposit? Eine aktuelle Standortbestimmung zahnärztlicher Füllungskomposite, Polyklinik für Zahnerhaltungskunde des Klinikums der Johannes Gutenberg-Universität Mainz.

Frentzen M., Koort H.J., Kermani O., Dardenne M.U.: Bearbeitung von Zahnhartgeweben mit einem Excimer-Laser – eine in-vitro Studie. Dtsch Zahnärztl Z 44, 1989, 431-435.

Frentzen M., Götz W., Ivanenko M., Afilal S., Werner M., Hering P.: Osteotomy with 80-µs CO_2 laser pulses – histological results. Lasers Med Sci 18, 2003, 119-124.

Frick H., Leonhardt H., Starck D.: Allgemeine Anatomie – Spezielle Anatomie. Taschenlehrbuch der gesamten Anatomie. Band 1, 4. Auflage, Georg Thieme Verlag Stuttgart, New York, 1992, 1, 692-703.

Fried D., Featherstone J.D.B., Visuri S.R., Seka W., Walsh J.T.: The Caries Inhibition Potential of Er:YAG and Er:YSGG Laser Radiation. Proc SPIE 3593, 1997, 73-78.

Fried N., Fried D.: Comparison of Er:YAG and 9.6-µm TE CO_2 Lasers for Ablation of Skull Tissue. Lasers Surg Med 29, 2001, 335-343.

Friesen L.R., Cobb C.M., Rapley J.W., Forgas-Brockman L., Spencer P.: Laser Irradiation of Bone: II. Healing Response Following Treatment by CO_2 and Nd:YAG Lasers. J Periodontol 70, 1999, 75-83.

Giachetti L., Russo D.S., Scarpelli F., Vitale M.: SEM Analysis of Dentine Treated with the Er:YAG Laser: A Pilot Study of the Consequences Resulting from Laser Use on Adhesion Mechanisms. J of Clinical Laser Med Surg 22(1), 2004, 35-41.

Glock K. G.: Bearbeitung von Zahnhartsubstanzen mit dem CO_2-Swiftlaser®-Lasersystem – eine in-vivo Studie. Dissertation, Fakultät für Medizin, Technische Universität München, 2000.

Goldman L., Hornby P., Mayer R., Goldman B.: Impact of the Laser on Dental Caries. Nature 203, 1964, 417.

Gürsoy T., Kazak M., Gokce K., Benerli Y.: Microleakage of Class I and Class V Resin composite Restorations after Burr or Er,Cr:YSGG Laser Preparation. JOLA 3(4), 2003, 229-233.

Hibst R., Keller U.: Experimental Studies of the Application of the Er:YAG Laser on Dental Hard Substances: I. Measurement of the Ablation Rates. Lasers Surg Med 9, 1989, 338-344.

Hibst R.: Mechanical Effects of Erbium:YAG Laser Bone Ablation, Lasers Surg Med 12, 1992, 125-130.

Hossain M., Nakamora Y., Yamada Y., Suzuki N., Murakami Y., Matsumoto K.: Analysis of Surface Roughness of Enamel and Dentine after Er,Cr:YSGG Laser Irradiation. J of Clinical Laser Med Surg 19 (6), 2001, 297-303.

Hossain M., Yamada Y., Nakamura Y., Morakami Y., Tamaki Y., Matsumoto K.: A Study on Surface Roughness and Microleakage Test in Cavities Prepared by Er:YAG Laser Irradiation and Etched Burr Cavities. Lasers Med Sci 18, 2003, 25-31.

http://physics.nist.gov

http://www.taylor-hobson.com/faqsurfacedetail.asp?faqid=69

Ivanenko M., Fahimi-Weber S., Mitra T., Wienrich W., Hering P.: Bone Tissue Ablation with sub-µs Pulses of a Q-switched CO_2 Laser: Histological Examination of Thermal Side Effects. Lasers Med Sci 17, 2002, 258-264.

Ivanenko M., Hering P.: Wet bone ablation with mechanically Q-switched high-repetition-rate CO_2 laser. Appl Phys B 67, 1998, 395-397.

Ivanenko M., Werner M., Afilal S., Klasing M., Hering P.: Ablation of Hard Bone Tissue with pulsed CO_2 Lasers. Medical Laser Applications, 19/5, 2005, in press.

Ivoclar Vivadent: Composite-Füllungsmaterial. Report Nr. 5, 1990.

Ivoclar Vivadent: Der gefüllte Zahn – ein komplexes Verbundsystem. Report Nr. 7, 1992.

Ivoclar Vivadent: SR Adoro im Fokus – Indirekte Komposite – Werkstoffkunde und Entwicklung. Report Nr. 15, 2004.

Ivoclar Vivadent: Wissenschaftliche Dokumentation. Die Tetric® Ceram Familie: Tetric® Ceram, Tetric® Ceram HB, Tetric® Flow, Tetric® Flow Chroma. Forschung Entwicklung. Wissenschaftlicher Dienst. 2000.

Jovanovic S., Schonfeld U., Prapavat V., Berghaus A., Fischer R., Scherer H., Muller G.: Effects of Pulsed Laser Systems on Stapes Footplate. Lasers Surg Med 21, 1997, 341-350.

Kalachandra S., Sankarapandian M., Shobha H.K., Taylor D.F., McGrath J.E.: Influence of Hydrogen Bonding on Properties of Bis-GMA Analogues. J Material Science: Materials in Medicine 8, 1997, 283-286.

Kamata M., Imahoko T., Ozono K., Obara M.: Materials Processing by Use of a Ti:Sapphire Laser with Automatically-Adjustable Pulse Duration. Appl Phys A, 2004.

Keller U., Hibst R., Mohr W.: Tierexperimentelle Untersuchungen zur Laserosteotomie mit dem Erbium:YAG-Laser. Dtsch Z Mund Kiefer GesichtsChir 15, 1991, 197-199.

Keller U.: Erbium-YAG-Laser in der Oralchirurgie, Dt. Zahnärztekalender 1998, 113-129.

Kim B. M., Feith M. D., Rubenchik A. M., Joslin E. J., Celliers P. M., Eichler J., Da Silva L. B.: Influence of Pulse Duration on Ultrashort Laser Pulse Ablation of Biological Tissues. J Biomedical Optics 6(3), 2001, 332-338.

Kimura Y., Yu D., Fujita A., Yamashita A., Murakami Y., Matsumoto K.: Effects of Erbium, Chromium:YSGG Laser Irradiation on Canine Manibular Bone. J Periodontol 72, 2001, 1178-1182.

Koechner W., Bass M.: Solid-State-Lasers. A Graduate Text. Springer Verlag, New York, 2003.

Kuhne O.: Photoablation an Hartgewebe. Diploma Thesis, Fachhochschule Aachen, Abteilung Jülich, Germany, 1998.

Kultermann G.: Moderne Adhäsivsysteme – Fortschritt oder Marketing. DFZ, 5, 2001, 36-41.

Kunzelmann K.H., Chen H.Y., Mehl A., Manhart J., Hickel R.: Effects of different light polymerisation concepts on composite shrinkage forces. J Dent Res 80, Divisional Abstracts, 1207, Abstract 53, 2001.

Lee C.: Procurement of Autogenous Bone from the Mandibular Ramus with Simultaneous Third-Molar Removal for Bone Graftin Using the Er,Cr:YSGG Laser: A Preliminary Report, J Oral Implant 31(1), 2005, 32-38.

Li Z., Reinisch L., Van de Merwe W.: Bone Ablation With Er:YAG and CO_2 Laser: Study of Thermal and Acoustic Effects. Lasers Surg Med 12, 1992, 79-85.

Liu J.M.: Simple Technique for Measurements of Pulsed Gaussian-Beam Spot Sizes. Optics Letters 7 (5), 1982.

Lizarelli R., Moriyama L.T., Bagnato V.S.: Ablation of Composite Resins Using Er:YAG Laser – Comparison with Enamel and Dentine. Lasers Surg Med 33, 2003, 132-139.

London R.A., Bailey D.S., Young D.A., Alley W.E., Feith M.D., Rubenchik A.M: Hydrodynamic Model for Ultrashort Pulse Ablation of Hard Dental Tissue. SPIE 2672, 1999, 231-242.

Lonnroth E., Shahnavaz H.: Use of polymer materials in dental clinics, case study. Swed Dent J, 21 (4), 1997, 149-159.

Lubatschowski H., Heisterkamp A., Will F., Singh A.I., Serbin J., Ostendorf A., Kermani O., Heermann R., Willing H., Ertmer W.: Medical Applications of Ultrafast Laser Pulses. RIKEN Review 50, 2002, 113-118.

Manual of the Hurricane-i Laser, Spectra-Physics, 2003.

Mitra T.: Ablation Biologischen Hartgewebes mit gepulsten IR-Lasern. PhD Thesis, Naturwissenschaftliche Fakultät der Heinrich-Heine-Universität Düsseldorf, 2002.

Moritz A., Beer F., Goharkhay K., Shoop U., Strassl M., Verheyen P., Walsh L.T., Wernisch J., Wintner E.: Orale Lasertherapie. Quintessenz Verlag, Berlin, 2006.

Moritz A., Gutknecht N., Schoop U., Goharkhay K., Wernisch J., Sperr W.: Alternatives in Enamel Conditioning: A Comparison of Conventional and Innovative Methods. J of Clinical Laser Med Surg 14 (3), 1996, 133-136.

Neev J., Da Silva L.B., Feith M.D., Perry M.D., Rubenchik A.M., Stuart B.C.: Ultrashort Pulse Lasers for Hard Tissue Ablation. IEEE J of Selected Topics in Quantum Electronics 2 (4), 1996 a, 790-800.

Neev J., Huynh D. S., Dan C.C., White J.M., Da Silva L.B., Feith M.D., D.L. Matthews, M.D. Perry, A.M. Rubenchik, B.C. Stuart: Scanning Electron Microscopy and Ablation Rates of Hard Dental Tissue Using 350 fs and 1 ns Laser Pulses. SPIE 2672, 1996 b, 250-261.

Nelson J., Orenstein A., Liaw L., Berns M.: Mid-Infrared Erbium:YAG Laser Ablation of Bone: The Effect of Laser Osteotomy on Bone Healing. Lasers Surg Med 9, 1989, 362-374.

Niemz M., Eisenmann L., Pioch T.: Vergleich von drei Lasersystemen zur Abtragung von Zahnschmelz. Schweiz Monatsschr Zahnmed 103, 1993, 1252-1256.

Niemz M.: Cavity Preparation with the Nd:YLF Picosecond Laser. J Dent Res 74 (5), 1995, 1194-1199.

Niemz M.: Investigation and Spectral Analysis of the Plasma-Induced Ablation Mechanism of Dental Hydroxyapatite. Appl Phys B 58, 1994, 273-281.

Niemz M.: Laser-Tissue Interactions: Fundamentals and Applications. Springer, Berlin, 1996.

Olivier W., Morgenroth K.: Experimentelle Osteotomien mit dem Er:YAG Laser im Vergleich zu konventionellen Techniken. Laser Journal 2, 2003, 10–14.

Ozono K., Obara M.: Tailored Processing of Advanced Biomedical Hydroxyapatite by Femtosecond Laser Pulses. Appl Phys A 77, 2003, 303-306.

Payne J., Peavy G., Reinisch L., Van Sickle D.: Cortical Bone Healing Following Laser Osteotomy Using 6.1 μm Wavelength. Lasers Surg Med 29, 2001, 38-43.

Peavy G., Reinisch L., Payne J., Venugopalan V.: Comparison of Cortical Bone Ablations by Using Infrared Laser Wavelengths 2.9 to 9.2 μm. Lasers Surg Med 26, 1999, 421-434.

Pourzaradian A., Watanabe H., Aoki A., Ichinose S., Sasaki K.M., Nitta H., Ishikawa I.: Histological and TEM Examination of Early Stages of Bone Healing after Er:YAG Laser Irradiation. Photomedicine and Laser Surgery 22 (4), 2004, 355-363.

Reider G.: Photonik. Eine Einführung in die Grundlagen. Springer Verlag, Wien, New York, 1997.

Rode A.V., Gamaly E.G., Luther-Davies B., Taylor B.T., Graissel M., Dawes J.M., Chan A., Lowe R.M., Hannaford P.: Precision Ablation of Dental Enamel Using a Subpicosecond Pulsed Laser. Australian Dental J 48(4), 2003, 233-239.

Rohanizadeh R., Jean A., Daculsi G.: Effects of Q-switched Nd:YAG Laser on Calcified Tissues. Lasers Med Sci 14, 1999, 221-227.

Romaos G., Deppe H., Ertl T., Gutknecht N., Purucker P.: Atlas der chirurgischen Laserzahnheilkunde. Urban und Fischer, München, Jena, 1999.

Rubenchik A.M., Da Silva L.B., Feith M.D., Lane S., London R., Perry M.D., Stuart B.C., Neev J.: Dental Tissue Processing with Ultrashort Pulse Laser. SPIE 2672, 1999, 222-230.

Rumpf C.: New minimally-invasive laser treatment in orthopaedics on spinal deformations and bone tumors. PhD Thesis, Kirchhoff-Institute of Physics, Rupertus Carola University of Heidelberg, Germany, 2001.

Rupprecht S., Tangermann K., Kessler P., Neukam F., Wiltfang J.: Er:YAG laser osteotomy directed by sensor controlled systems. Journal of Cranio-Maxillofacial Surgery 31, 2003, 337-342.

Salle B., Gobert O., Maynadier P., Perdrix M., Petite G., Semerok A.: Femstosecond and Picosecond Laser Microablation: Ablation Efficiency and Laser Microplasma Expansion. Applied Phyiscs A 69 (Suppl.), 1999, 381-383.

Sasaki K.M., Aoki A., Ichinose S., Ishikawa I.: Ultrastructural Analysis of Bone Tissue Irradiated by Er:YAG Laser. Lasers Surg Med 31, 2002, 322-332.

Sassi J.F., Chimello D.T., Borsatto M.C., Corona S.A.M., Pecora J.D., Palm-Dibb R.G.: Comparative Study of the Dentine/Adhesive Systems Interface after Treatment with Er:YAG Laser and Acid Etching using Scanning Electron Microscope. Lasers Surg Med 34, 2004, 385-390.

Scanlab Manual, 2005.

Schäfer C.B.: Die Erbium-Laser präparierte Kavität – Randständigkeit von Kompositversorgungen und Säurerestistenz der Kavitätenränder. PhD, Medizinische Fakultät der Rheinisch-Westfälischen Technischen Hochschule Aachen, 2003.

Schärer P., Chen L.: Komposite-Zemente und Dentinhaftmittel. Phillip J 11/12, 1998, 326-334.

Schwab B., Hagner D., Bornemann J., Heermann R.: The Use of Femtosecond Technoloy in Otosurgery. Appl Phys 96, 2004 a, 211-226.

Schwab B., Hagner D., Müller W., Lubatschowski H., Lenarz T., Heermann R.: Bone Ablation Using Ultrashort Laser Pulses. A New Technique for Middle Ear Surgery. Laryngo-Rhino-Otol 83, 2004 b, 219-225.

Seka W., Featherstone J.D.B., Fried D., Visuri S.R., Walsh J.T.: Laser Ablation of Dental Hard Tissue: From Explosive Ablation to Plasma-Mediated Ablation. SPIE 2672, 1996, 144-158.

Serbin J., Bauer T., Fallnich C., Kasenbacher A., Arnold W.H.: Femtosecond Lasers as Novel Tool in Dental Surgery. Appl Surf Sci 197-198, 2002, 737-740.

Spencer P., Payne J.M., Cobb C.M., Reinisch L., Peavy G.M., Drummer D.D., Suchman D.L., Swafford J.R.: Effective Laser Ablation of Bone Based on the Absorption Characteristics of Water and Proteins. J Periodontol 70 (1), 1999, 68-74.

Stehrer T.: Laser Induced Breakdown Spectroscopy with the Use of Fibres. Diploma Thesis, Institute of Applied Physics, Johannes-Kepler-Universität, Linz, 2005.

Stern R.H., Sognnaes R.F.: Laser Beam Effect on Dental Hard Tissue. J Dent Res 43, 1964, 873.

Stern R.H., Vahl J., Sognnaes R.F.: Lased Enamel: Ultrastructural Observations of Pulsed Carbon Dioxide Laser Effects. J Dent Res 51, 1972, 455-460.

Stock K., Hibst R., Keller U.: Comparison of Er:YAG and Er:YSGG Laser Ablation of Dental Hard Tissues. SPIE 3192, 0277-786X, 1997, 88-95.

Strassl M., Kasenbacher A., Wintner E.: Ultrashort Laser Pulses in Dentistry. JOLA 2 (4), 2002, 213-222.

Strassl M., Üblacker B., Bäcker A., Beer F., Moritz A., Wintner E.: Comparison of the Emission Characteristics of Three Erbium Laser Systems – A Physical Case Report. JOLA 4 (4), 2000, 263 -270.

Strassl M.: Novel Concepts for Maximum Conservative Dental Hard Tissue Preparation. PhD Thesis, 2007.

Vogel A., Venugopalan V.: Mechanisms of Pulsed Laser Ablation of Biological Tissues. Chem Rev 103, 2003, 577-644.

Walsh J.T., Deutsch T.F.: Er:YAG Laser Ablation of Tissue: Measurement of Ablation Rates. Lasers Surg Med 9, 1989, 327-337.

Wang X., Zhang C., Matsumoto K.: In vivo study of the healing processes that occur in the jaws of rabbits following perforation by an Er,Cr:YSGG laser. Lasers Med Sci 2005 Apr 1 (Epub ahead of print).

Wannop N.M., Dickinson M.R., King T.A.: Erbium:YAG Laser Radiation Interaction with Dental Tissue. SPIE 2080 Dental Applications of Lasers, 1993, 33-43.

Wintner E., Strassl M.: Grundlegendes zum Laser. Out of: Moritz A., Beer F., Goharkhay K., Shoop U., Strassl M., Verheyen P., Walsh L.J., Wernisch J., Wintner E.: Orale Lasertherapie. Quintessenz Verlag, Berlin, 2006.

Wintner E.: Ultra-Short-Pulse Laser Technology and Applications. Lecture notes, 2000/2001.

www.lib.umich.edu/dentlib/Dental tables/Density.html

www.see.ed.ac.uk/~jchick/Y5/Projects/04kilgour/

www.ubicampus.mh-hannover.de/~bmt/bio/kapitel_6/6_2.php

Zack L., Cohen G.: Pulp response to externally applied heat. Endotontics, OS, OM&OP 19 (4), 1965, 515-530.

8 PUBLICATIONS AS FIRST AUTHOR OR CO-AUTHOR

1. Strassl M., Kopecek H., Weinrotter M., Bäcker A., Al-Janabi A.H., Wieger V., Wintner E.: Novel applications of short and ultra-short pulses. Applied Surface Science 247, 2005, 561 – 570.

2. Strassl M., Wieger V., Winter E.: Novel Approach for Dental Hard Tissue Ablation by Ultra-Short Laser Pulses, OSA TOPS Proceedings 98, 2005, 819 – 825.

3. Wieger V., Strassl M., Wintner E.: Potential Painless Treatment of Teeth by Scanned Ultra-Short Laser Pulses, Student Research Conference Proceedings 2005.

4. Wieger V., Strassl M., Wintner E.: Laser Dental Hard Tissue Ablation: Comparison Er-Lasers and Scanned Ultra-Short Pulse Laser. Int J of Applied Electromagnetics and Mechanics 21, 2005. (in the press)

5. Wieger V., Strassl M., Wintner E.: Pico- and Microsecond Laser Ablation of Dental Restorative Materials, Laser and Particle Beams 24, 2006, 41 – 45.

6. Wieger V., Yousif A., Strassl M., Wintnter E.: Ultra-short laser pulses in dentistry – a solution towards painless dental treatment? Proceedings of SPIE, Advanced Laser Technologies 2005, Vol. 6344, 2006, 634403/1-6.

7. Wieger V., Brodoceanu D., Bäuerle D., Wintner E.: Ultra-Short Pulse Laser Ablation of Biological Hard Tissue, Biomaterials in Regenerative Medicien, Proceedings of the International Conference, Vienna, October 2006, 159-164.

8. Yousif A., Strassl M., Wieger V., Zoppel S., Wintner E.: Oral Applications of Ultra-Short Laser Pulses – a New Approach for Gentle and Painless Treatment? SPIE 6261-141, 2006. (accepted)

9. Wieger V., Wernisch J., Wintner E.: Novel oral applications of ultra-short laser pulses. SPIE Proc 6460-10, Photonics West Conference, San Jose, CA, January 2007. (accepted)

10. Wieger V., Beer F., Wintner E.: Novel non-linear laser applications in biomedical technology: bone treatment with ultra-short pulse lasers. SPIE Proc. for ILLA´06, Smolyan, Bulgaria, October 2006. (accepted)

11. Wieger V., Zoppel S., Wintner E.: Ultra-Short Pulse Laser Osteotomy, Laser Physics 17 (4), 2007. (in the press)

9 SUPERVISION OF BACCHELOR THESES

1. Kadlec P.: Ablation von Compositen durch Dentallaser, Novermber 2004.

2. Hofbauer R.: Ablation von verschiedenen Komposite durch zwei Lasersysteme, Mai 2005.

3. Hofbauer R.: Ablation verschiedener Knochengewebe durch Erbium-Lasersysteme, October 2005.

4. Tatic S.: Er,Cr:YSGG Laser in Bone Surgery, September 2006.